الجمهورية الجزائرية الديمقراطية الشعبية
REPUBLIQUE ALGERIENNE DEMOCRATIQUE ET POPULAIRE
وزارة التعليم العالي و البحث العلمي
Ministère de l'Enseignement Supérieur et de la Recherche Scientifique
جامعة أبي بكر بلقايد – تلمسان –
Université Aboubakr Belkaïd – Tlemcen –
Faculté de TECHNOLOGIE

THESE

Présentée pour l'obtention du **grade** de **DOCTORAT 3ème Cycle**

En : Hydraulique

Spécialité : Sciences et Technologies Hydrauliques

Par : KHETTAB Omar El Farouk

Sujet

Origin and Transport of Sediments in a Semi-Arid Environment

Origine et Transport de sédiments en Milieu Semi-Aride

Soutenue publiquement, le **18/ 02/ 2026**, devant le jury composé de :

Mme ABDELBAKI Chérifa	Professeur	Univ. Tlemcen	Présidente
Mr MEGNOUNIF Abdesselam	Professeur	Univ. Tlemcen	Directeur de thèse
Mr GHENIME Abderrahmane Nekkache	Professeur	Univ. Tlemcen	Co- Directeur de thèse
Mr GUEMOU Bouabdellah	MCA	Univ. Ain Temouchent	Examinateur 1
Mr BOUANANI Abderrazak	Professeur	Univ. Tlemcen	Examinateur 2

2025-2026

DEDICATION AND AKNOWLEGMENTS

To my sister Asmaa, my brothers Sid Ahmed and Houssem, and my parents Malika and Mohammed: words cannot fully express my appreciation and gratitude for your constant support, encouragement, and comforting presence. This was especially true during the difficult times of COVID-19 and the challenging period that followed. I could not have achieved this without your love and strength.

My deepest gratitude goes to Prof. Abdesselam MEGNOUNIF, whose guidance and presence were essential to the successful completion of this work. His scientific contributions laid the foundation upon which this project was built and reached new heights.

I am also sincerely grateful to Prof. Abderrahmane GHENIM, whose insights greatly enhanced the quality of this work. I extend my heartfelt thanks to Prof. Cherifa ABDELBAKI for her efforts in helping this research gain visibility, and my special commendation to Dr. Madani BESSEDIK for his encouragement and positive spirit.

I warmly thank Meriem DIAF for her generosity and willingness to share her datasets, without which this work would have been much more difficult.

I also wish to extend my heartfelt thanks to Dr. GUEMOU Bouabdellah and Prof. BOUANANI Abderazak for taking the time to examine this thesis.

To my friends, to all the kind people around me, and to those whose contributions were invisible yet meaningful,

THANK YOU.

Finally, a special dedication to my late family members:

I wish I could have shared this success with you.

Abstract

Sediment transport in fluvial systems is governed by complex, non-linear interactions between water discharge and suspended-sediment concentration, giving rise to hysteresis loops that standard rating curves cannot capture. This thesis introduces an integrated, automated workflow for concentration–discharge hysteresis analysis. We develop the concept of a "hysteresis signature," a systematic code that partitions each loop into linear, clockwise, and anticlockwise segments. We then quantify each segment both on a normalized scale (partial amplitudes) and in real discharge–concentration units via an asynchronous-load metric.

Applied to a large multi-parameter dataset, our method automatically classified 51 distinct hysteresis forms—far beyond traditional five-type schemes—and resolved classification ambiguities inherent in existing indices. This approach provides a powerful tool for understanding watershed dynamics in terms of sediment production and for identifying sediment sources at the catchment scale. In a semi-arid case study on the Mekerra River (NW Algeria), we validated the workflow against successive flood events and found that bank-and-bed sources contribute roughly 84 % of total suspended sediment yield.

The modular nature of the tool makes it readily adaptable to various climates and different watershed sizes, from large basins to small ones. The hysteresis signature method can also be applied to dissolved loads. The tool offers a robust, scalable approach for high-frequency monitoring, sediment-source apportionment, and watershed management.

Keywords: Sediment concentration–discharge hysteresis; Automated loop classification; Hysteresis signature; Semi-arid watershed case study; Sediment source apportionment; Hysteresis Index.

ملخص

يخضع نقل الرسوبيات في الأنهار لتفاعلات معقدة وغير خطية بين معدل الجريان وتركيز الرواسب العالقة، مما يؤدي إلى ظهور حلقات هسترة لا تستطيع المنحنيات التقليدية لمعادلة الجريان–التركيز تمثيلها بدقة. في هذه الأطروحة نقدّم مسار عمل آلياً ومتكاملاً لتحليل هسترة الجريان–التركيز. طوّرنا مفهوم «بصمة الهسترة»، وهو أسلوب ترميز يقسّم كل حلقة إلى مقاطع خطية، وأخرى باتجاه عقارب الساعة، وأخرى بعكس عقارب الساعة. بعد ذلك قمنا بقياس كل مقطع على مستويين: مقياس مُطَبَّع (سعات جزئية) ووحدات فعلية لمعدل الجريان–التركيز باستخدام مؤشر الحمل غير المتزامن.

عند تطبيق هذا المنهج على قاعدة بيانات واسعة ومتعددة المعايير، تمكّنا من تصنيف 51 شكلاً مختلفاً من الهسترة بشكل آلي، وهو عدد أكبر بكثير من المخططات التقليدية ذات الأنماط الخمسة، كما عالجنا مشكلات الغموض في التصنيف الموجودة في المؤشرات السابقة. يوفر هذا النهج أداة قوية لفهم ديناميكيات حوض التصريف من حيث إنتاج الرسوبيات ولتحديد مصادرها على مستوى الحوض .وفي دراسة حالة في مناخ شبه جاف على وادي مقرة (شمال غرب الجزائر)، تم التحقق من صحة المسار من خلال أحداث فيضانية متعاقبة، وأظهرت النتائج أن ضفاف وقاع النهر تساهم بحوالي 84٪ من إجمالي الرواسب العالقة المنقولة.

تُعد طبيعة الأداة قابلة للتكيف بسهولة مع مختلف المناخات والأحواض المائية ذات الأحجام المختلفة، من الكبيرة إلى الصغيرة. كما يمكن تطبيق أسلوب بصمة الهسترة على المواد الذائبة، مما يجعلها أداة قوية وقابلة للتوسع في الرصد عالي التواتر، وتحديد مصادر الرسوبيات، وإدارة الأحواض المائية.

الكلمات المفتاحية: هستيرية تركيز–الجريان الرواسب؛ التصنيف الالي للحلقات؛ بصمة الهستيرية؛ هيدرولوجيا الأحواض النهرية؛ تعيين مصادر الرواسب؛ مؤشر الهستيرية.

Résumé

Le transport des sédiments dans les systèmes fluviaux est régi par des interactions complexes et non linéaires entre le débit d'eau et la concentration en sédiments en suspension, générant des boucles d'hystérésis que les courbes de tarage classiques ne peuvent pas représenter. Cette thèse propose un processus intégré et automatisé pour l'analyse des hystérésis concentration–débit. Nous développons le concept de « signature d'hystérésis », un code systématique qui segmente chaque boucle en portions linéaires, horaires et anti-horaires. Nous quantifions ensuite chaque portion sur une échelle normalisée (amplitudes partielles) et en unités réelles de concentration et de débit via une métrique de charge asynchrone.

Appliquée à un vaste jeu de données multi-paramètres, notre méthode a automatiquement classifié 51 formes d'hystérésis distinctes—bien au-delà des cinq types traditionnels—et a levé les ambiguïtés de classification inhérentes aux indices existants. Cette approche offre un outil puissant pour comprendre la dynamique des bassins versants en termes de production de sédiments et pour identifier les sources de sédiments à l'échelle du bassin. Dans une étude de cas sur le bassin semi-aride de l'oued Mekerra (NW Algérie), la validation sur des crues successives a révélé que les apports des berges et du lit contribuent à environ 84 % du rendement total en sédiments en suspension.

La nature modulaire de l'outil le rend aisément adaptable à divers climats et à différentes tailles de bassins versants, des plus grands aux plus petits. De plus, la méthode de signature d'hystérésis peut également être appliquée aux matières dissoutes. L'outil offre une approche robuste et évolutive pour la surveillance à haute fréquence, le calcul des parts de sources sédimentaires et la gestion des bassins versants

Mots-clés : hystérésis concentration–débit ; classification automatisée des boucles ; signature d'hystérésis ; Bassin versant ; répartition des sources de sédiments ; indice d'hystérésis.

Table of Contents

List of Tables

List of Figures

Introduction

Introduction

1. Background

The natural landscape is in a constant state of evolution. The flux of sediments plays a crucial role in shaping landscapes and maintaining ecosystems. For instance, the Nile River has transported vast amounts of sediments from its headwaters in Africa to the Mediterranean Sea, forming the fertile and densely populated Nile Delta (e.g., Dumont, 2010; Sestini, 1989). Similarly, the Loess Plateau in China has been formed by the accumulation of fine, wind-blown sediments over thousands of years, creating thick, fertile soil layers (e.g., Sun, 2002; L. Wang et al., 2006; G. Zhao et al., 2013). In contrast, the landscape of the Atacama Desert, one of the driest places on Earth, has been shaped by sporadic fluvial activity and constant wind erosion, where rare rain events carve out valleys and canyons, and windblown sediments create dunes and other aeolian landforms (e.g., Arenas-Díaz et al., 2022; Bull et al., 2018; Houston, 2006; Jungers et al., 2013).

Sediments are detached from rock and soil bodies through natural processes such as rain, infiltration, evaporation, water flow, diurnal cycles, biological activity, and temperature fluctuations. These processes cause rocks and soils to break down into small, transportable aggregates. With sufficient transport capacity, these aggregates are carried away from their origin by wind and water, following a sequence of transport, deposition, and remobilization, described as a sediment cascade (Bracken et al., 2015; Collins & Walling, 2004; K. Fryirs, 2013; Harvey, 2002; Vercruysse et al., 2017). Sediment detachment, transport, and deposition dynamics are significantly influenced by anthropogenic activities. Urbanization, dam construction, deforestation, industrialization, and agricultural practices are key contributors to landscape transformations. These activities lead to the degradation of soils, fragmentation of rocks, detachment of sediments, and alteration of transport regimes and depositional rates, profoundly impacting downstream hydrological and hydrogeochemical conditions in lakes, wetlands, and coastal waters (R. Chalov et al., 2015).

Sediment flux can have physical, chemical, and ecological impacts. Sediment transport is crucial for maintaining aquatic ecosystem health, resilience, and function (Koiter et al., 2013; Owens, 2008). However, it also has negative effects. In agricultural catchments, sediment export leads to the loss of nutrient-rich soil, reducing agricultural productivity and potentially contributing

to land instability (e.g., den Biggelaar, Lal, Wiebe, & Breneman, 2003; den Biggelaar, Lal, Wiebe, Eswaran, et al., 2003). Sedimentation in water bodies can reduce water storage capacity, increase flood risks, and degrade soil, water quality, and aquatic habitats (Ben Slimane et al., 2016; Bunzel et al., 2015; Duvert et al., 2012; Gardner & Gerrard, 2003; Horowitz, 2008; Kassoul et al., 1997; Koiter et al., 2013; Owens et al., 2005; Sánchez-Chardi et al., 2009; Tananaev, 2015; Upadhayay et al., 2017; Urban et al., 2009; Vörösmarty et al., 2003, 2010; S. Wang et al., 2019).

The movement of sediment downstream is influenced by a complex interaction between watershed characteristics, storm events, and sediment properties, leading to variations in downstream sediment fluxes. This results in a non-linear behavior known as the hysteresis effect, where sediment concentration exhibits a lagged response to changes in water discharge, indicating a complex interaction between these variables. This asynchrony arises from dynamic sediment availability, channel morphology, and numerous other factors (Gharari & Razavi, 2018; Hamshaw et al., 2018; Prowse, 1984; Seeger et al., 2004; Zuecco et al., 2016). According to Phillips, (2003), hysteresis occurs when a single discharge value corresponds to multiple sediment concentrations.

Hysteresis analysis has become a cornerstone methodology for examining the non-linear relationship between suspended sediment concentration and stream discharge. By quantifying these patterns, researchers have not only verified the underlying mechanisms driving flow-sediment feedback loops but have also decoded complex mass transport dynamics unique to individual watersheds. Investigations into temporal variability have highlighted shifting seasonal regimes of sediment availability, while others have addressed how catchment scale modulates the resulting hysteresis profiles. Consequently, these diagnostics offer a robust standard for determining whether sediment flux is restricted by **source availability** (supply-limited) or **hydraulic capacity** (transport-limited). Furthermore, the framework has proven vital for identifying provenance, allowing scientists to assess, locate, and measure the primary geomorphic drivers within a system.

2. Research Gap and Study Objectives

Hysteresis Analysis is a crucial approach for studying the non-linear nature of the sediment-concentration discharge relationship. This analysis consists of two main components:

a. **Qualitative Analysis**: This involves the visual inspection of sediment concentration as a function of discharge plots. Various hysteresis patterns have been linked to specific

phenomena and processes, deduced from analyzing multiple potential mechanisms and watershed characteristics (e.g., land use, slopes, soil types). This process includes manual inspection of sedigraphs and hydrographs.

b. **Quantitative Analysis**: This involves computing metrics that describe the rotation, magnitude, and slope of hysteresis patterns (e.g., Aich et al., 2014; Andrea et al., 2006; Butturini et al., 2008; Langlois et al., 2005; Lawler et al., 2006; Lloyd et al., 2016b, 2016a; Poggi-Varaldo & Rinderknecht-Seijas, 2003; H. G. Smith & Dragovich, 2009; Vaughan et al., 2017; Zuecco et al., 2016)

To extract comprehensive information from hysteresis relationships, both qualitative and quantitative assessments are essential. Hysteresis analysis combines techniques from both these axes. Briefly described, at the event scale, hysteresis analysis is performed as follows:

(1) Hysteresis patterns are plotted and sorted according to a targeted classification (e.g., the Williams classification (G. P. Williams, 1989)). This classification can be manual or automated using techniques such as machine learning (e.g., Hamshaw et al., 2018), or based on hysteresis metrics (e.g., Butturini et al., 2008; S. D. Keesstra et al., 2019).

(2) Quantitative metrics such as hysteresis indices and slope are computed.

(3) Results are combined and analyzed.

However, hysteresis pattern sorting and the calculation of indices have often been conducted separately, leading to inconsistencies. To enhance the effectiveness of hysteresis analysis, it is crucial to integrate both qualitative and quantitative aspects, thereby improving quality of the results. This requires a more comprehensive classification approach to effectively sort and explore new hysteresis patterns, a unique quantitative analysis for each pattern, and consistency between classification and quantification. Additionally, automating these processes is essential for efficient handling of large datasets. In this study, we aim to address these methodological gaps by introducing an automated, comprehensive approach that meets these criteria and demonstrating it using a substantial dataset.

3. Thesis Structure

The study is divided into three main chapters, each addressing a specific aspect of sediment dynamics, from their origins to advanced analytical techniques for understanding their transport. Below is an overview of the structure of the study

Chapter I – Sediments from Origin to Outlet provides a comprehensive overview of sediment dynamics, beginning with the processes that lead to sediment detachment. It explores various mechanisms such as weathering—both physical and chemical—mass wasting, riverbank collapse, volcanic activity, forest fires, and anthropogenic activities. The chapter then delves into the properties of sediments and characteristics related to their origins. It continues with an examination of sediment transport, deposition, sedimentation, and the mixing processes of sediments from different sources. The chapter concludes by discussing the motivations and methods for identifying and understanding the contribution of various sediment sources. This chapter serves as a steppingstone for the following chapters by detailing crucial aspects of sediment transport dynamics.

Chapter II – The Sediment Concentration – Discharge Relationship focuses on the relationship between sediment concentration and water discharge, known as hysteresis. It introduces the basic concepts of this relationship and discusses the factors that control the configuration of concentration-discharge hysteresis, including sediment production and transport patterns. The chapter also covers various aspects of hysteresis analysis. The practical applications of hysteresis analysis, such as the classification and interpretation of hysteresis patterns and the determination of sediment sources, are explored. This chapter concludes with a brief review of the current state of hysteresis analysis, setting up the foundation for the next chapter.

Chapter III – Conception and Development of An Improved Concentration – Discharge Hysteresis Analysis Workflow presents the development and validation of a new method for hysteresis analysis. It starts with the background and objectives of the study, followed by a detailed description of the datasets used for validation. The chapter proceeds with a step-by-step description of the new and improved workflow for hysteresis analysis. A critical analysis of the method's performance is provided, highlighting the strengths and limitations of this new approach. The chapter concludes with the application of the method in a case study within a semi-

arid climate watershed, demonstrating the practical utility and implications of the improved hysteresis analysis workflow.

Chapter 1

Sediments from origin to outlet

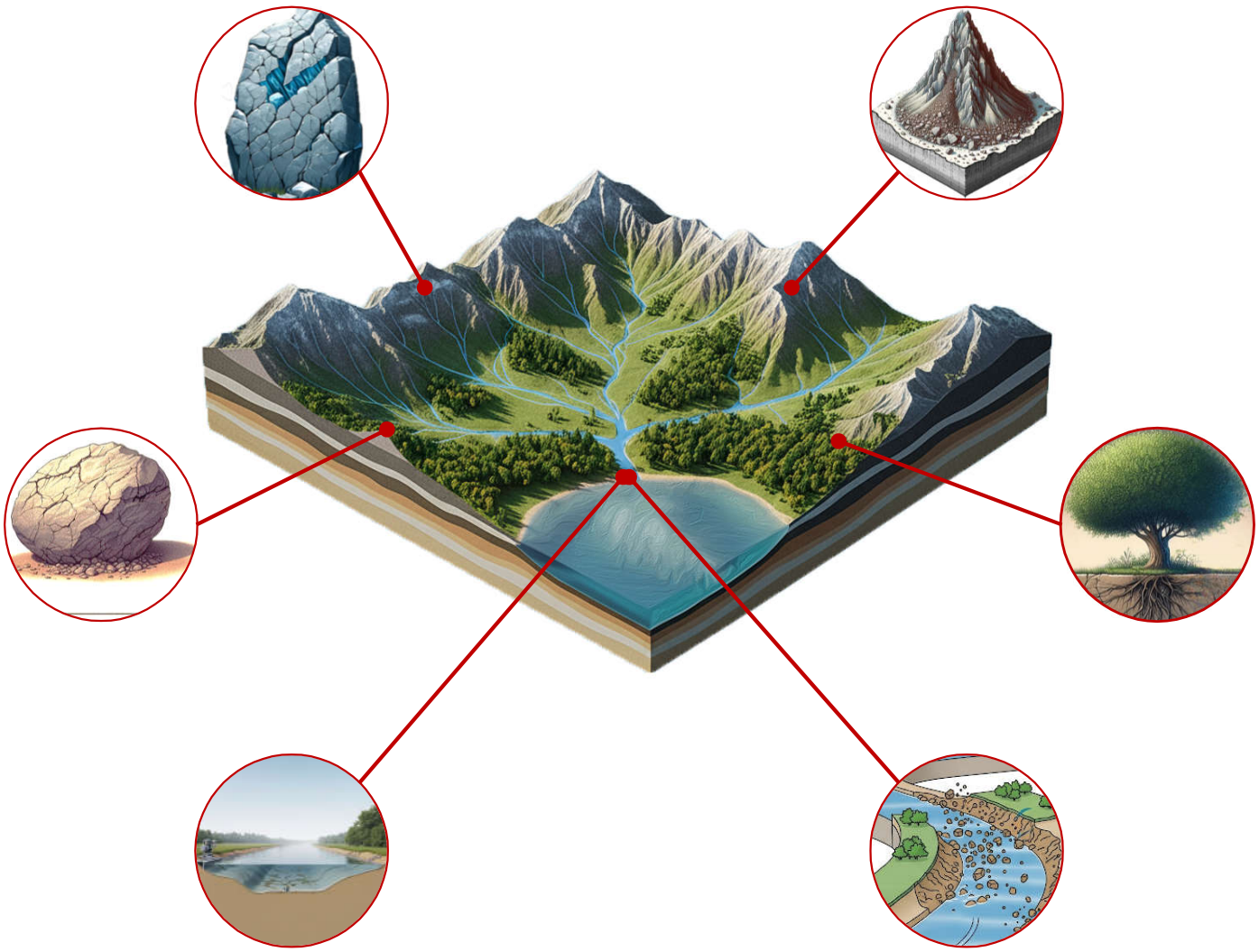

I. Chapter 1 – Sediments from origin to outlet

I-1. The Sediment Cascade: Processes from Origin to Outlet

The journey of sediments begins with detachment, where physical and chemical processes—augmented by mass movements, biological activity, and human interventions—release particles from parent materials. Liberated sediments have distinct properties tied to both their characteristics (such as grain size, composition, and structure) and their site of origin. These attributes not only determine their mobility but also influence their role in downstream processes.

Transport agents then convey sediments through hillslopes and channel networks, where they may be deposited temporarily or mixed with material from other sources. The mixing of sediments in transit creates complex signatures that integrate the diverse conditions of their pathways, offering valuable clues about their provenance and controlling mechanisms. Ultimately, this journey culminates in deposition, whether within floodplains, reservoirs, or coastal systems, where sediments leave lasting imprints on landscapes and human societies.

Understanding these interconnected processes is essential for unraveling sediment sources and fluxes at the watershed scale. Identifying where sediments originate and how they move provides the foundation for both scientific inquiry and practical management. This chapter explores the sediment cascade in its entirety—detachment, properties, transport, mixing, and source analysis—laying the groundwork for subsequent analyses of sediment dynamics through concentration–discharge relationships.

I-2. Sediment detachment

Sediment production processes are a diverse set of natural and anthropogenic phenomena that contribute to the generation and release of loose particles in the environment. These processes play a fundamental role in shaping landscapes, influencing ecosystems, and impacting human activities.

I-2.1. Weathering

Weathering is the process of breaking down rocks and minerals into smaller particles through physical, chemical, and biological processes (Figure I-1). Physical weathering includes mechanical actions such as freeze-thaw cycles, abrasion by wind or water, and root growth. Chemical weathering involves chemical reactions that alter the composition of rocks, such as dissolution, oxidation, and hydrolysis.

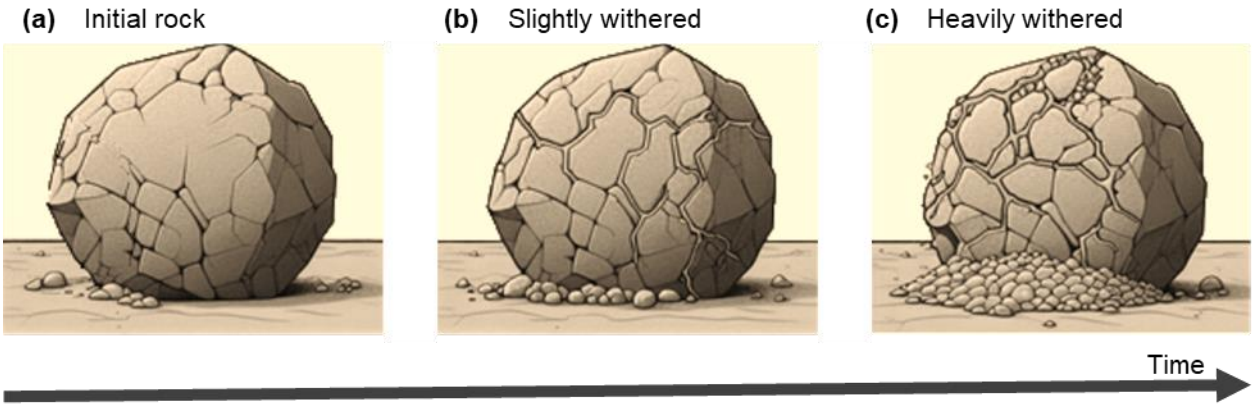

Figure I-1. Example Illustration of rock weathering.

I-2.2. Physical Weathering

Physical weathering encompasses a spectrum of processes that alter rocks without changing their internal mineral structure (Scheffers et al., 2015b). Unlike chemical weathering, which involves the transformation of minerals through chemical reactions, physical weathering focuses on the mechanical breakdown of rocks. Rocks, resilient as they may seem, are prone to fragmentation, and this can occur for a multitude of reasons. One of the primary mechanisms is stress along natural zones of weakness, such as joints or cracks (Scheffers et al., 2015b). In response to external forces, rocks can fracture into smaller fragments, ranging from sand-sized particles to fine silt. The susceptibility of rocks to such breakage stems from their vulnerability to bending, stretching, or compression induced by various exogenous factors including temperature fluctuations, frost action, plant root growth, and the impact of objects.

I-2.2.1.Frost Action (Frost Wedging):

Freezing and thawing processes (Figure I-2), occurring on a daily cycle, hold significant sway over the physical weathering of rocks, thereby playing a pivotal role in sediment production. Water seeping into cracks and pore spaces can freeze, causing expansion—approximately 9-11% at 0°C—thus exerting force across existing fractures or instigating cracks from ice-filled pore spaces (Jain, 2014; Price, 1995; Scheffers et al., 2015b). Crystals have been observed to lift substantial weights, highlighting the importance of crystal growth-induced pressure in this process (Becker & Day, 1905). Frost wedging, a form of mechanical disintegration, becomes active when temperatures hover around 0°C. This process hinges on the frequency of water transitioning from its fluid state to ice; more frequent changes lead to increased breakage (Scheffers et al., 2015b). Frost wedging occurs when water in a crack freezes, expands, and presses against the rock, thereby prying open the crack and facilitating weathering (Jain, 2014). Frost action emerges as a dominant force in breaking down solid bedrock into transportable sediments (Anderson, 1998; Deprez et al., 2020; Matsuoka & Murton, 2008). Despite a single freezing and thawing cycle not necessarily inducing immediate disintegration, the cumulative effect of sequential cycles leads to the deterioration of porous materials. This degradation manifests in an increase in porosity due to the introduction of micro-cracks (Deprez et al., 2020; Martínez-Martínez et al., 2013). Moreover, freezing and thawing indirectly contribute to hazards such as rock falls, slides, and debris flows, posing threats to infrastructure and human lives (Deprez et al., 2020; Matsuoka & Sakai, 1999). Changes in freezing and thawing activity in mountainous regions influence sediment delivery downslope (Anderson et al., 2013; Deprez et al., 2020; Sass & Oberlechner, 2012).

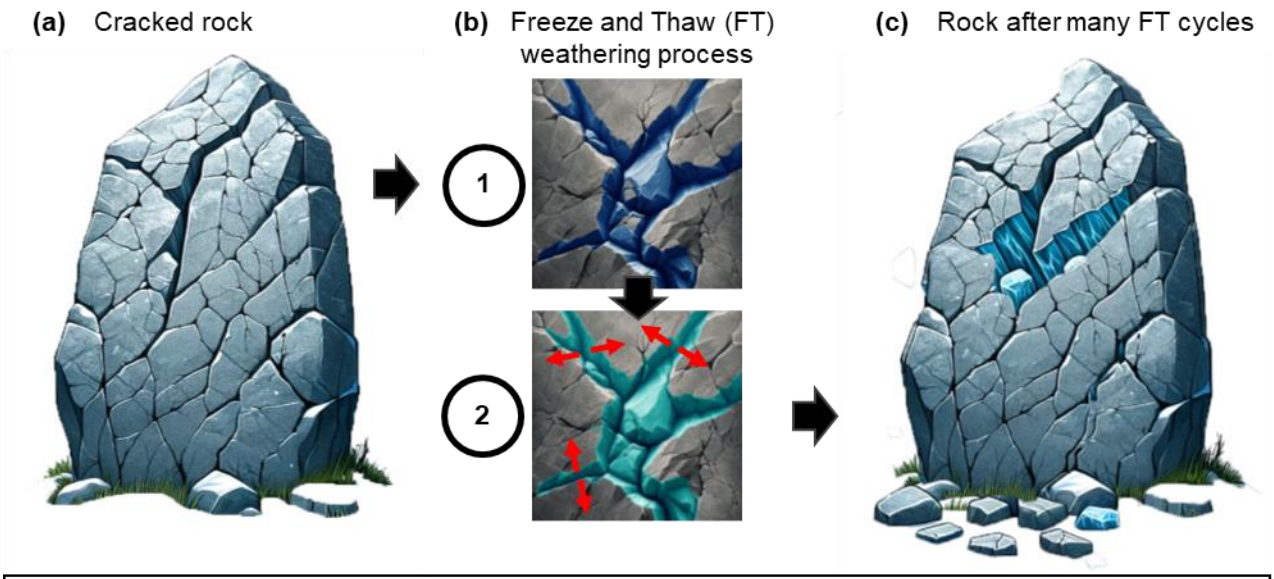

Figure I-2. Frost wedging weathering process

I-2.2.2.Thermal Stress:

Rocks, composed of multiple minerals (J. Liu et al., 2018; Yan & Zheng, 2017), undergo thermal cracking (Figure I-3) primarily due to thermal stress, resulting in damage to the rocks (Browning et al., 2016; C. David et al., 1999). Temperature changes induce the creation of new cracks and the reactivation of existing ones, even during uniform heating (Yan & Zheng, 2017). Thermal stress arises from differences in mineral thermal expansion coefficients and mineral thermal decomposition (Fredrich & Wong, 1986; Heap et al., 2013; J. Liu et al., 2018; Richter & Simmons, 1974; Yan & Zheng, 2017). Various mechanisms initiate thermal stress, including the disparity in mineral thermal expansion coefficients, anisotropic thermal expansion of minerals, and temperature thresholds (Browning et al., 2016; H. W. Cooper & Simmons, 1977; Fredrich & Wong, 1986; Heap, Baud, et al., 2014; Heap, Lavallée, et al., 2014; Keshavarz et al., 2010; Lin, 2002; J. Liu et al., 2018; Nasseri et al., 2009). Stress builds up between grains on heating or cooling, even

in monomineralic rocks with randomly oriented grains, exacerbating the situation in polymineralic rocks (Browning et al., 2016).

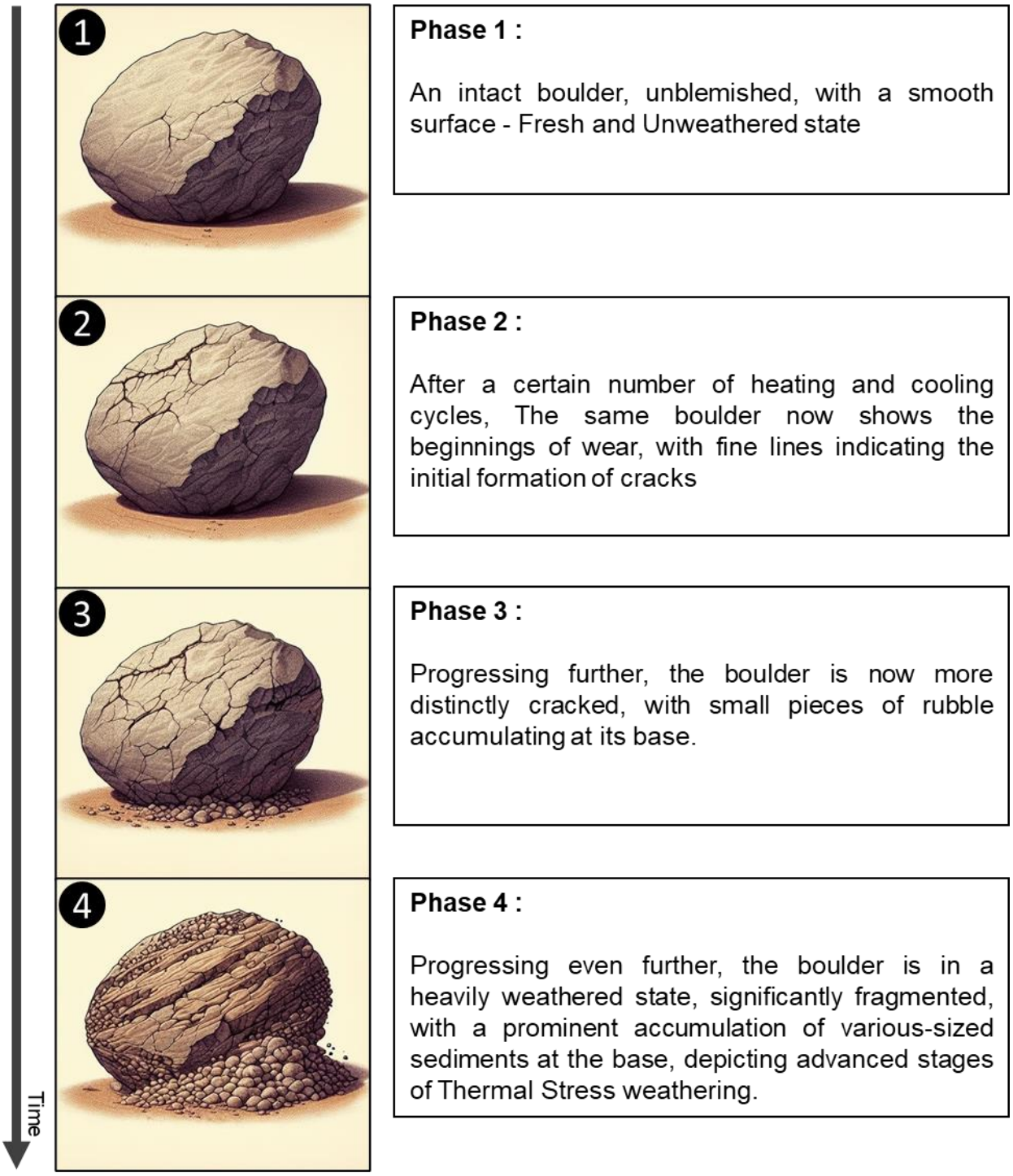

Figure I-3. Evolution of a boulder through thermal stress weathering process.

Differences in mineral thermal expansion coefficients are a primary factor causing thermal cracking (J. Liu et al., 2018; Yan & Zheng, 2017). This disparity extends and widens existing cracks, generating new inter and intra-granular cracks (J. Liu et al., 2018; Yan & Zheng, 2017). Furthermore, both old and new cracks can connect to form networks, altering rock permeability (Bauer & Handin, 1983; Fredrich & Wong, 1986; J. Liu et al., 2018). Thermal stress contributes to the creation of fine sediments by disaggregating rocks into fine aggregates, influencing porosity (Chaki et al., 2008; C. David et al., 1999; Griffiths et al., 2018; Nasseri et al., 2007; Reuschlé et al., 2003; X. Wang et al., 2013), reducing uniaxial strength (Griffiths et al., 2018; Nasseri et al., 2007), and stiffness (E. C. David et al., 2012; Griffiths et al., 2018; Walsh, 1965). In essence, thermal stress exacerbates various processes, contributing significantly to the transformation of rocks into fine sediments.

I-2.2.3.Salt Crystal Growth (Salt Wedging):

The growth of salt crystals in rock fissures and pores can exert pressure on the surrounding rock, causing it to crack and fragment (Figure I-4). The process of salt crystal growth poses a danger by exerting a wedging force as the salt solution in rock pores and cracks undergoes crystallization (Genkinger & Putnis, 2007; Oguchi & Yu, 2021; Ruiz-Agudo et al., 2013; Scherer, 1999, 2004; M. Steiger, 2005a, 2005b). This pressure is called crystallization pressure or crystal growth pressure and causes salt weathering in rocks, monuments, buildings, and other structures (Oguchi & Yu, 2021). This pressure is caused by a growth of the salt against the confining force of the rock (Oguchi & Yu, 2021) leading to rock cracking, fragmentation, increase in porosity, and permeability. A detailed description of salt weathering can be found in Espinosa-Marzal & Scherer, 2010a, 2010b, and Oguchi & Yu, 2021.

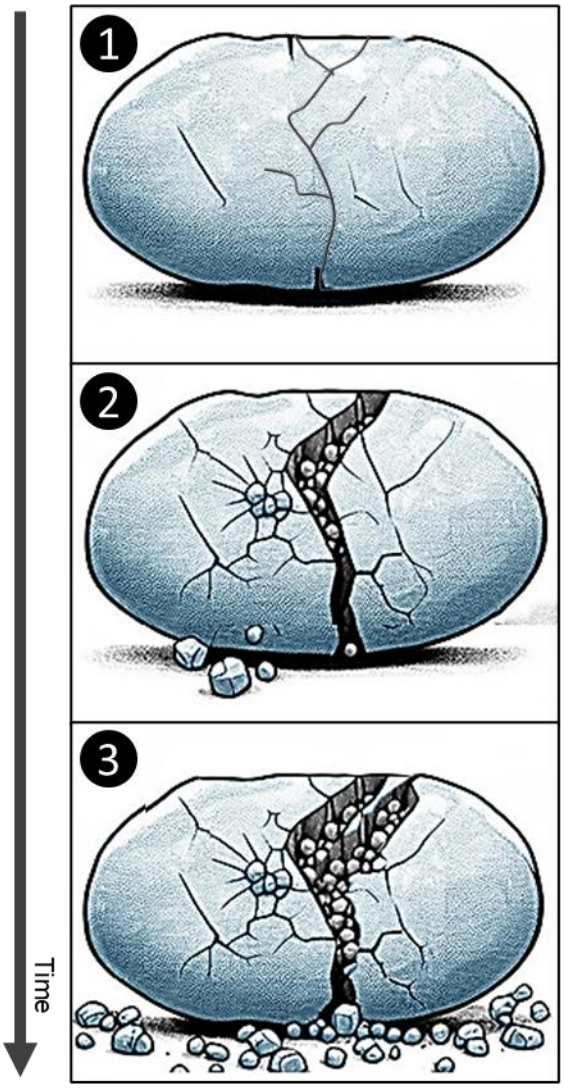

Phase 1 :

An intact boulder with a few visible but minor cracks. The boulder is solid with no significant signs of weathering or erosion.

Phase 2 :

The same boulder with increased cracking. A prominent crack has widened and branched, with smaller cracks surrounding it. The salt crystals within the cracks have started to expand, exerting pressure on the rock and causing further fracturing

Phase 3 :

Multiple cracks have widened, and there are now visible salt crystals forming and growing within these spaces. The process has resulted in pieces of the boulder breaking off, evident by the fragments and smaller rocks that have accumulated at the base, indicating advanced stages of salt wedging weathering.

Figure I-4. Evolution of a boulder through salt wedging process.

I-2.2.4.Pressure Release

Exfoliation weathering (Figure I-5), a type of physical weathering, occurs when large flat or curved sheets of rock detach from crystalline rock bodies (Scheffers et al., 2015b). This process is not directly tied to the interaction between climate and the lithosphere (Scheffers et al., 2015b). Fractures form in near-surface rocks experiencing high residual compression parallel to the surface, followed by pressure relief caused by events such as the buildup and melting of glaciers during

glacial periods or erosion of thick overlying sediment layers (Scheffers et al., 2015b). This "unloading" effect reduces the vertical confinement on subsurface strata, allowing the elastic matrix of the rock to expand toward the surface (Jain, 2014). This volumetric increase produces fractures roughly parallel to the topographic gradient (Earle, 2019; Jain, 2014). Over time, continued erosion exposes these fractured segments detach as distinct slabs along the decompression planes (Jain, 2014). The remaining resistant structures appear as expansive, rounded landforms termed exfoliation domes, while the shed material is categorized as exfoliation sheets (Jain, 2014).

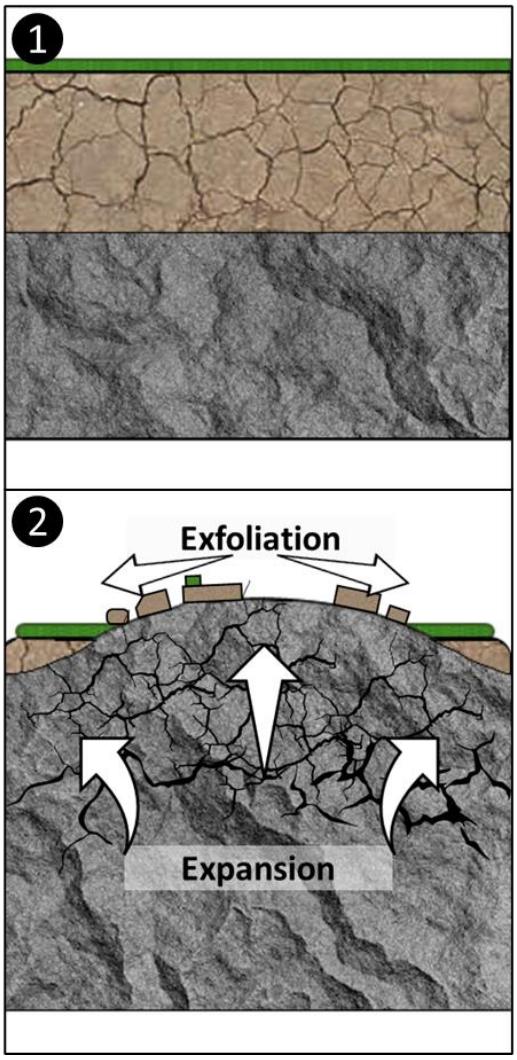

Stage 1 :

An intact soil profile above a bedrock layer. The soil is shown with a network of cracks, indicating initial stages of drying and cracking which could lead to erosion.

Stage 2 :

The subsequent stage where the bedrock begins to expand and crack. This expansion is due to the reduction of overlying pressure as the soil above is eroded away. The arrows indicate the outward and upward movement of the rock, demonstrating the process of exfoliation. This leads to the fracturing and separation of slabs of rock, driven by the release of confining pressure that occurs as the overlaying soil is removed.

Figure I-5. Exfoliation Process Schematic

I-2.2.5.Root Wedging

Biomechanical weathering, a phenomenon often attributed to the action of tree roots, plays a pivotal role in the gradual disintegration of bedrock (Figure I-6). Roots, as noted by various studies (Cross & Birot, 1967; Jain, 2014; Malik et al., 2019; Pitty, 2020), are capable of penetrating cracks in fractured bedrock, initiating a process that leads to their widening and, ultimately, the fragmentation of the rock body. The biomechanical interactions between tree roots and bedrock become particularly apparent when roots encounter gaps or weaker portions of the rock, such as elongated fissures or chemically altered joints (Pawlik et al., 2016). Remarkably, roots adapt to the shape of the rock cracks, exhibiting irregular or elongated growth on one or more axes, in contrast to the oval shape seen in roots growing in loose material (Malik et al., 2019).

The dynamics of root growth in rock cracks involve distinct stages. Initially, a growing root encountering a rock surface undergoes growth blocking. Subsequently, the crack widens, providing the root with new space and an opportunity for more intensive radial growth in the direction that was previously impeded (Malik et al., 2019). When roots grow in open cracks, they gradually fill them up; however, if injured by rock edges, they respond by forming irregular disturbed rings. This response is attributed to changes in crack shape, particularly when dislocated rock edges wound a root, allowing growth in new directions (Malik et al., 2019).

Observations suggest that the impact of roots on rock weathering is influenced by the inherent properties of the rock body, including the existing network of joints, cracks, and fissures (Little & Field, 2003; Pawlik et al., 2016; Phillips, 2009, 2016; Zwieniecki & Newton, 1995). A noteworthy case study by Jackson & Sheldon, (1949) observed tree roots growing in the rock fissures of a limestone cliff face. Their findings concluded that the penetration and expansion of tree roots enlarged rock fractures, causing rock fragmentation and the development of a scree slope beneath the cliff, ultimately contributing to the gradual retreat of the cliff. Additionally, sequences of wood anatomical features serve as indicators of crack widening in bedrock, providing further insights into the intricate processes of biomechanical weathering (Malik et al., 2019).

Phase 1 :

A young tree with a modest canopy and relatively shallow root system. The soil around the roots is mostly intact with no visible cracks, indicating the early stage of growth.

Phase 2 :

A more mature tree with a denser canopy and a more developed root system. The roots have thickened and deepened, causing slight cracking in the surrounding soil, which suggests the increasing influence of the root system as the tree grows.

Phase 3 :

A fully mature tree with a lush, thick canopy and a robust root system. The roots have now caused significant cracking and displacement of the soil, with large cracks visible. This panel indicates the advanced stage of growth and the substantial impact of the tree's roots on the environment around it.

Figure I-6. Impact of tree roots' development on their surrounding soil.

I-2.2.6.Wetting and Drying

Slaking, a fundamental process in weathering, involves the alternation of wetting and drying in rocks (Figure I-7). This phenomenon, driven by the ordered accumulation of water molecules between mineral grains, can be attributed to various causes. 'Slaking' may occur due to the volume expansion of clay minerals or be associated with the movement of moisture within the rock mass (Price, 1995). The process of hydration, a chemical attachment or incorporation of water molecules into specific minerals, exemplified by the transformation of anhydrite into gypsum, contributes to an increased mineral volume (Scheffers et al., 2015b). Interestingly, while hydration is fundamentally a chemical process, it manifests as a physical weathering process due to the mechanical pressure resulting from the increased volume (Scheffers et al., 2015b). The impact of slaking becomes evident as rock grains undergo tensional stress with the thickening of water layers. The repetitive cycle of wetting and drying serves as a potent agent of physical weathering. According to Jain (2014), after approximately 20 iterations, these transitions can compromise the integrity of rock samples. In soil environments, the process manifests as continuous swelling and shrinking, which destabilizes particle bonds and promotes structural breakdown.

Observations extend beyond theoretical considerations, as illustrated by the disintegration of mudrock cores stored outdoors in leaky core boxes after weeks of wetting and drying (Price, 1995). This phenomenon is not limited to controlled environments; similar disintegration may be observed in fresh cuts and natural exposures of mudrocks (Price, 1995). The broader context includes the role of abrasion in soil characteristics, where particles within the soil undergo abrasion, contributing to the fineness of sediments. Structural cracks emerge in dry soil environments as the matrix contracts, disrupting the uniformity of horizon interfaces(Jain, 2014).

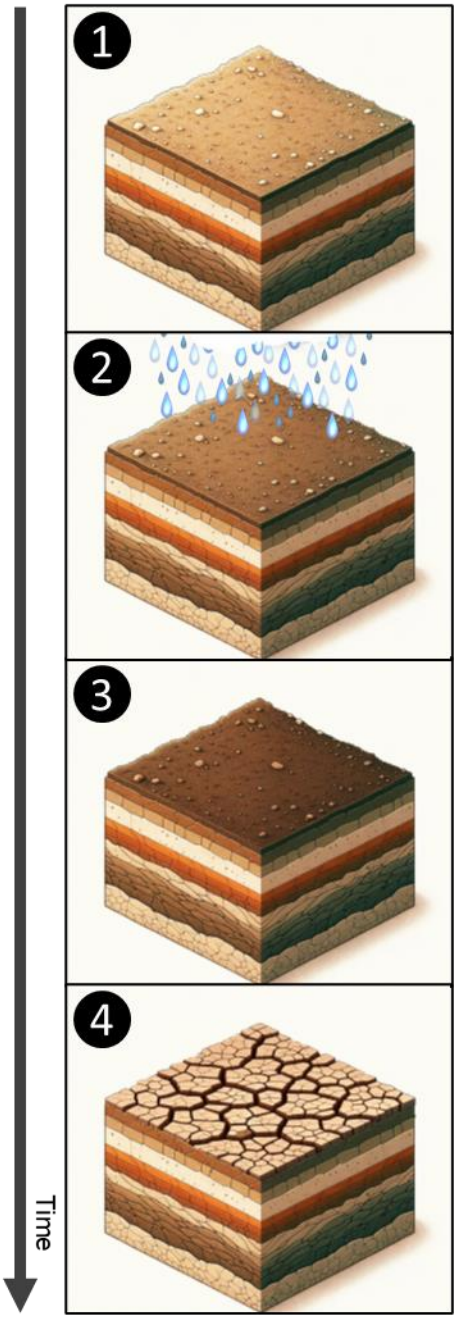

Phase 1 :

An isometric view of a cross-section of intact soil layers with no signs of moisture. The soil is uniform and undisturbed

Phase 2 :

Rain falls onto the soil, indicating the beginning of the wetting process, with the top layer of soil starting to darken as it absorbs water.

Phase 3 :

The soil immediately after the rain has stopped. The top layer of soil is now darker, suggesting that saturation with moisture from the recent rainfall.

Phase 4 :

The soil after it has dried out. The top layer shows significant cracking, indicative of the drying process where the soil has contracted and split apart due to the loss of moisture.

Figure I-7. The transformation of soil through wetting and drying.

I-2.2.7.Rainfall impact (Rain-splash effect)

Splash erosion (Figure I-8), a fundamental process in soil erosion, is characterized by the initial detachment of soil particles upon impact with raindrops, making it a key factor in the overall erosion dynamics (Gabet & Dunne, 2003; Le Bissonnais, 1996; Marzen et al., 2015; Pulley et al., 2022). Raindrop energy plays a pivotal role in overcoming soil particle bonds, resulting in the dislodgment of particles from the soil surface (Kinnell, 2005; J. Wang et al., 2020). The impact of raindrops transmits energy to the soil, causing the movement and disruption of particles and aggregates (Bisal, 1960; G. Li et al., 2017; Marzen et al., 2015; A. I. J. M. Van Dijk et al., 2002). The susceptibility to splash erosion is influenced by various factors, including particle size distribution, aggregate stability, slope, and raindrop characteristics like kinetic energy, impact angle, and size (Marzen et al., 2015; Riezebos & Epema, 1985). Infiltration capacity often falls short of immediately absorbing raindrops, leading to radial water expansion and the formation of a corona (Marzen et al., 2015).

Wind-driven rain-splash, a combination of splash detachment and wind impact, introduces additional complexities to the process. Wind alters the physical properties of surface-impacting raindrops, accelerating their fall velocity and modifying their size and form through increased turbulence and collisions (C. R. Umback and W. D. Lembke, 1966; Disrud et al., 1969; Erpul et al., 2000; Fister et al., 2012; Marzen et al., 2015; Pedersen & Hasholt, 1995). The collaborative impact of wind and rainfall significantly amplifies the amount of detached and transported material, as observed by Marzen et al. (2015), reporting an increase of about two orders of magnitude in eroded material.

Vegetation and other protective measures play crucial roles in mitigating raindrop impacts. Vegetation intercepts raindrops, rendering them with zero velocity upon reaching the soil surface (Díaz-Raviña et al., 2012; Fernández-Raga et al., 2017; Giménez-Morera et al., 2010; Lu et al., 2016; Ma et al., 2014). Moreover, a layer of water on the soil surface or overland flow can attenuate the erosive impact of raindrops, with the effectiveness depending on the ratio between flow depth and raindrop diameter (Gabet & Dunne, 2003; Kinnell, 1991, 1993; Moss & Green, 1983; Palmer, 1946). Overland flow exceeding raindrop diameter by 0.6 to 1.0 times can reduce the detachment rate (Dunne et al., 2010; Ghahramani et al., 2011; Torri et al., 1987). Ponding, sheet, and rill overland flow act as a protective mulch layer, shielding the soil from raindrop impacts (Fernández-

Raga et al., 2017; Kinnell, 2005; Mermut et al., 1997). Similarly, pre-detached soil particles, whether from overland flow or other protective measures, may offer ephemeral protection to the underlying soil by limiting the penetration of raindrops (Fernández-Raga et al., 2017; Kinnell, 2005).

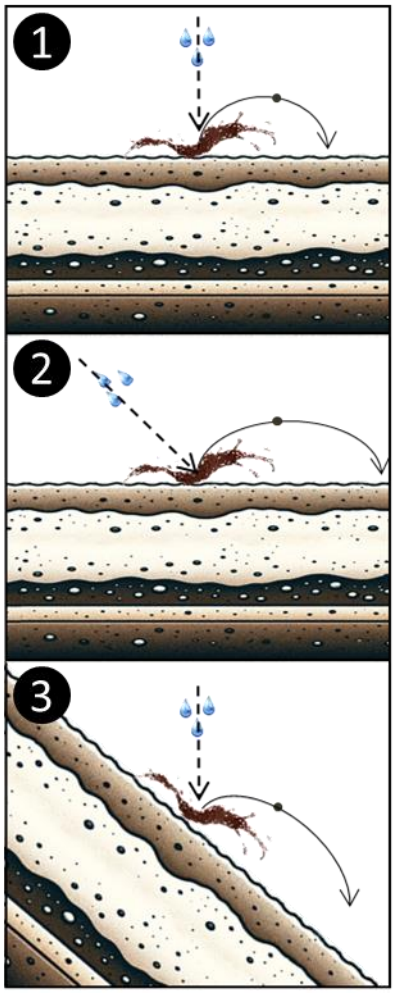

Type 1 :

A vertical rainfall impacting horizontal soil. A direct, perpendicular hit where the raindrop collides with the soil surface, causing particles to be ejected upwards and outwards in a symmetrical splash pattern.

Type 2 :

Wind-driven rain, where the raindrop impacts the horizontal soil at an angle. This results in an asymmetrical splash pattern, with soil particles being ejected more forcefully on the side opposite to the direction of the wind, indicating the influence of wind on rain splash erosion

Type 3 :

A raindrop falling on a sloped surface. The splash pattern here is affected by gravity, with soil particles being displaced downhill. On sloped surfaces, the rain splash effect contributes to the downward movement of soil, which can lead to greater erosion over time.

Figure I-8. Comparative Illustration of Rain Splash Erosion: (1) Vertical Raindrop, (2) Wind-driven Raindrop, and (3) Raindrop on a Sloped Surface.

I-2.2.8.Water flow and the associated matter

When water is in motion, it serves as a carrier for a diverse array of materials. Suspended sediments, encompassing fine particles like clay, silt, and sand, remain aloft in the water column (referred to as suspended sediments) (e.g., Asselman, 1999; Bisantino et al., 2011). Additionally, larger particles, such as gravel, pebbles, and cobbles, may traverse the river or stream bed as bedload (e.g., Mao et al., 2014). The flowing water can transport floating organic material, including leaves, branches, and plant debris (e.g., Bocchiola et al., 2006; Jacobson et al., 1999; Kramer & Wohl, 2017; MacVicar et al., 2009). During heightened flow or flooding events, water can also transport more substantial debris, including boulders and fallen trees (e.g., Bocchiola et al., 2006; Kehew et al., 2010; Kramer & Wohl, 2017; Lenzi, 2004). In cold regions, when ice starts to melt and break, it is transported as floating debris (e.g., Chen et al., 2023; Tao Shen et al., 1990; Turcotte et al., 2011). Water, along with the diverse matter it carries, plays a pivotal role in the detachment of sediments at both the particle and macro levels. This dynamic process is fundamental to reshaping landscapes, rivers morphologies, and ecosystems.

At the particle level, the detachment of cohesive and semi-cohesive sediments from the bed and banks by flowing water involves complex interactions. Water molecules, constituting the flowing stream, engage in frictional interactions with sediment particles in contact with the bed or banks. This frictional drag force, part of the overall viscous shear stress, arises from the movement of water molecules and their internal resistance to flow. As water flows over sediment particles, cohesive and adhesive forces between particles determine their resistance to shear stress. Collisions between water molecules and sediment particles, coupled with the generation of lift forces, contribute to the imparting of shear stress. These collisions provide kinetic energy to sediment particles, and higher flow velocities lead to more energetic impacts. The critical shear stress, representing the threshold at which applied shear stress overcomes cohesive and adhesive forces, defines the initiation of sediment particle movement. Once this critical threshold is surpassed, sediment particles start to move, potentially leading to their detachment from the bed or banks.

Materials transported by flowing water, including suspended sediments, bed load, organic matter, large debris, and river ice, play a significant role in the detachment of sediments from the bed and banks. As water moves, these materials interact with the streambed and banks, exerting forces that contribute to sediment detachment. Suspended sediments, carried within the water

column, impact the streambed through abrasion and bed scour, potentially leading to the removal of finer particles. Bed load, comprising larger sediment particles transported along the riverbed, can induce scouring and contribute to the reworking of bed sediments. Organic matter, such as leaves and branches, can influence sediment detachment through interactions with the bed and by altering flow patterns. Large debris and river ice, especially during high-flow events, enhance erosive forces and may lead to the dislodging of sediment particles from the bed and banks.

Stream banks and bed sediment contribution. Involve the following key processes:

- **Abrasion**: the wearing down of stream materials through abrasion serves as a fundamental mechanism for clast destruction in overland and fluvial flows (Le Bouteiller et al., 2011; J. Wang et al., 2020; J.-G. Wang et al., 2012, 2013, 2017). Defined by specialized actions such as grinding, crushing, and chipping (Kuenen, 1956; J. Wang et al., 2020). This process involves the mechanical wearing down of the stream banks and bed by the impact of sediment particles carried by the flowing water (e.g., the action of sandpaper on a surface).
- **Scouring**, or hydraulic surface erosion (Pike et al., 2018), is an intense, localized erosion of the stream bed, often associated with higher flow velocities, can lead to the removal of sediments and even bedrock material. Scour is commonly observed in the vicinity of structures such as bridges, piers, abutments, culverts, piles, islands, and groins (e.g., Dehghani et al., 2013; Deng & Cai, 2010; Koken & Constantinescu, 2008; Lança et al., 2013; Melville, 1997; Prendergast & Gavin, 2014; C. Wang et al., 2017). General scour can occur irrespective of the presence of such structures and may manifest as either long-term or short-term scour, involving the removal of sediments across the width of a channel (C. Wang et al., 2017). Contraction scour and local scour are specific types directly attributed to the presence of obstacles like bridges, piers, abutments, or erosion control devices obstructing the flow (e.g., Dehghani et al., 2013; Umbrell et al., 1998; C. Wang et al., 2017).
- **Cavitation**: The cavitation process in rivers is influenced by factors such as water velocity, the presence of obstacles, channel geometry, and other hydraulic conditions. When water flows rapidly over irregularities in the riverbed or encounters obstacles like rocks, the local pressure can drop, leading to the formation of vapor bubbles (Arndt, 1981; Carling et al., 2017; Sun et al., 2023; Whipple et al., 2000). Subsequently, as the water continues to flow and the pressure increases, these bubbles collapse violently, releasing energy in the form of shock waves (Ochiai et al., 2013; Sreedhar et al., 2017; Sun et al., 2023; Yusof et al., 2016).

This cyclic process of bubble formation and collapse is known as cavitation. Fluvial cavitation can have several effects on the river environment, including the collapse of cavitation bubbles near the riverbed can contribute to erosive processes by causing localized pressure changes and impacting the surrounding sediment and bedrock (Whipple et al., 2000).

- **Fluid stress**: shear stress plays a pivotal role in the detachment of sediments from the streambed and banks. As the velocity of flowing water increases, shear stress acts on cohesive or semi-cohesive sediments initially bound together. The cohesive forces, encompassing factors like electrostatic forces and surface tension, gradually yield to the mounting shear stress. This breakdown of cohesion leads to the detachment of individual or clustered sediment particles from the streambed and banks. The process initiates with the detachment of the most easily dislodged particles and progresses as shear stress continues to surpass the cohesive strength of channel sediments. Accordingly, the bed and banks are subject to sediment detachment as shear stress acts upon the materials constituting them.

I-2.3. Chemical weathering

Chemical weathering, a fundamental geological process, occurs when minerals within rocks react with the elements present in their environment, primarily water and air. This transformative process leads to a range of reactions, including dissolution and the formation of new minerals through combinations with molecules like oxygen, water, or carbon dioxide (Scheffers et al., 2015b). As minerals undergo these chemical alterations, rocks are fundamentally changed, decomposing, and decaying over time (Jain, 2014; M. Steiger et al., 2011). The impact of chemical weathering intensifies with increased precipitation, particularly in the form of rain, and higher temperatures, as water's essential role and elevated temperatures contribute to accelerated mineral degradation (Jain, 2014). Beneath the surface, chemical weathering operates through the movement of water within the mass and materials, with joints and other discontinuities serving as pathways. The distribution of mass weathering reflects both minor and major joint set spacing, orientation, and the presence of faults (Price, 1995). Chemical weathering results from the combined influences of precipitation, temperature, vegetation, topography, rock type, and time (Jain, 2014).

I-2.3.1.Dissolution and Solution

When rocks and minerals encounter water, dissolution occurs (Jain, 2014). Carbon dioxide, a common component in the atmosphere, dissolves in water to form carbonic acid, a weak acid known for its capacity to chemically react with minerals and initiate dissolution (Earle, 2019; Jain, 2014; M. Steiger et al., 2011). This reaction results in the alteration of minerals, either dissolving them entirely or transforming them into different compounds. As the dissolved material is transported away, it leaves behind voids in the rock, contributing to the development of geological features such as caves, exemplified in limestone terrains (Jain, 2014; Price, 1995). In regions where rocks contain minerals like calcium, magnesium, and potassium, the carbonic acid facilitates their conversion into carbonates, dissolving them in rainwater and creating unique karst topography characterized by sinkholes, caves, and caverns (Jain, 2014). The chemical activity of H+ ions, released during these reactions, enhances the weathering process as they easily infiltrate crystal structures, releasing other ions into the water (Jain, 2014; M. Steiger et al., 2011). The solubility of elements in this process follows a specific order, influencing the dissolution reactions in rocks (Price, 1995):

Calcium (Ca) > Sodium (Na) > Magnesium (Mg) > Potassium (K) > Silicon (Si) > Aluminum (Al) > Iron (Fe).

The rates of mineral dissolution reactions depend on: (1) the amount and contact time of liquid water; (2) the solubility of minerals; and (3) the availability of acidity, i.e., the pH of the solution in contact with minerals (M. Steiger et al., 2011). For instance, Iron (Fe) is about 100000 times more soluble at pH 6 than at pH 8.5 (Price, 1995).

I-2.3.2.Hydration

Hydration, a fundamental process in chemical weathering, plays a pivotal role in altering the composition and physical characteristics of minerals within soils. This mechanism involves the reaction of certain minerals with water and acid, resulting in the uptake of hydrogen and the removal of other cations (Jain, 2014). The chemical changes induced by hydration are exemplified in transformations such as Hematite converting to Limonite (Jain, 2014). Additionally, specific minerals like anhydrite ($CaSO_4$) undergo hydration with water (H_2O) to form gypsum ($CaSO_4 \cdot 2H_2O$) (Jain, 2014; Scheffers et al., 2015b).

As these minerals undergo hydration, their chemical structures enlarge, rendering them softer, more stressed, and prone to decomposition (Jain, 2014). The softened minerals, now more easily decomposed, become integral components in the breakdown of soil particles. This dual effect of chemical alteration and physical softening makes minerals more susceptible to the weathering forces that shape the Earth's surface.

I-2.3.3.Oxidation

Oxidation, a pivotal process in chemical weathering, involves the chemical combination of oxygen with compounds, leading to a change in the oxidation number of elements, characterized by the loss of electrons. This reaction prompts the formation of oxides as oxygen combines with compound elements in rocks (Jain, 2014), compelling their segregation from the crystal lattice (Scheffers et al., 2015b). Notably, oxidized minerals undergo an increase in volume and often exhibit decreased hardness (Jain, 2014). The alteration of the oxidation number disrupts the mineral's electrical neutrality, rendering it more susceptible to subsequent weathering by water and carbonic acid (Jain, 2014). This phenomenon is particularly evident in minerals containing iron and manganese, such as goethite and hematite, contributing to the distinct brown and red colors observed in soils and weathered rocks (Jain, 2014; Scheffers et al., 2015b). Additionally, higher temperatures and the presence of precipitation serve to accelerate the oxidation process, further influencing the chemical transformation of minerals in geological formations (Jain, 2014).

I-2.3.4.Hydrolysis

Hydrolysis, a transformative geological process, leaves its indelible mark on the Earth's soil profile, orchestrating changes that shape the landscape (Jain, 2014). As a precursor to hydrolysis, carbonic acid undergoes ionization, breaking down into hydrogen and bicarbonate ions, while concurrently, water dissociates into hydrogen and hydroxide ions (Jain, 2014; Scheffers et al., 2015b). These ions engage in intricate chemical reactions, recombining with the crystal lattice of minerals through ion substitution (Scheffers et al., 2015b). The free hydrogen ions play a pivotal role in altering the atomic structure of minerals by displacing other ions (Jain, 2014). Initiated by water, typically in the form of precipitation, hydrolysis disrupts the chemical composition and size of minerals, yielding less stable forms that are more susceptible to weathering (Jain, 2014).

Hydrolysis extends its influence by elevating the pH of the solution through the release of hydroxide ions (Jain, 2014). Particularly effective in the weathering of common silicate and alumino-silicate minerals due to their electrically charged crystal surfaces, hydrolysis leads to the destruction of primary minerals like feldspar (Jain, 2014; Scheffers et al., 2015b). This destruction, coupled with the formation of secondary clay minerals such as kaolinite, is accompanied by the removal, discharge, or dissolution of large amounts of silica (Scheffers et al., 2015b). In humid climates, where the weathering of feldspar in rocks like Granodiorite or Granite is prevalent, clay formation is a distinctive outcome of hydrolysis (Jain, 2014). Unveiling the pervasive impact of hydrolysis, this process contributes significantly to the composition of sedimentary rocks, with clays constituting nearly half of the Earth's sedimentary rock inventory, with quartz being the sole exception to clay formation (Jain, 2014).

I-2.3.5.Reduction

Reduction, while often overshadowed by oxidation reactions, holds significance, particularly in anaerobic environments like waterlogged soils, where the characteristic greenish-gray color is indicative of reduced iron oxides (Carroll, 1970; Depetris et al., 2014; Jain, 2014). Acting as a reducing agent, organic matter plays a crucial role in weathering processes, undergoing oxidation to produce CO2 or form new organic compounds (Depetris et al., 2014). The reduction of minerals results in the formation of electrically unstable, more soluble, or internally stressed compounds, ultimately leading to their accelerated decomposition (Jain, 2014). Microbial activity can contribute to sulfate ion reduction, where microbes utilize the oxygen in sulfates to oxidize organic material, producing sulfides that can further react, entering the gas pool as H2S or precipitating with metals as FeS or MnS (Depetris et al., 2014).

I-2.3.6.Carbonation and Acidification

Carbonation, a significant process in chemical weathering, involves the interaction of carbonate and bicarbonate ions with minerals, particularly in environments rich in carbon dioxide (Jain, 2014). Microbial and plant activities contribute to this process by providing CO2, fostering rock weathering, and facilitating carbonation reactions (H. Deng et al., 2023; Thorley et al., 2015; S. Wu et al., 2019). This reaction occurs as carbon in a gas or fluid reacts with silicate minerals,

forming solid carbonate minerals (E. M. Stewart et al., 2019). Carbonic acid, a product of CO2 and water, is instrumental in dissolving carbonates and decomposing mineral surfaces due to its acidic nature (Jain, 2014). When gaseous CO2 dissolves in water, it produces carbonic acid, which, as a weak acid, can dissociate into a negatively charged bicarbonate anion ($HCO^{-}3$) and a positively charged H+ cation (Jain, 2014; E. M. Stewart et al., 2019). Acidification, considered a form of dissolution, accelerates weathering in the presence of hydrogen ions derived from carbonic and organic acids (Jain, 2014). Carbonic acid enhances mineral dissolution compared to water alone, forming more soluble bicarbonates (Jain, 2014). In regions with limestone, acidification is responsible for the weathering of limestones and dolomites, resulting in the formation of geological features such as sinkholes and caves (Carroll, 1970; Jain, 2014).

I-2.4. Mass Wasting:

Mass wasting, also known as "Mass Movement," describes the downslope movement of rock, debris, soil, and regolith near the Earth's surface under the influence of gravity (Jain, 2014; Pradhan & Siddique, 2019; Van Beek et al., 2008). This progression operates across a vast dynamic range, varying from nearly static transfer to instantaneous mobilization (Pradhan & Siddique, 2019). The initiation of mass movement events is often preceded by weathering processes that weaken the massive bedrock structure along joints, faults, and predisposed bedding planes in sedimentary rocks (Scheffers et al., 2015a). For example, processes like frost wedging, driven by the pressure of freezing water and repeated freezing-thawing cycles in higher mountain areas, can trigger rockfalls (Scheffers et al., 2015a). Once a slope becomes unstable, a mass movement is likely to occur, requiring only a trigger to set it in motion. Such triggers can include ground vibrations from earthquakes, volcanic activities, or heavy rainfall during storms or monsoons (Pradhan & Siddique, 2019; Scheffers et al., 2015a). Ongoing weathering and erosion processes can gradually steepen slopes, contributing to the collapse of slope flanks (Scheffers et al., 2015a). Earth scientists classify different types of mass movements based on the nature of the material, velocity, physical nature of the movement, and the presence of water, air, or ice in the wasted material (Pradhan & Siddique, 2019; Scheffers et al., 2015a). Landslides, rockfalls, slumps, and debris flows are examples of mass wasting processes, each characterized by distinct features and behaviors (see Table I-1).

Table I-1. Mass Wasting Processes.

Mass Wasting Processes	Description
Rockfall	Rockfalls involve the rapid descent of detached rock fragments down a slope. Triggered by factors such as weathering, seismic activity, or undercutting, rockfalls are characterized by free-falling rocks, often bouncing and colliding as they descend.
Rock Avalanche	Rock avalanches are massive, fast-moving landslides predominantly comprising rock debris. They can travel at high speeds, causing extensive damage. The distinguishing feature is the catastrophic release of large volumes of rock down a slope.
Rockslide	Rockslides are characterized by the sudden and rapid movement of rock masses along well-defined shear surfaces. They often occur on steep slopes and are initiated by factors like heavy rainfall or seismic events.
Debris flow	Debris flows involve a mix of soil, rock, and water that moves downslope as a viscous fluid. These flows can be triggered by intense rainfall, rapid snowmelt, or volcanic activity, and they exhibit high velocities.
Debris Fall	Debris falls refer to the downslope movement of a mixture of rock and soil that breaks away and falls freely. While like rockfalls, debris falls involve a more significant proportion of soil and loose material.
Debris Avalanche	Debris avalanches consist of a rapid flow of fragmented rock and debris, often triggered by volcanic eruptions, earthquakes, or heavy rainfall. They can cover large areas and have destructive consequences.
Debris Slide	Debris slides involve the movement of loose rock, soil, and debris along a defined surface. They occur on moderately steep slopes and are characterized by the sliding motion of material.
Mudflows	Mudflows, or mudslides, are rapid movements of water-saturated soil and fine-grained debris. They often follow heavy rainfall, snowmelt, or volcanic activity, exhibiting fluid-like behavior.
Earthflow	Earthflows are slow-moving downslope flows of fine-grained soil and sediment. They typically exhibit a lobate or tongue-shaped appearance and can be triggered by prolonged rainfall or saturation.
Slumps	Slumps involve the rotational movement of a mass of rock and soil along a curved surface. They are characterized by a distinctive backward rotation, creating a slump block at the base.
Solifluction	Solifluction refers to the slow downslope movement of water-saturated soil over frozen or impermeable layers. It is common in periglacial environments and results in the gradual deformation of the landscape.
Earth Creep	Earth creep is the extremely slow and continuous downslope movement of soil and regolith. It is often imperceptible but can cause long-term landscape changes through the gradual displacement of soil.
Sediment Flows	Sediment flows involve the movement of loose sediment, including sand and silt, downslope. They can be triggered by various factors, such as heavy rainfall or human activities, and may exhibit diverse behaviors.
Slurry Flows	A type of sediment flow involving water-saturated, fine-grained mixtures that move like a thick slurry. They occur in rivers, on coasts, or due to rainfall, snowmelt, or human activity. Slurry flows behave fluid-like, transport large amounts of sediment, and can threaten infrastructure and ecosystems.
Granular Flows	Granular flows involve the downslope movement of sediment predominantly composed of larger, granular particles. These flows can range from dry granular materials to mixtures with varying moisture content. Factors such as slope instability, seismic events, or heavy rainfall can trigger granular flows. They may exhibit characteristics of both solid and fluid behavior, with particles interacting in a complex manner. Granular flows can pose hazards in mountainous terrain and are associated with phenomena like rockfalls and landslides.
Grain Flows	Grain flows consist of the downslope movement of individual grains or particles. They often occur in arid or desert environments and are influenced by factors like wind and slope instability.
Subsidence	Subsidence refers to the gradual sinking or settling of the Earth's surface. It can result from various factors, including the collapse of underground caves, mining activities, or the extraction of fluids from underground reservoirs. Subsidence may lead to the formation of sinkholes or ground depressions.

Friction and collision during the fall or slide of large rock bodies increase fragmentation, generating additional fine sediments and rock fragments of varying grain sizes. At the conclusion of mass wasting processes, diverse landforms and deposits emerge, contributing to material accumulation (Figure I-9). For instance, talus cones resulting from rockfalls exhibit distinct sorting arrangements, with finer particles generally at the top and coarser particles at the bottom (Scheffers et al., 2015a). Debris and alluvial fans, fan-shaped deposits of sediment, debris, and rocks, are landforms where transported material spreads out upon reaching flatter terrain (e.g., Baumann & Kaiser, 1999; Blair & McPherson, 2009; Cavalli & Marchi, 2008; Crosta & Frattini, 2004; De Haas et al., 2018; Liu et al., 2017). Toma landscapes, named after the Toma River in Japan, result from large, fast-moving landslides abruptly stopping, creating a chaotic, hummocky topography (e.g., Abele, 1974; Iturrizaga, 2012; Ostermann et al., 2020; Penck & Brückner, 1909). Scree slopes, covered with loose, fragmented rock debris, accumulate at the base of cliffs or steep slopes (e.g., Lucas, Fankhauser, et al., 2020; Lucas, Herzog, et al., 2020). Landslide dams, natural dams formed when landslide debris obstructs a river or stream channel, are also notable features (e.g., Duman, 2009; Fan et al., 2020, 2021). These landforms illustrate how mass wasting processes contribute to sediment detachment, landscape evolution, and the formation of sediment sources.

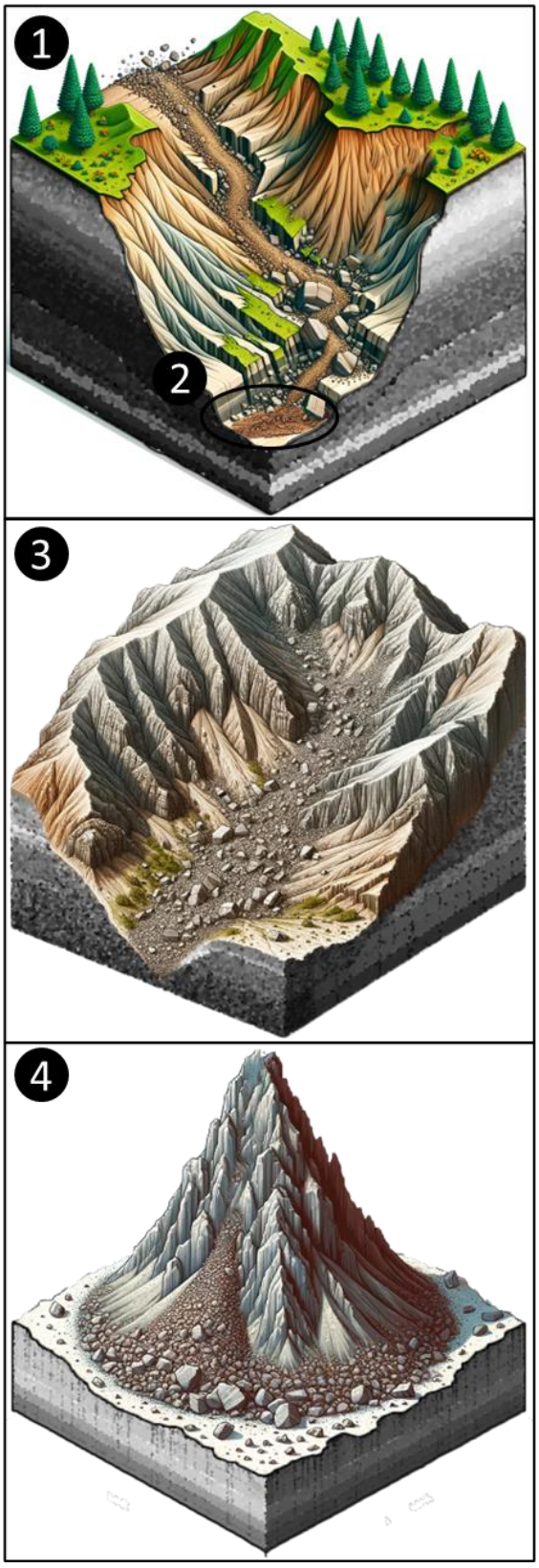

1. A landslide is characterized by a mass of earth and rocks sliding down a slope

2. A landslide toe which could be a debris fan where the landslide material has spread out at the base of the slope

3. A scree slope is a collection of broken rock fragments at the base of a cliff or mountain, typically resulting from physical weathering like freeze-thaw cycles.

4. A talus cone is a steep conical pile of rocks that have fallen from the adjacent cliff faces, forming an angle of repose at the base.

Figure I-9. Example mass movement landscapes.

I-2.5. Riverbank collapse

Bank collapse is a significant form of river channel transverse deformation, influenced by the interaction between river flow and bank soil (Xu et al., 2018). The process is driven by fluvial erosion, where material removal from the bank toe directly induces bank retreat and triggers mass instability indirectly (Langendoen, 2000). Various failure mechanisms contribute to bank collapse, each with distinct characteristics (Figure I-10). Rotational failure occurs with shallow slopes, involving bank materials sliding into the channel along a curved surface (Langendoen, 2000; Staley et al., 2006). In steeper banks, planar failure is observed, where a block of soil slides downward and outward into the channel, either through a planar slip or a toppling failure (Langendoen, 2000; Staley et al., 2006). Cantilevered collapse, prevalent in the concave bank of the bend during the dry season, results from the failure of an overhanging bank block formed by undercutting (Langendoen, 2000; Staley et al., 2006; Y. Wang et al., 2016). Piping or sapping failure, another mechanism, describes streambank collapse due to seepage, where erosion caused by soil piping undermines the upper cohesive layer, leading to the detachment and rotation of the failure block into the stream (Hagerty, 1991; Langendoen, 2000; Staley et al., 2006). Post-collapse, the sloping soil becomes a sediment source, significantly altering sediment inflow and concentration, consequently impacting downstream channel evolution (Tang et al., 2012; Xu et al., 2018).

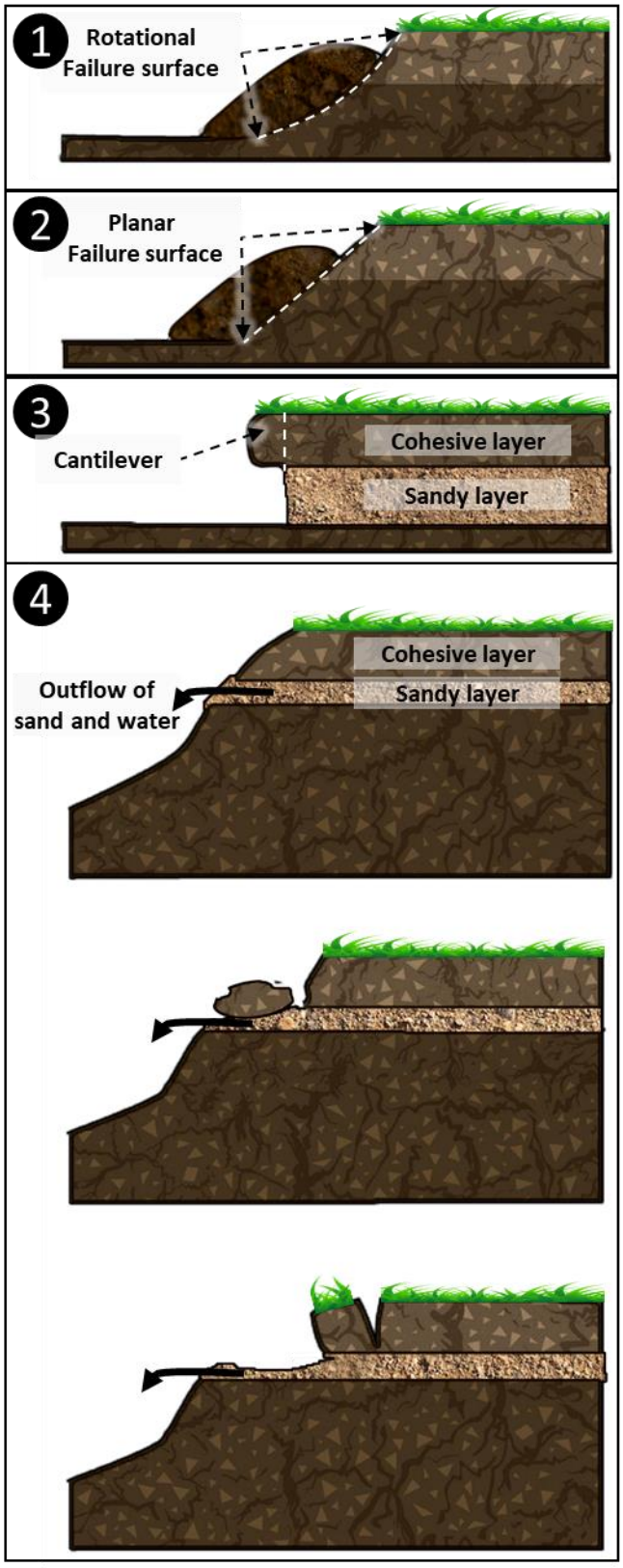

Rotational Failure

A mass of soil rotating out from the riverbank along a curved failure surface.

Planar Failure

The bank material is failing along a flat, inclined plane

Cantilever Failure

A block of soil projecting out over a weaker layer beneath it, resembling a cantilever. The failure occurs due to the weight of the cantilevered block and the lack of support from the undercut or weaker material below

Piping Failure

Seepage outflow from the river through the sandy layer causes the loss of material, creating voids and undermining the structural integrity of the layers above.

Due to the erosion and voids created by the seepage, the upper cohesive layer collapses as the supports are washed out, leading to blocks detaching from the bank.

The continuous outflow of water and sand causes further detachment and toppling of the undermined blocks, aggravating the failure and leading to a progressive collapse.

Figure I-10. Types of Riverbank Failures.

I-2.6. Volcanic Activity and Forest Fires:

Explosive volcanic eruptions (Figure I-11) can have profound impacts on river systems, altering hydrology and sediment transport significantly (Major, 2003). The physical and chemical effects of explosive volcanic eruptions and their products extend to rivers in the vicinity of volcanoes (Kataoka et al., 2019). These eruptions have the potential to disrupt the environment by depositing large volumes of erodible fragmental material, causing severe disturbances (Areu-Rangel et al., 2020). The consequences include the damaging, destroying, burying, or obliterating of vegetation and the widespread coverage of landscapes with centimeters to tens of centimeters of gravelly to silty sediment known as tephra or volcanic ash (Major, 2003). Volcanic eruptions result in the burial of landscapes with tephra, creating extensive areas with unstable surfaces (Arnalds et al., 2013; Del Moral & Grishin, 1999). Following an eruption, increased turbidity and suspended sediment transport are commonly observed, driven mainly by the erosion and remobilization of newly deposited, loosely packed eruptive material upstream of the catchment (Blong, 1984; Kataoka et al., 2019; C. Stewart et al., 2006). For example, the eruption of Unzen volcano in southwestern Japan from 1990 to 1995 led to a substantial accumulation of sediment at the periphery of the lava dome (Ogawa et al., 2007; Yamakoshi, 2005; Miyabuchi, 1999).

Intense fires have significant consequences on soil (Figure I-12), leading to the loss of ground cover and reduced infiltration rates due to the development of hydrophobic layers or surface sealing with ash and fine sediment, thereby enhancing runoff and surface erosion (Reneau et al., 2007; Shakesby & Doerr, 2006). The combustion process during a fire produces mobile, fine-grained wood ash, which is transported downstream in suspension, particularly in the initial flow events following the fire (Malmon et al., 2007; Ranalli, 2004; Reneau et al., 2007). This combustion transforms biomass, necromass, and soil organic matter into ash (Bodí et al., 2014; García-Comendador et al., 2020). The immediate aftermath of a wildfire results in a non-homogeneous ash layer covering the soil surface (García-Comendador et al., 2020). Although ash does not persist on the soil surface for an extended period, it is swiftly redistributed or removed in the days or weeks following a fire, often being transported in rivers in conjunction with fine sediment (Cerdà & Doerr, 2008; García-Comendador et al., 2020; Pereira et al., 2015) or gradually infiltrates the layers of soil below, contributing to the complex dynamics of post-fire soil conditions (Pereira et al., 2015).

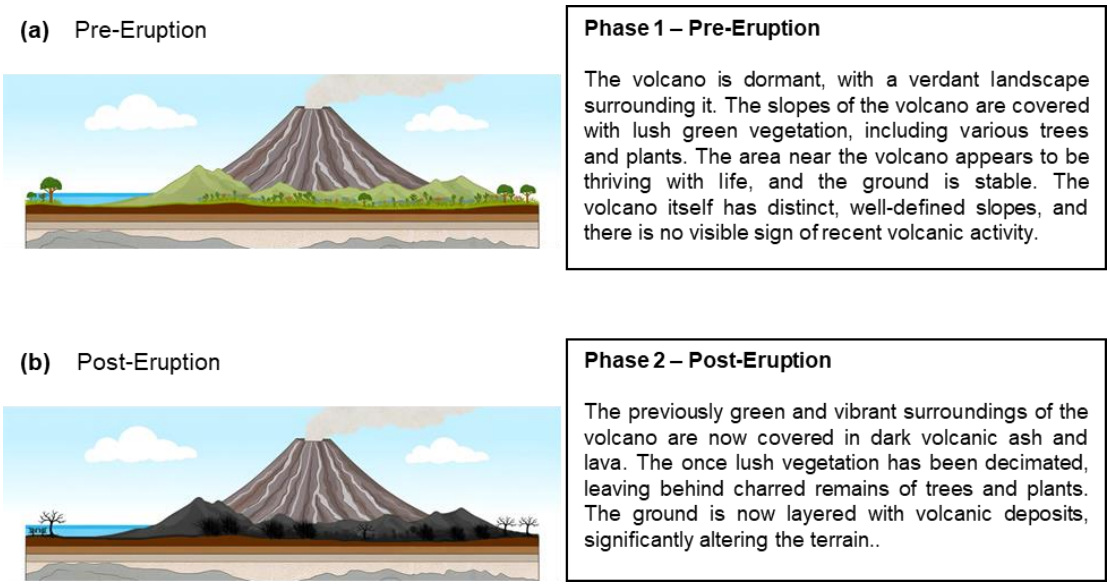

Figure I-11. Landscape Evolution Before and After a Volcanic Eruption.

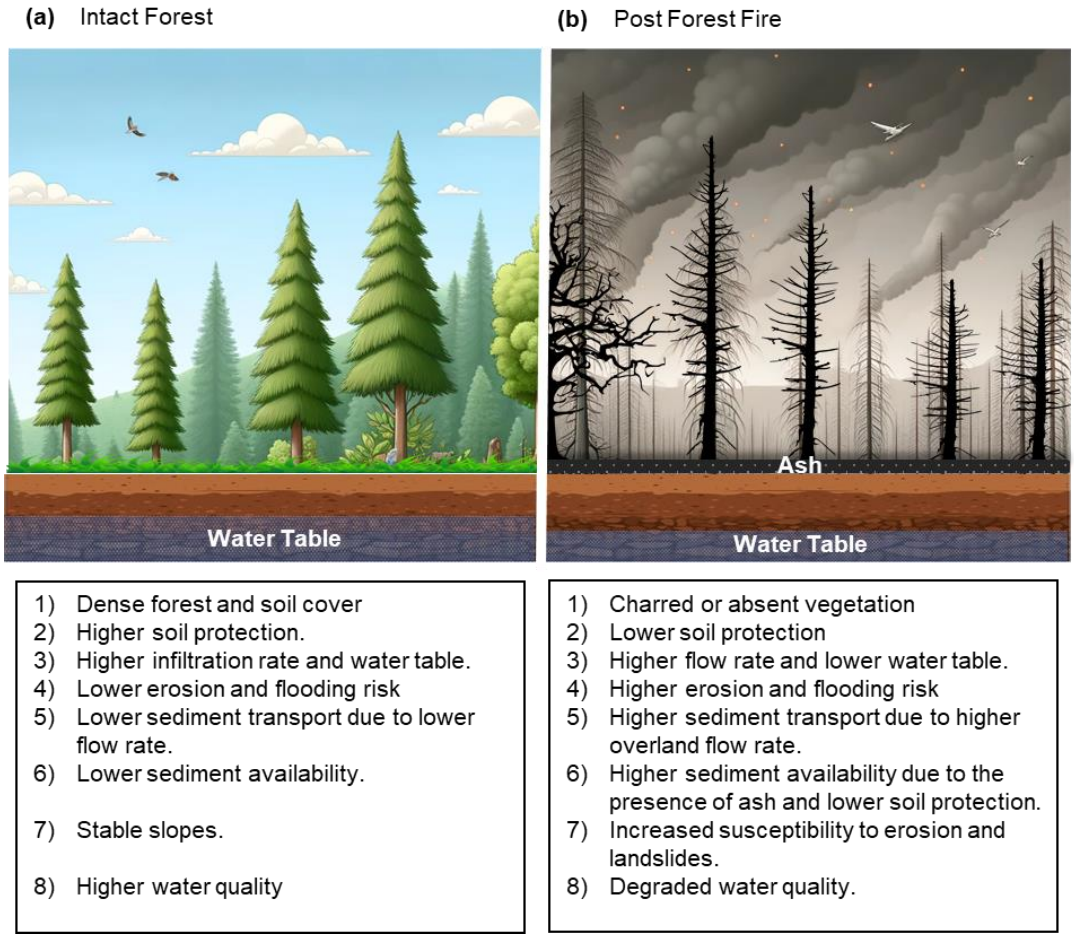

Figure I-12. Comparison Schematic of Forest Fires' Effect on Landscapes.

I-2.7. Anthropogenic Activities:

Human activities have long been a source of environmental challenges, with significant implications for water and soil resources worldwide (Ozcan et al., 2012; Q. et al., 2002). Urbanization, dam construction, deforestation, industrialization, and agricultural practices are key contributors to landscape transformations, leading to the degradation of soils, fragmentation of rocks, and detachment of sediments. These anthropogenic actions reshape natural terrains into disrupted environments. Inland human activities can profoundly impact downstream hydrological and hydrogeochemical conditions in lakes, wetlands, and coastal waters (R. Chalov et al., 2015). Notably, the suspended-phase transport of anthropogenically derived elements can dominate overall transport processes (Chalov et al., 2012; R. Chalov et al., 2015; Thorslund et al., 2012).

Agricultural practices, such as plowing and irrigation, disturb soil structures and significantly contribute to sediment mobilization. Pulley et al., 2022 found that post-plough periods accounted for a mean of 28.8% of monitored sediment flux, despite covering only 10.9% of the monitoring period. Human activities not only influence sediment production directly but also exacerbate other sediment detachment processes. Land pollution, arising from the release of heavy metals in mining and ore excavation (Malmström et al., 2008), nutrient and pesticide runoff in agricultural areas (Darracq & Destouni, 2005), and the release of various elements and chemicals, including persistent organic pollutants, in urban and industrial areas (Jarsjö et al., 2005), contributes to the environmental challenges associated with human activities. Furthermore, the release of chemicals and salts into the environment can infiltrate soils, enhancing chemical and physical weathering processes.

I-2.8. Sediments Global Properties

Sediment properties refer to the physical, chemical, and biological characteristics of sediment particles. These properties play a crucial role in understanding sediment behavior, transport, and their impact on the environment. Some of the key sediment properties are summarized in

Table **I-2** and

Table I-3. These sediment properties are interconnected and collectively determine sediment behavior, including erosion susceptibility, transport dynamics, and sedimentation patterns. Understanding and characterizing these properties are essential for various fields of study, including geology, geomorphology, hydrology, environmental science, and engineering, as they help predict and manage sediment-related processes and their impacts on the environment.

Table I-2. Physical Properties of Sediments

Property	Description	Example references
Grain Size	Size of individual sediment particles	Caldwell & Edmonds, (2014) Hartkamp et al., (1993) Horowitz & Elrick, (1987) Lepesqueur et al., (2019) Walling & Moorehead, (1989) S. Wang et al., (2022) W. Wu & Wang, (2006)
Porosity	Amount of open space between sediment particles	Edwin L. Hamilton, (1976) Hartkamp et al., (1993) Kamann et al., (2007) W. Wu & Wang, (2006)
Permeability	Ability of water to flow through sediment	J. R. Cooper et al., (2018) Hartkamp et al., (1993) Kamann et al., (2007)
Density	Mass per unit volume of sediment	Edwin L. Hamilton, (1976) Lepesqueur et al., (2019) Seng Low, (1989)
Sorting	Uniformity of grain size distribution	Blom et al., (2003) McCave, (2008) Powell, (1998)
Roundness (shape)	Shape of sediment particles	Blott & Pye, (2008) Harold L. Alling, (1950) W. Wu & Wang, (2006)
Cohesion	Internal strength or stickiness of sediment particles	Bui, (2000) Q. Li et al., (2017) W. M. Van Dijk et al., (2013)
Consistency	State of firmness or viscosity of sediment	Hasiotis et al., (2002) Milàn & Bromley, (2007) Smith, (1998)

Table I-3. Chemical and Environmental Properties of Sediments

Property	Description	Example References
Composition	Types and proportions of minerals in sediment	El Bilali et al., (2002) Hartkamp et al., (1993) Horowitz & Elrick, (1987) Nederbragt et al., (2006) Zhou et al., (2005)
Organic Content	Amount of organic material in sediment	Beaudoin, (2003) Tansel & Rafiuddin, (2016) Wicks et al., (2009)
Texture	General appearance and feel of sediment	Jeong et al., (2010) Rustomji, (2006) Schilirò et al., (2019)
Mineralogy	Study of minerals present in sediment	Herman et al., (2007) Jeong et al., (2010) River & Richardson, (2019)
Color	Visual appearance of sediment	Kabir & Ahmari, (2020a) Kabir & Ahmari, (2020b) Nederbragt et al., (2006)
pH	Acidity or alkalinity of sediment	Masscheleyn et al., (1991) Ravisangar et al., (2001) Zhou et al., (2005)

I-2.9. Sediment origin related characteristics

There are several sediment properties that tend to remain relatively unchanged as sediment is transported from its origin to its deposition site. These properties can provide crucial information regarding the origin of sediments and their history. Some sediment properties that often remain consistent and relate to its origin are summarized in Table I-4. By examining these unchanged sediment properties, scientists can infer crucial details about the sediment's origin, depositional processes, and the environmental conditions prevailing in the source area. These properties help reconstruct past landscapes, understand sediment transport dynamics, and provide a basis for interpreting geological and environmental changes over time.

Table I-4. Origin-Related Sediment characteristics.

Property	Description	Example Reference
Mineralogy	Identification and study of minerals present in sediment.	Andrews et al., (2018) Andrews & Eberl, (2012) River & Richardson, (2019)
Heavy Mineral Analysis	Examination of dense minerals in sediment.	Hounslow & Morton, (2004) Tsikouras et al., (2011) Wong et al., (2013)
Clay Mineralogy	Analysis of clay minerals present.	He et al., (2013) J. Liu et al., (2010) Veerasingam et al., (2014)
Geochemical Signatures	Chemical composition and distribution in sediments.	Amorosi et al., (2022) Franz et al., (2013) Raigani et al., (2019)
Color	Visual appearance and hue of sediment.	García-Comendador et al., (2020) Kieta et al., (2023) Krein et al., (2003) Pulley & Collins, (2021)
Texture	Particle arrangement and size in sediment.	David Krinsley, Pierre E. Biscaye, (1973)
Grain Size and shape	Measurement of particle size distribution and form.	Koiter et al., (2018) Sadeghi & Singh, (2017) Saukel et al., (2010) Zhang et al., (2023)
Organic Matter Composition	Analysis of organic materials present in sediment.	F. Chen et al., (2016) Koiter et al., (2015, 2018)
Magnetic Properties	Evaluation of sediment's response to magnetic fields.	Hatfield & Maher, (2008) Hounslow & Morton, (2004) Oldfield et al., (1979)
Isotopic Signatures	Identification of isotopic ratios in sediment.	Gellis & Noe, (2013) Lizaga et al., (2022) Upadhayay et al., (2017)

I-3. Transport and Sedimentation

Sediment transport dynamics from the origin to the outlet of a watershed involve a complex interplay of processes that determine the movement and deposition of sediments throughout the watershed. The journey of sediments can be divided into transport, mixing, and deposition phases. In a watershed, in addition to wind transport, rainfall and snowmelt can generate overland flow or runoff with sufficient capacity to pick up and mobilize sediments.

I-3.1. Wind Sediment Transport:

Wind sediment transport refers to the process by which wind moves and transports sediment particles across the Earth's surface. It is a natural phenomenon that plays a significant role in shaping landscapes, particularly in arid and semi-arid regions (Nickling & Neuman, 2009) where vegetation cover is sparse. During wind erosion, the force of the wind dislodges and lifts loose sediment particles from the ground, carrying them over short or long distances depending on wind strength and sediment size. The transported sediment can range from fine dust particles to larger sand grains (Nickling & Neuman, 2009), and even pebbles or small rocks in extreme cases. Wind sediment transport can lead to the formation of features such as sand dunes (Parteli et al., 2009; Tsoar, 2001), dust storms (Semenov, 2012; Sivakumar, 2005), and loess deposits (Pye, 1995; Sun, 2002), and it can have both erosional and depositional effects on the landscape. Additionally, wind-blown sediment can impact air quality, agricultural productivity, and ecosystem health in affected areas (Semenov, 2012).

I-3.2. Water transport

Water serves as a versatile carrier, capable of transporting a diverse range of materials depending on its capacity. The materials transported encompass dissolved particles, such as salts, nutrients, and pollutants (e.g., Butler & Ford, 2018; Chahinian et al., 2011; Xue et al., 2022), as well as finer particles like clay, silt, and sand that remain suspended in the water column, collectively referred to as suspended sediments (e.g., Asselman, 1999; Bisantino et al., 2011). Larger particles, including gravel, pebbles, and cobbles, can be transported along the stream bed as bedload (e.g., Mao et al., 2014). Additionally, flowing water has the capacity to transport organic

materials like leaves, branches, and plant debris (e.g., Bocchiola et al., 2006; Jacobson et al., 1999; Kramer & Wohl, 2017; MacVicar et al., 2009). During periods of high flows or flooding, water can carry more substantial debris, such as boulders and fallen trees (e.g., Bocchiola et al., 2006; Kehew et al., 2010; Kramer & Wohl, 2017; Lenzi, 2004). In colder regions, broken ice becomes a form of floating debris (e.g., Chen et al., 2023; Tao Shen et al., 1990; Turcotte et al., 2011). Accordingly, with enough capacity, it is evident that water can carry everything that it encounters in its path.

Sediment transport within flowing water is a dynamic process, and the initial phase, Sheet Flow or Overland Flow, plays a crucial role in reshaping landscapes. This phase occurs when water, primarily from rainfall or snowmelt, moves as a thin, unconfined sheet over the land surface, spreading evenly. Overland flow is triggered when the rate of water application exceeds the soil's infiltration capacity (Lavee & Poesen, 1991). Literature reports multiple types of overland flow, including Saturated Overland Flow, a flow that is not generated until the soil is saturated, Hortonian (or Horton) Overland Flow, induced by intense rainfall exceeding infiltration capacity, Concentration Overland Flow, occurring when water is locally concentrated on impermeable objects like stones, and Return flow, observed when subsurface flow resurfaces (Calvo-Cases et al., 2003, 2005; Cook, 1946; Ferreira et al., 2000; Gomi et al., 2008; Hewlett & Hibbert, 1967; Horton, 1933; Hueso-González et al., 2015; Lavee & Poesen, 1991; Ziegler et al., 2004). Horton Flow can be considered as the most important overland flow process. Hydrophobic soils can produce both localized areas of high Hortonian overland flow and preferential vertical infiltration (Gomi et al., 2008; Imeson et al., 1992; M. Kobayashi & Shimizu, 2007). Overland flow from hillslopes displays high spatial and temporal variability influenced by microtopographic patterns, causing variability in ponding and preferential infiltration (Dunne et al., 1991; Gomi et al., 2008; Julien & Moglen, 1990). Overland Flow contributes to the transport of fine-grained sediments, known as the "wash load", from hillslopes to the channel during runoff events (Yuill & Gasparini, 2011) where Hortonian Overland Flow has been identified as a significant contributor to soil loss in Mediterranean geomorphological systems (Beven, 2002; García-Ruiz et al., 2013; Hueso-González et al., 2015; Puech & Chabi-Gonni, 1984; Rao et al., 1998; Stomph et al., 2002).

As water progresses from sheet flow, the development of small channels known as rills becomes apparent, triggered by concentrated flow in specific areas (Casalí et al., 2006; Di Stefano & Ferro, 2011). Rill flow signifies the creation of incised channels in response to erosive forces. If erosive forces persist, rills can transform into larger, more defined features called gullies,

representing a significant concentration of water into distinct, eroded channels. The formation of these channels results from concentrated flow transporting sediment particles detached from interrill areas and scoured from the channels wetted perimeter (Di Stefano et al., 2013; Di Stefano & Ferro, 2011; Foster, 1982; Nearing et al., 1997). Rill formation and development contribute to an increase in total sediment transport efficiency (Di Stefano et al., 2013). Gullies and rills, common in cultivated soils globally, pose a threat of significant soil loss (Auzet et al., 1993; Benito et al., 1992; Bennett et al., 2000; Bryan, 1987; Casalí et al., 2006; De Santisteban et al., 2006; Di Stefano & Ferro, 2011; Govers & Poesen, 1988; Zheng & Huang, 2005). Detached sediments are carried by overland flow into the rill channels, where the concentrated linear flow is deeper and faster than the more dispersed overland flow, enhancing overall sediment transport efficiency (Bruno et al., 2008; Di Stefano et al., 2013). According to Gao, (2013), higher velocities in gullies ensure that sediment transport downslope exceeds that supplied from the surrounding surface and banks, leading to the enlargement of these channels.

Interflow, though concealed beneath the surface, plays a crucial role in subsurface water movement within the unsaturated zone. As water infiltrates the soil, it may traverse deeper into the ground, integrating into the groundwater system. Subsurface water flow is intricately associated with various processes such as heave, piping, concentrated leak erosion, contact erosion, and suffusion piping (Fleshman & Rice, 2014). Internal erosion, resulting from the transport and migration of soil particles, induces alterations in the hydraulic and mechanical characteristics of the soil (Sharif et al., 2015). A specific manifestation of this process is soil piping, also known as tunnel erosion, where concentrated flowing water creates linear voids in soils or unconsolidated sediments (Verachtert et al., 2011). Piping occurs when high-velocity flow erodes weak spots in the soil or rock, gradually enlarging voids and transporting detached material away, contributing to the growth of underground channels. Dissolution, another significant facet of piping, especially in scenarios where the soil or rock is susceptible to chemical breakdown by water, further influences the evolution of these channels (see *Chemical weathering*). These channels, formed by centralized subsurface flows, have implications for gully development and direct land degradation (Faulkner, 2006; Hosseinalizadeh et al., 2019; Nadal-Romero et al., 2011; Podmanicky et al., 2011; Poesen, 1989; G. Wilson, 2011). Piping can lead to the collapse of the soil surface, resulting in the formation of discontinuous gullies (Jones, 2004; Verachtert et al., 2011). However, this process remains less observed and studied because pipes become visible only after surface soils collapse

(Verachtert et al., 2011). Underground water has a substantial contribution to overall streamflow and baseflow significantly influencing surface sediment transport.

Ultimately, the culmination of various pathways converges in the creation of streams or rivers. Stream flow embodies the concentrated movement of water within clearly defined channels, amalgamating water and sediment contributions from overland flow, rills, gullies, and groundwater discharge. Streams and rivers thus exhibit heightened transport capacity and erosion efficiency, integrating sediments sourced from upstream hillslopes, rills, gullies, subsurface deposits, and locally detached sediments from the channel bed and banks.

I-3.3. Deposition and Sedimentation:

The integrated sediment transfer system operates as a physical progression of solid detachment and deposition spanning the terrestrial and aquatic zones. Soil disruption occurs via a combination of kinetic rainfall energy, surface runoff, biotic activity, and geochemical breakdown. Following the loss of structural integrity, wind and water serve as the primary transport vectors, displacing particles from their point of origin. These detached materials subsequently follow two distinct evolutionary tracks within the broader watershed landscape:

(1) Direct transport: Sediments moved by overland flow (e.g., rain or snowmelt) or wind to the nearest channel (natural or artificial) and are transported towards sediment deposition zones (e.g., reservoirs, lakes, deltas, estuaries, sinkholes, and alluvial fans);

(2) Temporary storage and remobilization: Sediments are temporarily deposited on hillslopes and within the channel, then re-entrained when transport agents resume or acquire enough capacity (e.g., stronger winds, more intense rains, and higher flow events).

The sequence of transport, deposition and remobilization is described as a sediment cascade (Bracken et al., 2015; Collins & Walling, 2004; K. Fryirs, 2013; Harvey, 2002; Vercruysse et al., 2017). Sediment deposition is intrinsically intertwined with sediment transport, representing the subsequent phase in the continuum of sediment movement. While this progression may seem sequential when viewed from the perspective of individual particles, it is important to recognize that these processes also occur concurrently when considering the collective behavior of sediment ensembles. Deposition and Transport are a dynamic interplay of factors influenced by geomorphological and geological conditions (e.g., parent material, tectonics, relief, landforms,

topography), climate (e.g., rainfall and temperature), biota (vegetation and fauna), and human activities (e.g., agriculture, grazing, fire, mining, roads).

In recent decades, the concept of connectivity has emerged as a valuable tool for analyzing and quantifying the influences on water and sediment fluxes across various scales (S. Keesstra et al., 2018). Connectivity refers to the degree to which the movement of water and sediment is facilitated within landscapes, encompassing aggregate, pedon, slope, and watershed scales (S. Keesstra et al., 2018; Najafi et al., 2021). Connectivity is seen to act on different spatial directions separated into (1) longitudinal (river channel), (2) lateral (hillslope/floodplain-channel), and (3) vertical (surface-subsurface) connectivity (K. A. Fryirs et al., 2007; S. Keesstra et al., 2018). Despite its importance, it's notable that instances of disconnection are prevalent within hydro-geomorphological systems, often due to factors such as the short duration of rainfall events or the presence of relief, vegetation, fauna, and reservoirs (K. A. Fryirs et al., 2007; S. Keesstra et al., 2018; Strohmeier et al., 2016). These disconnections disrupt the direct transfer of runoff and sediment from source areas to river channels, highlighting that runoff and sediment yield are not simply the sum of their sources (S. Keesstra et al., 2018). For example, studies in arid regions, such as those conducted by Yair & Lavee, (1985) have demonstrated that runoff generated in upper slope areas may not reach river channels due to infiltration into colluvium, resulting in disconnection from the drainage network. Consequently, connectivity can be understood as the collective set of factors that promote water and sediment fluxes, while disconnections represent impediments to these fluxes. High connectivity indicates efficient water and sediment transfer, leading to lower rates of deposition, whereas lower connectivity, characterized by a higher prevalence of disconnections, signifies inefficient water and sediment transfer, consequently promoting greater deposition.

Several factors can intensify overland flow and consequently promote sediment transport within a watershed. Deforestation, for instance, can significantly increase surface runoff by removing vegetation cover that intercepts rainfall and reduces infiltration (Anselmetti et al., 2007; C. Zhao et al., 2016). Similarly, changes in land management practices, such as ceasing tillage, can initially reduce soil infiltration, leading to increased surface runoff. Keesstra et al., (2018) note that soil recovery, facilitated by biota, is necessary for restoring infiltration rates over time. Intense rainfall events can exacerbate connectivity by removing vegetation from river channels, enhancing the conveyance of water and sediment. Additionally, natural forest fires can strip slopes of

vegetation, further contributing to increased overland flow and sediment transport (Nunes et al., 2018; Sanjuán et al., 2016). Furthermore, land abandonment can lead to the neglect of terrace maintenance, resulting in structural collapse. This transition from terraces that reduce connectivity to collapsed structures can enhance overland flow pathways (Arnáez et al., 2015).

In contrast, various factors can impede overland flow and promote sediment deposition within a watershed, leading to diverse depositional environments (Table I-5). Vegetation plays a crucial role in reducing the velocity of overland flow, promoting infiltration while decreasing surface connectivity (C. Zhao et al., 2016). Ant nests, while often overlooked, promote infiltration and overland flow disconnectivity (Cammeraat et al., 2002). Wildlife activities, such as wild boar burrowing, activate sediment availability and enhance soil stability, thereby reducing overland flow and sediment transport (S. Keesstra et al., 2018). Similarly, beavers significantly alter hydrological processes by impounding rivers through a natural dam construction, effectively reducing flow velocity (Nyssen et al., 2011; Westbrook et al., 2006). Land abandonment can reduce connectivity by means of and recovery of natural vegetation (S. Keesstra et al., 2018). Changes in practices of land use like tillage, can also influence surface runoff patterns. Under tillage, the soil remains permeable, allowing rainfall to infiltrate easily and reducing surface runoff (S. Keesstra et al., 2018). Additionally, anthropologic activities intentionally designed to decrease connectivity, such as terrace construction, contour afforestation, and damming, contribute to impeding overland flow and promoting sediment deposition (Poeppl et al., 2015; Pringle, 2003). Natural events, such as landslides and earthquakes, can further alter landscape morphology, creating lakes on slopes and in channels that disconnect parts of the fluvial system (Lanckriet et al., 2016).

Table I-5. Sedimentation Locations and Influencing Factors

Sedimentation Location	Description	Example Reference
Floodplains	Low-lying areas adjacent to rivers or streams prone to sediment deposition during floods	Asselman & Middelkoop, (1995)
Deltas	Coastal landforms formed by river carried sediment deposition	Moore, (1966)
Alluvial Fans	Fan-shaped deposits of sediment formed at the base of mountains or hills	Lanckriet et al., (2016).
Estuaries	Transitional zones where rivers meet the sea, characterized by sediment deposition due to mixing of freshwater and saltwater	Brush, (1989)
Backwaters	Sheltered areas behind obstacles such as islands or large rocks, where flow velocity decreases and sediments settle	Bhowmik & Demissie, (1989)
Levees	Raised embankments along rivers or streams, where sediments accumulate during floods	Asselman & Middelkoop, (1995)
Riparian Zones	Vegetated areas along the banks of rivers or streams, where sedimentation occurs due to reduced flow velocity and vegetation trapping	J. Steiger et al., (2001)
Oxbow Lakes	Curved, U-shaped bodies of water formed when a river changes course, where sediments settle due to reduced flow velocity	C. M. Cooper & McHenry, (1989)
Reservoirs	Artificial lakes created by damming rivers, where sediment deposition occurs as flow velocity decreases	Schleiss et al., (2016)
Ponds	Small bodies of standing water where sediment settles due to low flow velocity	D. R. Butler & Malanson, (1995)
Marshes	Wetlands dominated by herbaceous vegetation, where sediment accumulates in the stagnant water	Nolte et al., (2013)
Wetlands	Ecologically important areas with saturated soils and vegetation, where sedimentation is common due to low flow velocity	Wardrop & Brooks, (1998)
Depressions	Low-lying areas where water collects, leading to sediment deposition	Craft & Casey, (2000)
Channel Bars	Sand or gravel bars found within river channels, where sediment accumulates due to reduced flow velocity	Hooke, (1986)
Point Bars	Crescent-shaped sediment deposits found on the inside of river bends, formed by the gradual deposition of sediment	Bluck, (1971)
Bayous	Slow-moving, swampy streams or channels where sedimentation occurs due to low flow velocity	Guccione et al., (1999)
Lagoons	Shallow coastal bodies of water separated from the sea by reefs or islands, where sediment accumulates	Adriano et al., (2005)
Sloughs	Slow-moving or stagnant channels within marshes or wetlands, where sediment settles out of suspension	Neal & Anders, (2015)
Groundwater Recharge Zones	Areas where surface water infiltrates into the ground, leading to sediment deposition	Prathapar & Bawain, (2014)

I-4. Sediment Mixing

Sediment transport involves the dynamic movement of particles across various environments, driven by the forces of water, wind, or ice. The phenomenon of sediment mixing plays a crucial role in this journey, where individual particles undergo intricate interactions during their movement. When we take a water sample at a stream gauging station, the sediments carried within the water represent a mixture originating from diverse locations within the basin, including exo-basin sources brought in by wind transport.

I-4.1. Hillslope Sediment Mixing

Sediment mixing within a watershed is a dynamic process shaped by various factors, with the origins of sediments playing a crucial role. Particles from remote sediment sources follow two distinct paths before contributing to the streamgage mixture. These sources may either be directly linked to the channel or transported to other sediment sources where they undergo hillslope mixing before their entry into the channel.

The connectivity of these remote sources determines the pathway they follow, influencing the mixing processes they undergo. Direct connection implies an immediate engagement with channel dynamics, where sediments swiftly enter the stream network, undergoing direct channel mixing processes (e.g., Figure I-13 Zone 3.). In contrast, indirect connections involve sediments traveling through hillslopes and adjacent locations before reaching the channel, initiating hillslope mixing processes (e.g., Figure I-13 Zone 1 and 2).

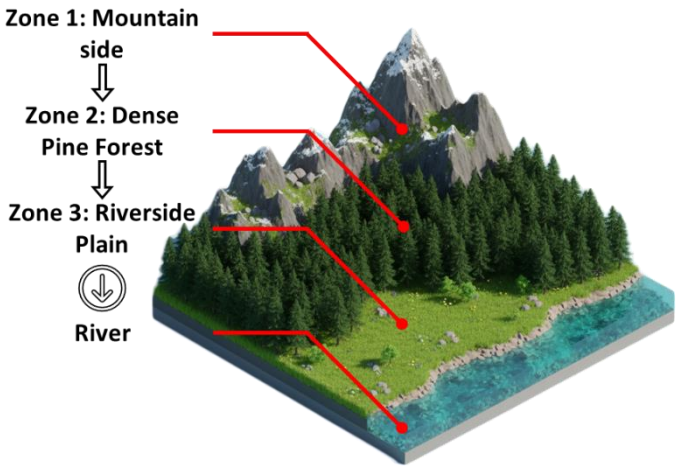

Figure I-13. Example Sediment Pathways for Different Zones of the Watershed.

The degree of connectivity further refines this process, delineating between strong and weak connections. A strong connection signifies a direct and efficient pathway, accelerating the travel rate of sediments toward the channel. This efficiency has implications for the rate and nature of hillslope mixing processes. On the other hand, weak connectivity implies a less efficient pathway, leading to a slower travel rate. Sediments with weaker connections may undergo more cycles of the transport-deposition process, resulting in a prolonged journey through hillslopes. This extended journey introduces the concept of aging, where sediments experience significant time gaps between detachment and arrival at the streamgage location. Aging involves physical and chemical changes to sediment particles, contributing to the complexity of sediment dynamics and challenging efforts to trace them back to specific sources within the watershed. Accordingly, the resulting mixtures at the streamgage include sediments of varying histories, blending freshly detached particles with those that have undergone extended journeys through the landscape.

Areas adjacent to the stream gauging station and the stream channel share crucial characteristics that shape their role in sediment mixing processes. Both types of areas serve as direct conduits to the stream channel, acting as key entry points for sediments into the stream network. These locations receive sediment contributions from nearby areas, establishing them as crucial nodes for hillslope mixing processes. Sediments arriving from proximal sediment sources settle alongside sediments previously deposited and locally detached sediments, creating a deposited sediment mixture, marking the final stage of hillslope processes before entering dynamic channel mixing. Their significance lies in being the last stops where hillslope-mixed sediments experience environmental conditions distinctive to their journey, setting the stage for their subsequent transport dynamics within the stream network.

I-4.2. Hydrographic Channel Network Sediment Mixing

The stream channel, a fundamental component of a watershed, encompasses the intricate network of watercourses that collectively form the drainage system. Its definition can vary, ranging from the main river channel to the entire hydrographic network, depending on the context and the perspective of the observer. Within this hydrographic network, a diverse array of sediments undergoes dynamic interactions and mixing processes. The sediment in the stream channel can be broadly categorized into distinct types, each with its origin and unique characteristics. These

include sediments delivered from hillslopes, those stored within the channel, particles detached by the flowing water from the bed and banks, and materials resulting from accidental processes such as bank collapse.

In understanding sediment mixing within a watershed, envisioning the hydrographic network as a converging tree network provides a useful framework. This representation views the various watercourses as branches converging toward the main stem, culminating at a stream gauging station—the sampling endpoint. Starting from the lowest level branches, akin to the smallest watercourses, we can systematically explore the sediment mixing dynamics within each segment, gradually working our way downstream to the main stem. This hierarchical approach allows us to simplify the intricate sediment mixing at different levels, providing insights into the complexities of channel mixing processes.

At the lowest level branch, representing the smallest watercourse, sediment mixing exhibits distinct characteristics. Here, we encounter a limited set of sediment mixtures, primarily originating from hillslope processes. These include mixtures from the left and right banks, along with a combination of deposited sediments lining the channel bed. Additionally, contributions arise from sediments detached from the bed and banks by the flow. These mixtures evolve to form a unique low level branch mixture (Figure I-14).

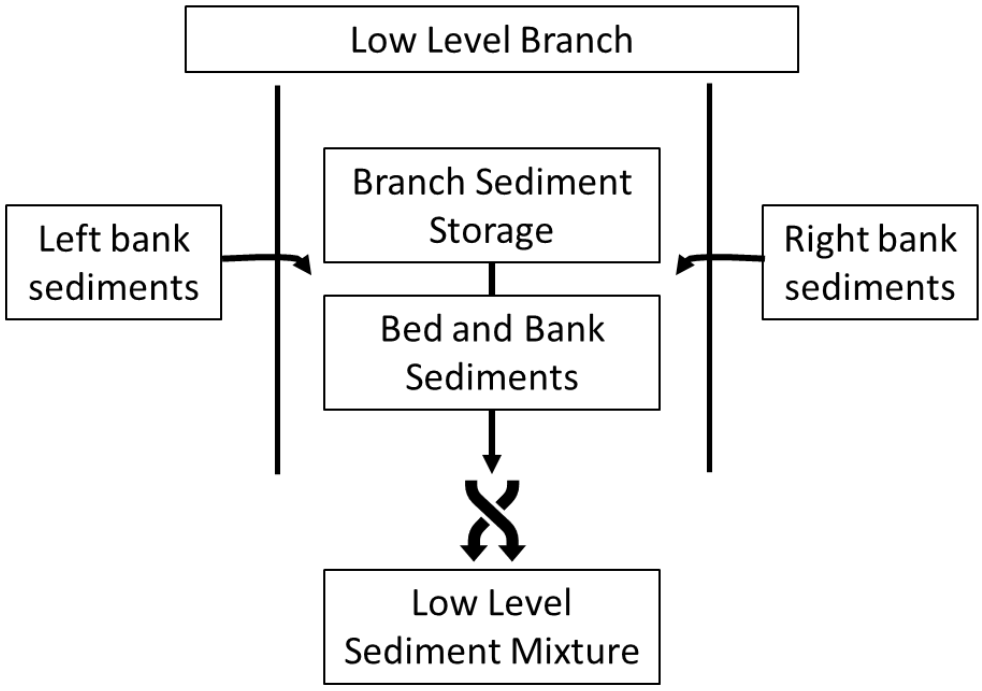

Figure I-14. Low level branch sediment mixing process schematic

In the second stage of channel mixing within intermediate level branches, the hydrographic network assimilates sediment mixtures from lower-level branches, adjacent hillslope compositions, and channel sediments, including those stored within the channel and particles detached by water flow (Figure I-15). This stage represents a critical juncture where various tributaries and watercourses contribute their distinct sediment blends to the evolving composition within the broader stream network.

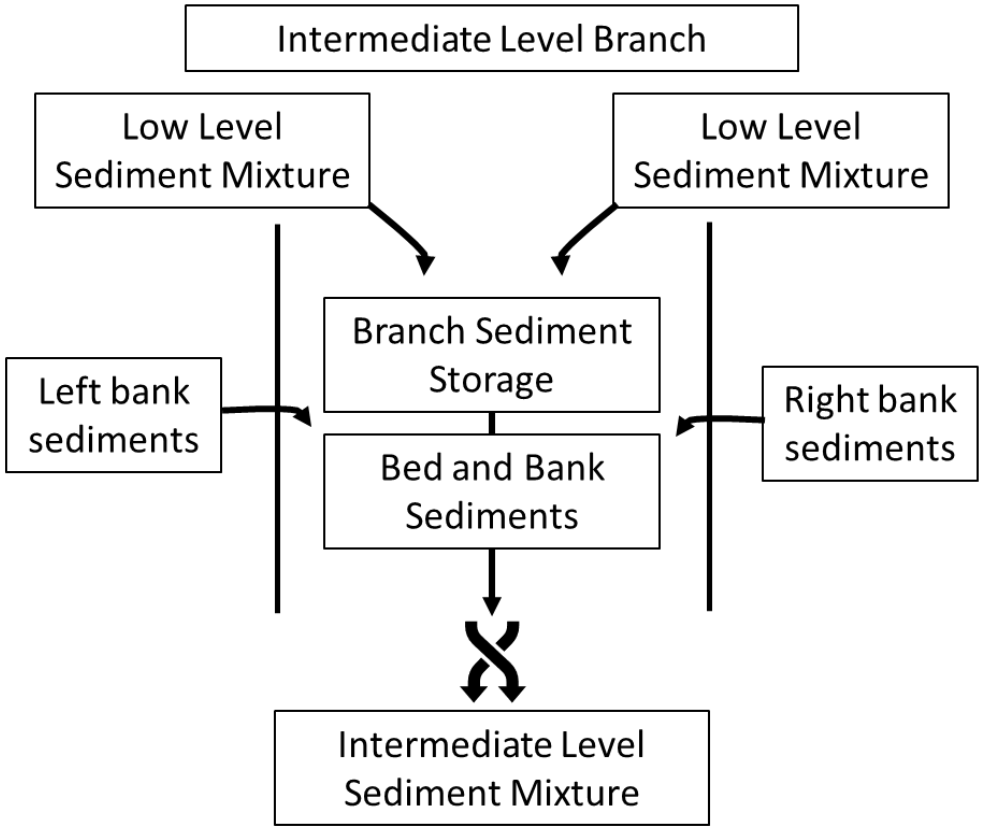

Figure I-15. Intermediate branch sediment mixing process schematic

Finally, at the highest-level branch leading to the streamgage, the channel integrates mixtures from low and intermediate level branches, adjacent hillslope mixtures, storage, and sediments detached from the bed and banks, culminating in the production of a final mixture at the streamgage (Figure I-16).

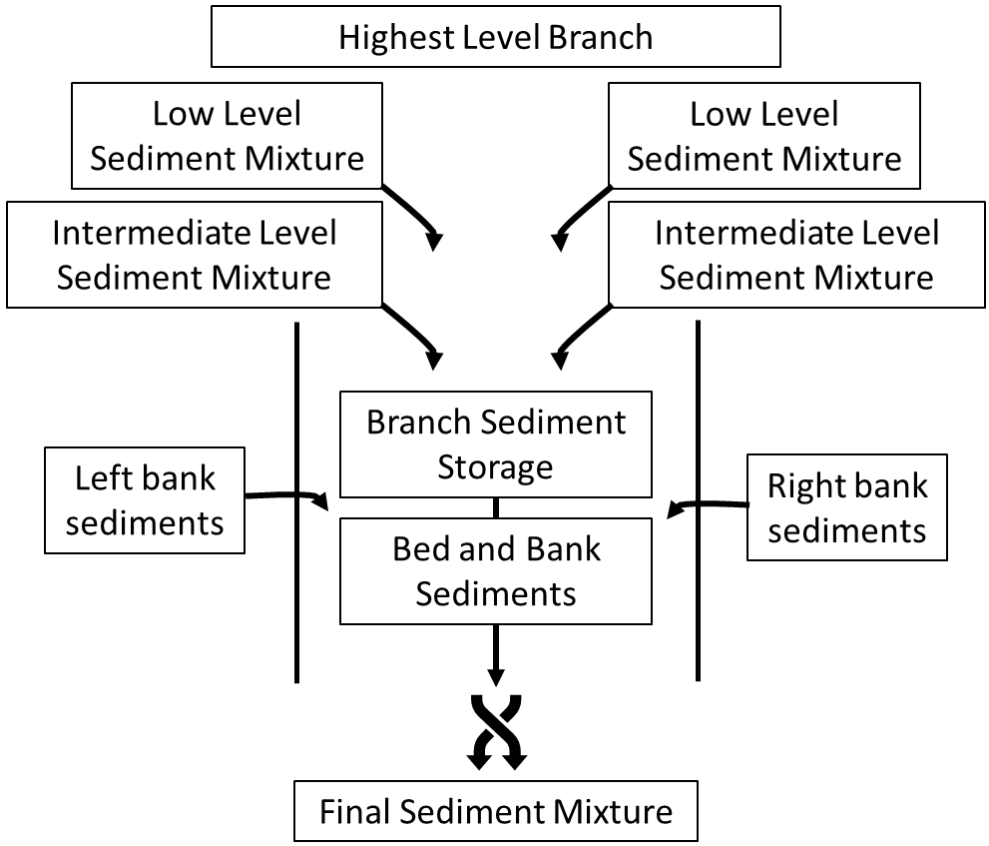

Figure I-16. Highest level branch sediment mixing process schematic

I-5. Sediment Sources Analysis

I-5.1. Motive

Sediment transport, a fundamental process in fluvial systems, plays a pivotal role in shaping landscapes, maintaining ecosystem health, and influencing socioeconomic activities. It involves the movement of sediment particles that contribute to the formation of landforms, river morphology, and the redistribution of nutrients and organic matter. Sediment transport is important for maintaining aquatic ecosystem health, resiliency and function (Koiter et al., 2013; Owens, 2008). However, alongside its natural significance, sediment transport also presents challenges and issues, particularly in human-altered landscapes and water management practices (Allan, 2004; Koiter et al., 2013; Owens et al., 2010; Syvitski et al., 2005).

One significant concern associated with sediment transport is sedimentation in water bodies, which can lead to reduced water storage capacity, increased flood risks, and degradation of soils, water quality, and aquatic habitats (Ben Slimane et al., 2016; Bunzel et al., 2015; Duvert et al., 2012; Gardner & Gerrard, 2003; Horowitz, 2008; Kassoul et al., 1997; Koiter et al., 2013; Owens et al., 2005; Sánchez-Chardi et al., 2009; Tananaev, 2015; Upadhayay et al., 2017; Urban et al., 2009; Vörösmarty et al., 2003, 2003; S. Wang et al., 2019). Indeed, excessive sedimentation can impair water quality, affecting aquatic ecosystems and compromising water supply for human consumption, agriculture, and industry. Moreover, sediment-laden water poses challenges for navigation, infrastructure maintenance, and hydropower generation, impacting local economies and livelihoods. Additionally, sediment erosion and deposition can exacerbate soil erosion, leading to loss of fertile land and reduced agricultural productivity and heightened vulnerability to natural hazards such as landslides and floods.

Given these multifaceted impacts, there is a growing recognition of the need to assess sediment transport processes and sources comprehensively. From a socioeconomic perspective, understanding sediment transport dynamics is crucial for sustainable water resource management, flood risk mitigation, and infrastructure planning and maintenance. By quantifying sediment fluxes, identifying sediment sources, and assessing sediment connectivity, decision-makers can develop effective strategies to mitigate sediment-related risks, enhance ecosystem resilience, and promote sustainable development. Moreover, from a scientific standpoint, studying sediment transport provides valuable insights into landscape evolution, ecosystem dynamics, and the interconnectedness of Earth's surface processes, advancing our understanding of geomorphology, hydrology, and environmental change. Therefore, efforts to assess sediment transport and sediment sources are essential for addressing both practical challenges and scientific inquiries, contributing to informed decision-making and holistic management of fluvial environments.

I-5.2. Methods

I-5.2.1. Modelling Sediment Transport

Sediment transport models are instrumental in numerically simulating the complex processes of sediment detachment, mobilization, and deposition within fluid environments (James et al., 2010). As Batista et al., (2019) emphasized, erosion models establish a formalized structure

for the mechanisms controlling the lifecycle of soil particles. These frameworks allow researchers to resolve the complex feedback loops between erosive forces and contributing environmental variables (Kumar, 2019). Furthermore, they act as indispensable diagnostic tools for quantifying the localized and watershed-scale impacts of siltation, facilitating evidence-based strategies for sustainable land management (Andualem et al., 2023).

Categorically, models of soil erosion are separated into: empirical, conceptual, and physical-based (Hajigholizadeh et al., 2018). Empirical models rely on observed data and mathematical equations but may make unrealistic assumptions about catchment physics (Andualem et al., 2023). Conceptual models aim to capture the overall functioning of catchments but may not accurately represent real-world processes (Andualem et al., 2023; Lørup & Styczen, 1990). Physically based models, on the other hand, aim to represent erosion mechanisms using comprehensive datasets and subprocesses, making them suitable for assessing sediment sources (Andualem et al., 2023; Lørup & Styczen, 1990). However, the complexity and data requirements of physically based models can pose significant challenges.

Indeed, uncertainty is inherent in sediment transport modeling due to hydrological process representation, model structure biases, data accuracy, and discrete measurements (Andualem et al., 2023; Refsgaard & Storm, 1990). Therefore, model calibration, validation, and testing against observed data are crucial for achieving desired accuracy levels (Andualem et al., 2023). However, testing soil erosion models can be challenging due to the difficulty and expense of collecting quantitative erosion data over multiple spatiotemporal scales (Batista et al., 2019; Nearing, 2000; Quinton, 2004; Stroosnijder, 2005). Consequently, the process of model selection, data collection, analysis, calibration, and validation can be resource-intensive and time-consuming, necessitating a long-term perspective and careful consideration of alternative approaches to achieve desired modeling objectives.

I-5.2.2. Sediment Fingerprinting

According to Vercruysse et al., (2017), sediments characterized by a natural signature or fingerprint (see Table I-4) tying sediments to their origin within a watershed. These properties are assumed to remain unchanged and thus allow to define the origin based on a comparison between the source and outlet samples (Koiter et al., 2013; Vercruysse et al., 2017; D. E. Walling, 2013).

Sediment fingerprinting offers a direct and robust framework for quantifying provenance, enabling researchers to determine the proportions of particulate matter originating from specific source (Du et al., 2019; Vale et al., 2016; C. G. Wilson et al., 2008). Achieving a reliable estimate of source contributions relies on a three-tier system:

- **Provenance Sampling:** Collecting representative material from hypothesized source categories.
- **Tracer Discrimination:** Identifying unique geochemical fingerprints to differentiate potential sources.
- **Mass-Balance Modeling:** Quantifying relative loads through models such as the Walling-Collins model (Collins et al., 1997; D. Walling et al., 1993), the Hughs model (A. O. Hughes et al., 2009) and a Bayesian model coupled with a discriminant function analysis (Du et al., 2019) (Figure I-17).

However, Pulley & Collins, (2021) stated that sediment fingerprinting methods are costly due to the required expertise, lengthy sample collection and preparation, and high-cost of tracer analyses. Indeed, according to Vercruysse et al., (2017), geochemical such techniques are very expensive and lengthy, which discourages a higher sampling frequency. Accordingly, studies are mostly applied using samples from deposited sediments rather than sediments in transit (i.e., streamflow samples) (e.g., Amorosi et al., 2022; He et al., 2013; Veerasingam et al., 2014; Wong et al., 2013).

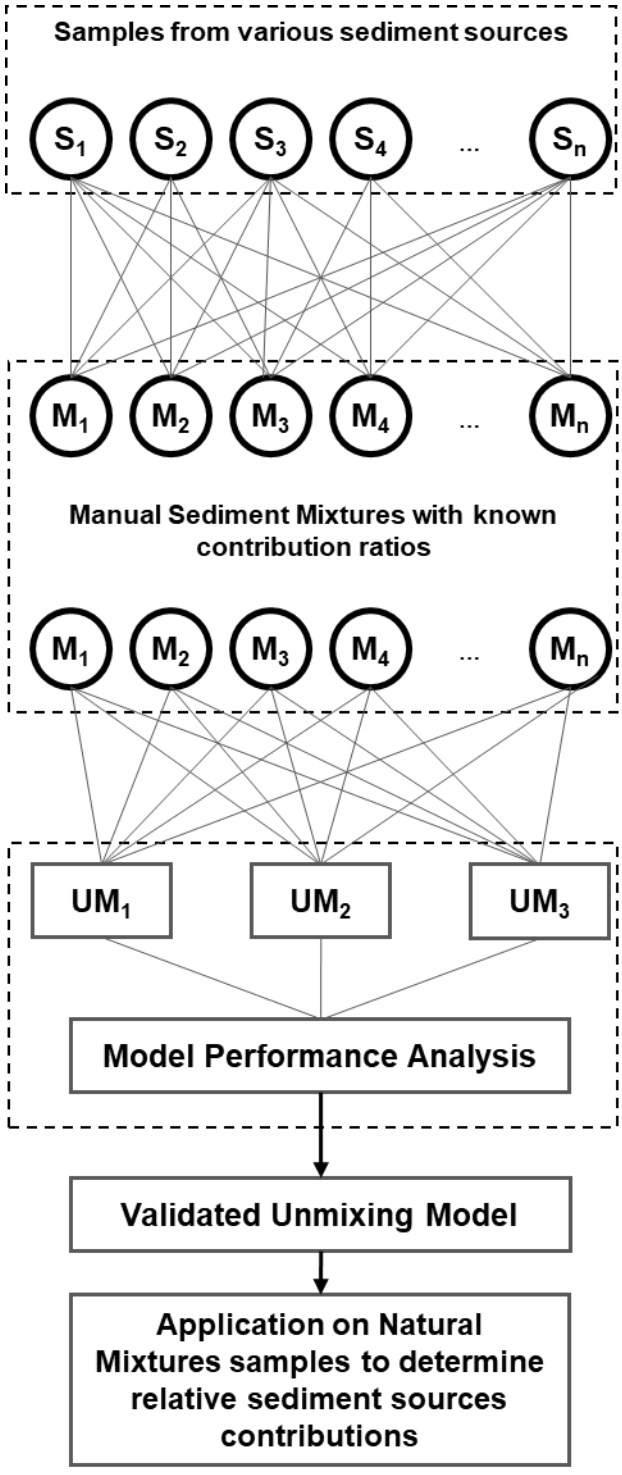

Phase 1 - Sample Collection

The process begins with the collection of sediment samples (S_1, S_2, S_3… S_n) from various potential sources, labeled. Each sample represents a unique sediment source in the environment.

Phase 2 - Manual Sediment Mixture Creation

From the collected samples, manual mixtures are created with known contribution ratios (M_1, M_2, M_3… M_n). These mixtures serve as controlled samples.

Phase 3 - Unmixing Model Application

The known mixtures are then subjected to one or more unmixing models (UM). These models are designed to statistically deduce the contribution of each source to a mixture.

Phase 4 - Model Performance Analysis

The results from the unmixing models are analyzed to assess the models' performance. This is done by comparing the known contribution ratios (from the manual mixtures) to the estimated contributions derived from the unmixing models.

Phase 5 - Model Validation

If the unmixing models' estimates closely match the known ratios, the model is considered validated. This means that the model is likely to be reliable for determining the contributions of different sediment sources in natural environmental samples

Figure I-17. Sediment Fingerprinting Approach Process.

I-5.2.3. Rating Curves and Hysteresis Analysis

Streamflow and sediment transport exhibit a direct relationship, prompting studies to analyze their correlation across various time scales (i.e., event, season, and year) using different time resolutions. Sediment rating curves, commonly established to depict the relationship between discharge and sediment concentration, are often in the form of power or log functions (e.g., Asselman, 1999; De Girolamo et al., 2015; Dickinson & Bolton, 1992; Fan et al., 2013; Irvine & Drake, 1987; Marttila & Kløve, 2010; Megnounif et al., 2007; Megnounif & Ouillon, 2018). Despite their simplicity, sediment rating curves face several challenges, including accuracy issues and an inability to explain the scatter around the curve due to spatiotemporal variations in sediment erosion and transport processes (Asselman, 1999; Vercruysse et al., 2017). This observation was highlighted by Dickinson & Bolton, (1992), stating that this issue is due to the hysteresis effect.

Hysteresis effect, observed when concentrations during the rising stage of flow differ from those during the falling stage, presents a challenge to sediment rating curves. Hysteresis analysis has emerged as a powerful tool to address these challenges where they have been useful in studying the different materials (as concentration) carried by natural flow (e.g., Andrea et al., 2006; Aubert et al., 2013; Bača, 2008; Eludoyin et al., 2017; S. D. Keesstra et al., 2019; L. A. Rose et al., 2018; S. Rose, 2003; Sherriff et al., 2016; Tananaev, 2015) allowing for a more nuanced understanding of sediment mixing dynamics. Indeed, early applications of hysteresis analysis to identify sediment sources and understand sediment transport patterns date back to 1956 (e.g. Dickinson & Bolton, 1992; Heidel, 1956; Irvine & Drake, 1987; Megnounif et al., 2013; Peart & Walling, 1982). Determining sediment sources through hysteresis analysis is an inductive method that requires knowledge of how different sources affect hysteresis loops. Quantifying sediment sources based on hysteresis analysis is not straightforward, and few methods have been developed for this purpose (e.g., Khettab, 2022; Megnounif et al., 2013). Khettab, (2022) notes that such methods give limited information about sediment sources compared to other approaches. Despite its challenges, hysteresis analysis remains a valuable tool in sediment transport studies, with detailed discussions to follow in subsequent chapters.

Chapter 2

The Sediment Concentration – Discharge Relationship

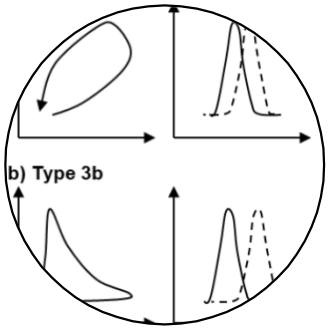

Concentration-Discharge

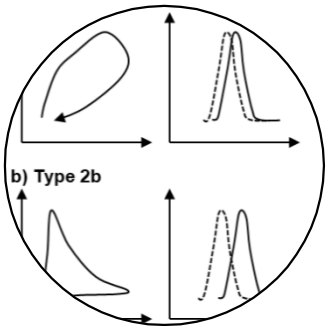

Hysteresis Loops

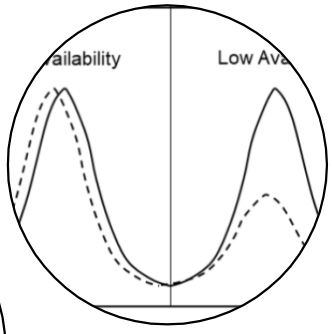

Sediment Availability

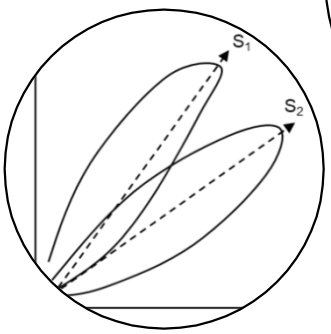

Sediment Sources

II. Chapter 2 – The Sediment Concentration – Discharge Relationship

II-1. Introduction To the Concentration – Discharge Relationship

The relationship between sediment concentration (C) and water discharge (Q) is crucial for understanding sediment transport dynamics in hydrological studies. Traditionally, this relationship has been described using sediment rating curves, which present significant challenges due to inherent inaccuracies and variability. Asselman, (1999, 2000) highlighted that errors in C-Q correlations can reach up to ±50%, often resulting in underestimations of sediment transport rates during low flows and overestimations during high flows. However, long-term observations suggest these discrepancies might balance each other out (Wolf et al., 2023).

Shields' (1936) concept of excess shear stress forms the basis for understanding sediment transport mechanics. It defines excess shear stress (τ^*) as the difference between the actual shear stress (τ) and the critical shear stress (τ_c) needed to initiate sediment movement.

$$\tau^* = \tau - \tau_c \qquad \text{(Equation II.1)}$$

This distinction is pivotal in predicting whether sediment transport will occur under specific flow conditions. However, additional equations are needed to quantitatively predict sediment transport rates (e.g. Bagnold, 1997; Brown, 1950; Einstein, 1942; Meyer-Peter & Müller, 1948). Among such equations the Meyer-Peter Müller Equation stands out:

$$q_s = \alpha \cdot (\tau - \tau_c)^{\beta} \qquad \text{(Equation II.2)}$$

Where:

- q_s is sediment transport rate per unit width.
- $\alpha \; and \; \beta$ are empirical coefficients

By substituting τ^* from Eq. II. 1 into Eq. II. 2, we derive:

$$q_s = \alpha \cdot \tau^{*\beta} \qquad \text{(Equation II.3)}$$

It is widely known that sediment discharge (Q_s), the total sediment transported per unit time, is also related to flow discharge (Q) through a power-law relationship:

$$Q_s = k \cdot \mathrm{Q}^{m+1} \quad \text{or} \quad C = k \cdot \mathrm{Q}^{m} \qquad \text{(Equation II.4)}$$

Where: k and m are empirical coefficients that encapsulate the effects of channel geometry, flow characteristics, and sediment properties in a generalized way.

While these equations are similar in structure, Eq. II. 4 is preferred due to its direct use of easily obtainable flow characteristics without compromising the essential physics of sediment movement.

However, assuming a strict correlation between suspended sediments and discharge oversimplifies the complexity of the C-Q response, ignoring multiple factors that influence sediment movement and leading to spurious correlations (McBean & Al-Nassri, 1988; Wolf et al., 2023). The inability of sediment rating curves to accommodate variations in erosion and transport processes contributes to the scatter observed around these curves, which Dickinson & Bolton, (1992) attributed to the hysteresis effect.

Hysteresis in the C-Q relationship represents a lagged response of sediment concentration to changes in water discharge, indicating a complex interaction between these variables. This asynchrony emerges from dynamic sediment availability, channel morphology, and other factors (Gharari & Razavi, 2018; Hamshaw et al., 2018; Prowse, 1984; Seeger et al., 2004; Zuecco et al., 2016). Phillips, (2003) suggests that hysteresis occurs when a single discharge value corresponds to multiple sediment concentrations, highlighting the complexity of the C-Q relationship.

Since the works of Haines, (1930), Marshall, (1933), and Richards, (1931) Hysteresis effect has been widely observed and documented (e.g., Aich et al., 2014; Bača, 2008; Chalov et al., 2012; Eder et al., 2010; Hamshaw et al., 2018; Khettab, 2022; Malutta et al., 2020; Megnounif et al., 2013; Misset et al., 2019; Moog & Whiting, 1998; Oeurng et al., 2010; Pietroń et al., 2015; R. Chalov et al., 2015; Seeger et al., 2004; Vale et al., 2016) spanning thousands of studies across a wide spectrum of meteorologic and geomorphologic conditions.

The complexity of this relationship is further compounded by seasonal variations, which exacerbate the scatter in sediment concentration predictions and influence hysteresis patterns in sediment transport dynamics (e.g., Megnounif et al., 2013; Oeurng et al., 2010; Wolf et al., 2023).

Such observations emphasize the need to consider a broader range of factors controlling sediment supply and transport in fluvial systems.

In summary, the limitations and challenges associated with using sediment rating curves for predicting sediment transport rates—accentuated by the hysteresis effect—call for a more nuanced approach. Recognizing the complex interdependencies within the C-Q relationship is essential for developing more accurate and reliable models for sediment transport prediction.

II-2. Hysteresis Patterns

In general, C-Q hysteresis loops have 4 traits: (1) the form, (2) the area, (3) the rotation, and (4) the slope (Aguilera & Melack, 2018). G. P. Williams, (1989) advanced a systematic description and classification of hysteresis relationships using five classes : (1) single-valued line, (2) clockwise, (3) anticlockwise, (4) single line plus loop, and (5) the figure-eight. Other forms exist but are not as widely used as these forms. Indeed, subsequent studies have expanded on this classification focusing on variations of classes (1) and (2) or multipeak hydrologic events (e.g., Gao & Josefson, 2012; Hamshaw et al., 2018; Nistor & Church, 2005; Tananaev, 2015).

II-2.1. Single-Valued Line

The single-valued line (or curve) is the simplest form among C-Q patterns (Figure II-1). Its unique characteristic is that for the same value of Q, the concentration on the hydrograph's rising limb equals the concentration on the falling limb (G. P. Williams, 1989). Three subgroups of this single-valued-line class are the straight line, the curve bending upward, and the curve bending downward (G. P. Williams, 1989). In all three subgroups, the relationship is positive (i.e., positive slope or C increases as Q increases).

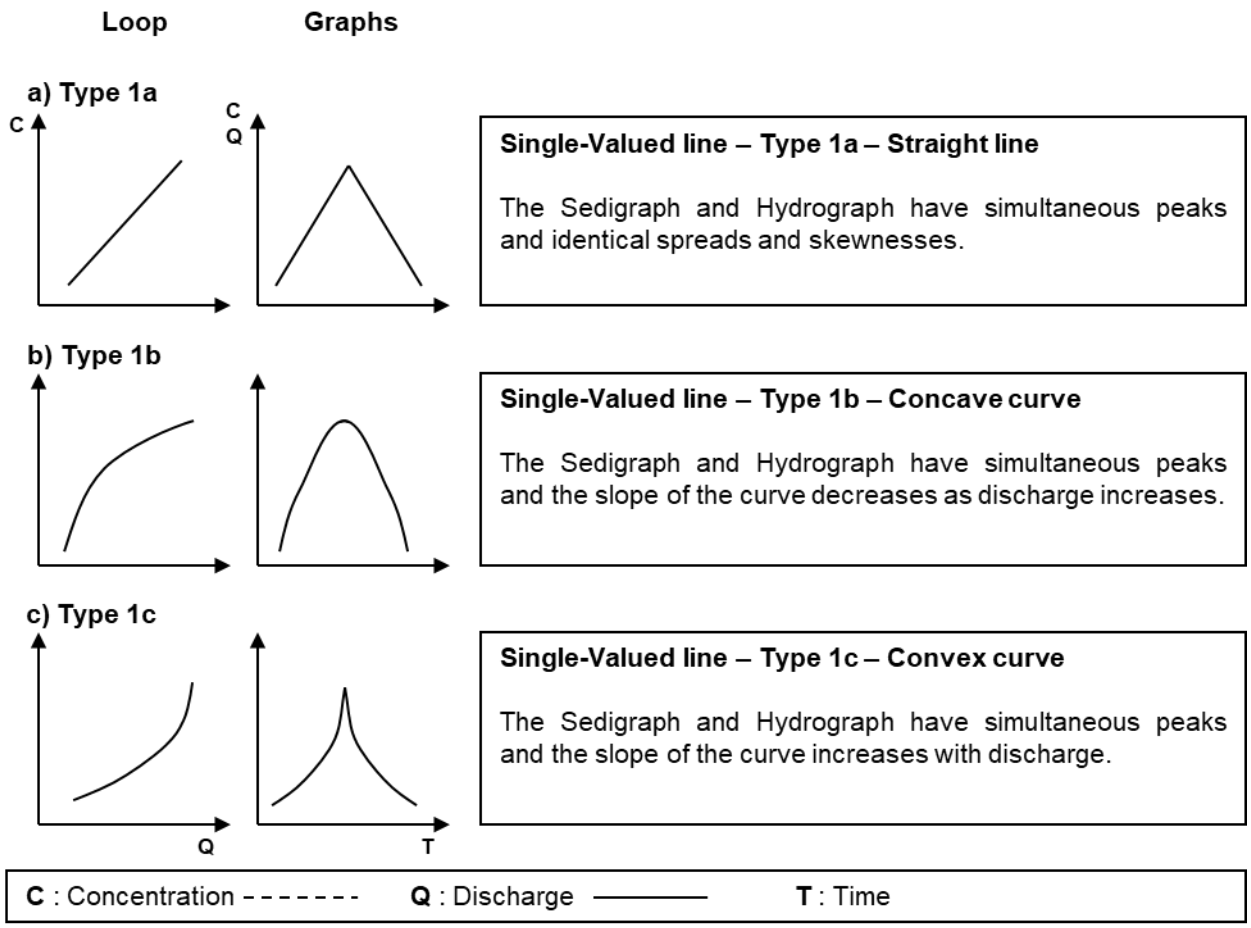

Figure II-1. Single-Valued line Concentration-Discharge Relationship.

II-2.2. Clockwise Loop

Clockwise loop, the most observed pattern among C-Q relationships (e.g., Aich et al., 2014; Hudson, 2003; Olive & Rieger, 1985), occurs when for all values of Q, the concentrations on the hydrograph's rising limb are higher than the concentrations on the falling limb (note: must exceed error margin). There exist multiple subgroups for this class of C-Q relationships depending on the timing of the concentration peak in comparison with hydrograph peak (Figure II-2).

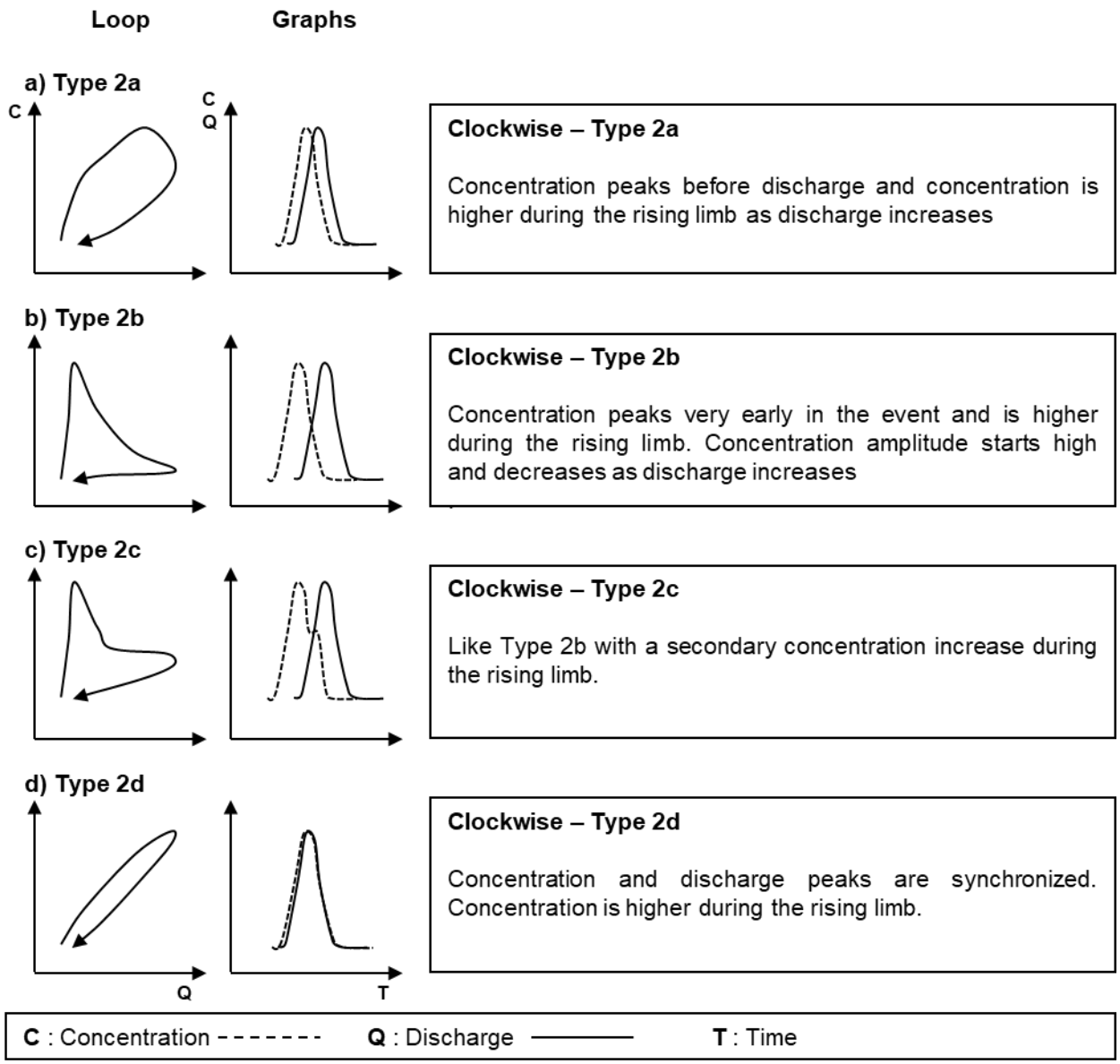

Figure II-2. Clockwise Concentration-Discharge Hysteresis Relationship – A Few Variations.

II-2.3. Anticlockwise Loop

Anticlockwise loops, commonly observed pattern, occurs when for all values of Q, the concentrations on the hydrograph's rising limb are lower than the concentrations on the falling limb. Depending on the timing of the concentration peak compared to the hydrograph peak, multiple subgroups for this class were reported (Figure II-3).

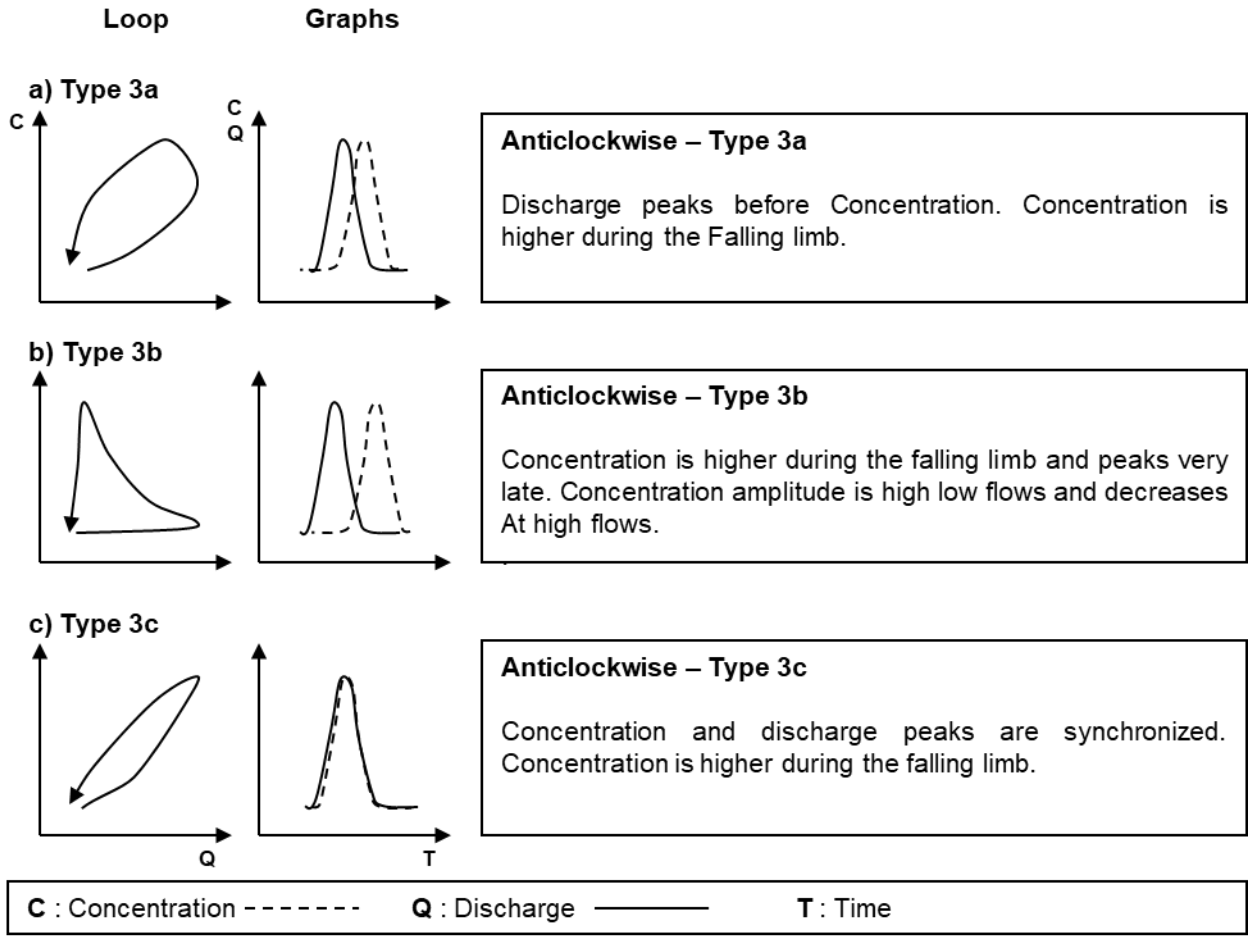

Figure II-3. Anticlockwise Concentration-Discharge Hysteresis Relationship – A Few Variations.

II-2.4. Single-Valued Line Plus Loop

Single-Valued Line plus Loops (Figure II-4) combine a single-valued line plus a clockwise or an anticlockwise sub-loop (Lloyd et al., 2016b; Megnounif et al., 2013; Yang & Lee, 2018). This

type of loop usually describes loops that have single-valued line at high flows and a loop at high flows. In other words, for low flows the concentration is similar whereas the concentration is different at high flows for the rising and falling of the hydrograph.

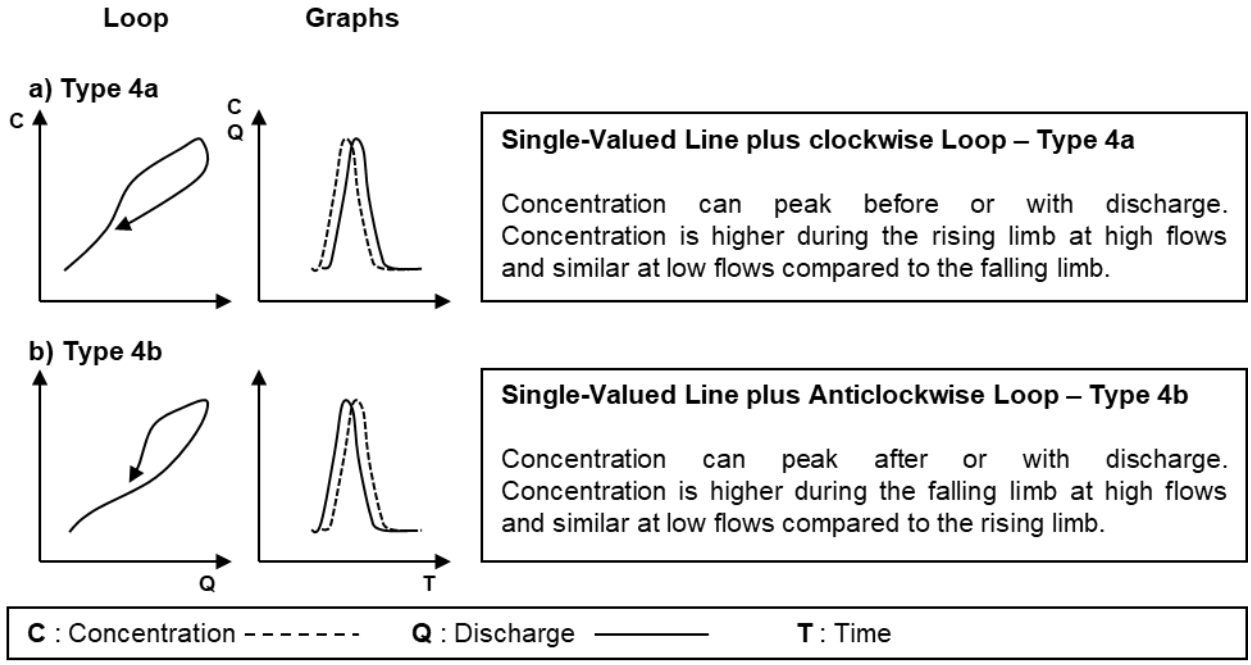

Figure II-4. Single-Valued Line Plus Loop Concentration-Discharge Hysteresis Relationships.

II-2.5. Figure of Eight Loop

Figure-of-eight loops (Figure II-5) combine clockwise and an anticlockwise subloop, caused by a shift in the form of the relationship between discharge and suspended sediment concentration during a single event (Lloyd et al., 2016b; Megnounif et al., 2013; Nadal-Romero et al., 2008; Nu-Fang et al., 2011; Seeger et al., 2004; G. P. Williams, 1989; Yang & Lee, 2018). Two sub-forms are commonly observed. The first has a clockwise subloop at low flows and an anticlockwise subloop at high flows whereas the order is reversed for the second.

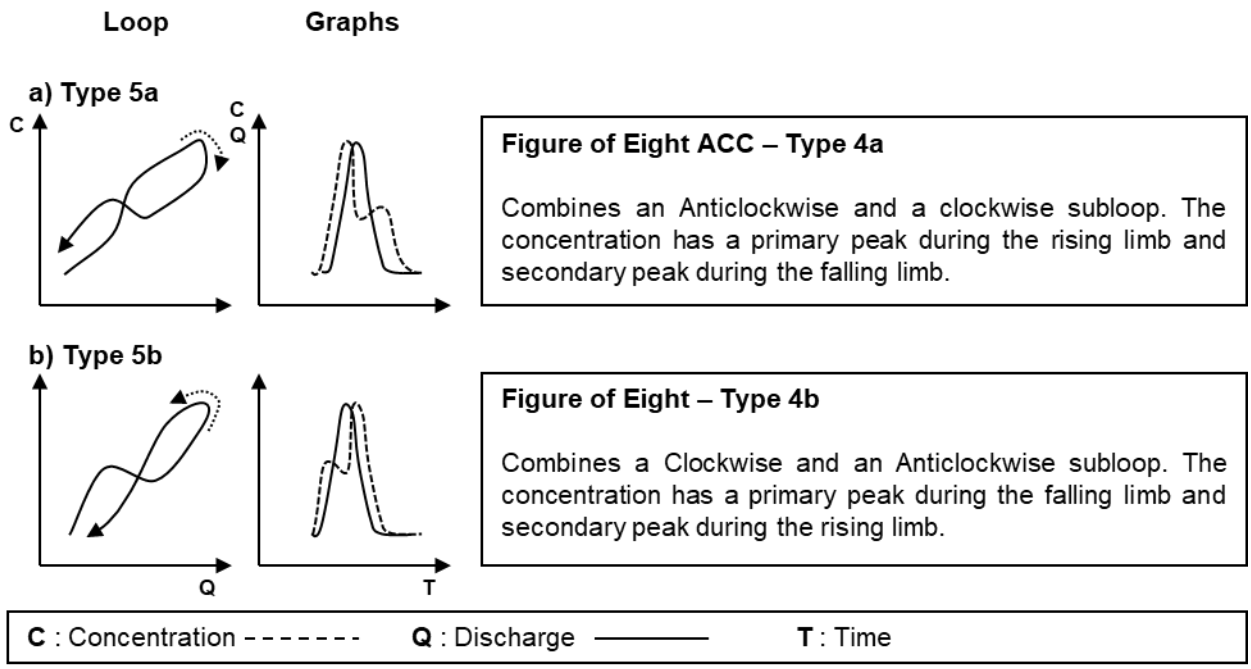

Figure II-5. Figure of Eight Concentration-Discharge Hysteresis Relationships.

II-2.6. Random and Other Hysteresis Patterns

There exist various other patterns that do not fit into the established classifications. These random or other hysteresis patterns may exhibit unique characteristics or combinations of behaviors that defy or are difficult to fit in a simple categorization. While less prevalent and less well-defined, these patterns still useful in the understanding of the complexities of sediment transport dynamics.

II-3. Factors controlling C-Q Hysteresis Configuration

The relationship is a direct function of the climatic and physiographic traits that regulate the transport regime throughout a hydrologic event. As established by Wilson, (1990), hydrograph morphology is governed by meteorological variables—including precipitation intensity and spatial coverage—alongside topographic and lithological factors such as catchment gradient and soil composition. In contrast, the sedigraph demonstrates heightened complexity due to the non-linear

interactions of sediment production, provenance availability, and the transient cycles of entrainment and deposition.

Sediment availability is considered a key factor influencing C-Q patterns (e.g. Asselman, 1999; Aubert et al., 2013; Buendia et al., 2016; Gao & Josefson, 2012; Lloyd et al., 2016a). Sediment availability and depletion is affected by several factors such as sediment production and transport patterns (i.e., the magnitude and frequency of flood events). There are other factors that influence the C-Q hysteresis form such as sediment sources proximity and basin size.

II-3.1. Sediment Production

Rovira & Batalla, (2006) describes a seasonal trend where sediment transport has two phases: (1) sediment preparation and (2) sediment mobilization and depletion. The first phase takes place during the period separating flow events, during which sediment availability is replenished. If the conditions permit it, sediment availability is increased at the start of storm through rainfall impact while some more sediments are produced (i.e., detached) during transport due to water stressing (see production processes in Chapter I).

The first part of sediment production consists of sediments that are produced independently of flow, denoted Independent Production (I_p). These sediments encompass hillslope, depositional, channel storage, Exo-basin (wind imported), and accidentally produced sediments (i.e., bank collapse and mass wasting sediments). The second part consists of sediments whose production depends on flow, denoted Dependent Production (D_p). The part of sediments is mainly associated with the erosion of the channel network.

Mathematically, sediment concentration (C) can be expressed with the following equation

$$C = \%I_p + \%D_p \qquad \text{(Equation II.5)}$$

Where:

- **$\%D_p$**: This variable is the percentage of transported sediment whose production is directly influenced by the flow rate. A higher $\%D_p$ indicates a strong input from the channel network.

- **$\%I_p$**: This variable is the percentage of transported sediment whose production is independent of the flow rate.

If we assume that channel network does not undergo a significant change during an event, leading to an alteration in the sediment production function associated with flow induced channel erosion, then $\%D_p$ is a linear relationship dependent upon the flow rate (as demonstrated in section II.II-1). As a result, EQ. 5 becomes:

$$C = \%I_p + a \cdot Q^{*b} \qquad \text{(Equation II.6)}$$

Where:

- Q is water discharge.
- a and b are empirical coefficients.

As a result, the portion of sediments whose production is independent of flow is the main component that causes the hysteresis effect. The manner this portion of sediments affects sediment availability, and as a result the C-Q patterns, is a function of transport patterns or events magnitude and frequency.

II-3.2. Sediment Transport Patterns

One crucial concept in sediment transport is transport capacity, which can be defined as the maximum amount of sediment that a flowing water body can carry under a given set of hydraulic conditions. Transport capacity is influenced by factors such as flow velocity, channel slope, sediment size, and water discharge. Essentially, it represents the ability of the flowing water to entrain, transport, and deposit sediment particles. In the other hand, Sediment Availability encompasses the total quantity of transport-ready sediment present in a basin. These sediments originate from various sources, including weathering and erosion of rocks and soils, human activities such as construction and mining, as well as biological processes.

In transport-limited settings, rivers have more sediments than they can carry, especially during floods or high flows. In other words, sediments are highly available whereas river flow lacks the capacity, due to the short duration or the magnitude of floods. This causes sediments to accumulate in the riverbed and floodplains, as the river cannot transport all the sediments it

receives. Over time, these accumulations can change the river's course, increase flood risks by elevating the riverbed and surrounding areas or create new sediment sources (sediment storage) for subsequent more potent floods. Conversely, in supply-limited situations, sediments are scarce, but the river has the capacity to carry more. This often happens when human activities, like dam construction or sediment extraction, reduce sediment supply, when a flood occurs in close succession to the previous, or when the flood is long and has sufficient magnitude to deplete sediments. Despite the lack of sediments, the river's ability to transport material leads to the erosion of riverbanks and beds. These terms describe the two ends of a spectrum that controls how sediment is moved and deposited in fluvial environments.

The response of a given basin lays somewhere in this spectrum. During the second phase reported by Rovira & Batalla, (2006) (i.e., sediment transfer and depletion), the exhaustion of the sediments is affected by flood events frequency (Malutta et al., 2020; Rovira & Batalla, 2006). Bača, (2008) argues a events' sediment transport is affected by the period separatin it from the previous one. Figure II-6 shows the succession of three floods. Flood 1 starts when sediment availability is high whereas Flood 2 starts in quick succession. Flood 3 takes a sufficient period to start. Flood 2 has a lower magnitude because sediments were exhausted during Flood 1. However, Flood 3 has a high magnitude due to the period separating it from Floods 1 and 2. Accordingly, if sediment supply will be replenished after some time has passed (Khettab, 2022; Malutta et al., 2020). Antecedent Dry Days, the number of days between events, is used in the sequential analysis of events. It indicates the length of the period of sediment preparation (e.g., sediment production by weathering) and thereby gives an insight into sediment availability. Many authors described sediment depletion within successive events (e.g., Khettab, 2022; Malutta et al., 2020; Nistor & Church, 2005; Olive & Rieger, 1985; Wood, 1977). Such events show a higher concentration during primary floods compared to subsequent ones desmontrating how a flood sequence afects sediment availability.

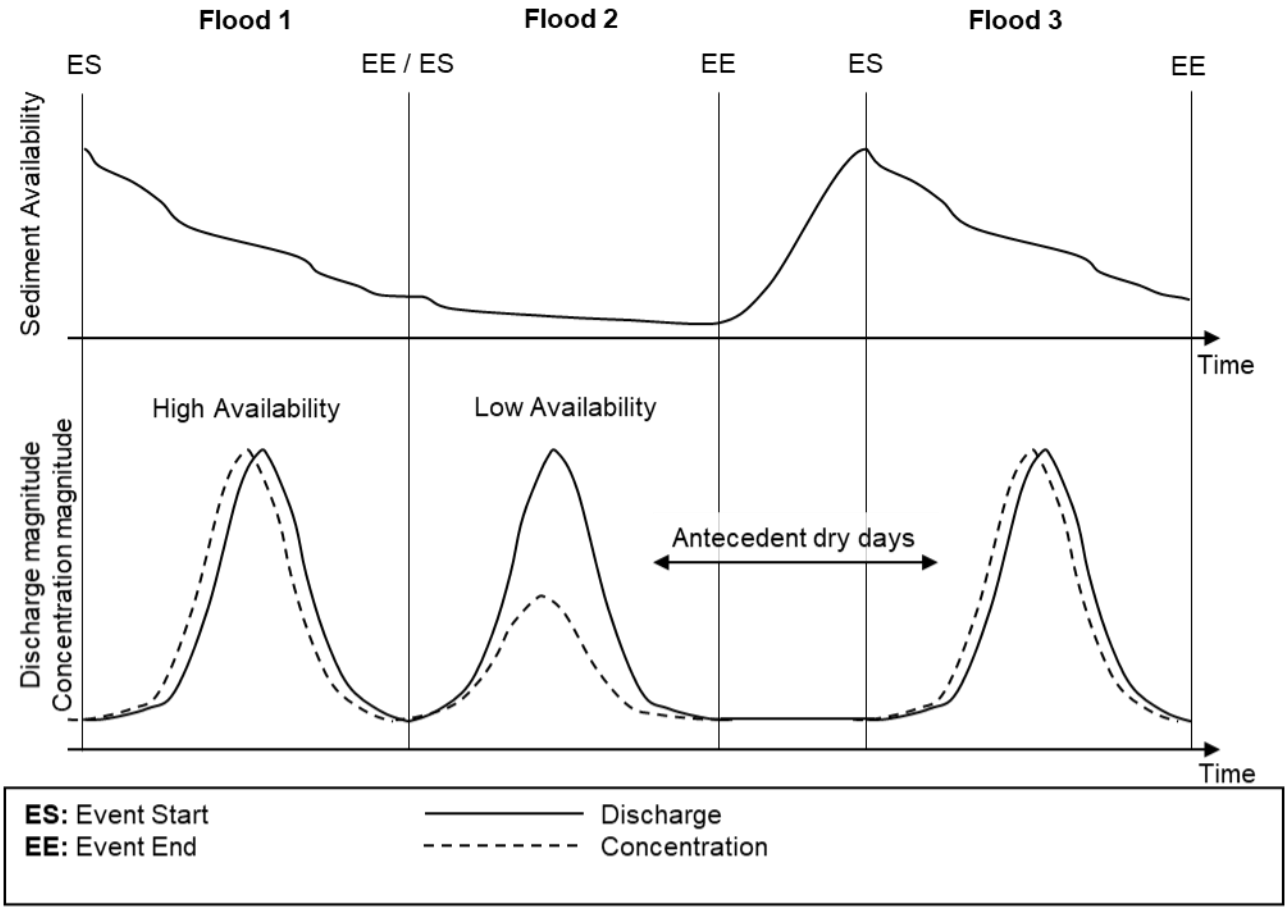

Figure II-6. Relationship between Flood events succession and Sediment Availability.

II-3.3. Other Factors

II-3.3.1. Particle Size

Sediment particle size gives insight into what is available for transport. For instance, fine particles are easily transportable. Hudson, (2003) reported that clockwise loops are due to a higher supply of washload from the nearby hillslopes. Fine sediments are usually responsible for early sediment concentration peaks due to their transportability. According to Lenzi & Marchi, (2000) and Malutta et al., (2020) the concentration of fine sediments lowers as discharge increases relative to the sediment source' particle size. Malutta et al., (2020) and Salant et al., (2008) reported that sand supply replenishes easily, something that does not occur in gravel-dominated basins.

II-3.3.2. Sediment Sources Proximity

The configuration of C-Q hysteresis loops is heavily affected by the proximity of sediment sources. For instance, input from sediment storage and areas close to the streamgage has been reported to result in an early concentration peak (Beel et al., 2011; Buendia et al., 2016; De Girolamo et al., 2015; Klein, 1984; McDonald & Lamoureux, 2009; Megnounif et al., 2013; Nadal-Romero et al., 2008; Nu-Fang et al., 2011; Oeurng et al., 2010; Pietroń et al., 2015; Salant et al., 2008; Seeger et al., 2004; H. G. Smith & Dragovich, 2009; Ziegler et al., 2014). In contrast, remote sediment sources are associated with delayed concentration peaks, mainly due to the long distances sediments have to cover before reaching the streamgage (Asselman, 1999; Beel et al., 2011; Buendia et al., 2016; De Girolamo et al., 2015; Duvert et al., 2010; Heidel, 1956; Hudson, 2003; Klein, 1984; Lenzi & Marchi, 2000; McDonald & Lamoureux, 2009; Megnounif et al., 2013; Rodríguez-Blanco et al., 2010; Seeger et al., 2004; Tian et al., 2016; Ziegler et al., 2014).

II-3.3.3. Basin Size and Meteorology

According to H. G. Smith & Dragovich, (2009) Hysteresis patterns are dependent on the characteristics of the basin, namely its size. For instance, a small basin favors sediment source proximity whereas a large basin creates both proximity and remoteness of sediments sources. For instance, Hudson, (2003), in a 98 227 km² basin, identified counterclockwise hysteresis because of the long distance sediments have to travel making the sediment wave travel slower than the discharge wave. Indeed, the spatiotemporal heterogeneity of a basin increases with its size. The C-Q configuration can cease being controlled by sediment availability and depletion of sediment sources. Hence, it becomes essential to identify which sub-basin contributes water and sediments and how each basin influences the hysteresis pattern. (Vercruysse et al., 2017).

As basin size increases, the spatial distribution of rainfall patterns becomes more pronounced. However, the effectiveness of rainfall parameters, including intensity and duration, remains critical. For instance, flash floods, characterized by sudden and intense rainfall lasting from minutes to a few hours, are often associated with meteorological phenomena such as convective storms and tropical cyclones. The swift accumulation of rainwater results in rapid runoff and elevated discharge rates, causing abrupt rises in water levels and swift flow velocities. While flash floods can inflict significant damage and transport substantial sediment loads, their brief

duration often allows for sediment settling in the channel. Conversely, longer duration and moderately intense rainfall events produce more evenly distributed hydrographs. These prolonged hydrological events are sufficient to deplete sediment availability within the basin within their span.

II-4. Hysteresis Analysis

The application of hysteresis analysis relies on the premise that C−Q relationships are determined by the location and nature of runoff generation and sediment mobilization (e.g., Aich et al., 2014; Gao & Josefson, 2012; S. D. Keesstra et al., 2019). By examining the variations in these loop patterns, scientists have identified clear signatures related to sediment sourcing and transport pathways (e.g., Gao & Josefson, 2012; Hamshaw et al., 2018; Megnounif et al., 2013; Seeger et al., 2004). This methodological approach has been instrumental in verifying the processes that trigger hysteretic behavior (e.g., Duvert et al., 2010; Pietroń et al., 2015; Seeger et al., 2004) Consequently, interpreting these patterns serves a dual purpose: confirming experimental geomorphology theories and providing quantitative insights into the sediment connectivity and dynamics within a study watershed (e.g., Gellis, 2013; Sherriff et al., 2016; H. G. Smith & Dragovich, 2009).

The application of hysteresis diagnostics is vital for resolving the underlying mechanics of sediment delivery. Specifically, researchers utilize these loops to determine whether a watershed is governed by source availability or the hydraulic capacity for transport (e.g., Asselman, 1999; Duvert et al., 2010; Gao & Josefson, 2012). This framework has proven robust for identifying sediment sources, such as localized bank destabilization, and assessing the overall connectivity of sub-basins to the main channel.(e.g., Aich et al., 2014; Buendia et al., 2016; Duvert et al., 2010; Eaton et al., 2010; A. Hughes et al., 2012; Lefrançois et al., 2007; Sherriff et al., 2016; H. G. Smith & Dragovich, 2009; Ziegler et al., 2014), determine the primary sediment sources, such as bank erosion (e.g., Lefrançois et al., 2007; H. G. Smith & Dragovich, 2009). Recent developments have even enabled the numerical quantification of sediment contributions, allowing for a clearer mass-balance of particulates moving through the watershed (e.g., Khettab, 2022; Megnounif et al., 2013).

Moreover, research has demonstrated hysteresis analysis to be widely applicable, extending to other hydrological parameters and phenomena such as the relationships summarized in Table II-1.

Table II-1. Example Hysteresis relationships in Hydrology.

Parameter A	Parameter B	Example reference
Temperature	Runoff	Schaefli, (2016) Subehi et al., (2010)
Soil moisture	Runoff	Matgen et al., (2012) Spence, (2010)
Runoff	Water table	McGlynn et al., (2004)
Hillslope contribution	Runoff	McGuire & McDonnell, (2010)
Temperature	Water conductance Runoff	Kobayashi et al., (1999)
Precipitation	Runoff	Andermann et al., (2012)
Runoff	Water temperature	Piccolroaz et al., (2016) Subehi et al., (2010)
Runoff	Groundwater level	Covino & McGlynn, (2007) Piccolroaz et al., (2016)
Runoff	Nutrient loads	Aguilera & Melack, (2018) Lloyd et al., (2016) McDiffett et al., (1989)

II-4.1. Pattern Analysis

The hysteresis pattern analysis has been the main approach to study Suspended Sediment Concentration – Discharge relationships. Each shape has been attributed to certain phenomena and processes. It is worth noting that the causes leading to each hysteresis loop vary with climatic and watershed characteristics, hence the diversity of explanations given to each pattern in literature. Indeed, researchers have analyzed multiple potential processes that afect the C-Q configuration (e.g., Hamshaw et al., 2018; Lloyd et al., 2016; Rodríguez-Blanco et al., 2010, 2018; Sherriff et al., 2016; Wood, 1977). The analysis is accompanied with statistical analysis to correlate C-Q configurations and controlling factors (e.g., Principal Component Analysis) (e.g. Aguilera & Melack, 2018; Beel et al., 2011; Buendia et al., 2016; Gellis, 2013; Giménez et al., 2012; Haddadchi & Hicks, 2021; S. D. Keesstra et al., 2019; Nadal-Romero et al., 2008; Oeurng et al., 2010; Rodríguez-Blanco et al., 2018). The interpretations associated with each pattern are summarized in Table II-2.

Table II-2. Common Hysteresis Patterns Interpretations.

Class	Interpretations and causes	References
I	• Abundance of fine-grained sediments in the channel.	Lloyd et al., (2016a) Yang & Lee, (2018)
	• Discharge travel time equals the sediment travel time.	Hudson, (2003)
	• Low availability of fine sediment.	Rodríguez-Blanco et al., (2010) Walling & Webb, (1982)
	• Uninterrupted supply of sediment.	Nistor & Church, (2005) Olive & Rieger, (1985) Rodríguez-Blanco et al., (2010) Smith & Dragovich, (2009) Williams, (1989) Wood, (1977)
	• The entrainment of bed material of the channel rather than on the supply of hillslope sediments.	Hudson, (2003) Megnounif et al., (2013)
	• Small Events	Mossa, (1996) Rodríguez-Blanco et al., (2010)
II	• Mobilization followed by depletion of in-channel/nearby sediment sources/ Wash-load (exhaustion effect/ initial flush of sediments)	Aich et al., (2014 Asselman, (1999) Buendia et al., (2016) Gao & Josefson, (2012) Hudson, (2003) Lloyd et al., (2016a) Megnounif et al., (2013) Nadal-Romero et al., (2008) Nu-Fang et al., (2011) Peart & Walling, (1982) Pietroń et al., (2015) Rovira & Batalla, (2006) Seeger et al., (2004) H. G. Smith & Dragovich, (2009) Williams, (1989) Wood, (1977) Yang & Lee, (2018)
	• Formation of armored layer before peak discharge	Williams, (1989) Yang & Lee, (2018)
	• Bank erosion	Smith & Dragovich, (2009)
	• Increased base flow or arrival of fresh water after peak discharge / Snowmelt Runoff events (Dilution effect)	Asselman, (1999) Buendia et al., (2016) Gonzales-Inca et al., (2018) Nadal-Romero et al., (2008) Wood, (1977)

Table II-2. Common Hysteresis Patterns Interpretations (continued).

III	• Flood wave traveling faster than mean flow velocity/ sediment wave travels slower than the discharge wave	Heidel, (1956); Williams, (1989) Lloyd et al., (2016a)
	• High soil erodibility	(Williams, (1989) Yang & Lee, (2018)
	• Bed and/or bank erosion	Asselman, (1999) Hudson, (2003) Pietroń et al., (2015)
	• Distant sediment source/upstream tributaries/late sediment supply by the tributaries	Aich et al., (2014) Asselman, (1999) Bača, (2008) Buendia et al., (2016) De Girolamo et al., (2015) Duvert et al., (2012) Gao & Josefson, (2012) Heidel, (1956) McDonald & Lamoureux, (2009) Megnounif et al., (2013) Pietroń et al., (2015) Rodríguez-Blanco et al., (2010) Seeger et al., (2004) Tian et al., (2016) Williams, (1989) Ziegler et al., (2014)
	• Seasonal variability in rainfall and sediment production	Williams, (1989)
	• Exhaustion of sediment available due to previous event	Gao & Josefson, (2012) Marttila & Kløve, (2010)
	• Valley slopes form the most important sediment source	Chalov et al., (2017) Pietroń et al., (2015)
	• The distribution of non-uniform sediment yield in the basin	Williams, (1989)
	• Small events with high rainfall intensity and very dry soil conditions	Eder et al., (2010)
	• During winter freezing – river cross-sections are often fully closed with ice	Tananaev, (2015)
	• Bank-collapse	(Asselman, (1999) De Girolamo et al., (2015) Marttila & Kløve, (2010) Megnounif et al., (2013) Rodríguez-Blanco et al., (2010)
	• Very high moisture and high antecedent rainfall conditions	Seeger et al., (2004)

Table II-2. Common Hysteresis Patterns Interpretations (continued).

IV	• Sediment travel time is distinct from the flow travel time in separate runoff states • Occurs under extreme dry conditions	Yang & Lee, (2018) Seeger et al., (2004)
V	• Sediment depletion followed by a second sediment wave (Exhaustion followed by replenishment of sediments)	Beel et al., (2011) Megnounif et al., (2013) Nadal-Romero et al., (2008) Nistor & Church, (2005) Nu-Fang et al., (2011) Vanmaercke et al., (2010)
	• Ice breakup	Williams, (1989)
	• Delayed contribution of sediment from sub-basins	Bača, (2008) Eder et al., (2010)
	• Influences of drainage system	Eder et al., (2010)
	• Multiple peaks	Eder et al., (2010) Gao & Josefson, (2012) Tananaev, (2015)
	• Sediment contribution from the streambed and its banks	Eder et al., (2010) Tananaev, (2015)

II-4.2. Direction and Magnitude Analysis

Hysteresis Analysis was previously conducted qualitatively. Hysteresis patterns were plotted and classified visually. Direction and Magnitude were also described visually as small or large (e.g., Bowes et al., 2015; Butturini et al., 2008; Eder et al., 2010; Evans & Davies, 1998; Vale & Dymond, 2020). Although, these qualitative descriptions have generated many insightful inferences, they do not allow a direct comparison between events. To solve this issue, Andrea et al., (2006) proposed a semi-automatic index (ΔR) calculated with:

$$\Delta R = R \cdot Loop_{Area} \cdot 100 \qquad \text{(Equation II.7)}$$

Researchers must visually assess and manually assign the direction (R in the equation) of each hysteresis loop to the index. If the C–Q hysteresis is clockwise, then R = 1; if it is counterclockwise, then R = -1; and if the hysteresis is unclear or inexistant, R = 0. Accordingly, ΔR ranges between -100 and 100. This requires considerable time and effort when dealing with large datasets, prompting a more general, numerical method to better quantify hysteresis loops.

Langlois et al., (2005) proposed a general hysteresis index ($H_{Langlois}$) based on the area of the map. The index calculation is the ratio of the area below the rising limb (A_{Rising}) and the area below the falling limb ($A_{Falling}$):

$$H_{Langlois} = \frac{A_{Rising}}{A_{Falling}} = \frac{\int_{Q_{min}}^{Q_{max}} C_{Rising}}{\int_{Q_{min}}^{Q_{max}} C_{Falling}} \quad \text{(Equation II.8)}$$

The reference value for $H_{Langlois}$ is 1. Accordingly, when $H_{Langlois} > 1$ the hysteresis is clockwise, when $H_{Langlois} < 1$, the hysteresis is anticlockwise, whereas when $H_{Langlois} \cong 0$, the hysteresis is balanced or a single-valued line. Langlois et al., (2005) advised that this index should be used on basic or mono-directional hysteresis patterns (clockwise, anticlockwise, single-valued line, and single-valued line plus loop) its application on patterns that combine clockwise and anticlockwise parts (e.g., figure of eight) could be confusing.

Lawler et al., (2006) developed an index (H_{Lawler}) based on mid-point (i.e., $Q_{50\%}$where $Q_{0\%} = Q_{min}$ and $Q_{100\%} = Q_{max}$). The index is the ratio of concentrations on the rising and falling limb at the mid-point of discharge. The index is then determined, for clockwise hysteresis where the concentration on the rising limb ($C_{mid_{Rising}}$) is higher than the concentration on falling limb ($C_{mid_{Falling}}$), simply as:

$$H_{Lawler} = \frac{C_{mid_{Rising}}}{C_{mid_{Falling}}} - 1 \quad \text{(Equation II.9)}$$

or, when the hysteresis is anticlockwise, i.e., where $C_{mid_{Falling}} > C_{mid_{Rising}}$, as:

$$H_{Lawler} = 1 - \frac{C_{mid_{Falling}}}{C_{mid_{Rising}}} \quad \text{(Equation II.10)}$$

Aich et al., (2014) stated that this index becomes skewed at higher concentrations, with a smaller index calculated for loops of the same shape and loop area in case of storms commencing at a higher concentration (Figure II-7a). Lloyd et al., (2016a) stated that calculating this at the mid-point can be misleading exemplified by figure of eight loops especially those which cross close to the mid-point (Figure II-7b).

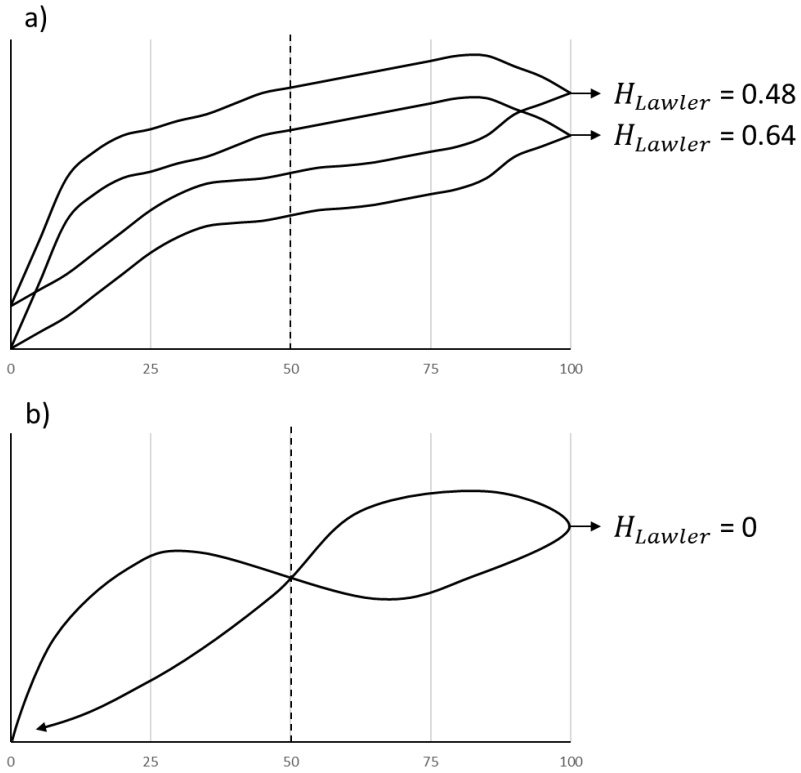

Figure II-7. Variations in H_{Lawler} values. a) Effect of initial values effect on H_{Lawler} where different values are associated with the same loop. b) Effect of a Figure of Eight loop that cross at (or close) to the mid-point effect on H_{Lawler}.

Aich et al., (2014) improved on this by proposing an index (H_{Aich}) using normalized values. The computation of the index consists of (1) splitting the hysteresis into a rising and falling curve by drawing a line that connects the concentration corresponding to Q_{max} and the concentration corresponding to the end of the event. Rectangular to this line, the maximum distance to the rising limb (D_{Rise}) and the falling limb (D_{Fall}), respectively are computed. Finally, hysteresis index is defined as:

$$H_{Aich} = D_{Rise} + D_{Fall} \qquad \text{(Equation II.11)}$$

The reference value for this index Is 0. For a clockwise loop, H_{Aich} is positive, for an anticlockwise loop it is negative.

These two indices (i.e, $H_{Lawler}$and H_{Aich}) (1) show the direction (sign) and magnitude in one single number, (2) they are dimensionless; and (3) they are straightforward and easy to compute. However, several points were raised regarding their limitations. Both Lloyd et al., (2016a) and Zuecco et al., (2016) agree that these indices did not consider complex forms (e.g., figure of eight). Additionally, they are positional indices. While H_{Lawler} is computed at the mid-point, H_{Aich} is computed on the largest section of the loop. Their positional nature can lead to an incomplete representation of hysteresis loops. To overcome these shortcomings, Lawler et al., (2006) suggested computing the index at multiple sections of the loop and use an averaged value to represent the event. However, Lloyd et al., (2016a) demonstrated that the index is still affected since it uses the ratio and the absolute values. Lloyd et al., (2016a) also demonstrated that it is more adequate to rely on normalized values.

Lloyd et al., (2016a) and Zuecco et al., (2016) proposed integrative (global) indices, H_{Lloyd} and H_{Zuecco} respectively, that consider multiple sections of the loop. For H_{Zuecco}, first, the definite integrals under the normalized rising and the falling limb for each interval (from 1 to k) are calculated. Then, for each interval, the difference between definite integrals from the rising and the falling limb are calculated. Finally, the index is simply the sum of these differences. On the other hand, H_{Lloyd} is the mean of the differences between normalized concentrations, described by the following equation:

$$H_{Lloyd} = \frac{1}{k}\sum_{i=1}^{k} C^{i}_{Normalized_{Rise}} - C^{i}_{Normalized_{Fall}} \qquad \text{(Equation II.12)}$$

Despite differences in the calculations the underlying idea of the quantification is identical. Both metrics have showed many advantages in application (e.g., Baker & Showers, 2019; Birkel et al., 2017; Lloyd et al., 2016b; L. A. Rose et al., 2018; Sherriff et al., 2016; Vaughan et al., 2017; M. R. Williams et al., 2018). While W. Liu et al., (2021) strongly recommends to use one of these two integrative indices, Hamshaw et al., (2018) showed that these indices do not offer a unique description for different hysteresis loops. Indeed, to observe the differences, researchers need to rely on the series of metrics representing each interval. Moreover, the sole use of normalized valued leads to a loss of information in the data compression and does not reflect the differences between events at a real scale. Among solutions, Misset et al., (2019) used a new weighted index to investigate the transport efficiency using the transported mass and H_{Lloyd}.

II-4.3. Hydro-Chemical Analysis – Loop Range and Slope Analysis

The slope describes the nature of the relationship between variables as positive (direct) for a positive slope (Figure II-8a) or negative (indirect) for a negative slope (Figure II-8b). Usually, the slope is related to the flushing index (e.g., Rose et al., 2018; Vaughan et al., 2017; Wymore et al., 2019) or the relative changes in solute concentration ΔC (Butturini et al., 2008). In solutes, negative slopes indicate solute dilution whereas a positive slope indicates solute flushing (Aguilera & Melack, 2018; Butturini et al., 2008; Lloyd et al., 2016b). Evans & Davies, 1998, Godsey et al., 2009, and Wymore et al., 2019 stated that the hysteresis slope is positive when material transport is considered transport-limited (flushing effect), negative where the transport of material is considered source limited (dilution effect), or chemostatic where concentrations are independent of discharge (horizontal slope). With suspended sediment concentration, the relationship is mostly positive. In this case, It is characterized by the slope steepness (Figure II-8c). Asselman, (1999) advanced that steep slopes are indicative of large quantities of sediment available for transport, whereas low slopes indicate a limited sediment availability.

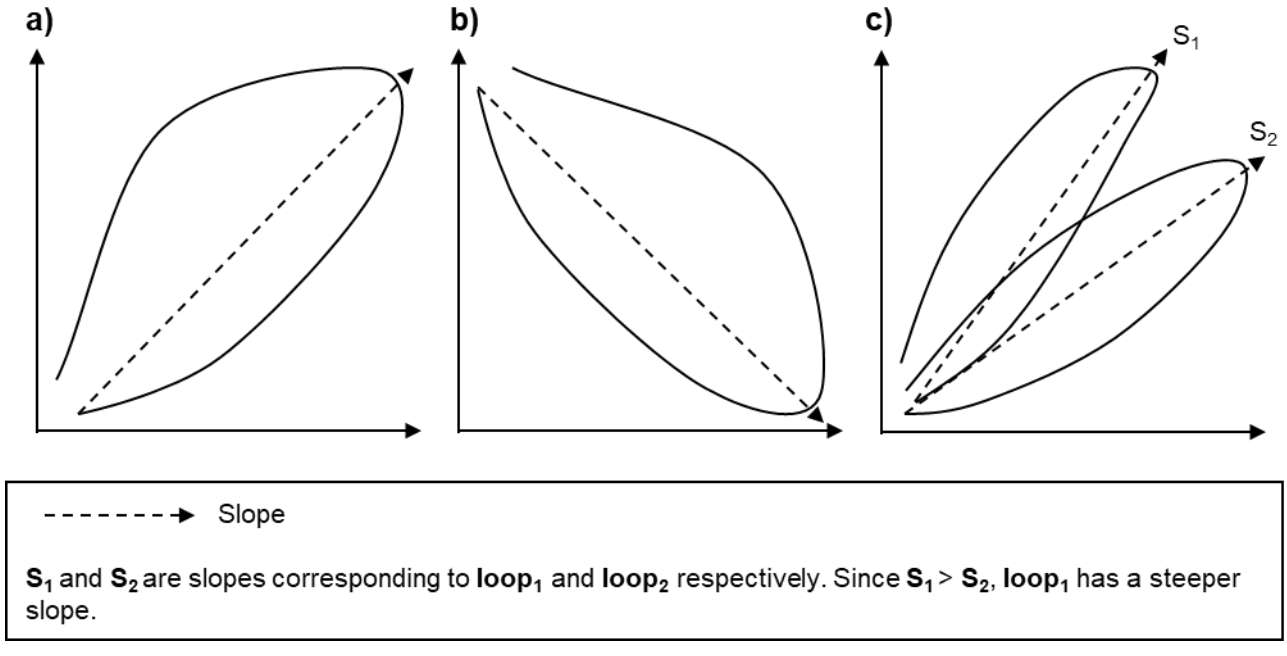

Figure II-8. Hysteresis Loop Slope Property.

II-5. Hysteresis Analysis Derived Applications

II-5.1. Hysteresis Classification

Hysteresis classification refers to the systematic categorization of hysteresis relationships based on one or multiple traits. These traits typically include pattern, rotation, size, and slope. Various classification schemes have been developed to classify hysteresis loops according to these traits:

a) **Pattern Classification:** This approach focuses on identifying recurrent forms of hysteresis patterns within the SSC-Q relationship.
b) **Size Classification:** Size classification categorizes hysteresis loops based on their magnitude or width. Loops may be classified as large, medium, or narrow, often using hysteresis indices.
c) **Rotation Classification:** Rotation classification assesses the directional rotation of hysteresis loops. This classification is also based on hysteresis indices and examines whether the loop rotates clockwise, anticlockwise, or exhibits a figure-eight pattern.
d) **Slope Classification:** Slope classification categorizes hysteresis loops based on their slope characteristics. Loops may be classified as positive, negative, or chemostatic, depending on the direction and steepness of the slope.
e) **Combined Classification:** Some classification schemes incorporate multiple traits to provide a comprehensive characterization of hysteresis relationships.

Several methods have been employed to classify hysteresis loops. For instance, G. P. Williams, (1989) proposed a systematic classification and description of the most recurring hysteresis patterns in literature in a time where works focused on specific forms (e.g., Olive & Rieger, 1985; Wood, 1977). The Williams classification consisted of the most recurrent forms at the time. However, due to necessity, this classification was later expanded upon (e.g., Butturini et al., 2008; Gao & Josefson, 2012; Hamshaw et al., 2018; Khettab, 2022; Nistor & Church, 2005; Tananaev, 2015; Zuecco et al., 2016). Hysteresis patterns are frequently inferred visually. However, with an increasing number of patterns in the classification (e.g., 14 forms in Hamshaw et al., (2018)), an increasing number of events, and larger datasets (e.g., Aguilera & Melack, 2018; Baker & Showers, 2019; Hamshaw et al., 2018; S. D. Keesstra et al., 2019), faster and reliable methods have become a necessity to classify hysteresis loops or to conduct hysteresis analysis in general.

Butturini et al., (2008) combined the hysteresis index (ΔR) and the relative changes in concentration (ΔC) to develop a 2-Dimensional diagram presentation to discriminate between different hysteresis patterns (Figure II-9). This method of combining a hysteresis index with ΔC or the flushing index proved to be an informative and a straightforward way to classify hysteresis loops (e.g., Aguilera & Melack, 2018; Darwiche-Criado et al., 2015; Strohmeier et al., 2013). Zuecco et al., (2016) utilized metrics such as the largest and smallest interval amplitudes and H_{Zuecco} to classify hysteresis loops. However, such methods still require additional effort (visual or manual). Moreover, many studies have considered hysteresis patterns with a negative slope as separate classes (e.g., Aguilera & Melack, 2018; Butturini et al., 2008; Lloyd et al., 2016b; Zuecco et al., 2016).

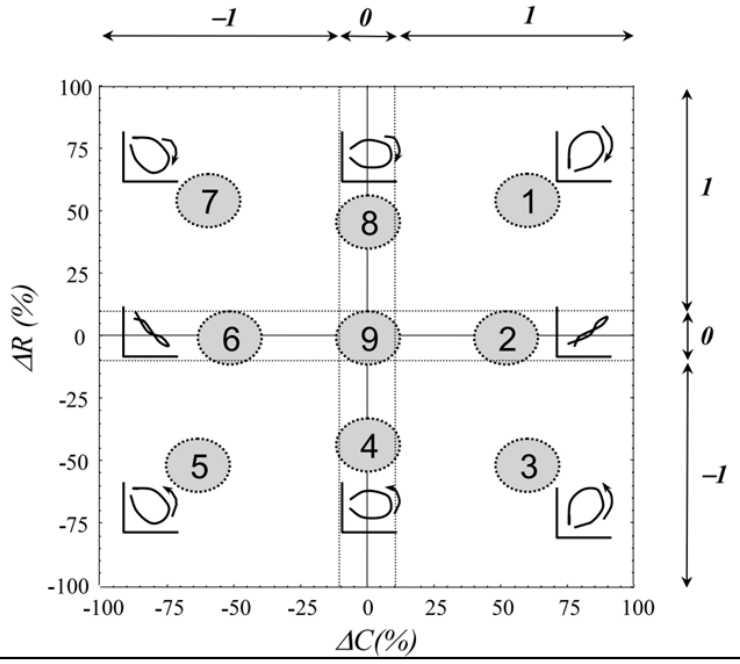

ΔR is the Hysteresis Index
ΔC the relative changes in concentration

Schematic representation of the unity plane **ΔC** versus **ΔR** that describes the diversity continuum across the geometrical forms of Concentration-Discharge responses. In this plane, the vertical and horizontal dotted lines delimit the nine discrete different types of Concentration-Discharge response.

Figure II-9. Hysteresis loop classification based on ΔR and ΔC as advanced by Butturini et al., (2008).

S. D. Keesstra et al., (2019) automated a method based on H_{Lloyd}. The method consists of computing the index for each discharge quartile and then based on the sign of the indices of each quartile the hysteresis pattern is identified (Table II-3). The authors were able to identify many patterns excluding some basic patterns (e.g., single valued line plus loop).

Table II-3. Event type separation procedure based on sign of H_{Lloyd} value for discharge quartiles (Q_u)

N°	H_{Lloyd} Q_u1	H_{Lloyd} Q_u2	H_{Lloyd} Q_u3	H_{Lloyd} Q_u4	Class
1	+	+	+	+	Clockwise
2	+	+	+	-	
3	-	+	+	+	
4	-	-	-	-	Anti-Clockwise
5	-	-	-	+	
6	+	-	-	-	
7	+	+	-	-	Figure of Eight
8	+	+	-	+	
9	+	-	-	+	
10	-	-	+	+	
11	-	-	+	-	
12	-	+	+	-	
13	+	-	+	+	Complex
14	+	-	+	-	
15	-	+	-	+	
16	-	+	-	-	

Hamshaw et al., (2018) proposed utilizing image-recognition techniques through a Restricted Boltzmann Machine (RBM) to streamline hysteresis analysis. This workflow requires predefining event shapes and training the algorithm on an established library before attempting automated classification. Despite demonstrating sensitivity to specific loop variants, the model showed a drop in accuracy from 85% in the training phase to 70% in application. A distinct advantage of this machine-learning approach is its potential for iterative improvement through continuous exposure to new events. However, the reported 8% error rate in directional classification presents a significant challenge that more training might not fully eliminate.

Ultimately, the RBM framework functions as a qualitative tool; consequently, the researchers utilized the H_{Lloyd} metric to calculate the actual geometrical intensity of the loops.

II-5.2. Sediment sources determination

II-5.2.1. Principle

Sediments carried by natural flow can originate from the river network (bed and bank erosion) and from the watershed. The combination of sediments from different sources often generates variability within the carried concentration (Gellis, 2013; G. P. Williams, 1989). While stream derived sediments' production and transport are fully dependent upon flow, catchment and storage sediments only depend on streamflow for transport, whereas their production (detachment) is function of various other processes (Chapter I). The second part of sediments is limited in terms of quantity and transfer. In other words, this portion of sediments' delivery into the stream can either be exhausted or interrupted (when transfer agents are ceased or lack the transport capacity). Hence, there is a direct causation between sediments from different origins and the hysteretic effect observed in the relationship.

As described above, sediment sources are qualitatively identified through pattern analysis. For instance, when the C-Q relationship showed a clockwise pattern, it was attributed to the mobilization and depletion of in-channel or nearby sediment sources (i.e., Wash-load, exhaustion effect, and the initial flush of sediments) (Aich et al., 2014; Asselman, 1999; Bača, 2008; Buendia et al., 2016; De Girolamo et al., 2015; Duvert et al., 2012; Gao & Josefson, 2012; Heidel, 1956; McDonald & Lamoureux, 2009; Megnounif et al., 2013; Pietroń et al., 2015; Rodríguez-Blanco et al., 2010; Seeger et al., 2004; Tian et al., 2016; G. P. Williams, 1989; Ziegler et al., 2014). Due to the difficulty of separating and quantifying different sediment sources directly from hysteresis analysis, the acquired information remained qualitative or based on separate methods.

II-5.2.2. Estimation Concept

Megnounif et al., (2013) developed an unmixing model, based on hysteresis analysis, to separate sediments into two portions: (1) sediments from the stream channel, and (2) sediments from the watershed surface, stream storage, and other sediment sources. The authors proceeded to

a sediment transport phase-by-phase breakdown, leading to the development of a mathematical model for several hysteresis loops, graphically simplified and represented in Figure II-10.

As explained in Chapter II – Section II-3.1, sediment can be divided into two categories based on the nature of their origin. The first category includes sediments produced independently of flow, such as those from hillslopes, depositional areas, channel storage, exo-basin (wind-transported) sources, and accidental events like bank collapse and mass wasting. The second category comprises sediments whose production is flow-dependent, primarily associated with the erosion of the channel network.

Khettab, (2022) mathematically represented the concentration of sediment recorded at the streamgage with the following equation:

$$C = \mathrm{ES} + P_Q \qquad \text{(Equation II.13)}$$

Where:

- **ES (External Sources)** represents the sediment produced independently of flow. This includes contributions from hillslopes, depositional areas, channel storage, exo-basin sources, and accidental sediments.
- **P_Q** denotes the sediment production from the stream channel. It is highly dependent on the erosive power of flow. Assuming a constant channel erosivity, the rersulting relationship is linear.

Both Megnounif et al., (2013) and Khettab, (2022) agree that the quantity of sediments delivered from external sources is limited by sediment availability as well as overland flow capacity and duration. In other words, these sediment sources can be exhausted when their availability is depleted, or their supply can be interrupted when transport agents stop or lose capacity. Meanwhile, the channel remains a continuous sediment source throughout a flood event. This implies that the status of external sediment supply (active, exhausted, or interrupted) causes the hysteretic effect observed in the Concentration-Discharge relationship. During certain periods of the event, external sediment supply may be inactive, making the channel the only active sediment source.

The authors suggest that this phase can be deduced from analyzing the hydrograph, sedigraph, and hysteresis loop. As shown in Figure II-10, there are two distinct flow phases:

- **Phase (a)** corresponds periods of transport when multiple sediment sources are active (Both ES and P_Q are active).

- **Phase (b)** corresponds periods of transport when the channel is the only active sediment sources (P_Q is active and ES ≈ 0).

In summary, when both ES and P_Q are active, sediment concentration is higher compared to when only P_Q is active. Therefore, the authors associate the lower bound curve of the hysteresis loop with the stream channel contribution, while the excess concentration (or loop area) is attributed to external sediment sources.

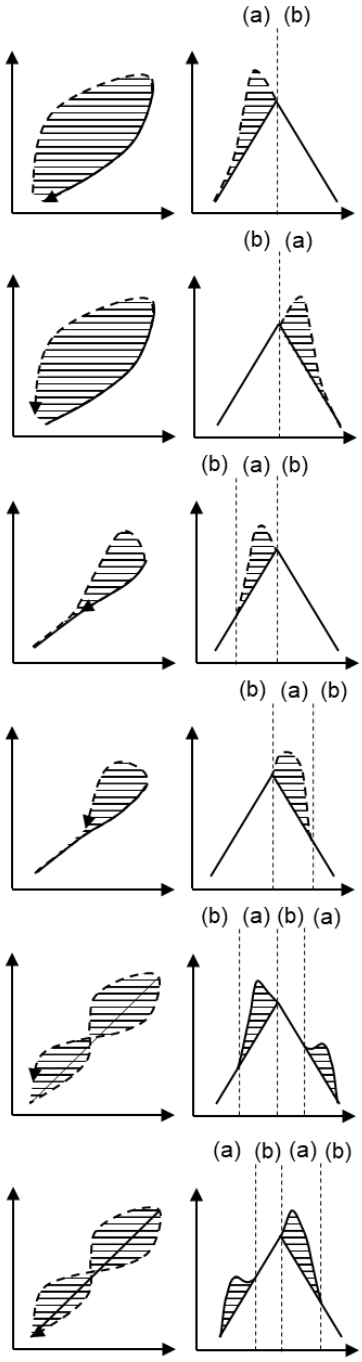

Sediment Sources Contribution

Clockwise	
Rising Limb	**Falling Limb**
• Channel Contribution • External Sources Contribution	• Channel Contribution

Anticlockwise	
Rising Limb	**Falling Limb**
• Channel Contribution	• Channel Contribution • External Sources Contribution

Single-Valued Line plus Clockwise Loop	
Rising Limb	**Falling Limb**
• Channel Contribution • External Sources Contribution (High flow Only)	• Channel Contribution

Single-Valued Line plus Anticlockwise Loop	
Rising Limb	**Falling Limb**
• Channel Contribution	• Channel Contribution • External Sources Contribution (High flow only)

Figure of Eight Anticlockwise-Clockwise	
Rising Limb	**Falling Limb**
• Channel Contribution • External Sources Contribution (High flow only)	• Channel Contribution • External Sources Contribution (Low flow only)

Figure of Eight Clockwise-Anticlockwise	
Rising Limb	**Falling Limb**
• Channel Contribution • External Sources Contribution (Low flow only)	• Channel Contribution • External Sources Contribution (High flow only)

Catchment, channel storage, and temporary sediment sources contribution (External Sources)

Channel contribution to suspended sediment concentration

Sedigraphs are split into transport phases (a) and (b) where:
(a) corresponds to phases of transport when multiple sediment sources are active
(b) corresponds to phases of transport when the channel is the sole sediment source

Figure II-10. Sediment sources contribution breakdown schematic as given by Megnounif et al., (2013)

II-5.2.3. Concept Criticism

The method might not be directly applicable since there is no general agreement on the factors behind of C-Q hysteresis patterns (Table II-2). For instance, while some agree that a sediment availability is the main factor, others attribute hysteresis effect to other factors including armored layer formation or breakage, bank erosion, and sediment dilution effect (Asselman, 1999; Buendia et al., 2016; Gonzales-Inca et al., 2018; Nadal-Romero et al., 2008; H. G. Smith & Dragovich, 2009; G. P. Williams, 1989; Wood, 1977; Yang & Lee, 2018). Indeed, the core of this concept is based on several conditions, each when not met lead to an inadequate sediment sources separation.

The first condition for the applicability of this concept is the absence of external sediment sources. However, this condition might not be met. Many studies have described cases where hysteresis loops in multi-peak and successive floods are stacked, with the hysteresis loop of the primary event being higher and having a steeper slope (e.g., Khettab, 2022; Nistor & Church, 2005; Olive & Rieger, 1985; Wood, 1977). In such cases, the contribution from external sources remains active, leading to an overestimation of the channel's contribution (Figure II-11a).

The second condition requires external sources to be the primary factor responsible for the hysteresis effect. This condition is not met when dilution effects occur. For example, Nadal-Romero et al., (2008) advanced that the clear water from forested headwaters can cause dilution without affecting the transported mass. Similarly, Wood, (1977) observed that increased groundwater input leads to the dilution of sediment concentration (Figure II-11b). However, it is crucial that the clean water input occurs close to the streamgage; otherwise, it will only dilute the external sediment supply.

The third condition requires the channel sediment contribution to have a linear relationship with discharge (Figure II-11c). This condition is not met when there is a significant change in the channel's contribution. Such changes can occur during a flood event due to factors like landslides, the formation or melting of glacier armor, or variations in stream erosivity during prolonged floods. These events cause significant alterations in the state of the stream, disrupting the linear relationship between the channel sediment contribution and discharge.

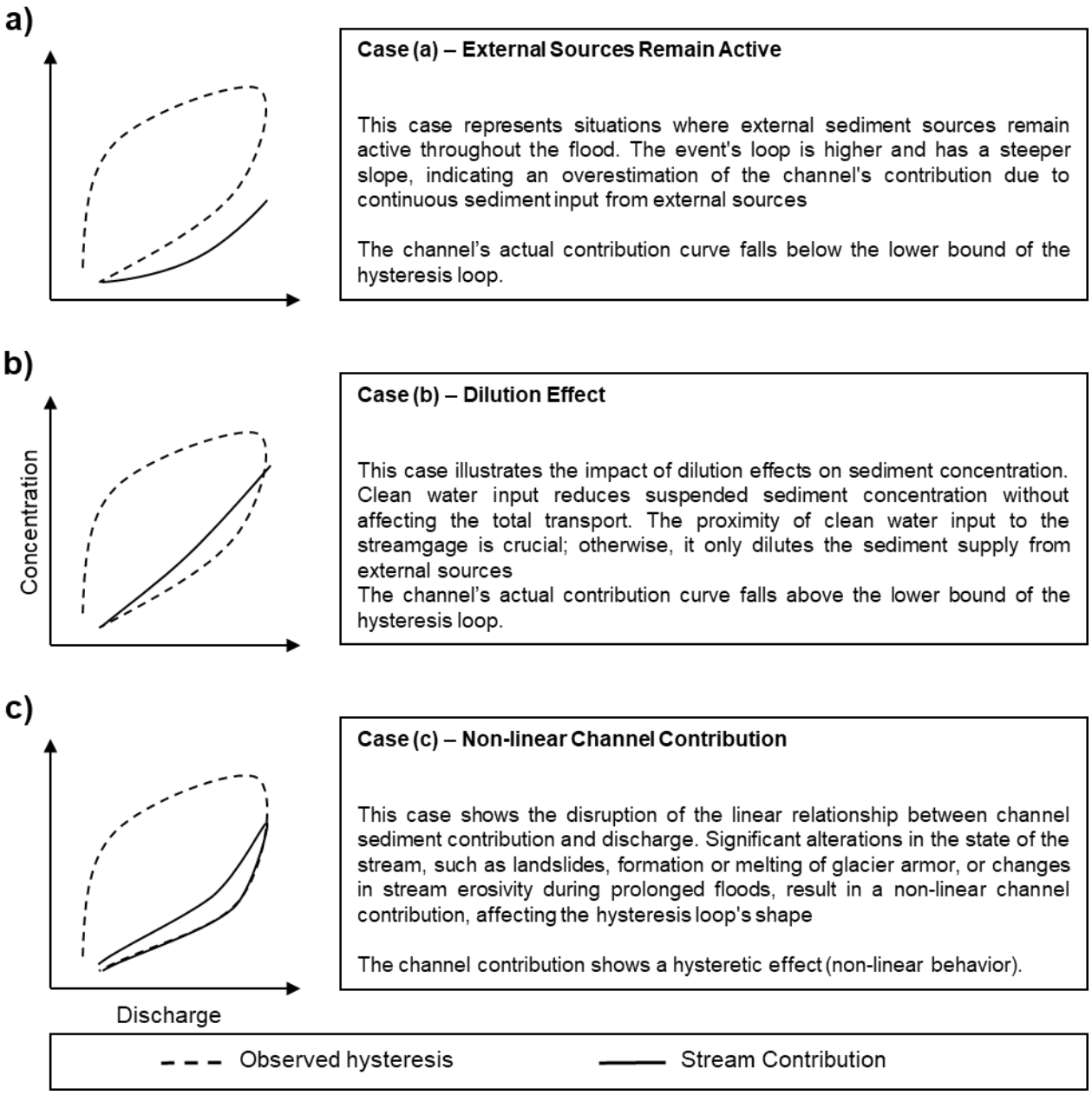

Figure II-11. Cases where the lower bound curve does not represent the stream contribution.

II-5.2.4. Concept Validation

For the concept to be applicable, all three conditions must be fulfilled. Verifying the inactivity of external sources is not straightforward. Except for cases showing a single-valued line behavior (fully or partially), there is no clear indication of external sediment sources being inactive

and that the lower bound of the hysteresis loop represents the channel contribution. Therefore, verification may require additional data, further analysis, and more adequate approaches.

Khettab, (2022) proposed a validation process using hysteresis analysis, specifically targeting situations where data is limited to discharge and concentration measurements. This validation process involves assessing multi-peak and successive floods. As shown in Figure II-6, when floods are sequential and sediment availability is the main controlling factor, the expected result is a decrease in concentration magnitude for the same discharge. Accordingly, the author proposed an indicator based on the slope of the normalized concentration by discharge ratio (Figure II-12a). A negative value indicates sediment depletion, whereas a positive value indicates sediment replenishment. This indicator highlights that sediment availability is the primary factor affecting the C-Q patterns.

The second part of the validation process is a visual inspection of hysteresis loops using multi-peak and grouped successive floods. After confirming sediment depletion, the visual assessment aims to identify one of two observations:

(1) **Shared Segment Observation:** When two or more flood events reach the depletion or interruption of external sediment sources, the loops of these individual flood events are expected to share a segment (Figure II-12b). Since the channel contribution is the sole common factor between these floods, and initial conditions are different, observing this shared segment indicates that the loop area is indeed associated with the contribution of external sources.

(2) **Single-Valued Curve Observation**: Continuous depletion throughout events leads to the appearance of a linear behavior in later events, positioned the lowest (Figure II-12c). When this case is observed, it indicates that the loop area reflects the contribution of external sources. Their depletion results in the stream channel becoming the only active sediment source, leading to the appearance of a single-valued line later on.

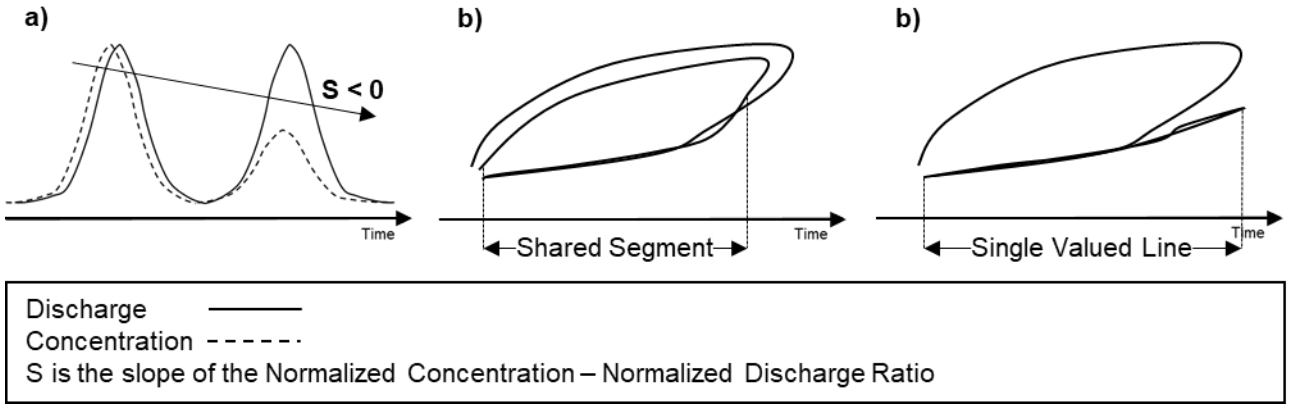

Figure II-12. Observations required for the validation of the Hysteresis Analysis based Unmixing Model.

These two observations confirm that, for a given discharge, the contribution of the channel bank and bed discrepancies for each discharge measurement are negligible. Consequently, both the depletion indicator and these observations ensure that all conditions are fulfilled and thereby validate the concept of the method.

However, this validation method relies on multi-peak and closely occurring flood events. Therefore, this process might not be useful when flood events are isolated and multi-peak floods are minimal, necessitating additional data or different methods for estimating sediment sources. Nonetheless, Khettab, (2022) states that despite these limitations, the lower bound of the curve remains the closest estimation of the in-channel contribution. The author compared the computation of the channel contribution to sediment yield using single-peak and grouped successive and close-occurrence floods, finding that the change in estimation was adjusted by a maximum of about 6.5%. The author attributes this slight adjustment to the domination of large and medium events with enough duration and capacity to exhaust external sediment sources.

II-6. Current State of Hysteresis Analysis

The process of Concentration-Discharge hysteresis analysis typically begins by establishing clear objectives, which serve as the foundation for subsequent analytical steps. Assuming comprehensive analysis is the goal, the next phase involves extracting flood events from the

concentration-discharge data timeseries. A secondary dataset can be set up where multipeak events are not separated, and successive floods are grouped together. Following flood event extraction, the classification of hysteresis patterns is performed, followed by a subsequent computation of metrics such as Hysteresis Indices and the Flushing Index (or slope). Finally, to discern sediment source contributions, events undergo analysis using hysteresis-based unmixing models. These sequential steps encapsulate the key components of Concentration-Discharge hysteresis analysis, providing a structured framework for understanding sediment transport dynamics. However, there is ongoing work to refine and enhance these operations and the overall process of Hysteresis Analysis.

Achieving a comprehensive understanding of hysteresis dynamics necessitates the integration of both qualitative and quantitative frameworks. While visual diagnostics are subject to human limitations, numerical methodologies provide exact data on loop attributes such as magnitude, orientation, and gradient. Over the past decade, a variety of quantitative indices have been developed to standardize cross-watershed comparisons (e.g., Aich et al., 2014; Langlois et al., 2005; Lawler et al., 2006; Lloyd et al., 2016b, 2016a; Poggi-Varaldo & Rinderknecht-Seijas, 2003; Smith & Dragovich, 2009; Zuecco et al., 2016). However, as dataset volumes grow, manual sorting becomes increasingly impractical. Automated solutions, such as the machine learning algorithm introduced by Hamshaw et al. (2018), offer potential efficiency but often require extensive training data and prior shape knowledge. Similarly, the automated protocol established by Keesstra et al. (2019) lacks the flexibility to categorize certain complex geometric hybrids.. Furthermore, existing indices may not fully capture the physical significance of the loop, leading to ambiguity in quantifying complex shapes.

Current indexing methods often struggle to represent the true physical complexity of transport events. Evidence suggests that they may conflate different loop shapes (Hamshaw et al. 2018) or create interpretative confusion when rotational directions shift within a single event (Langlois et al. 2005) highlighted the potential confusion in applying the hysteresis index to shapes combining clockwise and anticlockwise components. To enhance analysis consistency and reliability, a more flexible classification method and unique quantitative analysis for each hysteresis pattern are necessary, alongside the automation of these operations for efficient handling of large datasets. These points are explored in more depth in the following chapter.

Chapter 3

Conception and Development of An Improved Concentration – Discharge Hysteresis Analysis Workflow

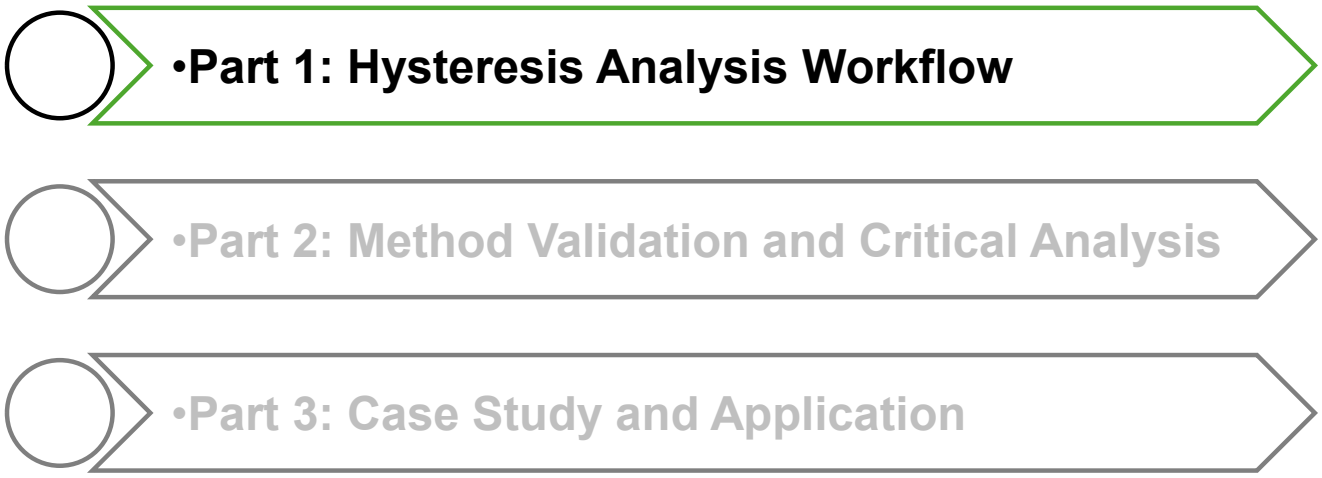

III. Chapter 3 – Conception and Development of An Improved Concentration – Discharge Hysteresis Analysis Workflow

III-1. Background and Study Objectives

Concentration-Discharge (C-Q) hysteresis analysis begins with setting specific objectives that guide the choice of analytical techniques. Initially, this involves isolating flood events from time series data on concentration and discharge, often using automated tools (e.g., Fischer et al., 2021; Oppel & Mewes, 2020). These tools automatically identify the start and end points of flow events within continuous time series data

Subsequently, the extracted flood events undergo classification of hysteresis patterns. This classification can be visual, involving manual inspection of C-graphs, Q-graphs, and hysteresis loops, and subsequent categorization into predefined classes. This approach can be either targeted, based on existing classifications, or exploratory, to identify new patterns or sub-patterns of hysteresis. Despite disregarding the comprehensiveness of a targeted classification, manually sorting hysteresis is labor-intensive, particularly in extensive studies such as regional analyses or those involving long historical data sets and various parameters (e.g., Aguilera & Melack, 2018; Baker & Showers, 2019; Hamshaw et al., 2018; S. D. Keesstra et al., 2019). This complexity prompts the need for an automated classification process that simplifies these tasks. However, existing methods (e.g., Butturini et al., 2008; Hamshaw et al., 2018; S. D. Keesstra et al., 2019; Zuecco et al., 2016) often lack comprehensiveness, are only semi-automatic, or face issues with misclassification.

To thoroughly analyze hysteresis relationships, both qualitative and quantitative assessments are necessary. Graphical inspections of hysteresis loops are limited and need numeric descriptions of the loop's geometrical features—such as size, rotation, and slope—to reveal their hydrological implications. Researchers have developed various hysteresis metrics and indices to quantify these aspects and determine the loop's orientation and strength (Aich et al., 2014; Langlois et al., 2005; Lawler et al., 2006; Lloyd et al., 2016b, 2016a; Poggi-Varaldo & Rinderknecht-Seijas, 2003; H. G. Smith & Dragovich, 2009; Zuecco et al., 2016). These indices compare the metrics to a baseline value, indicating clockwise or anticlockwise motion, and serve as diagnostic tools for

comparing hydrological events across different channels or watersheds, enhancing understanding of sediment transport dynamics (Aich et al., 2014; L. A. Rose et al., 2018; Sherriff et al., 2016).

Automating these indices ideally provides both qualitative and quantitative insights into hysteresis loops. However, hysteresis in hydrology often exhibits complex patterns beyond simple directional loops, and current indices, which are primarily geometrical, may not adequately reflect the physical processes involved (Lloyd et al., 2016a). Furthermore, the same index value can correspond to different loop shapes (Hamshaw et al., 2018), and indices can be misleading when applied to mixed-direction loops, such as figure-eight shapes (Langlois et al., 2005). Consequently, there remains a need for more precise and distinct quantification methods to accurately characterize hysteresis shapes and their variations over time.

For suspended sediment concentration – discharge relationships, it is possible to derive a computation method to estimate the stream channel contribution to sediment yield (Khettab, 2022; Megnounif et al., 2013). The automation computation method advanced by Megnounif et al., (2013) requires the automation of pattern classification. As a result, classification accuracy is necessary to correctly estimate the stream channel contribution portion and reduce errors. Meanwhile, the automated computation method by Khettab, (2022) was designed to remove the requirement for hysteresis classification. However, the author insists that hysteresis analysis is still required to validate the concept of the computation method.

Historically, the classification of hysteresis loops and the calculation of their metrics have been conducted separately, leading to inconsistencies. To enhance the effectiveness of hysteresis analysis, it is crucial to integrate the qualitative and quantitative aspects, thereby improving the reliability of the results. This requires a more flexible classification approach to effectively sort and explore new hysteresis patterns, a unique quantitative analysis for each pattern that differentiates not just shapes but also sizes and impacts, and consistency between classification and quantification. Additionally, automating these processes is essential for efficiently handling large datasets.

In this study, we aim to address these methodological gaps by introducing an automated, comprehensive approach that meets these criteria. We demonstrate this method using a substantial dataset focusing on discharge and associated water parameters. Our objectives are two-fold:

1. We introduce the "Hysteresis Signature" as a concept to classify hysteresis shapes, including standard and novel forms.
2. We also introduce a new numeric analysis format corresponding to the signature. It is used to individually characterize segments of the loop using dual-metrics (real-scale and normalized). This approach also aims to highlight and address the limitations of existing metrics and highlighting the necessity for this dual quantification method.

III-2. Study Data

III-2.1. Main Data Collection

Datasets were systematically selected and retrieved from the United States Geological Survey (USGS) sources, including the National Water Information System: Web Interface (https://waterdata.usgs.gov/nwis) and USGS Real-Time Water Quality Data for the Nation (https://nrtwq.usgs.gov/). An initial data quality assessment was conducted using the data portal's visualization tools. Stations with minimal missing data were selected for further analysis (Table III-1).

Hydrological events were subsequently identified from the time series data. The delineation of events can be performed manually or using automated methods such as the ones described by Fischer et al., (2021) and Oppel & Mewes, (2020). For this study, a semi-automatic tool was developed to facilitate flood event extraction, details of which are provided below. The isolated events were then individually subjected to the hysteresis analysis methods described later.

Table III-1. Station details and hysteresis variables.

Region	USGS Station ID	Area (km²)	Event count	Secondary dataset
Suspended-Sediment Concentration				
Hawaii	USGS 16200000	3.57	105	
	USGS 16210500	101.68		
	USGS 16226200	10.41		
	USGS 16226400	11.91		
	USGS 16238000	6.4		
Colorado	USGS 07105800	1295	80	Yes
Turbidity-based suspended-sediment concentration				
Indiana	USGS 03353200	274.5	81	Yes
	USGS 05516665	976.4	50	
Arkansas	USGS 07194880	89.87	21	Yes
	USGS 07263296	189.1	35	Yes
Pennsylvania	USGS 01479820	73.3	56	Yes
	USGS 01480870	232.8	181	
New York	USGS 0136219503	76.7	18	Yes
Maryland	USGS 01649190	33.9	38	
Kansas	USGS 07144100	3209	97	
Turbidity				
Pennsylvania	USGS 01473169	53.87	123	
Virginia	USGS 02035000	16192.6	96	
	USGS 01673000	2792	89	
Georgia	USGS 02203863	22.35	121	
Maryland	USGS 01589025	779.6	90	
Missouri	USGS 07061270	135.2	92	
Texas	USGS 08181500	3411	60	
Total			1433	

These sites are managed and maintained by the U.S Geological Survey (USGS). All the events included in this study correspond to a period of record approved by the USGS. Data sampling and automated retrieval measures can be found in the Water Data Web Interface (https://waterdata.usgs.gov/nwis).

III-2.2. Main Dataset Description

At all selected stations, discharge is monitored continuously, with data recorded at intervals ranging from 5 to 15 minutes. Turbidity measurements are taken every 15 minutes. Suspended-sediment samples are collected under various hydrological conditions using automatic samplers and manually during routine water-quality assessments, adhering to the protocols specified in the USGS National Field Manual (U.S. Geological Survey, 2015). Laboratory-analyzed suspended-sediment concentrations are integrated with in-stream turbidity readings to calculate real-time concentrations.

The stations retained for analysis are situated in diverse regions and vary in watershed sizes. These stations measure three key determinants against discharge. Despite the high time-resolution of data collection, analysis of hydrograph types via the rising limb duration revealed a tendency toward extremely skewed hydrographs. Typically, the rising limb phase is brief, with the minimum duration recorded as short as two measurements (5 to 15 minutes). This often results in hydrographs where the rising limb appears almost as a straight line, while the falling limb contains more detailed data. Conversely, longer rising limbs were less frequent across the sampled events.

The field data testing collection comprised:

- Events from stations across various regions and catchment sizes.
- Analysis of different water parameters.
- Mixed data quality during events, characterized as:
    a) Low during the rising limb and high during the falling limb.
    b) Balanced quality across phases.
    c) High during the rising limb and slightly low during the falling limb.

This variety deemed the field data collection sufficiently diverse for further testing, which included trials with manually generated datasets.

The quality check for each parameter is the following:

- **Suspended Sediment Concentration (SSC)**: Six stations were chosen, with five in Oahu, Hawaii, which exhibited excellent data quality due to minimal missing data. The station in Colorado, despite some data interruptions, provided a significant number of events.

- **Turbidity-Based SSC**: Nine stations from six regions were retained, showing satisfactory data quality. Turbidity-based SSC, utilizing frequent turbidity measurements, offered more detailed sedigraphs compared to regular SSC. This method allows for finer time-step monitoring, enhancing the detail in the data.
- **Turbidity**: Widely available and of adequate quality, turbidity data was collected from seven stations across six states, encompassing 671 hydrologic events. This ample dataset highlights turbidity as a representative of non-concentration water quality parameters.

III-2.3. Manually Generated Dataset

To validate the flexibility and compatibility of our method with various data characteristics, we conducted complementary tests using manually generated hysteresis events. These tests also aimed to illuminate specific hydrologic conditions not covered by observed data. The manually generated events were divided into two sets:

- **First Set**: This set explored a range of hysteresis forms at varying time resolutions, starting from very low (as few as three measurements) to very high, which introduced noise into the hysteresis loops. Certain data resolutions were limited to specific possible forms.
- **Second Set**: Utilizing the same events from the first set, this set included modifications to the sign of the data (incorporating both positive and negative values) and alterations to the slope (negative, neutral, mixed).

While real observed data provides insights into the method's performance under actual conditions, manually generated datasets are crucial for pushing the method to its limits and ensuring its applicability to a broader range of hysteretic relationships and data characteristics.

III-3. Hysteresis Classification Concept

In Hysteresis analysis, three fundamental hysteresis behaviors are identified based on the relationship between discharge and concentration. These behaviors form the basis for classifying hysteresis patterns observed during flood events:

- **Linear**: similar concentrations between the rising and falling limbs.
- **Clockwise**: higher concentrations during the rising limb compared to the falling limb.
- **Anticlockwise**: higher concentrations during the falling limb compared to the rising limb.

All observed hysteresis loops are combinations of these basic behaviors. These combinations can be categorized into two primary subgroups:

- **Simple**: Comprised of single, consistent behaviors throughout.
- **Complex**: Combinations of two or more behaviors that occur at different phases of the flood event.

Common forms reported in literature include simple classes such as:

(1). **Linear (Class I)**: This behavior occurs when the concentration is similar in both limbs of the hydrograph, indicating a direct, proportional relationship between discharge and concentration without any delay or lag effects.
(2). **Clockwise (Class II)**: This behavior is observed when the concentrations are higher during the rising limb.
(3). **Anticlockwise (Class III)**: In contrast, anticlockwise pattern occurs when the concentration is higher during the falling limb. This could be indicative of delayed responses in the watershed, where the mobilization of materials like sediments or pollutants occurs after the peak discharge.

Additionally, known combined forms that account for more complex hydrological and hydrochemical interactions during flood events include:

(4). **Single-Valued line plus Loop (Class IV)**: Represents a combination of linear behavior with either clockwise or anticlockwise behavior, suggesting a transition in hydrological or chemical processes.
(5). **Figure of Eight (Class V)**: This combined form involves a loop that exhibits both clockwise and anticlockwise behaviors, resembling a figure of eight. This pattern indicates multiple phases of concentration response relative to discharge.

While these forms are commonly reported, numerous other combinations based on specific flood event characteristics exist. By automating the process of identifying and coding these combinations at different discharge increments, we can efficiently and accurately classify a wide range of hysteresis loops. This approach enables the merging of qualitative classification and quantitative analysis into a single cohesive procedure.

III-4. Flood Events Extraction

A simple flood event begins when discharge rises above baseflow, reaches its peak, and then decreases back to baseflow. Consecutive or multi-peak events can differ, with overlapping peaks that do not always return to baseflow between them. To simplify the extraction of hydrologic events from continuous data, a straightforward algorithm was developed for event separation. The extraction process involves three key steps:

1. **Automated Event Extraction**: The algorithm identifies flood events by first pinpointing the peak discharge. It then marks data points to the left of the peak (rising limb) until baseflow is reached, indicating the start of the event. A similar process is applied to the right of the peak, marking the end of the event when baseflow is reached. Data points are flagged to avoid rechecking, and the process repeats for each flood event, sorted in descending order by peak magnitude.

    - The upper bound of baseflow is the first parameter needed. If unknown, it can be approximated by automatically using the average discharge or manually through graphical inspection.

    - The second required parameter is the flattening criterion, defined as the difference between two consecutive discharge observations. In this study, it was set to zero. The algorithm allows for separate criteria for the rising and falling limbs.

    - For each event, the algorithm generates plots of the hydrograph and the associated water parameters, with identifiers, and tabulates the start, end, and identifier for each event.

2. **Event Validation and Manual Adjustment**: The plots generated during the automated process help identify events requiring attention. Any event with substantial missing data in either the streamflow or the associated water parameters is rejected (e.g., Figure III-1d), as are multi-peak events that cannot be separated (e.g., Figure III-1d). Rejections are noted in the tabulated data (Figure III-1a).

    - Accepted events are marked in the master dataset, and multi-peak events that need attention are manually separated at their midpoint. Multi-peak events are considered separable when the section below the midpoint is less than 50% of the peak. Separating such events at higher discharges can result in incomplete analysis.

    - During this step, start and end points can be adjusted to salvage events where missing data is found at low flows, allowing partial analysis at high flows.

3. **Final Automated Event Extraction**: Once validated and adjusted, the final flood events are re-extracted from the master dataset and sorted in chronological order.

In Phase 2, the semi-automatic tool allows for validating extracted events and making manual adjustments as needed (Figure III-2). Depending on the objective, this phase allows to perform the following operations:

(1) **Single-Peak Hysteresis Analysis**: Removing inseparable multi-peak flood events and separating others into distinct single-peak events. Optional adjustments to the start and end of floods can also be made.

(2) **Mixed Hysteresis Analysis**: Events generally do not require specific treatments. However, optional adjustments can be made to the start and end of floods.

(3) **Sediment Sources Unmixing Model Validation**: Following the validation method advanced by Khettab, (2022), events that occur closely together can be grouped into a single multi-peak event, with an optional adjustment to the start and end of events

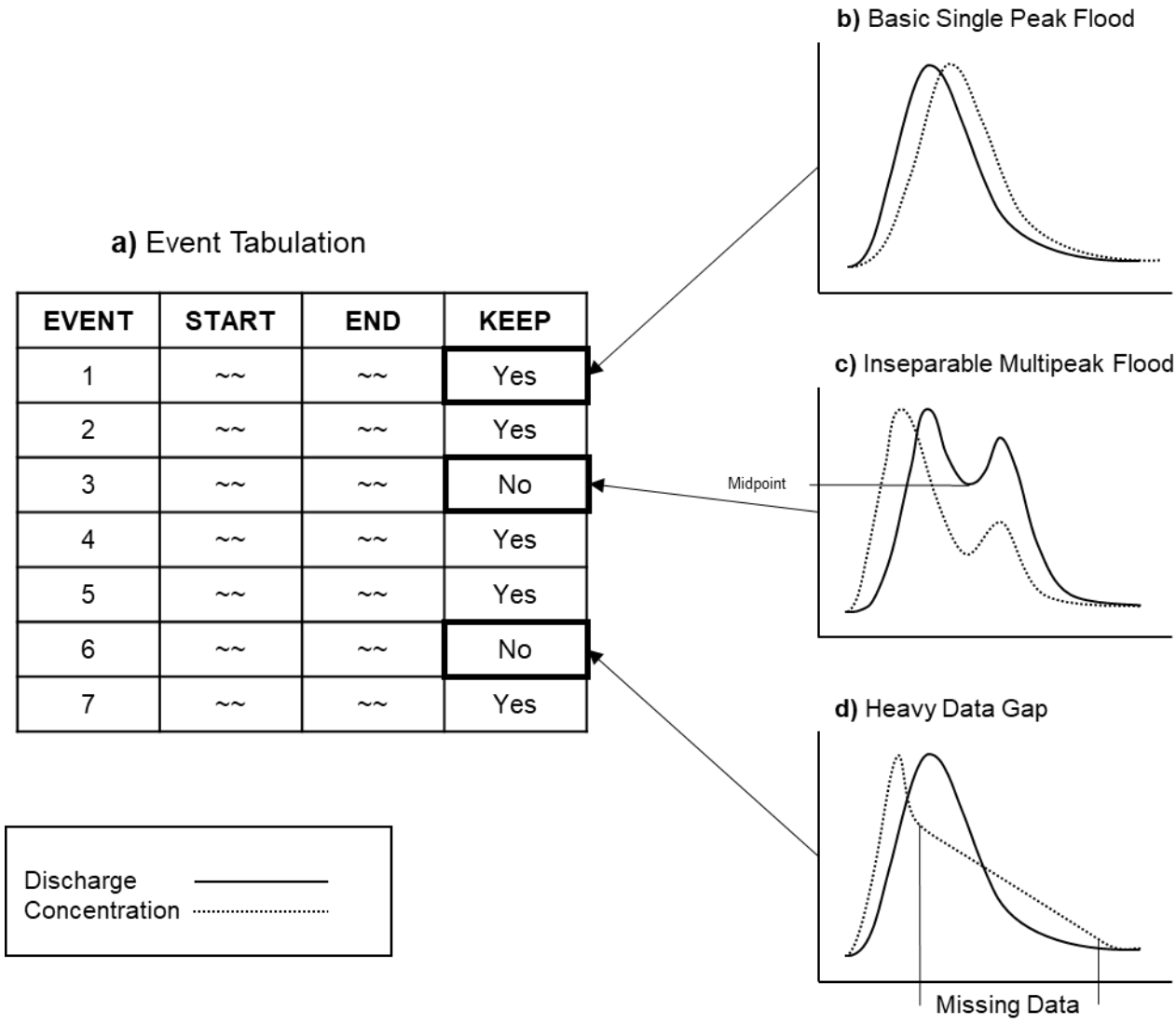

Figure III-1. Flood events validation and treatment phase schematic

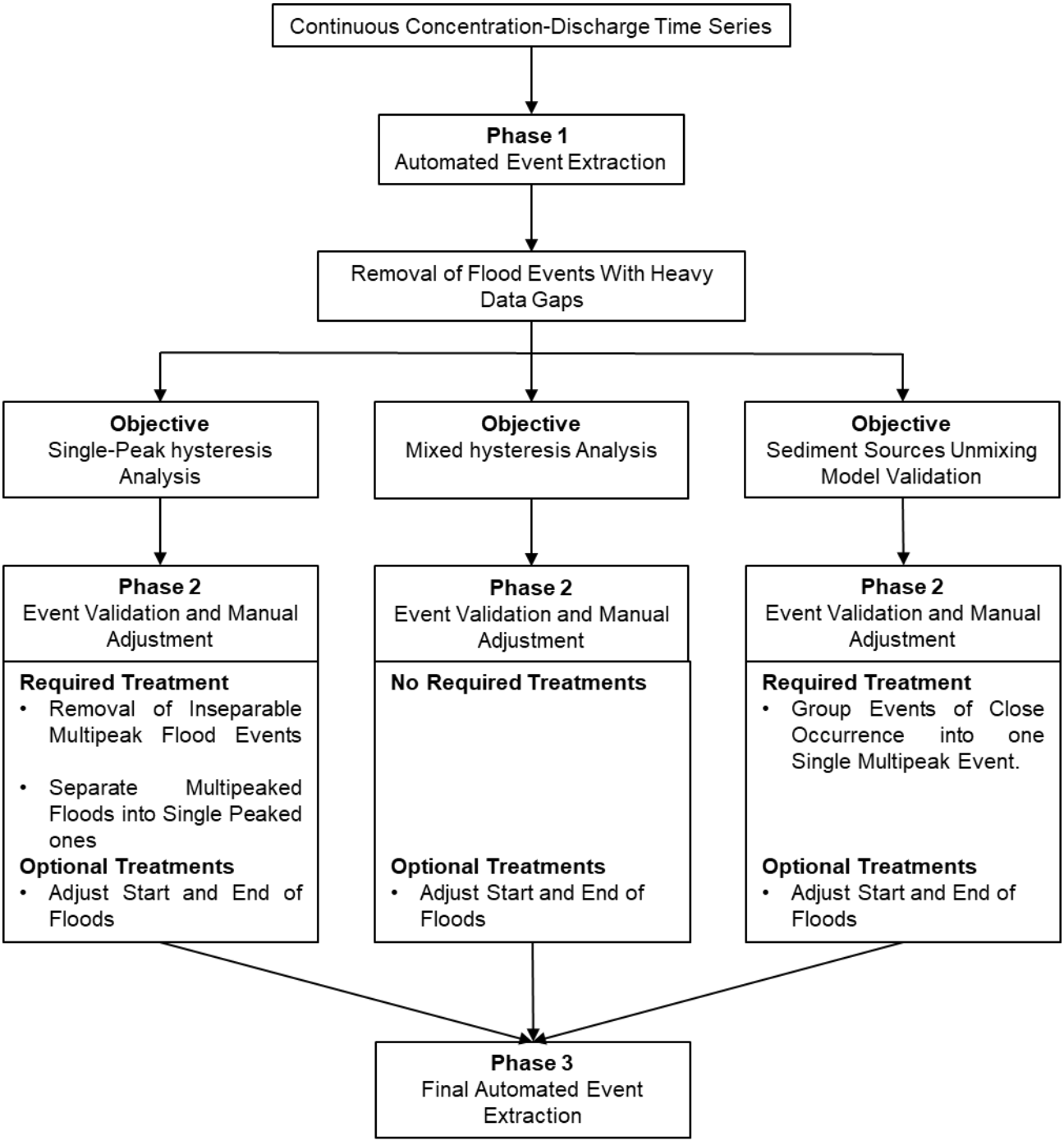

Figure III-2. Flowchart of the Semi-Automated Tool Process for Event Extraction, Validation, and Adjustment.

III-5. Procedure

III-5.1. Data Pre-Processing

The preprocessing stage involves segmenting the hydrograph into uniform discharge intervals to ensure comparability across events. With Q_{max} and Q_{min} establishing the scale, n equal divisions determine the nodes for calculation. These intervals are established numerically:

$$Q_{Sel}^{i} = Q_{min} + i.\frac{Q_{max}-Q_{min}}{n} \quad \text{(Equation III.1)}$$

Where $i = 0,1,\dots,n$, $Q_{Sel}^{0} = Q_{min}$, and $Q_{Sel}^{n} = Q_{max}$.

By projecting these standardized discharge values onto the hydrograph to find time (T_{Sel}^{i}) and then onto the concentration series (C_{Sel}^{i}), we create a nodal framework. This method relies on the assumption of temporal linearity between measurements. The final reconstructed loop represents a cleaned version of the hydrologic event, effectively purging measurement artifacts and irregularities from the source data to yield a technically smooth hysteresis profile (Figure III-3).

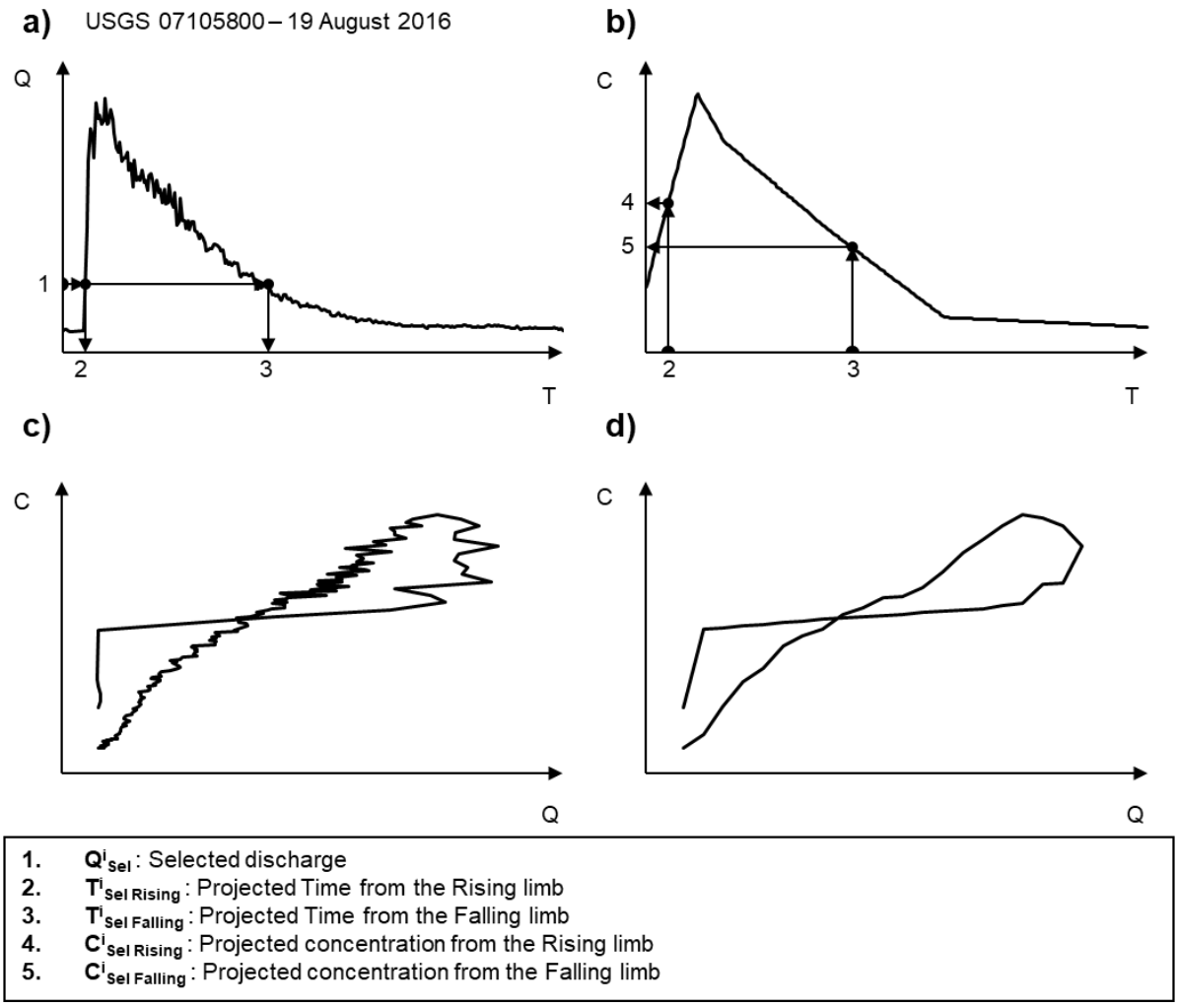

Figure III-3. Visual workflow of the data reconstruction process. a) Selected discharges projection to obtain the corresponding times followed by b) the projection of times to obtain the corresponding concentration. c) The original hysteresis loop. d) the hysteresis loop after treatment.

III-5.2. Data Pre-Processing Validation

The effectiveness of data subdivision levels was tested to determine if higher resolutions resolve complex hysteresis traits more accurately. While earlier work by Lloyd et al., (2016b) found no distinct advantage to exceeding 20 intervals, our comparative analysis suggests that 100-interval models offer marginal refinements in both visual topology and concentration metrics.

As illustrated in Figure III-4 and Figure III-5 , the increased granularity provides a slightly more nuanced representation. However, since smaller subdivisions provide greater adaptability across varied hydrological conditions, the 20-interval partition was selected as the optimal standard for the proposed methodology.

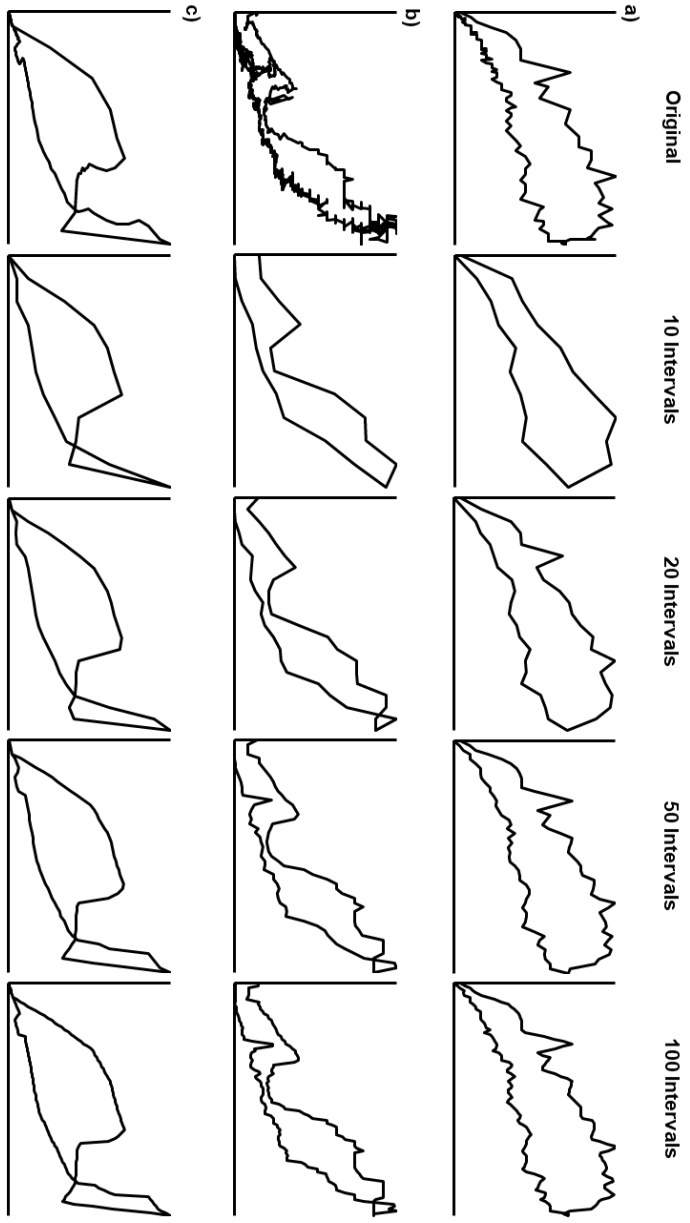

Figure III-4. Example visual validation of different loop subdivisions.

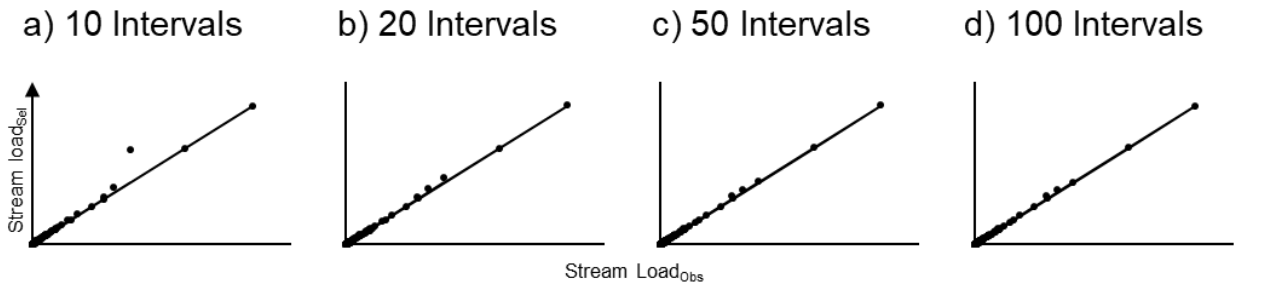

$\bar{R}$	MAPE	R^2	Slope
1.042	4.73	0.98	1.061

$\bar{R}$	MAPE	R^2	Slope
1.016	2.86	0.99	1.018

$\bar{R}$	MAPE	R^2	Slope
1.015	2.08	0.99	1.0149

$\bar{R}$	MAPE	R^2	Slope
1.013	1.88	0.99	1.0126

Stream load$_{Obs}$ and **Stream load$_{Sel}$** : estimations deduced from observed and treated data respectively
$\bar{R}$: Mean Ratio
MAPE : Mean Absolute Percentage Error
R^2 : Regression Coefficient of determination
Slope : Regression slope (a)

Figure III-5. Qualitative validation of different loop subdivisions using Concentration-based parameters.

III-5.3. Hysteresis Signature Determination

For standard hysteresis analysis, the discharge and concentration time series are initially normalized:

$$Q_N^i = \frac{Q_{Sel}^i - Q_{min}}{Q_{max} - Q_{min}} \qquad \text{(Equation III.2)}$$

$$C_N^i = \frac{C_{Sel}^i - C_{min}}{C_{max} - C_{min}} \qquad \text{(Equation III.3)}$$

Each discrete flow interval is then quantified using a normalized Partial Amplitude (PA), representing the geometric area bounded by the $C_N^i - Q_N^i$ curves of the hydrograph's respective phases, computed via the trapezoidal rule (Figure III-7a):

$$PA_i = \frac{1}{2}\left(Q_N^{i+1} - Q_N^i\right)\left(C_{NR}^i + C_{NR}^{i+1}\right) - \frac{1}{2}\left(Q_N^{i+1} - Q_N^i\right)\left(C_{NF}^i + C_{NF}^{i+1}\right) \qquad \text{(Equation III.4)}$$

With C_{NR}^i and C_{NF}^i are the normalized concentrations on the rising and falling limb, respectively.

In this normalized framework, each integration interval is set at a constant 5% (1/20):

$$PA_i = \frac{1}{40}\left[\left(C_{NR}^{i} + C_{NR}^{i+1}\right) - \left(C_{NF}^{i} + C_{NF}^{i+1}\right)\right] \qquad \text{(Equation III.5)}$$

Structural signatures are then derived through parametric thresholding of the PA_i values. As illustrated in Figure III-7b specific parameters are assigned based on directional dominance:

- Intervals with a PA_i between −0.005 and 0.005 are categorized as "x", signifying a single-valued or near-linear relationship.
- Values exceeding 0.005 receive the "y" parameter (clockwise dominance);
- Values below −0.005 are assigned "z" (anticlockwise dominance).

This specific threshold was validated by benchmarking multiple synthetic datasets to ensure the separation of linear and hysteretic behaviors (Figure III-6).

Consecutive intervals sharing the same parameter are aggregated into a single, unified sequence. The total flow range and net amplitude for these sequences are determined by their cumulative widths and partial amplitudes.

When sequential segments yield identical parameters, they are merged into a continuous sequence defined by the total flow span and aggregate area (Figure III-7).

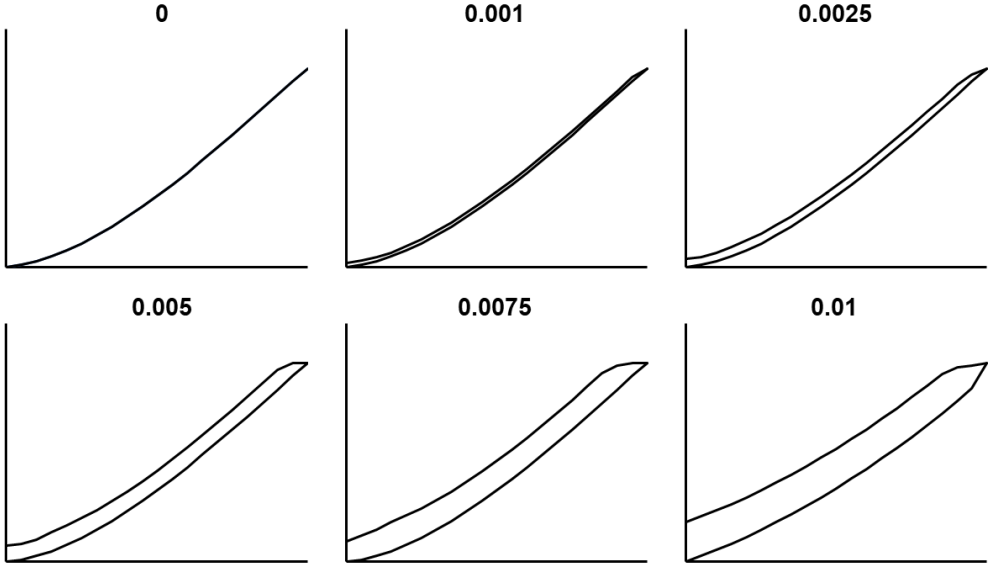

Figure III-6. Threshold visual analysis synthetic events and different loop openings.

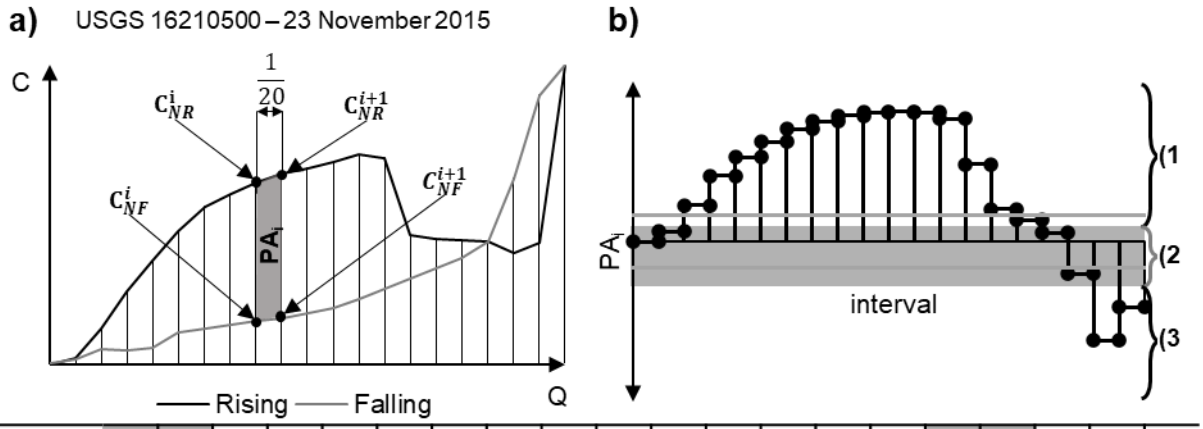

Interval i	1	2	3	4	5	6	7	8	9	10	11	12	13	14	15	16	17	18	19	20
PA_i	0	0+	0.01	0.01	0.02	0.02	0.02	0.02	0.02	0.02	0.02	0.02	0.02	0.01	0.01	0+	0+	-0.01	-0.02	-0.01
Parameter	x	x	y	y	y	y	y	y	y	y	y	y	y	y	y	x	x	z	z	z
Sequence*	x		y													x		z		
Amplitude	0+		0.24													0+		-0.04		
Width	10%		65%													10%		15%		
Signature**	y																	z		
Amplitude	0.24																	-0.04		
Width	85%																	15%		

C^i_{NR} : Normalized concentration from the Rising limb
C^i_{NF} : Normalized concentration from the Falling limb
PA_i: Partial Amplitude
* Obtained by merging intervals with the same parameter
** Obtained by merging Sequence Parameters with a <15% width to the adjacent sequence parameter of the same sign

Figure III-7. Visual representation of the hysteresis signature derivation framework: (a) Partitioning of Partial Amplitudes. b) Rotational classification categories including (1) clockwise, (2) linear, and (3) anticlockwise. Following threshold filtering and directional merging, the illustrated event yields a "yz" signature.

Minor segments involving minimal intervals can periodically encumber the primary hysteresis signature. These negligible segments occur during initial state returns, transitional limb crossings, or limb convergences at peak flow as well as stochastic noise, such as bank-cavings or measurement spikes (Figure III-7 and Figure III-8). To ensure the macro-scale loop form is not distorted by these micro-variations, a merging protocol :

- **Case A**: Segments under the 15% width requirement merge into the widest adjacent parameter of identical polarity.
- **Case B**: If multiple segments are under 15% and share a sign, the one exhibiting higher amplitude is prioritized
- **Case C**: For segments under 15% bounded by opposing polarities, the 10% limit acts as the final buffer; 5% segments are merged immediately.

The 15% criteria marks the transition from computational noise to interpretative significance. Segments exceeding this width indicate meaningful shifts in hydraulic phases or transport quantity that warrant individual parametric representation.

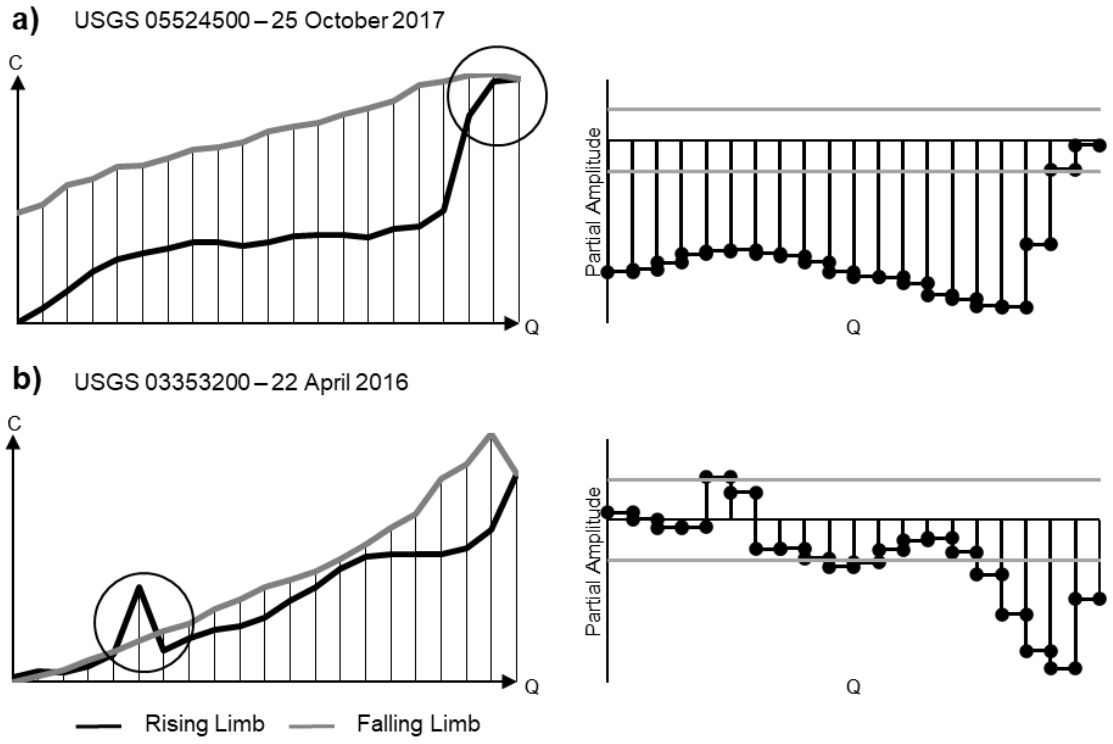

Figure III-8. Examples of low-significance loop segments requiring parametric merging: (a) Narrowing limb convergence; (b) Singular, high-frequency concentration spikes.

Comprehensive analysis confirms that a hysteresis loop is definitively characterized by its unique signature, which maps the event to a specific class and morphological form. Fundamental

classes, comprising linear, clockwise, and anticlockwise rotations, are designated by single-parameter identifiers: “x”, “y”, and “z”, respectively. For more complex, composite classes that exhibit shifting behaviors across varying flow stages, the resulting signature consists of a sequence of two or more parameters. This parametric progression tracks distinct segments of the loop from initiation at low flows to the peak discharge. Within this framework, “x” denotes a single-valued segment, while “y” and “z” represent clockwise and anticlockwise components. The final signature serves as a directional road map, with loop thickness for each sequence being assessed through a standardized, dimensionless quantifier (e.g., Figure III-7).

III-5.4. Hysteresis Loop Hydrologic Qantification

III-5.4.1. Computation

The real-scale framework converts gemetrical loop characteristics into hydrologically significant values. In the context of sediment transport, this involves calculating the Asynchronous Load, effectively bridging the gap between concentration-discharge plots and total transported mass. Intervals defined by signatures “y” and “z” are quantified according to the specific computational concept illustrated in Figure III-9a and Figure III-9b, respectively. Once individual segments are processed, their respective sediment loads are synthesized in alignment with the event's hysteresis signature.

In segments designated as “x,” where concentration offsets between hydraulic limbs are minimal, the algorithm assigns a quantification protocol based on dominant polarity: if concentrations are higher during the rising phase, the segment is processed as a “y” interval; conversely, it is treated as a “z” interval.

It is essential to recognize that real-scale descriptions are intrinsically variable and contingent upon the specific parameters analyzed. Therefore, diverse hysteretic relationships may necessitate distinct adaptive calculations to achieve an accurate physical characterization.

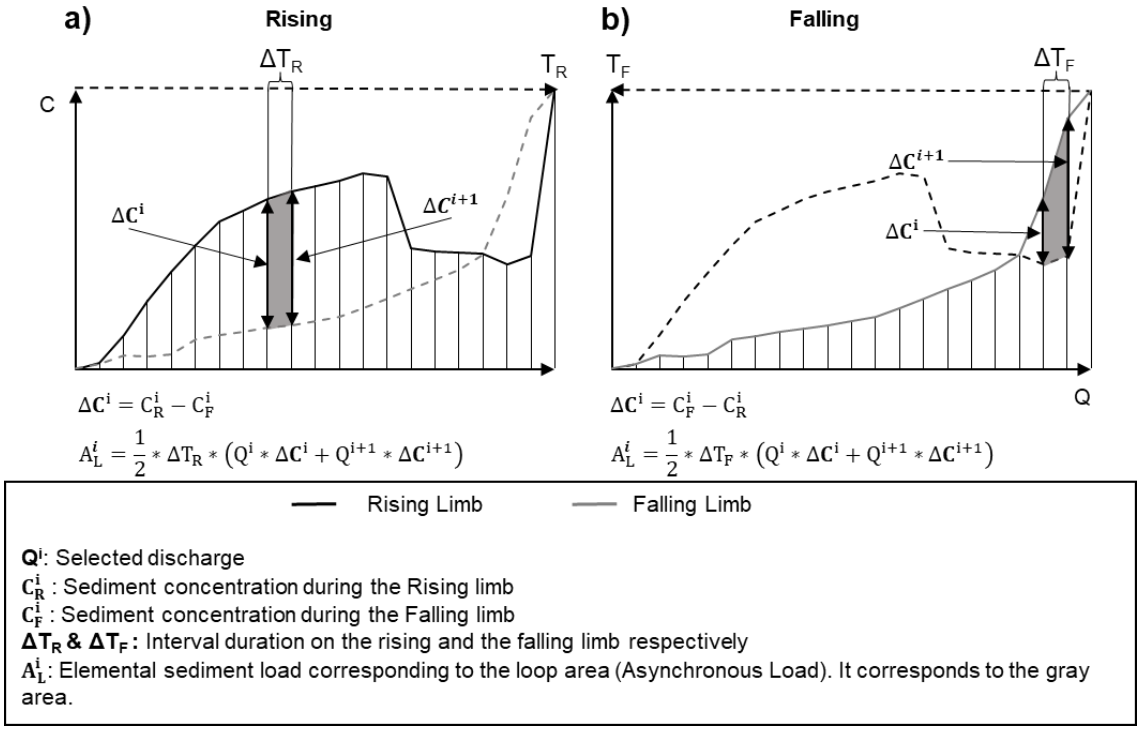

Figure III-9. Conceptual framework for stream load partitioning: (a) Quantification of a clockwise interval; (b) Quantification of an anticlockwise segment.

III-5.4.2. Interpretation

The Asynchronous Load (A_L) is a metric designed for water parameters based on concentraction (sediments, solutes, nutrients, and pollutants). It is used to differentiate between hysteresis loops and between subloops (more details are given in section III-6.2). It encompasses the effect of flow range and duration, two parameters that are not typically included in hysteresis analysis and whose effect is lost in the data compression.

In Sediment transport, when external sources are responsible for the hysteretic effect, the Asynchronous Load can be associated to the contribution of these sediment sources while the difference between the Total and the Asynchronous Load is the channel contribution to sediment yield. This condition can be verified with the validation process described in Chapter II – Section II-5.2.4.

Chapter 3

Conception and Development of An Improved Concentration – Discharge Hysteresis Analysis Workflow

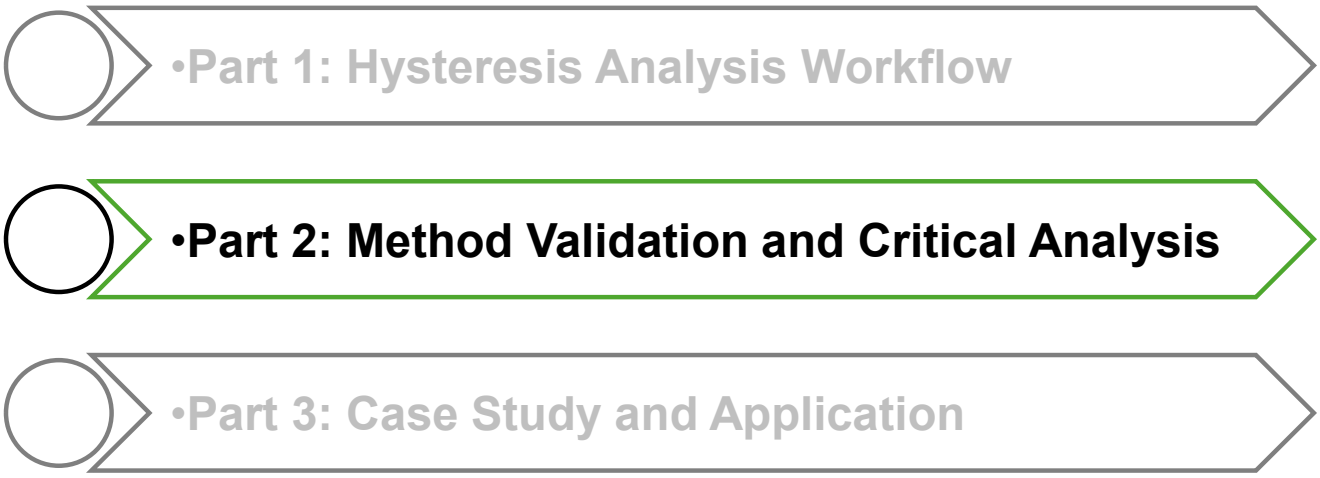

III-6. Method Validation

III-6.1. Automated hysteresis classification

The study generated 51 independent signatures by processing flow events without a predefined classification. This unbiased workflow allowed signatures to be defined purely by data-driven attributes, which were subsequently audited via plot analysis and Partial Area (PA) distribution checks. These 51 signatures provide a confirmed baseline for distinct hysteresis pattern identification. Importantly, the modular nature of this method ensures that while 51 signatures were observed here, the system remains capable of detecting a much wider spectrum of loops.

Signatures S1 through S7 (Figure III-10) correspond to the standard five-category model established in literature (e.g., G. P. Williams, 1989), representing 62% of the dataset. The presence of recurrent "complex" forms indicates that many patterns historically considered noise are actually predictable hydrological features. If a novel form appears with high frequency, it must be recognized as a fundamental component of the watershed dynamic rather than a rare process combination. Our analysis shows that simpler profiles (those with three parameters or fewer) occur with high regularity. Expanding the standard classification to encompass these 21 signature types allows for a robust characterization of 95% of hysteresis events, providing a more comprehensive analytical lens.

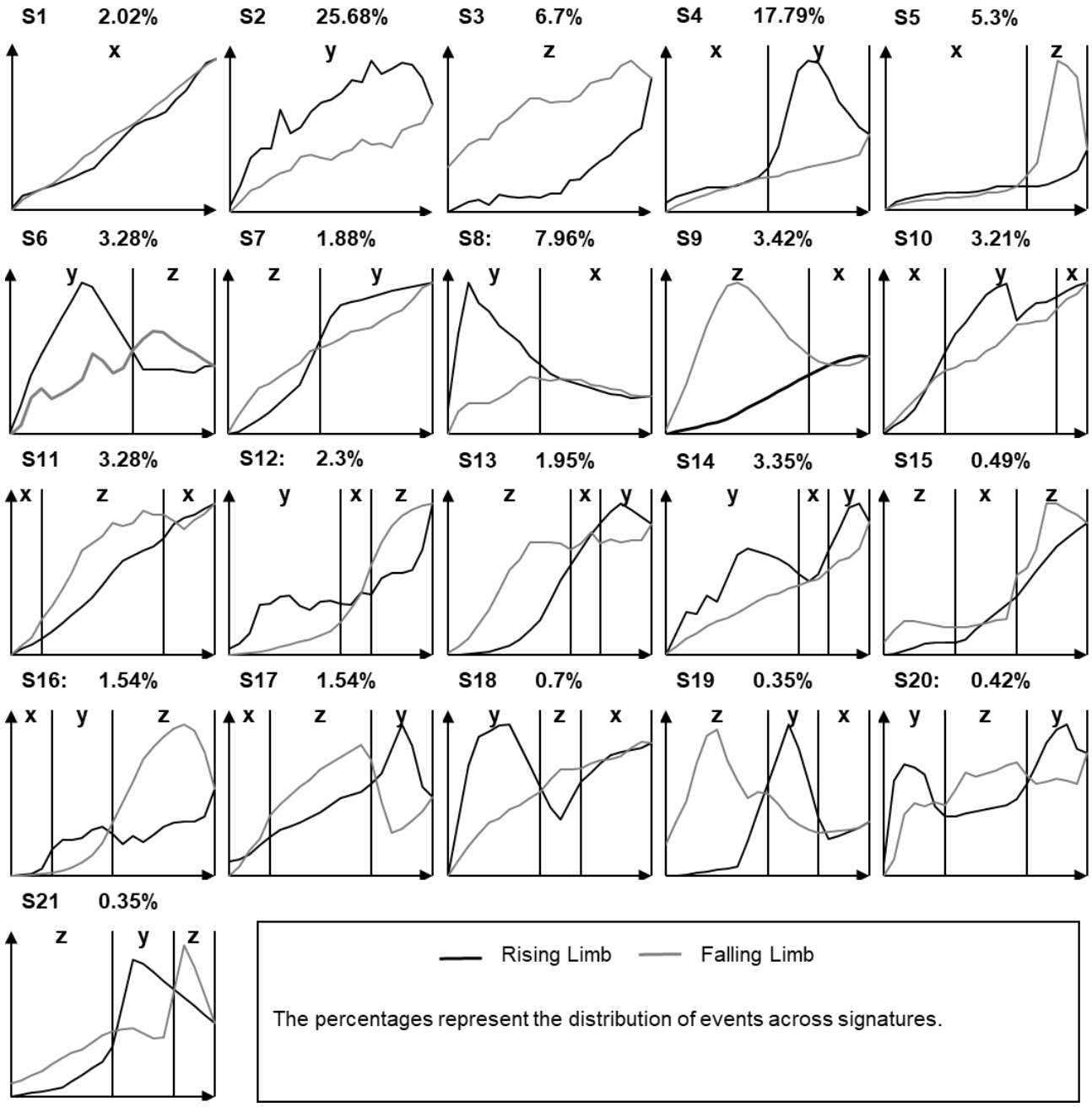

Figure III-10. Events characterized by a signature length of one to three..

While the vast majority of events follow simpler patterns, a small fraction (5%) exhibit complex structures requiring four to six parameters to define. These rare signatures often arise in cases of subtle loop geometry (e.g., Figure III-11 S25 and S31), where the parameter “x” where the parameter “x” is frequently observed. Analysis shows that 18 of these elaborate forms appeared repeatedly, whereas 12 were single, transient events..

Computational and visual classification protocols produced concurrent findings for the majority of events. However, long-signature events pose a visual challenge due to their characteristic narrow geometries. While most loop segments remained visually clear, the transition toward linear amplitudes in certain events rendered subtle geometric shifts undetectable by sight alone. For these specific cases, the distribution of partial amplitudes checks were essential to support the classification. The algorithm's ability to identify subtle distinctions between the "x," "y," and "z" parameters, despite these being visually unnoticeable, verifies the system's operational sensitivity and confirms the validity of the automated output (Figure III-12).

In specific scenarios, the boundary between clockwise and anticlockwise components shifts away from the central intersection of the hydrograph limbs. Because this intersection does not necessarily align with established interval limits, and given that proximal intervals often exhibit narrow amplitudes, the algorithm characterizes these zones with the "x" parameter. When these segments fail to meet the defined 15% width threshold, they are integrated into adjacent parameters sharing the same directional sign. Analysis confirms that this merging process preserves output accuracy and exerts minimal to no influence on quantitative hysteresis metrics. Should higher precision be required for specific applications, these artifacts are easily addressable during the post-processing phase.

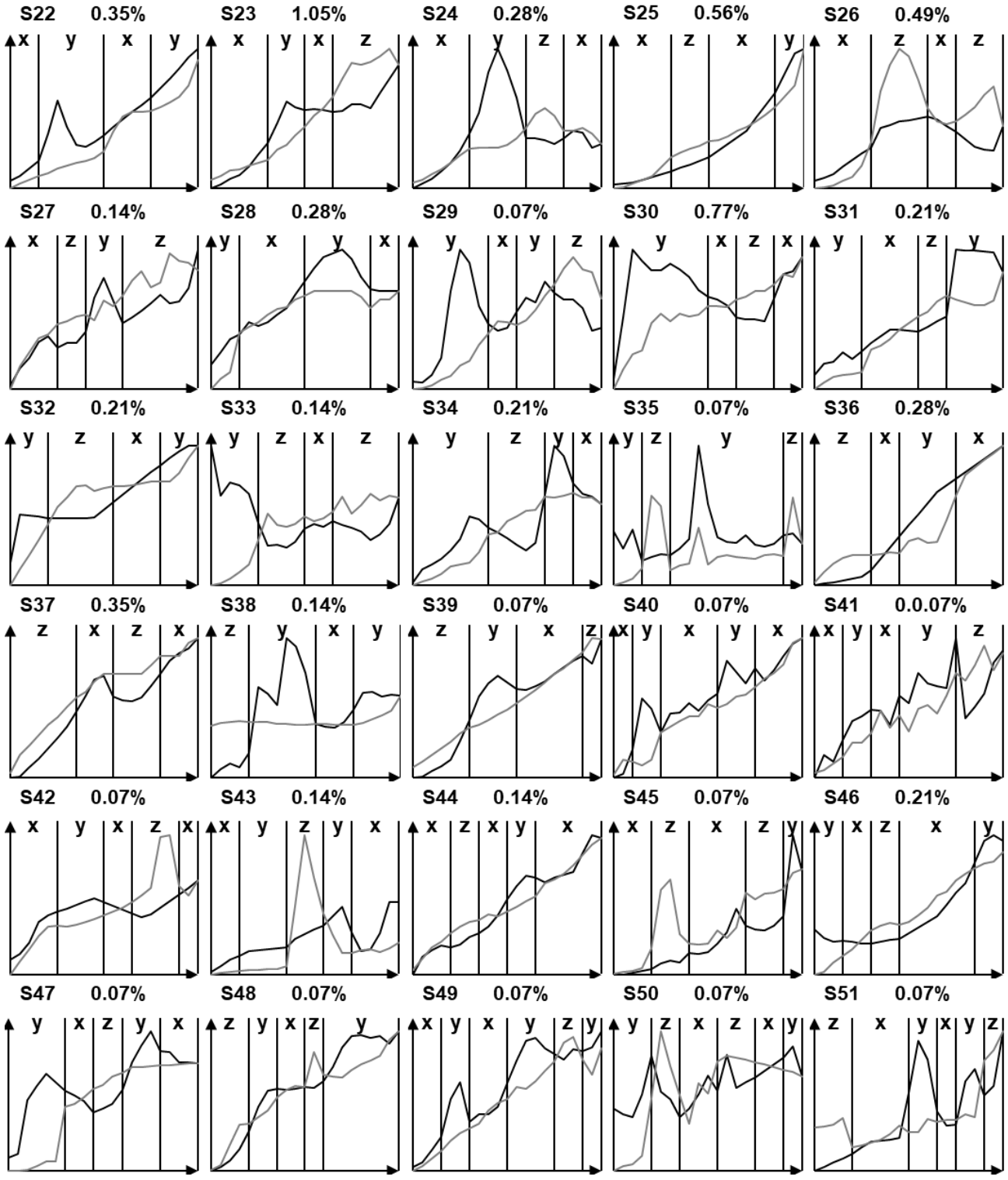

Figure III-11. Events characterized by a signature length of four to six.

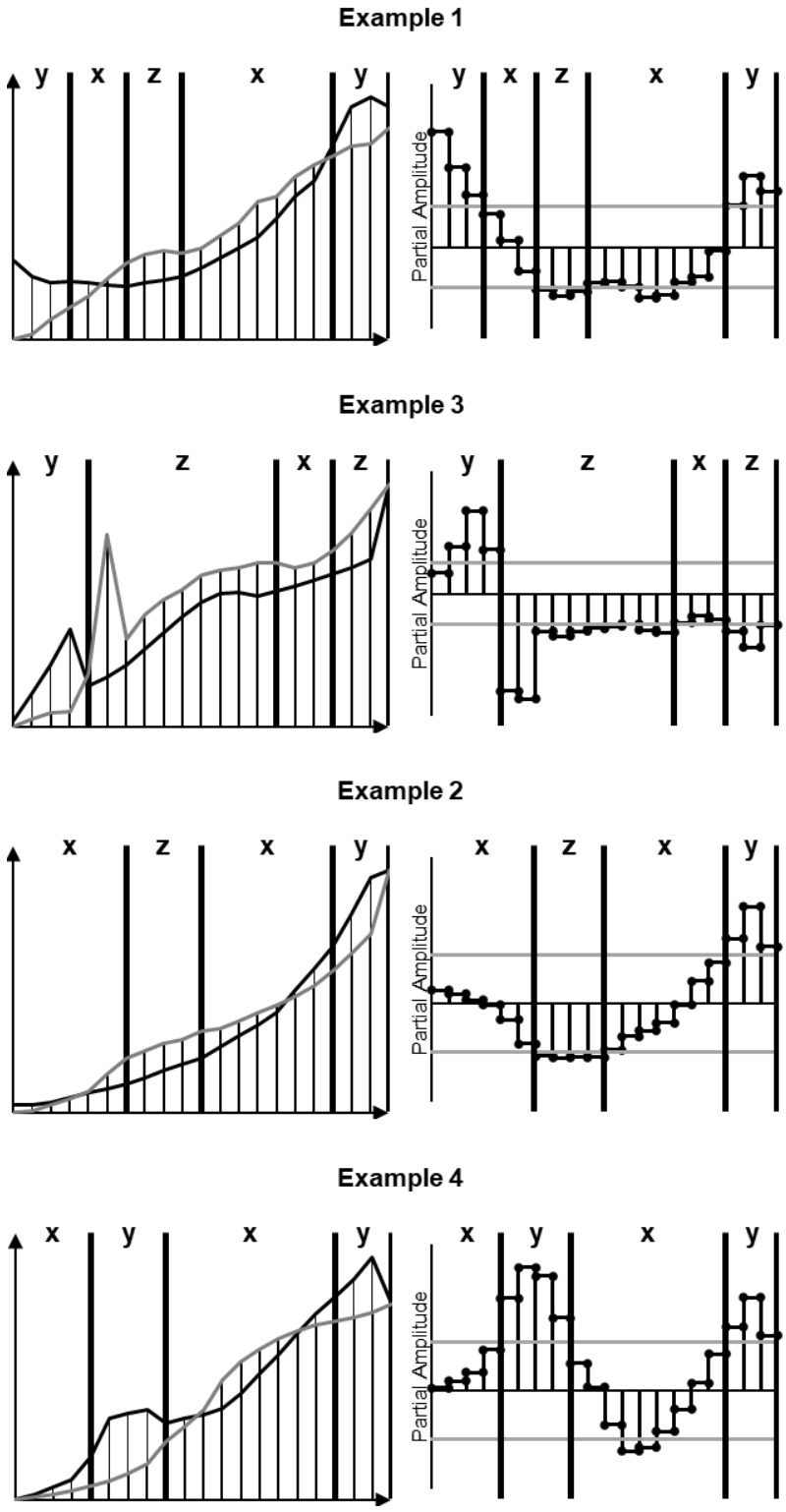

Figure III-12. Detailed examples of hysteresis forms' part separation to compare visual and automated classification for narrow hysteresis loops.

III-6.2. Numerical Constraints in Hysteresis Quantification

The diagnostic power of hysteresis classification is limited to identifying general trends in watershed behavior over time. However, because events labeled under a single signature can represent vastly different transport scales and geometric widths, the qualitative framework must be augmented. Quantitative quantification is required to bridge the gap between categorical sorting and physical process representation.

III-6.2.1. The Lack of Descriptive Uniqueness in Global Indices

We identified a core limitation regarding the representational uniqueness of standard indices. Specifically, Figure III-13. illustrates that distinct loop signatures can map to identical index values, a phenomenon recorded across 407 unique pairs in this study. This confirms that indices function as a low-resolution scale for rotational balance rather than a high-fidelity description of form. Consequently, there is a clear divergence between the pattern a loop and its quantitative index. As previously noted by Hamshaw et al., (2018), this lack of sensitivity suggests that such values cannot act as a surrogate for shape, necessitating a review of whether this statistical "aliasing" limits our understanding of watershed processes..

Historically, research on hysteresis magnitude has often relied on subjective classifications, labeling events simply as "small" or "large" (Andrea et al., 2006; Bowes et al., 2015; Butturini et al., 2008; Evans & Davies, 1998; Jansson, 2002; Lowe & Eyring, 1975; Schaefli, 2016). To move beyond these qualitative descriptions, many scholars introduced numerical indices to provide an objective measurement of loop strength and orientation (e.g. Aich et al., 2014; Langlois et al., 2005; Lawler et al., 2006; Lloyd et al., 2016a, 2016b; Poggi-Varaldo & Rinderknecht-Seijas, 2003; Smith & Dragovich, 2009; Zuecco et al., 2016). These metrics were designed to standardize the description of loop geometry, allowing for cross-comparisons between individual flow events or diverse drainage basins (Aich et al., 2014; Lloyd et al., 2016b, 2016a; Zuecco et al., 2016).

Fundamentally, these indices serve as geometric surrogates intended to characterize physical processes through spatial patterns. Consequently, evaluating whether such indices remain reliable, despite their failure to provide unique descriptions, hinges on their capacity to maintain

accuracy in identifying magnitude and direction. This representational uncertainty justifies a rigorous comparative study between standard indices and the proposed signature-based quantification format.

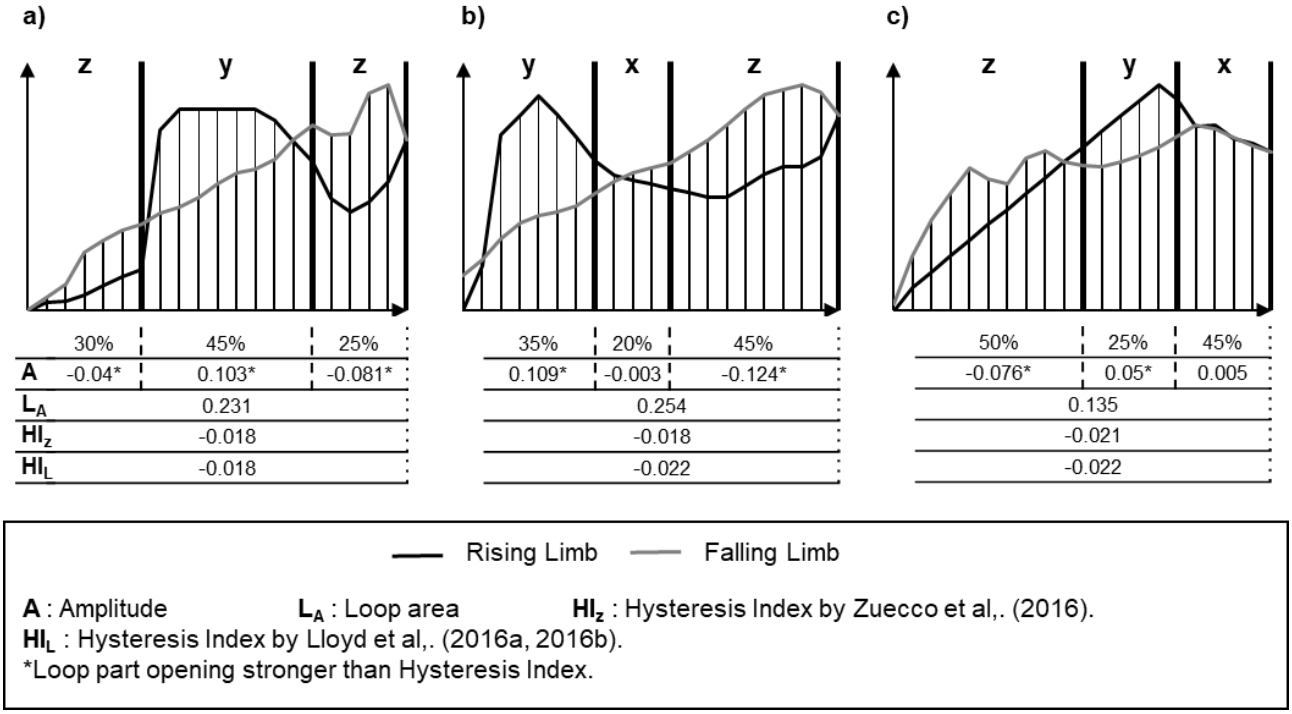

Figure III-13. Evidence of index saturation: Demonstrating the failure of unique single values to account for geometric diversity in hysteresis patterns.

III-6.2.2. The Structural Limitations of Indices

The representational accuracy of hysteresis indices was assessed to determine if the lack of a unique description distorts the physical analysis. Our findings indicate that for complex loops—those exhibiting bi-directional movement—the internal compensation between opposing segments leads to an artificially weak HI. This phenomenon effectively masks the true extent of the hysteretic effect. When benchmarked against sequence parameters (Figure III-13), the HI proved to be a less sensitive metric for capturing total transport dynamics. As Langlois et al., (2005) observed, such indices lack clarity when handling multi-phase rotations. In this case, the index is neither

representative of the size nor the direction. Furthermore, in instances where identical parameters occur multiple times within a single event (Figure III-10 S14-15 and S20-21). the HI cannot differentiate between subloops. These repeated segments, despite sharing a parameter, often originate from different geomorphic processes, necessitating a framework that acknowledges separate transport stages rather than collapsing them into a single, unrepresentative value.

This limitation has led several researchers to propose high-resolution alternatives. For example, Lloyd et al., (2016a) suggested evaluating a distribution of values throughout various loop sections alongside the global average (i.e., H_{Lloyd}) arguing that this provides a more rigorous characterization of complex geometries like figure-eight forms. Similarly, Aguilera & Melack, (2018) opted for a segmented representation, calculating independent values for each quartile of the loop's progression. Furthermore, Zuecco et al., (2016) introduced a complementary metric involving the variance between definite integrals of the hydrograph's rising and falling limbs.

This research suggests that the vulnerabilities of current indices can be overcome by segmenting loops before index assignment. Because single-peak events are essentially combinations of simple rotational variations, modularizing the loop ensures that each component receives a unique, hydrologically sensitive numeric description. This segmentation prevents the statistical underestimation typically caused by amplitude compensation, leading to precise accounts of loop magnitude and orientation. Consequently, partial description modernizes the application of hysteresis indices, making them resilient to complex, multi-phase transport scenarios.

III-6.2.3. The hydrologic problem

Generally, loop magnitude measures the phase-shift difference, but normalized descriptions fail to account for the physical weight of hydrologic parameters. Identical hysteretic behavior, when analyzed via concentration-based metrics, produces vastly different sediment transport outcomes depending on the flow range and duration involved. By simulating an event where a fixed concentration increase is applied across various flow levels (Figure III-14) we can visualize this discrepancy. Although the indices remain consistent (Figure III-14c-h), the sediment load is clearly sensitive to flow stages—increasing markedly at higher discharges. Furthermore, the discrepancies between the rising and falling flow phases at constant flows demonstrate the critical role of

duration. Ultimately, this evidence points to the limitations of relying on normalized partial quantification to interpret physical hydrological phenomena.

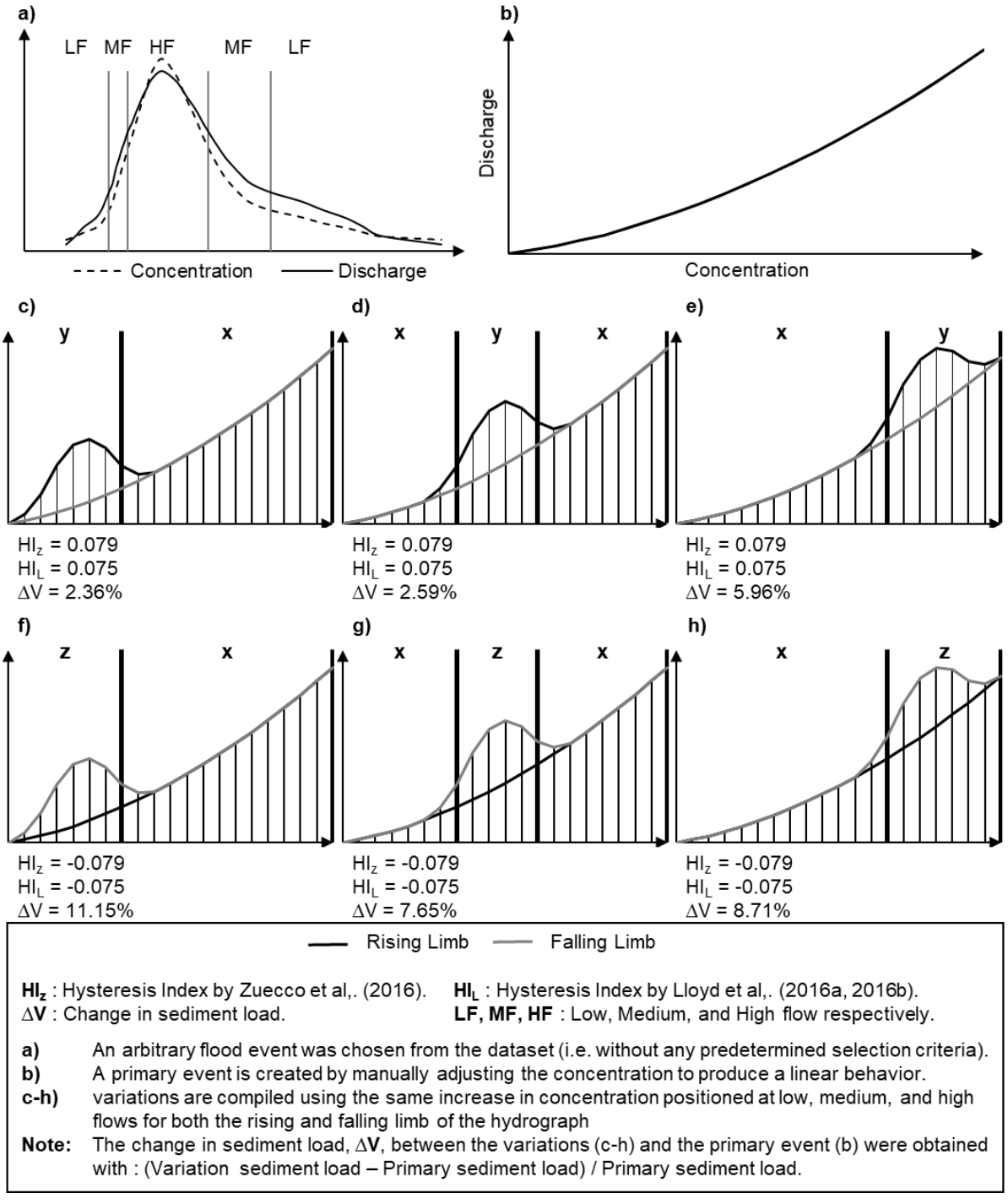

Figure III-14. Sensitivity of hysteresis metrics to temporal scales and flow intensity: A comparative analysis.

The solution involves re-evaluating loop segments using hydrologic parameters that influence their physical significance, specifically flow levels. Existing studies demonstrate the utility of this approach. Khettab, (2022) and Megnounif et al., (2013) successfully linked the geometric area of the loop to actual sediment loads to distinguish between watershed contributions and accidental sediment processes. Furthermore, Misset et al., (2019) refined the analysis of transport efficiency by applying a weighted index to the transported mass, a progression from the traditional indices established by Lloyd et al., (2016a).

The Asynchronous Load (AL) was developed in this research to provide a real-scale quantification for concentration-based variables. Experimental data matches the example in Figure III-14, showing that the multiplier effect of discharge and concentration makes high-flow stages critical to sediment transport. Because the rising limb is often short, the resulting hysteresis can govern sediment dynamics in a condensed timeframe. This confirms that flow intensity and duration are the true metrics of dominance, often diverging from what the largest normalized segment of the loop might suggest (Figure III-15).

Exclusively utilizing normalized metrics fails to provide the depth necessary for robust hydrological interpretation. For example, prioritizing the most "prominent" loop segments based only on normalized values may lead to erroneous conclusions; this is because normalized results often mask minor segments that possess substantial real-scale magnitude (as illustrated in Figure III-15). A truly comprehensive quantification requires a dual-metric approach for every segment. Assessing each component through both normalized and real-scale lenses ensures a nuanced understanding of the interplay between temporal duration, discharge levels, and constituent concentrations.

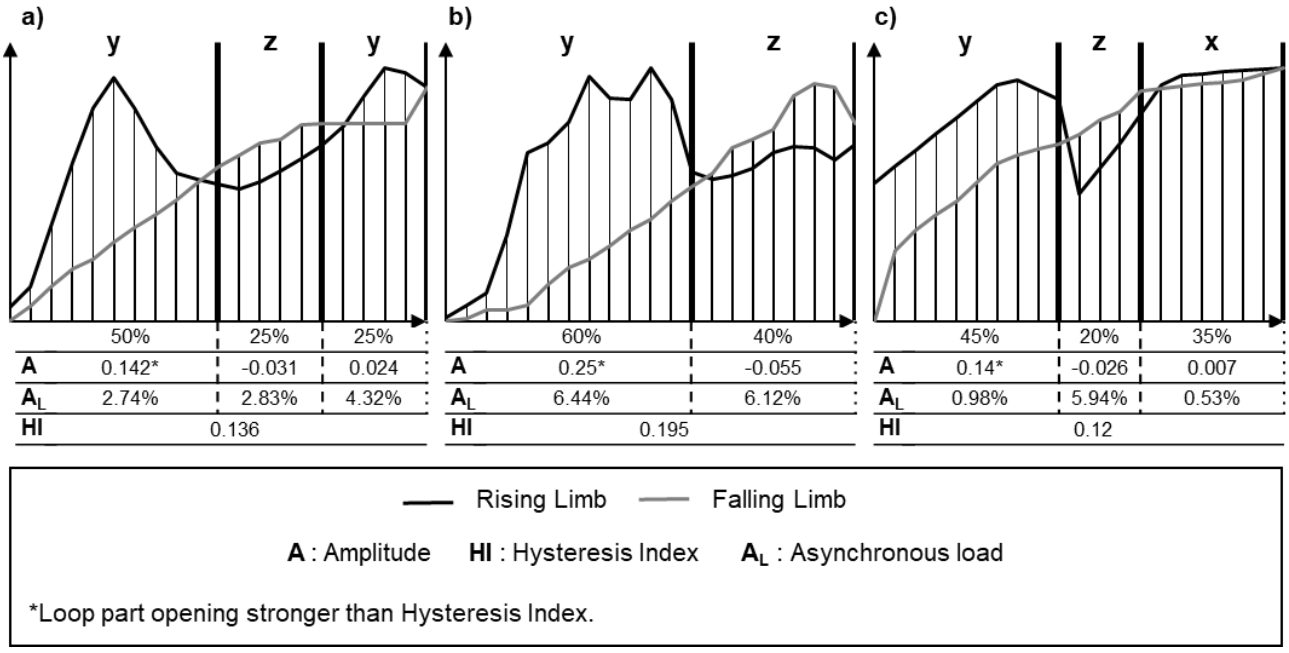

Figure III-15. Comparative analysis of hysteresis loops: Demonstrating the divergence between normalized metrics and physical hydrologic observations.

III-7. Method's Performance Critical Analysis

III-7.1. Hysteresis Classification and Quantification Tool

Hysteresis analysis can be divided into two parts: (1) the qualitative part which is usually performed graphically and therefore the obtained information is of an observational nature, and (2) the quantitative part which considers all the numerical derivations extracted from the hysteresis relationship such as size and slope. Many works have addressed issues related to each part albeit considering each issue individually. As a result, the available methods are inconsistent with each other. For instance, the classification of events is performed manually (same type of information when using machine-learning image identification however manual classification is more accurate). Then, hysteresis indices are calculated. All the limitations related to each method are passed down when they are coupled. Indeed, only classes I, II, and III are characterized correctly. Class IV is characterized as Class II or III disregarding the flow level whereas Class V and similar loops are mostly mis-characterized because of the combination of positive and negative metrics.

Signature-based hysteresis analysis is built so that such inconsistencies and drawbacks are solved. As shown in Figure III-16, the computation bloc of the method performs all the operations simultaneously then outputs the results all together. This intricate build relates all the calculations and sequencing to individual intervals. Then, partial amplitudes, elemental sequence parameters, and initial sediment loads per interval are reduced simultaneously. As a result, the output results are coherent:

- The signature identifies the form.
- Each sequence parameter in the signature identifies a part that constitutes the form.
- The position of each sequence parameter identifies the position of the part in the hysteresis form going from left to right and thereby from low to high flow, respectively.
- The width and position of each sequence parameter identify the flow range associated with the hysteretic event
- The amplitude of each sequence parameter describes both its geometrical significance and hysteretic strength on a normalized scale.
- The real-scale metrics of each sequence parameter characterize its physical (hydrological) impact and relates its hysteretic strength to its natural counterpart.

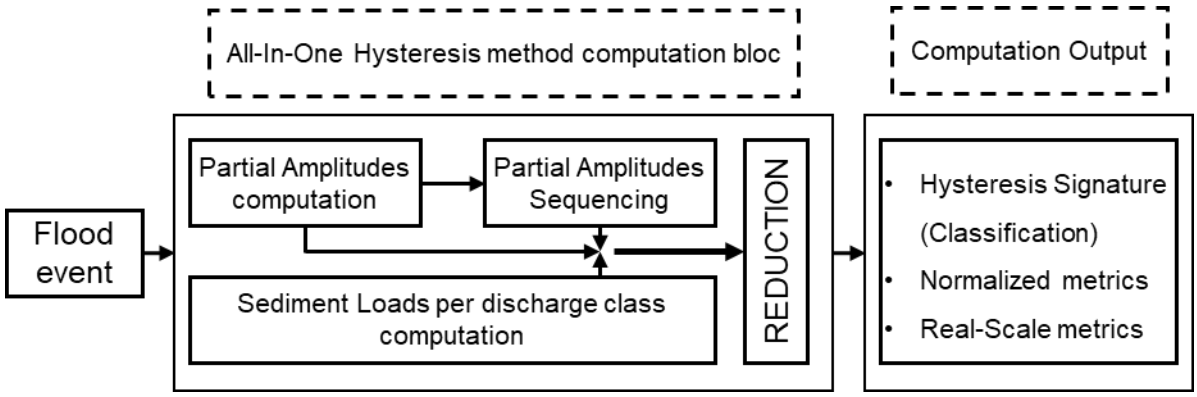

Figure III-16. Signature-based hysteresis analysis computation and output format schematic.

III-7.2. Method's Additional Performance Validation

Data records from different parameters vary in scale, data sign, time resolution, and relationship direction (positive/negative). Field data allowed us to test some data variations such as scale and mixed data quality (mostly low on the rising limb and high on the falling limb). However, there was still room for more testing to validate the data compatibility of the approach. To this end, we tested the procedure on manually generated events to figure out whether different combinations of data characteristics have any effect on the results.

High resolution data showed that the treatment process balances the number of points between the rising and the falling limb. As an effect, when a high-resolution dataset is used, the number of measurements is decreased, smoothing the loop in the process (e.g., Figure III-3). Meanwhile, when a low-resolution dataset is used, the number of measurements is increased. This observation was also made with observed data, prompting the need for a qualitative and a quantitative validation for several subdivisions, which were adequate (Chapter III – Section III-5.2). Hence, we concluded that the data quality does not affect the processing.

Data normalization standardizes the scale and sign of the values. Partial amplitudes depend only on the area enclosed between the rising and falling curves (Figure III-17). Consequently, the approach can classify and quantify the loop unaffected by the slope and data sign. As a result, we concluded that the approach successfully treats hysteresis loops unaffected by data sign and scale.

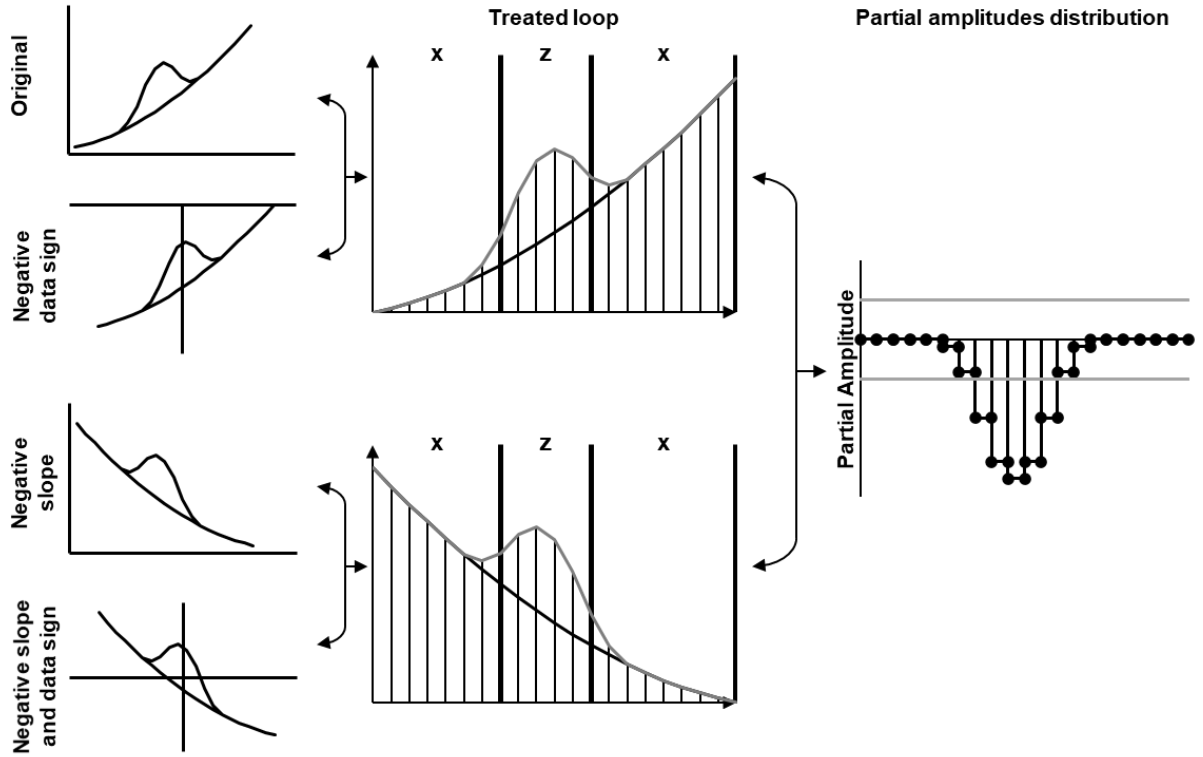

Figure III-17. Data treatment compatibility with different data variations and the same hysteretic effect.

III-7.3. Sediment Sources Separation

III-7.3.1. Hydrologic consideration

As stated in Chapter II - Section II-5.2 and detailed in Table II-2, there is no consensus among authors on the controls of C-Q hysteresis patterns where one pattern is associated with multiple possible processes. Hence, it is required to ascertain that the lower bound of the loop is the contribution of the stream channel while the loop area is the contribution from other sediment sources. Accordingly, the workflow to verify whether the Asynchronous load (A_L) is dependent upon External Sources being the main factor responsible for the hysteresis effect (Figure III-18).

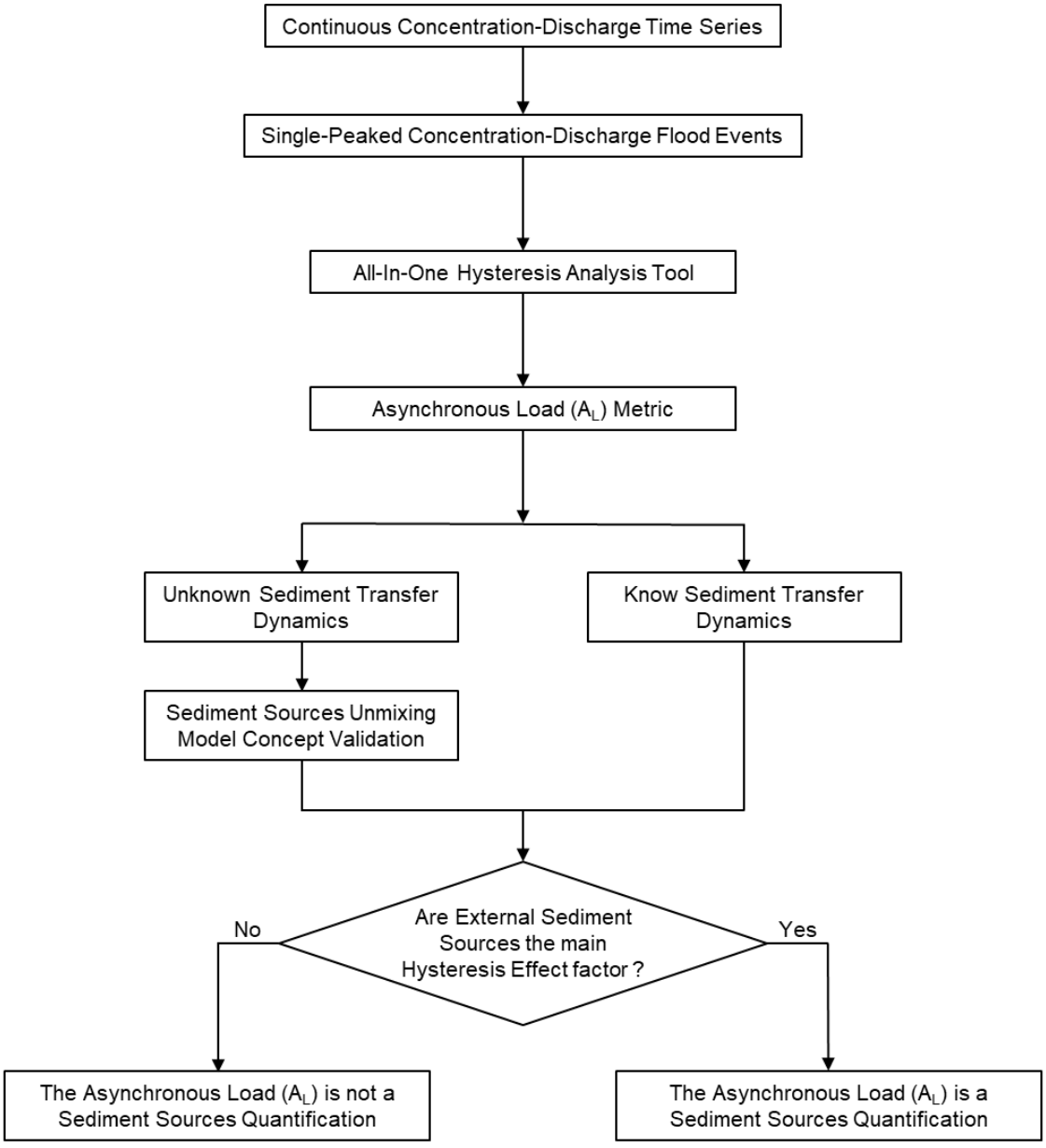

Figure III-18. Decision Tree for Interpretation of Sediment Sources Quantification using the Asynchronous Load.

As shown in Figure III-18, There exists two workflows to assess whether the asynchronous load (or loop area) is the contribution of External Sources. The first path is when sediment transfer dynamics are known. This path does not require any further verification. For instance, Megnounif et al., (2013) used their unmixing model to study the case of Oued Sebdou (Northwest of Algeria). Their application was straightforward since sediment dynamics are known due to the sheer amount of conducted studies in the region (Ghenim, 2013; Ghenim et al., 2007; Megnounif et al., 2005, 2007, 2013; Megnounif & Ghenim, 2016; Megnounif & Ouillon, 2018).

Meanwhile, it becomes more intricate when sediment dynamics are unknown. In this case, it is essential to substantiate whether the model's concept adheres to the basin's sediment response behavior. Appropriately, the options to validate the applicability of the model range from data-analysis techniques (such as hysteresis classification, and Hydrograph and sedigraph analysis) to in-field and lab-work small studies (such as in-situ channel dimensions monitoring, sediment fingerprinting, and short-term stream sampling at successive cross-sections). In brief, the second flow path is when sediment transfer dynamics are unknown and thus require further validation (e.g., the validation process advanced by Khettab, (2022)).

It is worth noting that when external sediment sources' contribution is not the main factor controlling hysteresis pattern, might be indicated by a failure in the validation process, the Asynchronous Load might not reflect a sediment sources quantification. Regardless, it remains a useful indicator to analyze hysteresis loops for concentration-based water parameters as demonstrated in Chapter III – Section III-6.2.

III-7.3.2. Example Sediment Sources Unmixing Model Concept Validation

The workflow when whether sediment availability-depletion is the main factor is unknown can use hysteresis analysis of successive flood events and thereby the analysis of multiple flood events (Chapter II – Section II-5.2.4). To demonstrate the validation process, a multipeak event was arbitrarily selected from the dataset. The flood was extracted from the station located in Colorado, United States (USGS station 07105800). The duration of the event is 10 days and consists of 9 main peaks (Figure III-19). The processing results of the separated floods are summarized in Table III-2.

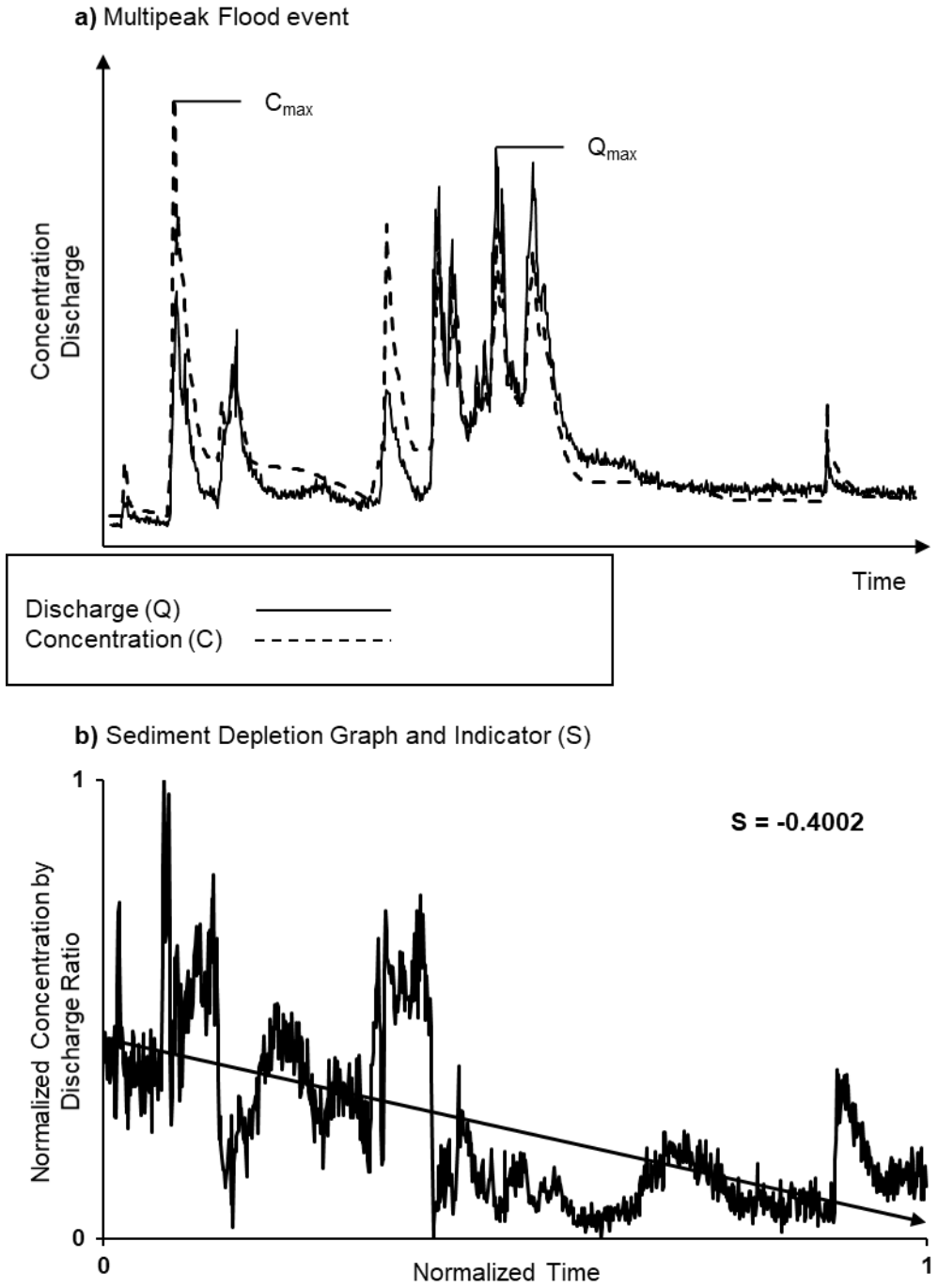

Figure III-19. Multipeaked flood and sediment depletion graphs example for Sediment Unmixing Model concept validation.

Table III-2. Multipeaked Flood Hysteresis Analysis Results summary

Peak	Signature	Hysteresis Class	Asynchronous Load (in metric ton)	Normalized Loop Area
1	y	Clockwise	968.64	0.265
2	yzyx	Complex	351.05	0.176
3	zxy	Figure of 8	530.14	0.138
4	zx	Linear + Anti Clockwise LA3	1114.23	0.209
5	zy	Figure of 8	272.03	0.261
6	zxy	Figure of 8	52.95	0.185
7	zxy	Figure of 8	52.21	0.151
8	x	Linear	229.75	0.041
9	x	Linear	564.59	0.038

As shown in Figure III-19, sediment depletion is evident since the slope of the normalized concentration by discharge ratio is a negative value. Indeed, the maximum concentration (C_{max}) occurs at the early stages of the event compared to the maximum discharge (Q_{max}). This indicates that sediments are highly available at the start and progressively decrease as the flood progresses. This observation is reinforced by the successive classification of individual peaks. As summarized in Table III-2, the last two floods in the succession are a single-valued curve. The depletion is also shown in the size of the loop area, as it is constantly decreasing going from Peak 1 to Peak 9. This depletion can also be seen in the decrease in slope of individual peaks (Figure III-20b). As shown in Figure III-20b, Peak 1 has a steeper slope indicating a high sediment availability. As shown in Figure III-20a Peak 1 is positioned above all the other floods. Peak 3, also has a steeper slope possibly due to a heavy rainfall episode. Meanwhile, the remaining peaks have a lower slope and are superposed. This superposition leads to the appearance of a significant shared segment at the lower bound of the curve. The shared segment, and the appearance of a single-valued curve, or in this case two, at the end of the event indicates the depletion of external sources the stream channel becoming the sole contributor to sediment yield and thus indicating the success of the validation process.

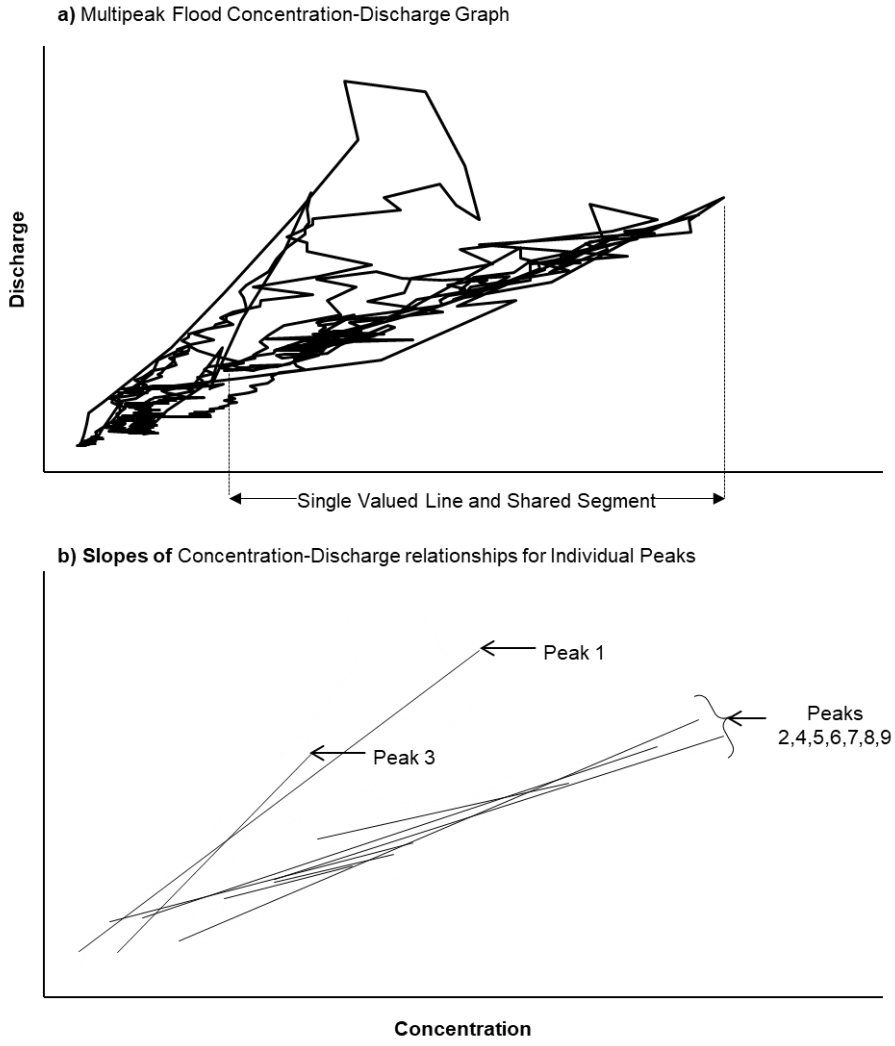

Figure III-20. Multipeaked Flood Concentration-Discharge Graph and Individual Peaks' Slopes.

III-7.4. Method Implications

III-7.4.1. Method Limitations

While signature-based hysteresis analysis effectively solves the many methodological issues of current hysteresis analysis, it is still only compatible with single-peak events. Multi-peak events either need to be separated or treated differently. However, their treatment is riddled with

technical difficulties and hydrological considerations. While their detection is easy, because they fail the data preprocessing validation, their data treatment is a case-by-case approach. In other words, each type of multipeak event has its own treatment. More technical considerations such as the difference between a fluctuation, an inconsequential spike (due to data errors or equipment malfunction), and an actual discharge peak increase the difficulty to obtain a robust automated procedure. Moreover, there is also the consideration of which and how different flow phases are compared. While single-peak events directly compare the rising and the falling limb, multipeak events have multiple rising and falling phases. Defining which phases of flow to compare not only is a technical challenge but needs to be defined under a hydrological aspect. Finally, multipeak events are both diverse and scarce, and therefore tend to be overlooked, and consequently, they remain an open challenge for future work and studies.

III-7.4.2. Method Generalization and Future Directions

The detailed analysis and inspection of the extensive method application on the main and manually generated datasets confirmed that the method can be applied on various datasets. In other words, the method can be applied to analyze various other hysteresis relationships in hydrology and across other domains. Indeed, hysteresis effect has been observed between many hydrologic parameters ranging from concentration-based parameters (suspended and bedload sediments, solutes, nutrients, and pollutants) to conductance, temperature, and groundwater level against discharge to name a few (see Chapter II – Section II-4).

The method has a modular nature where the computation of results can be split into two parts (1) the signature and normalized metrics calculations and (2) real-scale metrics computation. Accordingly, the first block is universally applicable (as shown in section III-7.2). The second block presented in this study is only applicable to concentration-based parameters against discharge. For other parameters, adequate calculations are required. These calculations can be easily implanted due to the method's flexible structure.

Chapter 3

Conception and Development of An Improved Concentration – Discharge Hysteresis Analysis Workflow

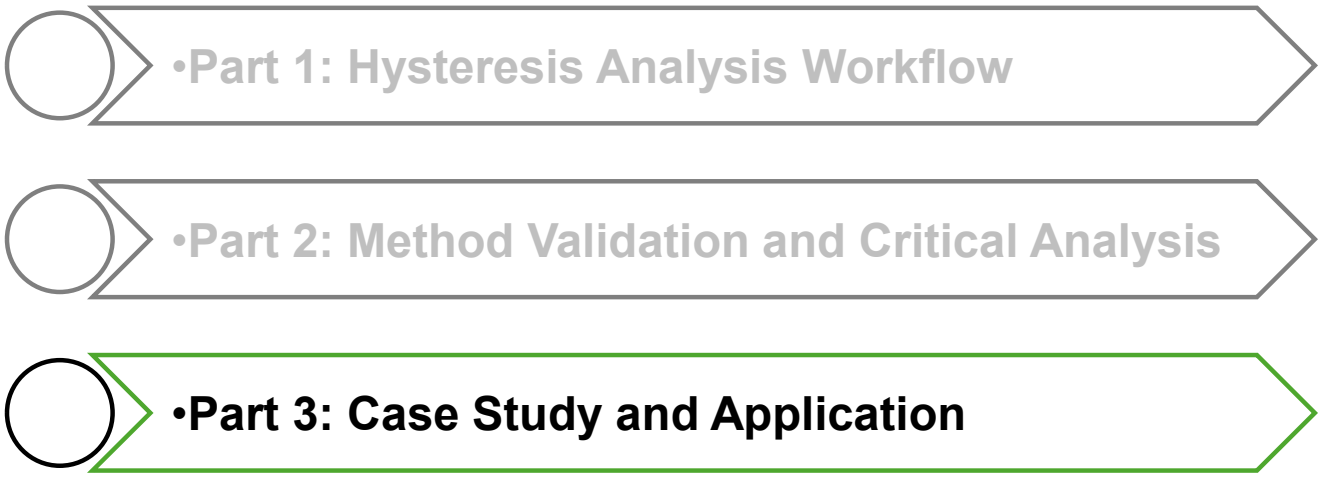

III-8. Method Application – Case Study.

III-8.1. Background

Semi-arid zones, also known as drylands or steppe regions, are geographical areas characterized by limited and irregular rainfall, resulting in a unique set of ecological, climatic, and socio-economic challenges, covering a significant portion of the Earth's surface. Arid and semi-arid areas comprise about 30% of the earth's surface (Huang et al., 2008; Tietjen & Jeltsch, 2007) among which semi-arid regions cover about 15 % (Huang et al., 2016). Semi-arid zones are typically found in the transition zones between deserts and more humid regions. They are characterized by low average annual rainfall, erratic precipitation patterns, high evaporation rates, and often extreme temperature fluctuations. These climatic conditions contribute to the formation of a distinct ecosystem, adapted to survive in water-scarce environments.

In recent years, the challenges associated with semi-arid zones have been exacerbated by climate change and human activities (e.g., Charney, 1975; Huang et al., 2016; Y. Xue, 1996). Rising temperatures, increased frequency of droughts, and land degradation pose significant threats to the delicate balance of these ecosystems.

One of the primary water challenges in semi-arid zones is the scarcity of rainfall (Ammar et al., 2016). These regions often receive low and irregular precipitation, which leads to a limited natural replenishment of water sources. The lack of reliable water supply poses significant hardships for communities that rely on agriculture, livestock, and domestic use. Insufficient rainfall can result in crop failures, reduced food production, and economic instability, leading to food insecurity and poverty (Ammar et al., 2016).

Another water challenge in semi-arid zones is the high rate of evaporation (Yaseen et al., 2020). With intense heat, water evaporates quickly from surface water bodies, soil, and vegetation. This exacerbates the water scarcity issue and further limits the availability of usable water resources. It also contributes to soil degradation and reduces the productivity of agricultural lands.

In semi-arid zones, where the amount of rainfall is limited, every drop of water is valuable. However, erosion processes can contribute to the loss of soil and sediment transport, which can

have significant implications for water resources. When rainfall occurs, the eroded soil particles are carried away by runoff, resulting in sedimentation in rivers, streams, reservoirs, and other water bodies. The deposition of sediments reduces the overall volume of water that can be stored. As sediments accumulate, the capacity of reservoirs and water storage structures diminishes, limiting the amount of water available for various purposes such as irrigation, drinking water supply, and industrial use. This aggravates the water scarcity issue, particularly during prolonged dry spells or droughts.

Managing sediment transport and studying sediment sources in semi-arid regions can help improve water management strategies and address water challenges. By understanding the origins, composition, and transport mechanisms of sediments, targeted interventions to address water challenges can be developed. Implementing soil conservation measures can help prevent erosion and reduce sedimentation in water bodies and improve soil structure and stability. By minimizing soil erosion, the amount of sediment carried by runoff can be significantly reduced, preserving the storage capacity of water reservoirs, and improving water quality.

III-8.2. Motive, Study Area, and Objectives

Algeria has limited natural water resources, with a notable scarcity in arid and semi-arid areas (Nadir & Boualem, 2016; Soltani et al., 2020). A large portion of northern Algeria falls within semi-arid climate regions, whereas the southern part is arid. Sediment transport in the region exacerbates the water stress situation. According to Guesri et al., (2020), an average of 45 million m^3 of siltation is deposited annually at the bottom of dams. It is reported that siltation in Algerian dams has caused a significant loss of annual water storage capacity, ranging between 2-5% (Benselama et al., 2019; Kassoul et al., 1997; Megnounif et al., 2013).

Among regions of interest in northern Algeria, the Mekerra basin stands out. The basin of Oued Mekerra, a sub-basin of the Macta watershed, is mostly located in the Sidi-Bel-Abbès Province, northwest of Algeria. To the north of the basin are the Tassala mountain range, where the elevation ranges between 1000 and 1100 meters; to the west are the mountains of the Tlemcen Province, with elevations around 1200 meters; to the south are the highlands of the Ras El Ma region, with elevations ranging from 1200 to 1260 meters; and to the east are the Telagh plateau

and Saïda mountains. The southern part of the basin is mostly covered with alfalfa and brushwood (Cherif et al., 2009). The central part of the watershed is forested, primarily with Aleppo pine and holm oak (Diaf et al., 2020). To the north, the region consists mainly of agricultural plantations and farmland (Cherif et al., 2009).

The Mekerra watercourse's flow is influenced by a semi-arid climate, characterized by irregular rainfall with an average annual precipitation ranging between 300-450 mm (Benmansour & Haddouche, 2019; Chehibi et al., 2024; Cherif et al., 2009; Diaf et al., 2020; Maref & Seddini, 2018; Otmane et al., 2017). Rainfall is inconsistent, with long drought periods and high-intensity rainfall events. The drought periods do not support the development of a dense soil cover, leaving surfaces exposed to significant rain splash effects during intense rainfall (BENKHADRA, 1997; Diaf et al., 2020).

The main course of the Mekerra originates in the south, from the high valleys of Ras El Ma. The basin can generally be divided into three areas: highlands in the south (1640-750 m), middle elevation areas (750-493 m), and the plain of Sidi Bel Abbès in the north (493-350 m) (Benmansour & Haddouche, 2019; Maref & Seddini, 2018; Otmane et al., 2017). Accordingly, the watercourse has three streamgages along its course (Cherif et al., 2009; Meddi & Ben Abbes, 2014; Otmane et al., 2017):

- **Hacaiba streamgage** controls the upper Mekerra basin, which has a drainage area of 938 km².
- **Sidi Ali Benyoub streamgage** controls the upper and middle Mekerra basin, with a drainage area of 1871 km².
- **Sidi Bel Abbès streamgage** controls the entirety of the watershed (upper, middle, and lower) with a drainage area of 3000 km².

The Mekerra watercourse is known to flood parts of the towns in the lower Mekerra, namely the city of Sidi Bel Abbès (e.g., Benmansour & Haddouche, 2019; Chehibi et al., 2024; Meddi & Ben Abbes, 2014; Otmane et al., 2017). In addition to reducing dam storage, sediments can settle along, or clog infrastructure designed for flood mitigation, thereby increasing flooding risks. Flooding prone urban areas, the Tabia dam, and the Sarno dam are located downstream of the Sidi

Ali Benyoub streamgage, making this station a crucial node for studying sediment transport and assessing sediment sources to address these issues.

Accordingly, in this section, the improved hysteresis analysis method is applied to study concentration-discharge relationships at this station. To further validate the enhanced hysteresis analysis workflow, the objectives of this application are to:

1. Study sediment dynamics in the watershed.
2. Verify whether the watershed response presents any challenges to the application of the method.

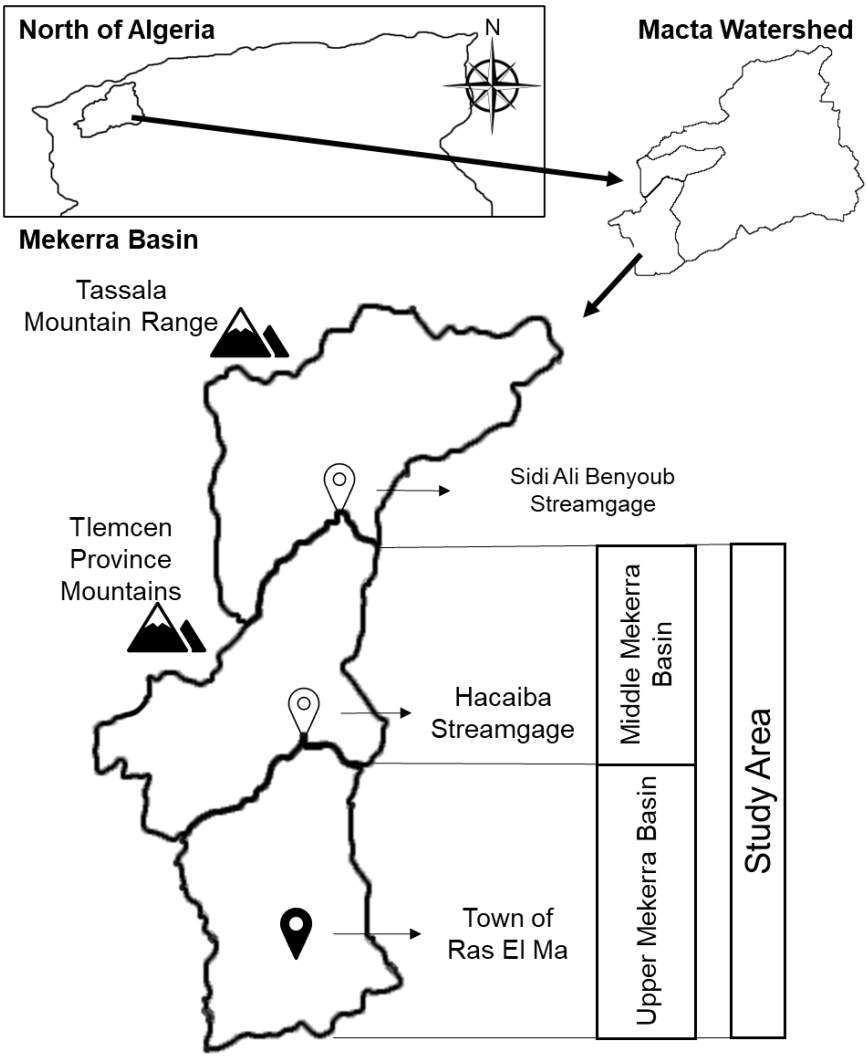

Figure III-21. Mekerra Basin Map

III-8.3. Data Collection, Preliminary Analysis, and Processing Path

The dataset utilized in this study comprises suspended sediment concentration and discharge measurements collected at the Sidi Ali Benyoub Streamgage. These data records, spanning from 1988 to 2009, were compiled by the Algerian National Agency of Hydraulic Resources (ANRH). The sampling frequency was adaptive: during baseflow conditions, samples were recorded less frequently, while during high flow periods, sampling frequency is increased to as frequent as every 15 minutes. The steps involved in data processing and analysis are summarized in Figure III-22.

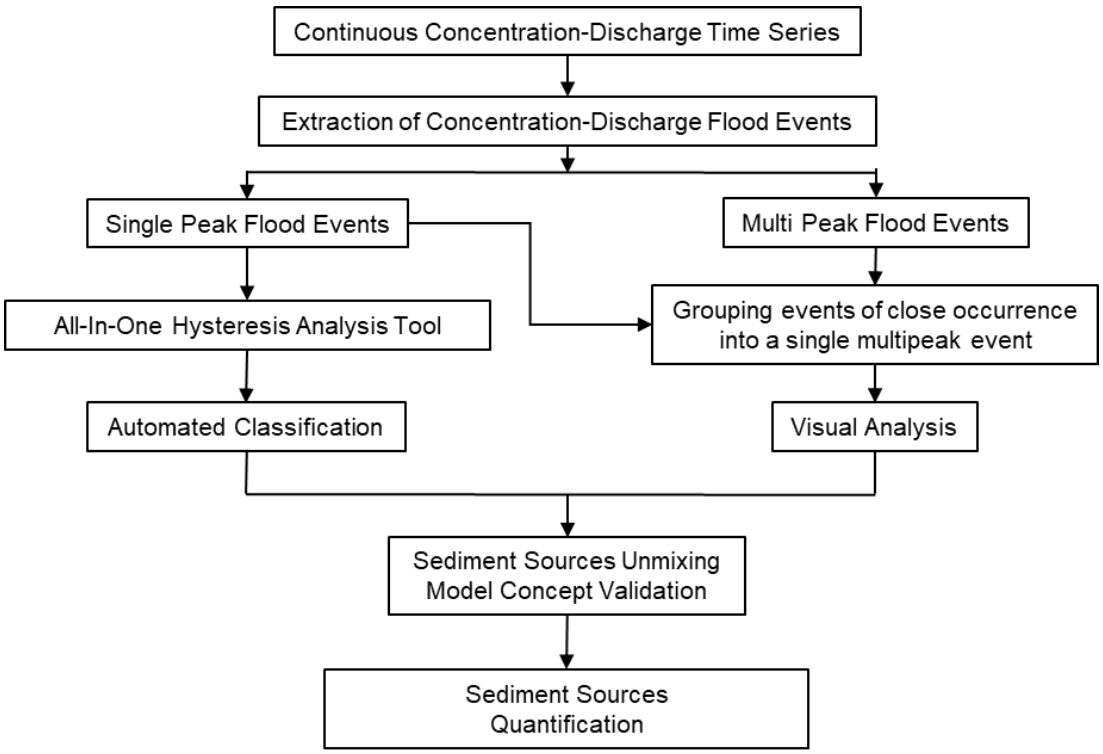

Figure III-22. Data processing and analysis flowchart

Flood events were extracted from the dataset using a semi-automatic algorithm. The start and end of these events were then manually verified and corrected as necessary (as described in Chapter III – Section III-4). Multi-peak events were separated into single-peak events when

possible. From the dataset, 91 hydrologic events were identified, of which 82 were single-peak events, while the remaining 9 were multi-peak floods.

The events underwent a preliminary assessment to evaluate their characteristics. The asynchrony of the sedigraphs was analyzed (Figure III-23). As shown in the comparison of maximum discharge concentration against peak discharge, the sedigraphs peaked around the same time as the discharge, with 24.2% peaking before the discharge, 37.4% peaking after the discharge, and 38.4% being synchronized. However, for most asynchronized events, the peaks of the sedigraphs occurred within a short timeframe relative to the discharge peak.

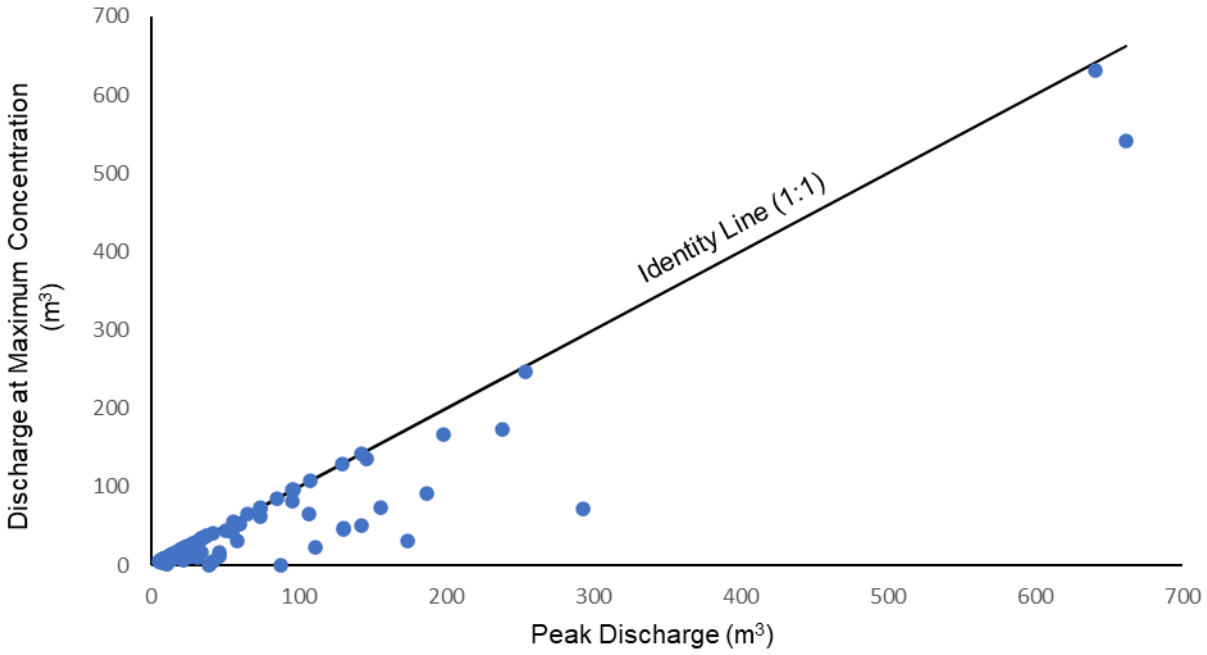

This plot compares the discharge at which the maximum concentration was recorded with the peak discharge for each event. The 1:1 identity line is included for reference.

Points that fall below the identity line indicate that the discharge at which the maximum concentration occurred was lower than the peak discharge. This highlights the asynchrony between the sedigraph and the hydrograph.

Figure III-23. Sedigraph asynchrony analysis versus discharge.

The events were characterized by an abrupt rise and a short rising limb. The hydrographs can be categorized as extremely skewed (negatively skewed or of a prior-peak shape, according to Yue et al., (2002)). The hydrographs also exhibit an impulse-like shape with a sharp rise and fall followed by a long tail flow recession phase (Figure III-24). Floods tended to be separated by long drought and baseflow periods, ranging from a few weeks to several months, with an average drought period of about 71 days. This separation led to the dominance of isolated flood events, which could pose an obstacle in the sediment source concept validation phase.

Finally, single-peak events were processed using the all-in-one hysteresis tool described in Chapter III – Section III-5 to obtain the automated classification of hysteresis loops. Both single-peak and multi-peak events were considered for grouping floods of close occurrence to validate the applicability of the sediment sources unmixing model. However, even after grouping events of close occurrence into successive and multi-peak events, the dataset still consisted predominantly of single-peak floods. Therefore, the validation of sediment sources relied on the analysis of both single-peak events and grouped events, as shown in Figure III-22.

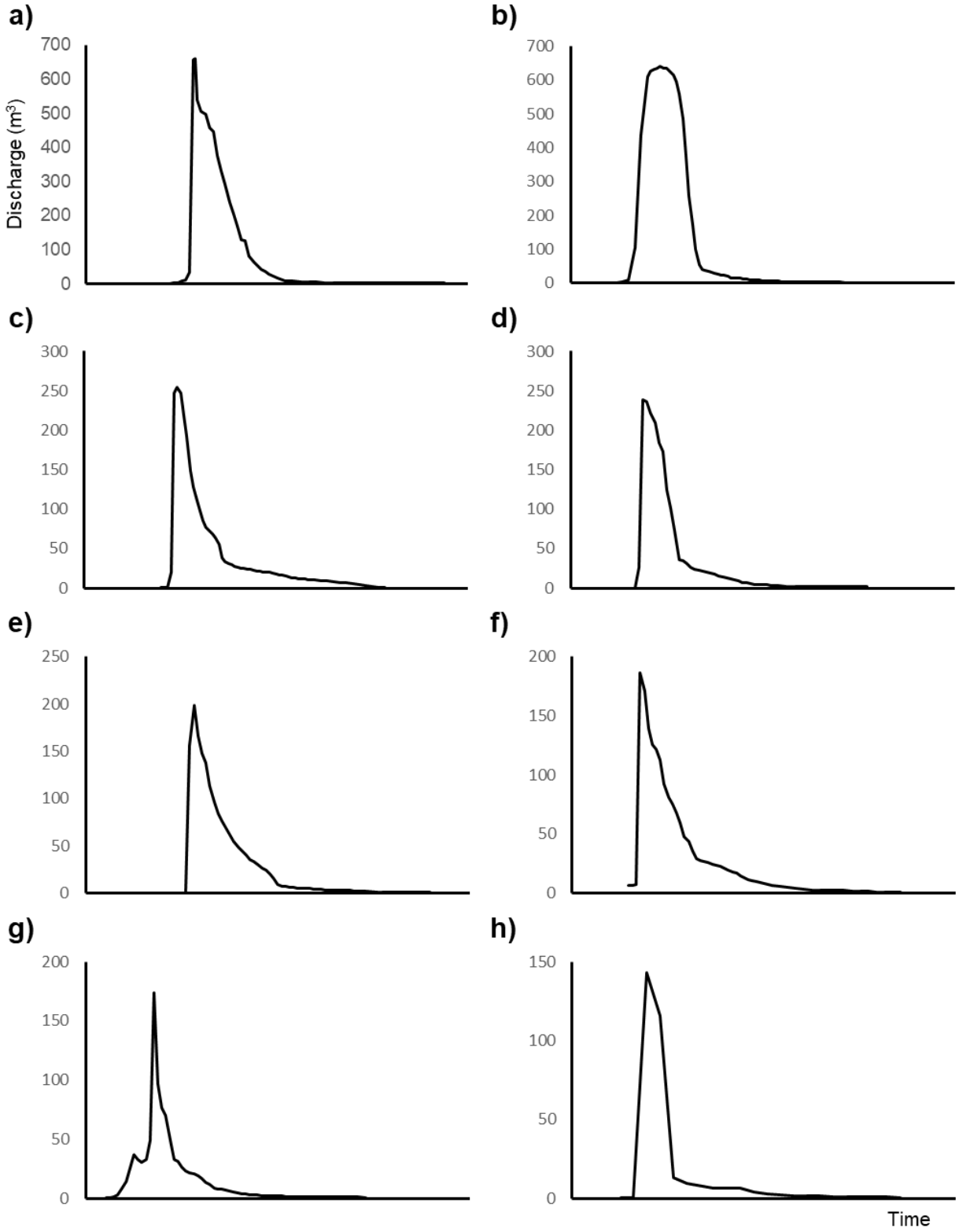

Figure III-24. Examples of the dominant hydrograph shape and distribution.

III-8.4. Results and Discussion

III-8.4.1. Concentration-Discharge Hysteresis Relationships

The processing results, summarized in Table III-3, reveal a diverse set of C-Q hysteresis relationships within the Mekerra watershed, encompassing combinations of single-valued lines, clockwise, and anticlockwise loop segments. The most frequently occurring classes were single-valued line plus clockwise and single-valued line plus anticlockwise loop (25.27% and 19.7% respectively). The diversity of C-Q relationships strongly suggests that the watershed is not dominated by a single type of hydrological response but is influenced by multiple, interacting sediment sources and transport mechanisms.

The distinctive sediment transport behavior observed in the Mekerra basin can be attributed to its meteorologic and geomorphologic properties. Rainfall events in the region tend to be sporadic and intense, which limits the development of dense land cover and leaves the soil exposed and vulnerable to rainfall erosivity, continuously refreshing the availability of loose sediments across the drainage area just prior and during runoff events, contributing to heightened sediment mobilization.

Prolonged drought periods between high-flow events significantly influences sediments available during a flood event. Bača, (2008) highlighted that sediment transport during a flood is influenced by the time elapsed since the previous event. Similarly, Malutta et al., (2020) emphasized that longer intervals allow for the replenishment of sediment supply. Rovira & Batalla, (2006) further described sediment dynamics as a two-phase process involving sediment preparation followed by sediment transfer and depletion. In the Mekerra watershed, extended drought and baseflow conditions between high-flow events promote the accumulation of sediments both within the basin and in-channel storage. The prevalent impulse like hydrologic response is also a factor that favors in-channel sediment accumulation and therefore sediment resuspension, leading to the frequent occurrence of early sediment peaks during subsequent floods.

Sediments from distant upstream sources must traverse significant distances before reaching the streamgage station. The disparity between the movement of water and sediment is further amplified by the basin's hydrological response, where flow events exhibit a sudden and

steep rise from baseflow to peak discharge over a short duration. This abrupt and rapid increase in water discharge allows the flood wave to propagate much faster than the sediment wave, accentuating the lag in sediment transport and shaping the observed hysteresis patterns. This phenomenon has been widely documented, with studies attributing anticlockwise hysteresis behavior to delayed sediment supply from upstream tributaries or the slower movement of sediment compared to flood waves (e.g., Heidel, 1956; Lloyd et al., 2016; Williams, 1989; Yang & Lee, 2018). Other studies have linked this behavior to sediments from distant sources or late sediment contributions (e.g., Aich et al., 2014; Asselman, 1999; Bača, 2008; Buendia et al., 2016; De Girolamo et al., 2015; Duvert et al., 2012; Gao & Josefson, 2012; McDonald & Lamoureux, 2009; Megnounif et al., 2013; Pietroń et al., 2015; Rodríguez-Blanco et al., 2010; Seeger et al., 2004; Tian et al., 2016; Ziegler et al., 2014).

Table III-3. Classification summary for Oued Mekerra Flood Events

Signature	Hysteresis Class	Count	Portion
x	Single-valued line plus loop	4	4.40%
y	Clockwise	7	7.69%
z	Anticlockwise	8	8.79%
xy	Single-valued line plus clockwise loop Type A	8	8.79%
xyx	Single-valued line plus clockwise loop Type B	3	3.30%
yx	Single-valued line plus clockwise loop Type C	12	13.19%
xz	Single-valued line plus Anticlockwise loop Type A	7	7.69%
xzx	Single-valued line plus Anticlockwise loop Type B	2	2.20%
zx	Single-valued line plus Anticlockwise loop Type C	9	9.89%
yz	Figure of Eight (Clockwise – Anticlockwise)	4	4.40%
yxz		4	4.40%
zy	Figure of Eight (Anticlockwise – Clockwise)	2	2.20%
zxy		2	2.20%
xyxz	Other	2	2.20%
xzxz		1	1.10%
yxy		1	1.10%
yzx		6	6.59%
Multipeak		9	9.89%

These combined factors drive the coexistence of both clockwise and anticlockwise hysteresis behaviors in the Mekerra basin, contributing to their frequent occurrence alongside more complex loop patterns, such as figure-of-eight configurations, which reflect the dynamic nature of sediment transport. The recurrent observation of single-valued line behavior suggests similar sediment transport rates between rising and falling flow phases, potentially indicating the depletion or temporary interruption of external sediment sources. This observation is particularly significant to validate sediment separation concept (Chapter II - Concept Validation).

III-8.4.2. Sediment Sources Separation Concept Validation

The main requirement to apply the lower bound curve method is to assess whether it is an adequate representation of the channel network contribution to sediment transport. The first part of the validation involved the grouping of events of close occurrence. Although floods tended to be separated by long droughts and baseflow periods, several multipeak and successive (or closely occurring) events were observed. These events were classified into three categories:

(1) Small events grouped with a major event, where the latter dominates, rendering the smaller ones inconsequential.

(2) Individual flood hysteresis loops showing a decreasing slope and size, indicating reduced sediment availability, without a shared segment or the presence of a single-valued line.

(3) Stacked or superposed hysteresis loops sharing a segment of the lower bound curve or displaying a single-valued line in secondary events.

In the first and second categories, it is unclear whether the lower bound curve represents solely the contribution of internal sources. Meanwhile, the third category provides the strongest indicator. Indeed, as initial conditions such as sediment storage, soil moisture, and storm characteristics vary between successive events, the streambed and banks remain the only consistent sediment sources. When sediments from external sources are absent or depleted, the dominant sediment supply shifts to the channel bed and banks, resulting in shared segments of the lower bound curve across successive floods (Figure III-25).

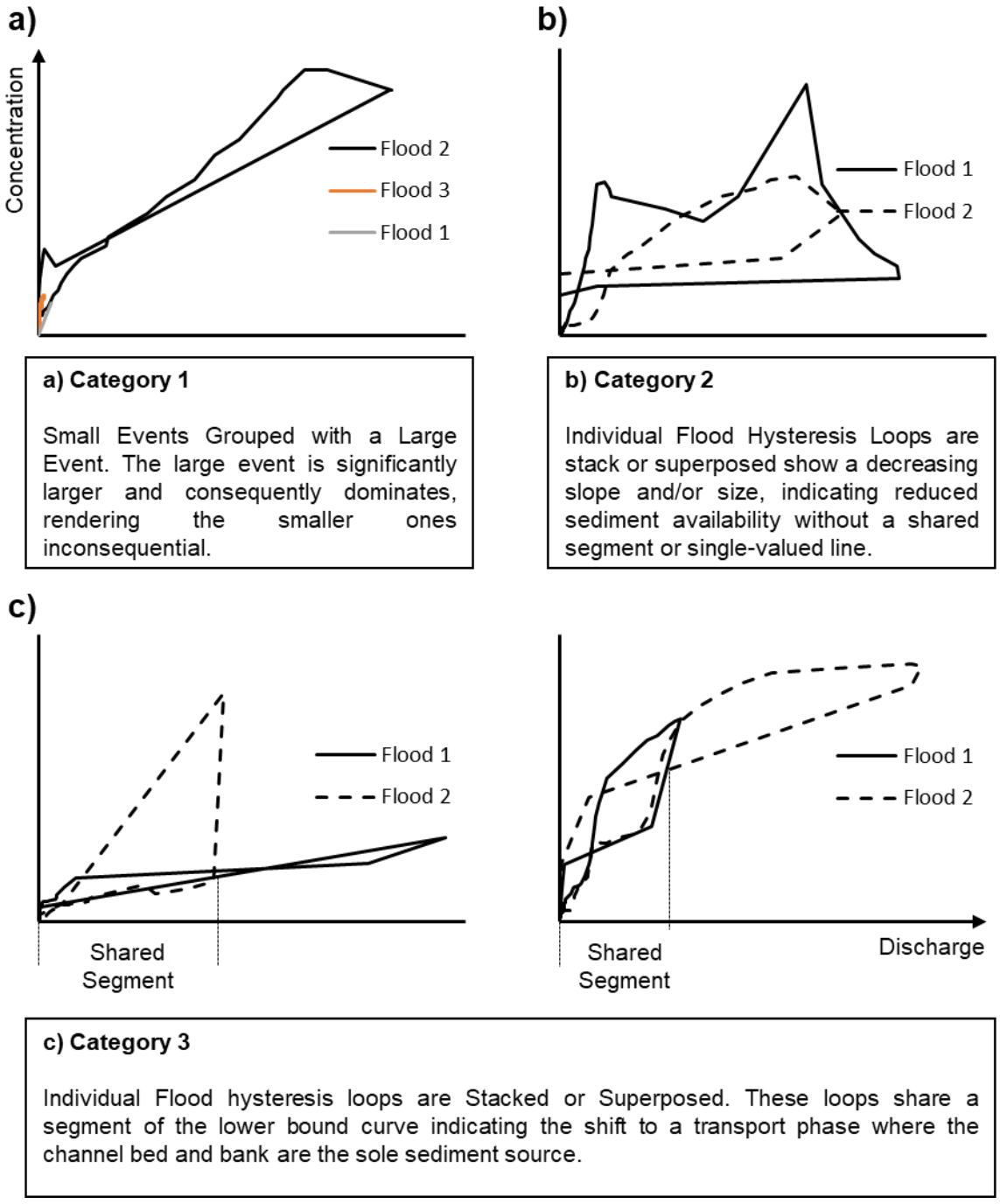

Figure III-25. Successive Flood Categories Examples

Although the third category provided strong evidence, most events were isolated single-peak events, requiring further analysis. In previous studies**,** a single-valued line is mainly attributed to an uninterrupted sediment supply (Nistor & Church, 2005; Olive & Rieger, 1985; Rodríguez-Blanco et al., 2010; H. G. Smith & Dragovich, 2009; G. P. Williams, 1989; Wood, 1977). Rodríguez-Blanco et al., (2010) and Walling & Webb, (1982) attribute this behavior to limited fine sediment availability. Since external sources are subject to variable supply and potential depletion, a single-valued line behavior is associated with the entrainment of channel material rather than hillslope-derived sediments (Hudson, 2003; Khettab, 2022; Megnounif et al., 2013).

The hysteresis signature plays a crucial role in distinguishing transport phases by highlighting concentration differences between the rising and falling limbs of the hydrograph. This distinction allows for easier isolation of phases exhibiting single-valued line behavior. This behavior was identified in approximately 60% of the events (e.g., Figure III-26), suggesting that during these events, external sources were either depleted or absent, leading to similar concentrations between the rising and falling limbs. In accordance with previous studies and successive flood observations (e.g., Figure III-25 – Category 3), a single-valued line behavior strongly indicates sediment contributions originating from the stream channel. It is worth noting that figure-of-eight loops containing a single-valued line behavior were excluded, since in these cases, the single-valued segment represents a transition between clockwise and anticlockwise subloops rather than a phase devoid of external sediment inputs.

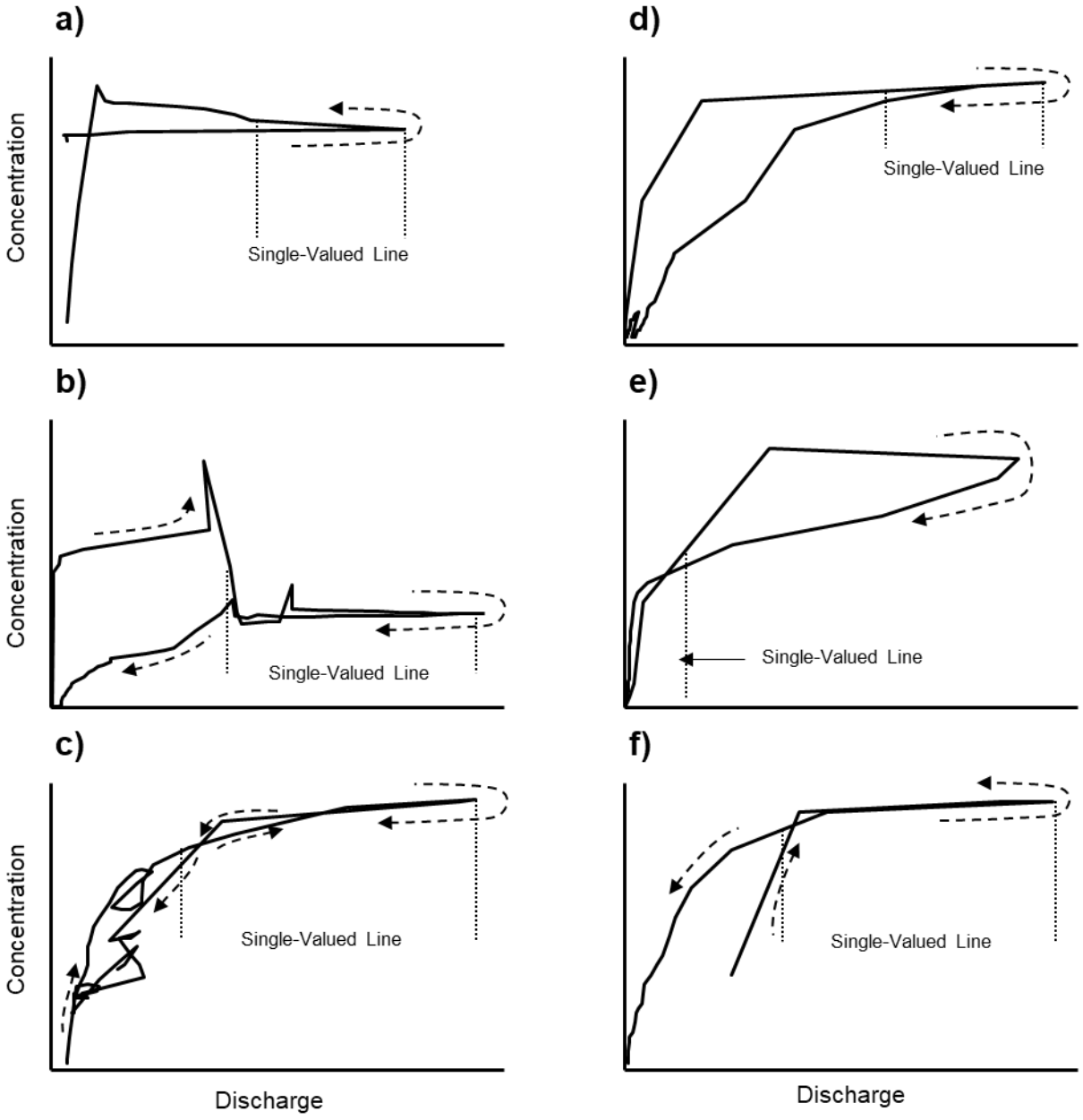

Figure III-26. Example Flood Events showing a single-valued curve segment

III-8.5. Sediment Sources Estimations

From the analysis of both single-peak and grouped flood events, it was evident that external sediment sources play a major role in shaping C–Q loop configurations in the Mekerra watershed. Results indicate that the geometrical base of the loop reliably represents channel network contributions, allowing for a straightforward estimation of stream channel-derived sediment yield.

Estimations showed that the channel network contributed approximately 84% of the total sediment transport making external contributions to be limited to only 16%. Phase-based sediment yield separation offers deeper insights into sediment transport dynamics. As shown in Table III-4, the rising limb accounts for approximately 33% of the total sediment transport, while the falling limb contributes 67%. This is a direct reflection of the hydrographs' asymmetry. Indeed, although clockwise effect was more frequent compared to the anticlockwise effect, duration plays a crucial role in defining which effect is dominant.

Table III-4. Sediment yield partitioning by source and flow phase.

Category	Sediment Yield (%)
Channel Network Contribution	84.07%
External Sources Contribution	15.93%
Sediment transport during rising limb	33.21%
Sediment transport during falling limb	66.79%

The dominant role of the channel network in sediment transport is closely tied to well-documented hydrologic processes. Sheet Flow or Overland Flow occurs when water moves as a thin, unconfined sheet over the land surface, spreading evenly transporting fine-grained sediments from hillslopes to the channel during runoff events (Yuill & Gasparini, 2011). Sediments are carried by overland flow into the channel network, where the flow is deeper and faster enhancing the overall sediment transport efficiency (Bruno et al., 2008; Di Stefano et al., 2013). Higher velocities in the channel network ensure that sediment transport downslope is dominant. For instance, Trimble, (1997) performed a long-term survey in San Diego Creek, California, United Stated, and found that the channel contribution amounts to about two thirds of the total sediment yield. Fraley

et al., (2009) conducted a study on Valley Creek, Pennsylvania, United Stated, and found that the combined contribution of bed erosion and bank erosion accounted for approximately 75% of the estimated sediment load from July 2004 to July 2005. Megnounif et al., (2013) studied sediment yield in Oued Sebdou Basin, Algeria, and found that the channel network contributed 77% of the total sediment transport.

The findings from the present study, which estimate the channel contribution to total sediment yield at ~84%, align closely with these documented values. This reinforces the notion that in semi-arid environments like the Mekerra basin, channel stabilization measures should be a primary focus for sediment management. Since channel processes largely govern sediment transport, mitigation efforts—such as bank reinforcement, riparian vegetation restoration, and flow regulation—could significantly reduce sediment loads and enhance watershed resilience.

III-8.6. Conclusions and End Notes

The analysis of sediment dynamics and concentration-discharge relationships in the Mekerra basin provided significant insights into its sediment transport mechanisms. The study highlights the substantial variability of sediment transport dynamics and on water resource management, particularly in an area that is prone to irregular and intense rainfall, dam siltation, and flood risk.

Key findings from the hysteresis analysis reveal that the watershed's response is complex, characterized by diverse hysteresis patterns striking a balance between clockwise and anticlockwise behavior. These patterns show the variability in sediment availability and transport mechanisms influenced by factors such as irregular precipitation, long drought periods, and the watershed form and size.

The predominance of single-valued curves and the successive events with stacked hysteresis loops with a significant shared lower bound segment provides a nuanced understanding of sediment source contributions during flood events and concluded that external sediment sources contribution (or sediment availability) is the main factor controlling hysteresis loops. This indicates

that the sediment sources concept (described in Chapter II – Section II-5.2) is applicable to the Mekerra basin.

The identification of the stream channel as the primary sediment source, accounting for approximately ~84% of total sediment yield during hydrologic events, emphasizes the need for targeted interventions towards the channel network to manage sediment transport effectively. These findings are crucial for developing strategies to mitigate sedimentation impacts on water storage infrastructure and mitigate the risk of flooding in the Mekerra basin.

Conclusion

Conclusion

The movement of sediment is a dual-edged process: it is essential for healthy river morphology and nutrient dispersion, yet it poses risks through the siltation of water bodies and resulting socioeconomic strain. Achieving sustainable management requires a comprehensive diagnostic approach to sediment sources and transport pathways. This knowledge facilitates a clearer understanding of landscape evolution and environmental change, linking hydrological patterns to geomorphic outcomes. Establishing a robust framework for source-based sediment assessment is therefore indispensable for modern environmental science.

Sediment particles are detached, transported, and deposited through various natural processes and anthropogenic actions. Chapter I provides a comprehensive overview of sediment dynamics, beginning with an introduction to the fundamental concepts. It delves into the mechanisms of sediment detachment, exploring both physical and chemical weathering processes such as frost action, thermal stress, salt crystal growth, and various chemical reactions like dissolution, oxidation, and hydrolysis. The chapter also examines other significant contributors to sediment detachment, including mass wasting, riverbank collapse, volcanic activity, forest fires, and human activities.

Following the detachment mechanisms, the chapter transitions to sediment transport and sedimentation. It addresses the movement of sediments by wind and water, discussing the processes of deposition and sediment mixing within different environments, such as hillslopes and hydrographic channel networks. The chapter concludes with an overview of sediment source analysis, presenting the motivations and methods used. This includes modeling sediment transport, sediment fingerprinting, and the use of rating curves and hysteresis analysis to assess sediment sources and dynamics.

As a steppingstone for the subsequent chapters, Chapter I lays the groundwork for understanding the sediment concentration-discharge relationship explored in Chapter II. The detailed examination of sediment detachment, transport, and source identification is crucial for analyzing hysteresis patterns, factors controlling these patterns, and the overall sediment dynamics within fluvial systems. This foundational knowledge is essential for the development of improved methodologies in hysteresis analysis presented in Chapter III.

Chapter II focuses on the relationship between streamflow and concentration. It begins by introducing the fundamental concepts of the concentration-discharge relationship, linking back to the processes of sediment detachment and transport discussed in Chapter I. The chapter then explores various hysteresis patterns, including single-valued lines, clockwise and anticlockwise loops, and other complex configurations.

Next, it delves into the factors controlling the configuration of concentration-discharge hysteresis. These include sediment production, sediment transport patterns, particle size, sediment source proximity, basin size, and meteorological conditions. These factors are directly related to the mechanisms covered in Chapter I.

The chapter also covers hysteresis analysis techniques, such as pattern analysis, direction and magnitude analysis, and hydro-chemical analysis. Practical applications of hysteresis analysis, including hysteresis classification and sediment source determination, are explored in detail. The chapter concludes with an overview of the current advancements and gaps linked to hysteresis analysis, setting the stage for the methodological advancements presented in Chapter III.

Chapter III represents the practical phase of this research, focusing on the development and validation of a novel methodological framework for hysteresis analysis. The chapter starts by meticulously outlining the procedure for an improved hysteresis analysis workflow. Method validation follows, encompassing both automated classification and quantitative analysis assessment.

Hysteresis is a frequent occurrence in hydrology and other fields, making its analysis a crucial tool for understanding the underlying mechanisms of a phenomenon. This chapter addresses common challenges in existing hysteresis analysis methods by introducing a more refined and precise approach to analyzing hysteresis loops. Accordngly, two primary contributions are established in this work. First, the Hysteresis Signature was engineered to segment loops into recognizable components, facilitating more efficient data reading and organization. Second, Partial Quantification builds upon these signatures to provide robust numerical analysis through both normalized and real-scale variables, a process validated through broad empirical testing.

The resulting 51-signature classification system offers a comprehensive baseline that can be easily extended via automated processing. The algorithm demonstrated impressive sensitivity,

distinguishing loop components even in instances of narrow, ambiguous geometry. This detailed exploration exposed gaps in existing metrics, specifically regarding distinctiveness and hydrologic accuracy. To address these deficiencies, the study proposes real-scale metrics and partial quantification as a more reliable standard. Even when real-scale data is unavailable, the normalized partial metrics provide a solid analytical foundation. Ultimately, the synergy between signature-based sorting and partial quantification creates a cohesive, high-fidelity framework for studying hysteresis.

The reliability of this method stems from its ability to ignore external data properties during processing. Normalized metrics and classification outcomes are determined exclusively by loop area, rendering them immune to variations in resolution or sign. While adaptive algorithms ensure real-scale metrics remain unaffected by these same factors, their use is strongly encouraged to achieve a meaningful physical characterization of the phenomena.

The scope of this approach is limited to single-peak events, yet the complexities of sequential, multi-peak occurrences warrant specialized consideration. Examining these events directly would deepen our understanding of inter-event dynamics, such as the progression of hysteresis across a series. Managing these intricate flow patterns remains an open challenge, providing a rich opportunity for scholars to build upon this work in future investigations.

This research demonstrates the significance of understanding sediment processes for accurate hysteresis analysis and highlights the practical applications of the new method in real-world scenarios. The integrated approach presented in this thesis attempts to advance the fields of geomorphology, hydrology, and environmental science by offering valuable insights and tools for sustainable water resource management and landscape evolution studies. A key strength of the proposed method is its independence from specific variables, making it a versatile tool applicable to a wide range of hydrological parameters, such as nutrients and solutes, and extending its utility to other scientific disciplines where hysteresis is a fundamental concept.

Bibliography

Abele, G. (1974). Bergsturze in den Alpen. Ihre Verbreitung, Morphologie und Folgeerscheinungen. *Wiss. Alpenvereinshefte*, *25*. https://cir.nii.ac.jp/crid/1573950400969034496

Adriano, S., Chiara, F., & Antonio, M. (2005). Sedimentation rates and erosion processes in the lagoon of Venice. *Environment International*, *31*(7), 983–992. https://doi.org/10.1016/j.envint.2005.05.008

Aguilera, R., & Melack, J. M. (2018). Concentration-Discharge Responses to Storm Events in Coastal California Watersheds. *Water Resources Research*, *54*(1), 407–424. https://doi.org/10.1002/2017WR021578

Aich, V., Zimmermann, A., & Elsenbeer, H. (2014). Quantification and interpretation of suspended-sediment discharge hysteresis patterns: How much data do we need? *CATENA*, *122*, 120–129. https://doi.org/10.1016/j.catena.2014.06.020

Allan, J. D. (2004). Landscapes and Riverscapes: The Influence of Land Use on Stream Ecosystems. *Annual Review of Ecology, Evolution, and Systematics*, *35*(1), 257–284. https://doi.org/10.1146/annurev.ecolsys.35.120202.110122

Ammar, A., Riksen, M., Ouessar, M., & Ritsema, C. (2016). Identification of suitable sites for rainwater harvesting structures in arid and semi-arid regions: A review. *International Soil and Water Conservation Research*, *4*(2), 108–120. https://doi.org/10.1016/j.iswcr.2016.03.001

Amorosi, A., Sammartino, I., Dinelli, E., Campo, B., Guercia, T., Trincardi, F., & Pellegrini, C. (2022). Provenance and sediment dispersal in the Po-Adriatic source-to-sink system unraveled by bulk-sediment geochemistry and its linkage to catchment geology. *Earth-Science Reviews*, *234*, 104202. https://doi.org/10.1016/j.earscirev.2022.104202

Andermann, C., Longuevergne, L., Bonnet, S., Crave, A., Davy, P., & Gloaguen, R. (2012). Impact of transient groundwater storage on the discharge of Himalayan rivers. *Nature Geoscience*, *5*(2), 127–132. https://doi.org/10.1038/ngeo1356

Anderson, R. S. (1998). Near-surface Thermal Profiles in Alpine Bedrock: Implications for the Frost Weathering of Rock. *Arctic and Alpine Research*, *30*(4), 362–372. https://doi.org/10.1080/00040851.1998.12002911

Anderson, R. S., Anderson, S. P., & Tucker, G. E. (2013). Rock damage and regolith transport by frost: An example of climate modulation of the geomorphology of the critical zone. *Earth Surface Processes and Landforms*, *38*(3), 299–316. https://doi.org/10.1002/esp.3330

Andrea, B., Francesc, G., Jérôme, L., Eusebi, V., & Francesc, S. (2006). Cross-site Comparison of Variability of DOC and Nitrate c–q Hysteresis during the Autumn–winter Period in Three Mediterranean Headwater Streams: A Synthetic Approach. *Biogeochemistry*, *77*(3), 327–349. https://doi.org/10.1007/s10533-005-0711-7

Andrews, J. T., & Eberl, D. D. (2012). Determination of sediment provenance by unmixing the mineralogy of source-area sediments: The "SedUnMix" program. *Marine Geology*, *291–294*, 24–33. https://doi.org/10.1016/j.margeo.2011.10.007

Andrews, J. T., Klein, A. J., Jenner, K. A., Jennings, A. E., & Campbell, C. (2018). The variability of Baffin Bay seafloor sediment mineralogy: The identification of discrete glacial sediment sources and application to Late Quaternary downcore analysis. *Canadian Journal of Earth Sciences*, *55*(6), 620–639. https://doi.org/10.1139/cjes-2017-0223

Bibliography

Andualem, T. G., Hewa, G. A., Myers, B. R., Peters, S., & Boland, J. (2023). Erosion and Sediment Transport Modeling: A Systematic Review. *Land*, *12*(7), 1396. https://doi.org/10.3390/land12071396

Anselmetti, F. S., Hodell, D. A., Ariztegui, D., Brenner, M., & Rosenmeier, M. F. (2007). Quantification of soil erosion rates related to ancient Maya deforestation. *Geology*, *35*(10), 915. https://doi.org/10.1130/G23834A.1

Arenas-Díaz, F., Fuentes, B., Reyers, M., Fiedler, S., Böhm, C., Campos, E., Shao, Y., & Bol, R. (2022). Dust and aerosols in the Atacama Desert. *Earth-Science Reviews*, *226*, 103925. https://doi.org/10.1016/j.earscirev.2022.103925

Areu-Rangel, O. S., Bonasia, R., Di Traglia, F., Del Soldato, M., & Casagli, N. (2020). Flood Susceptibility and Sediment Transport Analysis of Stromboli Island after the 3 July 2019 Paroxysmal Explosion. *Sustainability*, *12*(8), 3268. https://doi.org/10.3390/su12083268

Arnáez, J., Lana-Renault, N., Lasanta, T., Ruiz-Flaño, P., & Castroviejo, J. (2015). Effects of farming terraces on hydrological and geomorphological processes. A review. *CATENA*, *128*, 122–134. https://doi.org/10.1016/j.catena.2015.01.021

Arnalds, O., Thorarinsdottir, E. F., Thorsson, J., Waldhauserova, P. D., & Agustsdottir, A. M. (2013). An extreme wind erosion event of the fresh Eyjafjallajökull 2010 volcanic ash. *Scientific Reports*, *3*(1), Article 1. https://doi.org/10.1038/srep01257

Arndt, R. E. A. (1981). Cavitation in Fluid Machinery and Hydraulic Structures. *Annual Review of Fluid Mechanics*, *13*(1), 273–326. https://doi.org/10.1146/annurev.fl.13.010181.001421

Asselman, N. E. M. (1999). Suspended sediment dynamics in a large drainage basin: The River Rhine. *Hydrological Processes*, *13*(10), 1437–1450. https://doi.org/10.1002/(SICI)1099-1085(199907)13:10%253C1437::AID-HYP821%253E3.0.CO;2-J

Asselman, N. E. M. (2000). Fitting and interpretation of sediment rating curves. *Journal of Hydrology*, *234*(3–4), 228–248. https://doi.org/10.1016/S0022-1694(00)00253-5

Asselman, N. E. M., & Middelkoop, H. (1995). Floodplain sedimentation: Quantities, patterns and processes. *Earth Surface Processes and Landforms*, *20*(6), 481–499. https://doi.org/10.1002/esp.3290200602

Aubert, A. H., Gascuel-Odoux, C., & Merot, P. (2013). Annual hysteresis of water quality: A method to analyse the effect of intra- and inter-annual climatic conditions. *Journal of Hydrology*, *478*, 29–39. https://doi.org/10.1016/j.jhydrol.2012.11.027

Auzet, A. V., Boiffin, J., Papy, F., Ludwig, B., & Maucorps, J. (1993). Rill erosion as a function of the characteristics of cultivated catchments in the north of France. *CATENA*, *20*(1–2), 41–62. https://doi.org/10.1016/0341-8162(93)90028-N

Bača, P. (2008). Hysteresis effect in suspended sediment concentration in the Rybárik basin, Slovakia / Effet d'hystérèse dans la concentration des sédiments en suspension dans le bassin versant de Rybárik (Slovaquie). *Hydrological Sciences Journal*, *53*(1), 224–235. https://doi.org/10.1623/hysj.53.1.224

Bagnold, R. A. (1997). The flow of cohesionless grains in fluids. *Philosophical Transactions of the Royal Society of London. Series A, Mathematical and Physical Sciences*, *249*(964), 235–297. https://doi.org/10.1098/rsta.1956.0020

Baker, E. B., & Showers, W. J. (2019). Hysteresis analysis of nitrate dynamics in the Neuse River, NC. *Science of The Total Environment*, *652*, 889–899. https://doi.org/10.1016/j.scitotenv.2018.10.254

Batista, P. V. G., Davies, J., Silva, M. L. N., & Quinton, J. N. (2019). On the evaluation of soil erosion models: Are we doing enough? *Earth-Science Reviews*, *197*, 102898. https://doi.org/10.1016/j.earscirev.2019.102898

Bauer, S. J., & Handin, J. (1983). Thermal expansion and cracking of three confined water-saturated igneous rocks to 800□C. *Rock Mechanics and Rock Engineering*, *16*(3), 181–198. https://doi.org/10.1007/BF01033279

Baumann, F., & Kaiser, K. F. (1999). The Multetta Debris Fan, Eastern Swiss Alps: A 500-year Debris Flow Chronology. *Arctic, Antarctic, and Alpine Research*, *31*(2), 128–134. https://doi.org/10.1080/15230430.1999.12003290

Beaudoin, A. (2003). A comparison of two methods for estimating the organic content of sediments. *Journal of Paleolimnology*, *29*(3), 387–390. https://doi.org/10.1023/A:1023972116573

Becker, G. F., & Day, A. L. (1905). The Linear Force of Growing Crystals. *Proceedings of the Washington Academy of Sciences*, *7*, 283–288.

Beel, C. R., Orwin, J. F., & Holland, P. G. (2011). Controls on slope-to-channel fine sediment connectivity in a largely ice-free valley, Hoophorn Stream, Southern Alps, New Zealand: ALPINE SLOPE-TO-CHANNEL FINE SEDIMENT CONNECTIVITY. *Earth Surface Processes and Landforms*, *36*(7), 981–994. https://doi.org/10.1002/esp.2154

Ben Slimane, A., Raclot, D., Evrard, O., Sanaa, M., Lefevre, I., & Le Bissonnais, Y. (2016). Relative Contribution of Rill/Interrill and Gully/Channel Erosion to Small Reservoir Siltation in Mediterranean Environments. *Land Degradation & Development*, *27*(3), 785–797. https://doi.org/10.1002/ldr.2387

Benito, G., Gutie´rrez, M., & Sancho, C. (1992). Erosion rates in badland areas of the central Ebro Basin (NE-Spain). *CATENA*, *19*(3–4), 269–286. https://doi.org/10.1016/0341-8162(92)90002-S

BENKHADRA, H. (1997). *Battance, ruissellement et erosion diffuse sur les sols limoneux cultives determinisme et transfert d'echelle de la parcelle au petit bassin versant* [These de doctorat, Orléans]. https://theses.fr/1997ORLE2070

Benmansour, N., & Haddouche, D. (2019). Modélisation déterministe de l'oued Mekerra pour l'identification de la zone inondable de Sidi Bel-Abbès (Nord-Ouest algérien). *Techniques Sciences Méthodes*, *4*, 59–67. https://doi.org/10.1051/tsm/201904059

Bennett, J. S., Casalí, J., M. Robinson, K., & C. Kadavy, K. (2000). CHARACTERISTICS OF ACTIVELY ERODING EPHEMERAL GULLIES IN AN EXPERIMENTAL CHANNEL. *Transactions of the ASAE*, *43*(3), 641–649. https://doi.org/10.13031/2013.2745

Benselama, O., Mazour, M., Hasbaia, M., Djoukbala, O., & Mokhtari, S. (2019). *Analysis of the suspended sediment yield at different time scales in Mediterranean watershed, case of Wadi El Maleh (North-West of Algeria)*. *11*(Journal of Mediterranean Earth Sciences (2019), 11). https://doi.org/10.3304/JMES.2019.001

Beven, K. (2002). Runoff generation in semi-arid areas. *Dryland Rivers: Hydrology and Geomorphology of Semi-Arid Channels*, 57–105.

Bhowmik, N. G., & Demissie, M. (1989). Sedimentation in the Illinois River valley and backwater lakes. *Journal of Hydrology*, *105*(1–2), 187–195. https://doi.org/10.1016/0022-1694(89)90103-0

Birkel, C., Broder, T., & Biester, H. (2017). Nonlinear and threshold-dominated runoff generation controls DOC export in a small peat catchment. *Journal of Geophysical Research: Biogeosciences*, *122*(3), 498–513. https://doi.org/10.1002/2016JG003621

Bisal, F. (1960). The effect of raindrop size and impact velocity on sand-splash. *Canadian Journal of Soil Science*, *40*(2), 242–245. https://doi.org/10.4141/cjss60-030

Bisantino, T., Gentile, F., & Liuzzi, G. T. (2011). Continuous monitoring of suspended sediment load in semi-arid environments. *Sediment Transport*, 296–312.

Blair, T. C., & McPherson, J. G. (2009). Processes and Forms of Alluvial Fans. In A. J. Parsons & A. D. Abrahams (Eds.), *Geomorphology of Desert Environments* (pp. 413–467). Springer Netherlands. https://doi.org/10.1007/978-1-4020-5719-9_14

Blom, A., Ribberink, J. S., & De Vriend, H. J. (2003). Vertical sorting in bed forms: Flume experiments with a natural and a trimodal sediment mixture. *Water Resources Research*, *39*(2), 2001WR001088. https://doi.org/10.1029/2001WR001088

Blong, R. J. (1984). *Volcanic Hazards: A Sourcebook on the Effects of Eruptions*. Elsevier.

Blott, S. J., & Pye, K. (2008). Particle shape: A review and new methods of characterization and classification. *Sedimentology*, *55*(1), 31–63. https://doi.org/10.1111/j.1365-3091.2007.00892.x

Bluck, B. J. (1971). Sedimentation in the meandering River Endrick. *Scottish Journal of Geology*, *7*(2), 93–138. https://doi.org/10.1144/sjg07020093

Bocchiola, D., Rulli, M. C., & Rosso, R. (2006). Transport of large woody debris in the presence of obstacles. *Geomorphology*, *76*(1–2), 166–178. https://doi.org/10.1016/j.geomorph.2005.08.016

Bodí, M. B., Martin, D. A., Balfour, V. N., Santín, C., Doerr, S. H., Pereira, P., Cerdà, A., & Mataix-Solera, J. (2014). Wildland fire ash: Production, composition and eco-hydro-geomorphic effects. *Earth-Science Reviews*, *130*, 103–127. https://doi.org/10.1016/j.earscirev.2013.12.007

Bowes, M. J., Jarvie, H. P., Halliday, S. J., Skeffington, R. A., Wade, A. J., Loewenthal, M., Gozzard, E., Newman, J. R., & Palmer-Felgate, E. J. (2015). Characterising phosphorus and nitrate inputs to a rural river using high-frequency concentration–flow relationships. *Science of The Total Environment*, *511*, 608–620. https://doi.org/10.1016/j.scitotenv.2014.12.086

Bracken, L. J., Turnbull, L., Wainwright, J., & Bogaart, P. (2015). Sediment connectivity: A framework for understanding sediment transfer at multiple scales. *Earth Surface Processes and Landforms*, *40*(2), 177–188. https://doi.org/10.1002/esp.3635

Brown, C. B. (1950). Sediment transportation. *Engineering Hydraulics*, *12*, 769–857.

Browning, J., Meredith, P., & Gudmundsson, A. (2016). Cooling-dominated cracking in thermally stressed volcanic rocks. *Geophysical Research Letters*, *43*(16), 8417–8425. https://doi.org/10.1002/2016GL070532

Bruno, C., Stefano, C. D., & Ferro, V. (2008). Field investigation on rilling in the experimental Sparacia area, South Italy. *Earth Surface Processes and Landforms*, *33*(2), 263–279. https://doi.org/10.1002/esp.1544

Brush, G. S. (1989). Rates and patterns of estuarine sediment accumulation. *Limnology and Oceanography*, *34*(7), 1235–1246. https://doi.org/10.4319/lo.1989.34.7.1235

Bryan, R. (Ed.). (1987). *Rill erosion: Processes and significance*. Catena Verlag.

Buendia, C., Vericat, D., Batalla, R. J., & Gibbins, C. N. (2016). Temporal Dynamics of Sediment Transport and Transient In-channel Storage in a Highly Erodible Catchment: LINKING

SEDIMENT SOURCES, RAINFALL PATTERNS AND SEDIMENT YIELD. *Land Degradation & Development*, *27*(4), 1045–1063. https://doi.org/10.1002/ldr.2348

Bui, T. D. (2000). Cohesive Sediment Transport in Natural Streams: State of Knowledge. *Building Partnerships*, 1–10. https://doi.org/10.1061/40517(2000)268

Bull, A. T., Andrews, B. A., Dorador, C., & Goodfellow, M. (2018). Introducing the Atacama Desert. *Antonie van Leeuwenhoek*, *111*(8), 1269–1272. https://doi.org/10.1007/s10482-018-1100-2

Bunzel, K., Schäfer, R. B., Thrän, D., & Kattwinkel, M. (2015). Pesticide runoff from energy crops: A threat to aquatic invertebrates? *Science of The Total Environment*, *537*, 187–196. https://doi.org/10.1016/j.scitotenv.2015.08.011

Butler, B. A., & Ford, R. G. (2018). Evaluating Relationships Between Total Dissolved Solids (TDS) and Total Suspended Solids (TSS) in a Mining-Influenced Watershed. *Mine Water and the Environment*, *37*(1), 18–30. https://doi.org/10.1007/s10230-017-0484-y

Butler, D. R., & Malanson, G. P. (1995). Sedimentation rates and patterns in beaver ponds in a mountain environment. *Geomorphology*, *13*(1–4), 255–269. https://doi.org/10.1016/0169-555X(95)00031-Y

Butturini, A., Alvarez, M., Bernal, S., Vazquez, E., & Sabater, F. (2008). Diversity and temporal sequences of forms of DOC and NO_3 -discharge responses in an intermittent stream: Predictable or random succession? *Journal of Geophysical Research*, *113*(G3), G03016. https://doi.org/10.1029/2008JG000721

C. R. Umback and W. D. Lembke. (1966). Effects of Wind on Falling Water Drops. *Transactions of the ASAE*, *9*(6), 805–0808. https://doi.org/10.13031/2013.40102

Caldwell, R. L., & Edmonds, D. A. (2014). The effects of sediment properties on deltaic processes and morphologies: A numerical modeling study. *Journal of Geophysical Research: Earth Surface*, *119*(5), 961–982. https://doi.org/10.1002/2013JF002965

Calvo-Cases, A., Boix-Fayos, C., & Arnau-Rosalen, E. (2005). Chapter 3 patterns and thresholds of runoff generation and sediment transport on some Mediterranean hillslopes. In *Developments in Earth Surface Processes* (Vol. 7, pp. 31–51). Elsevier. https://doi.org/10.1016/S0928-2025(05)80009-4

Calvo-Cases, A., Boix-Fayos, C., & Imeson, A. C. (2003). Runoff generation, sediment movement and soil water behaviour on calcareous (limestone) slopes of some Mediterranean environments in southeast Spain. *Geomorphology*, *50*(1–3), 269–291. https://doi.org/10.1016/S0169-555X(02)00218-0

Cammeraat, L. H., Willott, S. J., Compton, S. G., & Incoll, L. D. (2002). The effects of ants' nests on the physical, chemical and hydrological properties of a rangeland soil in semi-arid Spain. *Geoderma*, *105*(1–2), 1–20. https://doi.org/10.1016/S0016-7061(01)00085-4

Carling, P. A., Perillo, M., Best, J., & Garcia, M. H. (2017). The bubble bursts for cavitation in natural rivers: Laboratory experiments reveal minor role in bedrock erosion. *Earth Surface Processes and Landforms*, *42*(9), 1308–1316. https://doi.org/10.1002/esp.4101

Carroll, D. (1970). *Rock Weathering*. Springer US. https://doi.org/10.1007/978-1-4684-1794-4

Casalí, J., Loizu, J., Campo, M. A., De Santisteban, L. M., & Álvarez-Mozos, J. (2006). Accuracy of methods for field assessment of rill and ephemeral gully erosion. *CATENA*, *67*(2), 128–138. https://doi.org/10.1016/j.catena.2006.03.005

Cavalli, M., & Marchi, L. (2008). Characterisation of the surface morphology of an alpine alluvial fan using airborne LiDAR. *Natural Hazards and Earth System Sciences*, *8*(2), 323–333. https://doi.org/10.5194/nhess-8-323-2008

Chahinian, N., Tournoud, M.-G., Perrin, J.-L., & Picot, B. (2011). Flow and nutrient transport in intermittent rivers: A modelling case-study on the Vène River using SWAT 2005. *Hydrological Sciences Journal*, *56*(2), 268–287. https://doi.org/10.1080/02626667.2011.559328

Chaki, S., Takarli, M., & Agbodjan, W. P. (2008). Influence of thermal damage on physical properties of a granite rock: Porosity, permeability and ultrasonic wave evolutions. *Construction and Building Materials*, *22*(7), 1456–1461. https://doi.org/10.1016/j.conbuildmat.2007.04.002

Chalov, S., Golosov, V., Tsyplenkov, A., Theuring, Ph., Zakerinejad, R., Märker, M., & Samokhin, M. (2017). A TOOLBOX FOR SEDIMENT BUDGET RESEARCH IN SMALL CATCHMENTS. *GEOGRAPHY, ENVIRONMENT, SUSTAINABILITY*, *10*(4), 43–68. https://doi.org/10.24057/2071-9388-2017-10-4-43-68

Chalov, S., Zavadsky, A., Belozerova, E., Bulacheva, M., Jarsjö, J., Thorslund, J., & Yamkhin, J. (2012). SUSPENDED AND DISSOLVED MATTER FLUXES IN THE UPPER SELENGA RIVER BASIN. *GEOGRAPHY, ENVIRONMENT, SUSTAINABILITY*, *5*(2), 78–94. https://doi.org/10.24057/2071-9388-2012-5-2-78-94

Charney, J. G. (1975). Dynamics of deserts and drought in the Sahel. *Quarterly Journal of the Royal Meteorological Society*, *101*(428), 193–202. https://doi.org/10.1002/qj.49710142802

Chehibi, O., Hamidi, M., & Roukh, Z. E. A. (2024). *A geodecisional method based in Analytical Hierarchy Process and Geographic Information System to the flood susceptibility mapping of the Sidi Bel Abbes Territory (NW of Algeria)*. https://doi.org/10.21203/rs.3.rs-3938260/v1

Chen, F., Fang, N., & Shi, Z. (2016). Using biomarkers as fingerprint properties to identify sediment sources in a small catchment. *Science of The Total Environment*, *557–558*, 123–133. https://doi.org/10.1016/j.scitotenv.2016.03.028

Chen, Y., Lian, J., Zhao, X., Guo, Q., & Yang, D. (2023). Advances in Frazil Ice Evolution Mechanisms and Numerical Modelling in Rivers and Channels in Cold Regions. *Water*, *15*(14), 2582. https://doi.org/10.3390/w15142582

Cherif, E. A., Errih, M., & Cherif, H. M. (2009). Modélisation statistique du transport solide du bassin versant de l'Oued Mekerra (Algérie) en zone semi-aride méditerranéenne. *Hydrological Sciences Journal*, *54*(2), 338–348. https://doi.org/10.1623/hysj.54.2.338

Collins, A. L., & Walling, D. E. (2004). Documenting catchment suspended sediment sources: Problems, approaches and prospects. *Progress in Physical Geography: Earth and Environment*, *28*(2), 159–196. https://doi.org/10.1191/0309133304pp409ra

Collins, A. L., Walling, D. E., & Leeks, G. J. L. (1997). Source type ascription for fluvial suspended sediment based on a quantitative composite fingerprinting technique. *CATENA*, *29*(1), 1–27. https://doi.org/10.1016/S0341-8162(96)00064-1

Cook, H. L. (1946). The infiltration approach to the calculation of surface runoff. *Eos, Transactions American Geophysical Union*, *27*(5), 726–747. https://doi.org/10.1029/TR027i005p00726-2

Cooper, C. M., & McHenry, J. R. (1989). Sediment accumulation and its effects on a Mississippi River oxbow lake. *Environmental Geology and Water Sciences*, *13*(1), 33–37. https://doi.org/10.1007/BF01666569

Cooper, H. W., & Simmons, G. (1977). The effect of cracks on the thermal expansion of rocks. *Earth and Planetary Science Letters*, *36*(3), 404–412. https://doi.org/10.1016/0012-821X(77)90065-6

Cooper, J. R., Ockleford, A., Rice, S. P., & Powell, D. M. (2018). Does the permeability of gravel river beds affect near-bed hydrodynamics? *Earth Surface Processes and Landforms*, *43*(5), 943–955. https://doi.org/10.1002/esp.4260

Covino, T. P., & McGlynn, B. L. (2007). Stream gains and losses across a mountain-to-valley transition: Impacts on watershed hydrology and stream water chemistry: STREAM GAINS AND LOSSES ACROSS A TRANSITION. *Water Resources Research*, *43*(10). https://doi.org/10.1029/2006WR005544

Craft, C. B., & Casey, W. P. (2000). Sediment and nutrient accumulation in floodplain and depressional freshwater wetlands of Georgia, USA. *Wetlands*, *20*(2), 323–332. https://doi.org/10.1672/0277-5212(2000)020%255B0323:SANAIF%255D2.0.CO;2

Cross, G. R., & Birot, P. (1967). General Physical Geography. *British Journal of Educational Studies*, *15*(1), 104. https://doi.org/10.2307/3119610

Crosta, G. B., & Frattini, P. (2004). Controls on modern alluvial fan processes in the central Alps, northern Italy. *Earth Surface Processes and Landforms*, *29*(3), 267–293. https://doi.org/10.1002/esp.1009

Darracq, A., & Destouni, G. (2005). In-Stream Nitrogen Attenuation: Model-Aggregation Effects and Implications for Coastal Nitrogen Impacts. *Environmental Science & Technology*, *39*(10), 3716–3722. https://doi.org/10.1021/es049740o

Darwiche-Criado, N., Comín, F. A., Sorando, R., & Sánchez-Pérez, J. M. (2015). Seasonal variability of NO3− mobilization during flood events in a Mediterranean catchment: The influence of intensive agricultural irrigation. *Agriculture, Ecosystems & Environment*, *200*, 208–218. https://doi.org/10.1016/j.agee.2014.11.002

David, C., Menéndez, B., & Darot, M. (1999). Influence of stress-induced and thermal cracking on physical properties and microstructure of La Peyratte granite. *International Journal of Rock Mechanics and Mining Sciences*, *36*(4), 433–448. https://doi.org/10.1016/S0148-9062(99)00010-8

David, E. C., Brantut, N., Schubnel, A., & Zimmerman, R. W. (2012). Sliding crack model for nonlinearity and hysteresis in the uniaxial stress–strain curve of rock. *International Journal of Rock Mechanics and Mining Sciences*, *52*, 9–17. https://doi.org/10.1016/j.ijrmms.2012.02.001

David Krinsley, Pierre E. Biscaye,. (1973). Argentine Basin Sediment Sources as Indicated by Quartz Surface Textures. *SEPM Journal of Sedimentary Research*, *Vol. 43*. https://doi.org/10.1306/74D72739-2B21-11D7-8648000102C1865D

De Girolamo, A. M., Pappagallo, G., & Lo Porto, A. (2015). Temporal variability of suspended sediment transport and rating curves in a Mediterranean river basin: The Celone (SE Italy). *CATENA*, *128*, 135–143. https://doi.org/10.1016/j.catena.2014.09.020

De Haas, T., Densmore, A. L., Stoffel, M., Suwa, H., Imaizumi, F., Ballesteros-Cánovas, J. A., & Wasklewicz, T. (2018). Avulsions and the spatio-temporal evolution of debris-flow fans. *Earth-Science Reviews*, *177*, 53–75. https://doi.org/10.1016/j.earscirev.2017.11.007

De Santisteban, L. M., Casalí, J., & López, J. J. (2006). Assessing soil erosion rates in cultivated areas of Navarre (Spain). *Earth Surface Processes and Landforms*, *31*(4), 487–506. https://doi.org/10.1002/esp.1281

Dehghani, A. A., Azamathulla, H. Md., Hashemi Najafi, S. A., & Ayyoubzadeh, S. A. (2013). Local scouring around L-head groynes. *Journal of Hydrology*, *504*, 125–131. https://doi.org/10.1016/j.jhydrol.2013.09.020

Del Moral, R., & Grishin, S. Y. (1999). Volcanic disturbances and ecosystem recovery. *Ecosystems of the World*, 137–160.

den Biggelaar, C., Lal, R., Wiebe, K., & Breneman, V. (2003). The Global Impact Of Soil Erosion On Productivity: I: Absolute and Relative Erosion-induced Yield Losses. In *Advances in Agronomy* (Vol. 81, pp. 1–48). Elsevier. https://doi.org/10.1016/S0065-2113(03)81001-5

den Biggelaar, C., Lal, R., Wiebe, K., Eswaran, H., Breneman, V., & Reich, P. (2003). The Global Impact Of Soil Erosion On Productivity*: II: Effects On Crop Yields And Production Over Time. In *Advances in Agronomy* (Vol. 81, pp. 49–95). Elsevier. https://doi.org/10.1016/S0065-2113(03)81002-7

Deng, H., Sonnenthal, E., Arora, B., Breunig, H., Brodie, E., Kleber, M., Spycher, N., & Nico, P. (2023). The environmental controls on efficiency of enhanced rock weathering in soils. *Scientific Reports*, *13*(1), 9765. https://doi.org/10.1038/s41598-023-36113-4

Deng, L., & Cai, C. S. (2010). Bridge Scour: Prediction, Modeling, Monitoring, and Countermeasures—Review. *Practice Periodical on Structural Design and Construction*, *15*(2), 125–134. https://doi.org/10.1061/(ASCE)SC.1943-5576.0000041

Depetris, P. J., Pasquini, A. I., & Lecomte, K. (2014). Chemical Weathering Processes on the Earth's Surface. In P. J. Depetris, A. I. Pasquini, & K. L. Lecomte, *Weathering and the Riverine Denudation of Continents* (pp. 33–46). Springer Netherlands. https://doi.org/10.1007/978-94-007-7717-0_4

Deprez, M., De Kock, T., De Schutter, G., & Cnudde, V. (2020). A review on freeze-thaw action and weathering of rocks. *Earth-Science Reviews*, *203*, 103143. https://doi.org/10.1016/j.earscirev.2020.103143

Di Stefano, C., & Ferro, V. (2011). Measurements of rill and gully erosion in Sicily. *Hydrological Processes*, *25*(14), 2221–2227. https://doi.org/10.1002/hyp.7977

Di Stefano, C., Ferro, V., Pampalone, V., & Sanzone, F. (2013). Field investigation of rill and ephemeral gully erosion in the Sparacia experimental area, South Italy. *CATENA*, *101*, 226–234. https://doi.org/10.1016/j.catena.2012.10.012

Diaf, M., Hazzab, A., Yahiaoui, A., & Belkendil, A. (2020). Characterization and frequency analysis of flooding solid flow in semi-arid zone: Case of Mekerra catchment in the north-west of Algeria. *Applied Water Science*, *10*(2), 59. https://doi.org/10.1007/s13201-019-1132-4

Díaz-Raviña, M., Martín, A., Barreiro, A., Lombao, A., Iglesias, L., Díaz-Fierros, F., & Carballas, T. (2012). Mulching and seeding treatments for post-fire soil stabilisation in NW Spain: Short-term effects and effectiveness. *Geoderma*, *191*, 31–39. https://doi.org/10.1016/j.geoderma.2012.01.003

Dickinson, A., & Bolton, P. (1992). A programme of monitoring sediment transport in north central Luzon, the Philippines. *Erosion and Sediment Transport Monitoring Programmes in River Basins*, 483–492.

Disrud, L. A., Lyles, L., & Skidmore, E. (1969). HOW WIND AFFECTS SIZE AND SHAPE OF RAINDROPS. *Agricultural Engineering*, *50*(10), 617.

Du, P., Huang, D., Ning, D., Chen, Y., Liu, B., Wang, J., & Xu, J. (2019). Application of Bayesian model and discriminant function analysis to the estimation of sediment source

contributions. *International Journal of Sediment Research*, *34*(6), 577–590. https://doi.org/10.1016/j.ijsrc.2019.05.005

Duman, T. Y. (2009). The largest landslide dam in Turkey: Tortum landslide. *Engineering Geology*, *104*(1–2), 66–79. https://doi.org/10.1016/j.enggeo.2008.08.006

Dumont, H. J. (Ed.). (2010). *The Nile: Origin, environments, limnology and human use* (Reprint). Springer.

Dunne, T., Malmon, D. V., & Mudd, S. M. (2010). A rain splash transport equation assimilating field and laboratory measurements. *Journal of Geophysical Research: Earth Surface*, *115*(F1), 2009JF001302. https://doi.org/10.1029/2009JF001302

Dunne, T., Zhang, W., & Aubry, B. F. (1991). Effects of Rainfall, Vegetation, and Microtopography on Infiltration and Runoff. *Water Resources Research*, *27*(9), 2271–2285. https://doi.org/10.1029/91WR01585

Duvert, C., Gratiot, N., Evrard, O., Navratil, O., Némery, J., Prat, C., & Esteves, M. (2010). Drivers of erosion and suspended sediment transport in three headwater catchments of the Mexican Central Highlands. *Geomorphology*, *123*(3–4), 243–256. https://doi.org/10.1016/j.geomorph.2010.07.016

Duvert, C., Nord, G., Gratiot, N., Navratil, O., Nadal-Romero, E., Mathys, N., Némery, J., Regüés, D., García-Ruiz, J. M., Gallart, F., & Esteves, M. (2012). Towards prediction of suspended sediment yield from peak discharge in small erodible mountainous catchments (0.45–22km2) of France, Mexico and Spain. *Journal of Hydrology*, *454–455*, 42–55. https://doi.org/10.1016/j.jhydrol.2012.05.048

Earle, S. (with Panchuk, K.). (2019). *Physical geology* (2nd edition). BCcampus, BC Open Textbook Project.

Eaton, B. C., Moore, R. D., & Giles, T. R. (2010). Forest fire, bank strength and channel instability: The 'unusual' response of Fishtrap Creek, British Columbia. *Earth Surface Processes and Landforms*, *35*(10), 1167–1183. https://doi.org/10.1002/esp.1946

Eder, A., Strauss, P., Krueger, T., & Quinton, J. N. (2010). Comparative calculation of suspended sediment loads with respect to hysteresis effects (in the Petzenkirchen catchment, Austria). *Journal of Hydrology*, *389*(1–2), 168–176. https://doi.org/10.1016/j.jhydrol.2010.05.043

Edwin L. Hamilton. (1976). Variations of Density and Porosity with Depth in Deep-sea Sediments. *SEPM Journal of Sedimentary Research*, *Vol. 46*. https://doi.org/10.1306/212F6F3C-2B24-11D7-8648000102C1865D

Einstein, H. A. (1942). Formulas for the Transportation of Bed Load. *Transactions of the American Society of Civil Engineers*, *107*(1), 561–577. https://doi.org/10.1061/TACEAT.0005468

El Bilali, L., Rasmussen, P. E., Hall, G. E. M., & Fortin, D. (2002). Role of sediment composition in trace metal distribution in lake sediments. *Applied Geochemistry*, *17*(9), 1171–1181. https://doi.org/10.1016/S0883-2927(01)00132-9

Eludoyin, A. O., Griffith, B., Orr, R. J., Bol, R., Quine, T. A., & Brazier, R. E. (2017). An evaluation of the hysteresis in chemical concentration–discharge ($C - Q$) relationships from drained, intensively managed grasslands in southwest England. *Hydrological Sciences Journal*, *62*(8), 1243–1254. https://doi.org/10.1080/02626667.2017.1313979

Erpul, G., Gabriels, D., & Janssens, D. (2000). Effect of wind on size and energy of amall simulated raindrops: A wind tunnel study. *International Agrophysics*, *14*(1).

http://agro.icm.edu.pl/agro/element/bwmeta1.element.agro-article-3577d924-43cf-41ce-bb1f-51c3c5f8d3b8

Espinosa-Marzal, R. M., & Scherer, G. W. (2010a). Advances in Understanding Damage by Salt Crystallization. *Accounts of Chemical Research*, *43*(6), 897–905. https://doi.org/10.1021/ar9002224

Espinosa-Marzal, R. M., & Scherer, G. W. (2010b). Mechanisms of damage by salt. *Geological Society, London, Special Publications*, *331*(1), 61–77. https://doi.org/10.1144/SP331.5

Evans, C., & Davies, T. D. (1998). Causes of concentration/discharge hysteresis and its potential as a tool for analysis of episode hydrochemistry. *Water Resources Research*, *34*(1), 129–137. https://doi.org/10.1029/97WR01881

Fan, X., Dufresne, A., Siva Subramanian, S., Strom, A., Hermanns, R., Tacconi Stefanelli, C., Hewitt, K., Yunus, A. P., Dunning, S., Capra, L., Geertsema, M., Miller, B., Casagli, N., Jansen, J. D., & Xu, Q. (2020). The formation and impact of landslide dams – State of the art. *Earth-Science Reviews*, *203*, 103116. https://doi.org/10.1016/j.earscirev.2020.103116

Fan, X., Dufresne, A., Whiteley, J., Yunus, A. P., Subramanian, S. S., Okeke, C. A. U., Pánek, T., Hermanns, R. L., Ming, P., Strom, A., Havenith, H.-B., Dunning, S., Wang, G., & Tacconi Stefanelli, C. (2021). Recent technological and methodological advances for the investigation of landslide dams. *Earth-Science Reviews*, *218*, 103646. https://doi.org/10.1016/j.earscirev.2021.103646

Fan, X., Shi, C., Shao, W., & Zhou, Y. (2013). The suspended sediment dynamics in the Inner-Mongolia reaches of the upper Yellow River. *CATENA*, *109*, 72–82. https://doi.org/10.1016/j.catena.2013.05.010

Faulkner, H. (2006). Piping Hazard on Collapsible and Dispersive Soils in Europe. In J. Boardman & J. Poesen (Eds.), *Soil Erosion in Europe* (1st ed., pp. 537–562). Wiley. https://doi.org/10.1002/0470859202.ch40

Fernández-Raga, M., Palencia, C., Keesstra, S., Jordán, A., Fraile, R., Angulo-Martínez, M., & Cerdà, A. (2017). Splash erosion: A review with unanswered questions. *Earth-Science Reviews*, *171*, 463–477. https://doi.org/10.1016/j.earscirev.2017.06.009

Ferreira, A. J. D., Coelho, C. O. A., Walsh, R. P. D., Shakesby, R. A., Ceballos, A., & Doerr, S. H. (2000). Hydrological implications of soil water-repellency in Eucalyptus globulus forests, north-central Portugal. *Journal of Hydrology*, *231–232*, 165–177. https://doi.org/10.1016/S0022-1694(00)00192-X

Fischer, S., Schumann, A., & Bühler, P. (2021). A statistics-based automated flood event separation. *Journal of Hydrology X*, *10*, 100070. https://doi.org/10.1016/j.hydroa.2020.100070

Fister, W., Iserloh, T., Ries, J. B., & Schmidt, R.-G. (2012). A portable wind and rainfall simulator for in situ soil erosion measurements. *CATENA*, *91*, 72–84. https://doi.org/10.1016/j.catena.2011.03.002

Fleshman, M. S., & Rice, J. D. (2014). Laboratory Modeling of the Mechanisms of Piping Erosion Initiation. *Journal of Geotechnical and Geoenvironmental Engineering*, *140*(6), 04014017. https://doi.org/10.1061/(ASCE)GT.1943-5606.0001106

Foster, GR. (1982). Modelling the erosion processes. *Hydrologic Modelling of Small Watersheds*. https://cir.nii.ac.jp/crid/1571417125546980224

Fraley, L. M., Miller, A. J., & Welty, C. (2009). Contribution of In-Channel Processes to Sediment Yield of an Urbanizing Watershed. *JAWRA Journal of the American Water Resources Association*, *45*(3), 748–766. https://doi.org/10.1111/j.1752-1688.2009.00320.x

Franz, C., Makeschin, F., Weiß, H., & Lorz, C. (2013). Geochemical signature and properties of sediment sources and alluvial sediments within the Lago Paranoá catchment, Brasilia DF: A study on anthropogenic introduced chemical elements in an urban river basin. *Science of The Total Environment*, *452–453*, 411–420. https://doi.org/10.1016/j.scitotenv.2013.02.077

Fredrich, J. T., & Wong, T. (1986). Micromechanics of thermally induced cracking in three crustal rocks. *Journal of Geophysical Research: Solid Earth*, *91*(B12), 12743–12764. https://doi.org/10.1029/JB091iB12p12743

Fryirs, K. (2013). (Dis)Connectivity in catchment sediment cascades: A fresh look at the sediment delivery problem. *Earth Surface Processes and Landforms*, *38*(1), 30–46. https://doi.org/10.1002/esp.3242

Fryirs, K. A., Brierley, G. J., Preston, N. J., & Kasai, M. (2007). Buffers, barriers and blankets: The (dis)connectivity of catchment-scale sediment cascades. *CATENA*, *70*(1), 49–67. https://doi.org/10.1016/j.catena.2006.07.007

Gabet, E. J., & Dunne, T. (2003). Sediment detachment by rain power. *Water Resources Research*, *39*(1). https://doi.org/10.1029/2001WR000656

Gao, P. (2013). 7.11 Rill and Gully Development Processes. In *Treatise on Geomorphology* (pp. 122–131). Elsevier. https://doi.org/10.1016/B978-0-12-374739-6.00156-1

Gao, P., & Josefson, M. (2012). Event-based suspended sediment dynamics in a central New York watershed. *Geomorphology*, *139–140*, 425–437. https://doi.org/10.1016/j.geomorph.2011.11.007

García-Comendador, J., Martínez-Carreras, N., Fortesa, J., Borràs, A., Calsamiglia, A., & Estrany, J. (2020). Analysis of post-fire suspended sediment sources by using colour parameters. *Geoderma*, *379*, 114638. https://doi.org/10.1016/j.geoderma.2020.114638

García-Ruiz, J. M., Nadal-Romero, E., Lana-Renault, N., & Beguería, S. (2013). Erosion in Mediterranean landscapes: Changes and future challenges. *Geomorphology*, *198*, 20–36. https://doi.org/10.1016/j.geomorph.2013.05.023

Gardner, R. A. M., & Gerrard, A. J. (2003). Runoff and soil erosion on cultivated rainfed terraces in the Middle Hills of Nepal. *Applied Geography*, *23*(1), 23–45. https://doi.org/10.1016/S0143-6228(02)00069-3

Gellis, A. C. (2013). Factors influencing storm-generated suspended-sediment concentrations and loads in four basins of contrasting land use, humid-tropical Puerto Rico. *CATENA*, *104*, 39–57. https://doi.org/10.1016/j.catena.2012.10.018

Gellis, A. C., & Noe, G. B. (2013). Sediment source analysis in the Linganore Creek watershed, Maryland, USA, using the sediment fingerprinting approach: 2008 to 2010. *Journal of Soils and Sediments*, *13*(10), 1735–1753. https://doi.org/10.1007/s11368-013-0771-6

Genkinger, S., & Putnis, A. (2007). Crystallisation of sodium sulfate: Supersaturation and metastable phases. *Environmental Geology*, *52*(2), 329–337. https://doi.org/10.1007/s00254-006-0565-x

Ghahramani, A., Ishikawa, Y., Gomi, T., & Miyata, S. (2011). Downslope soil detachment–transport on steep slopes via rain splash. *Hydrological Processes*, *25*(15), 2471–2480. https://doi.org/10.1002/hyp.8086

Gharari, S., & Razavi, S. (2018). A review and synthesis of hysteresis in hydrology and hydrological modeling: Memory, path-dependency, or missing physics? *Journal of Hydrology*, *566*, 500–519. https://doi.org/10.1016/j.jhydrol.2018.06.037

Ghenim, A. (2013). Estimation de la précision de la relation en puissance reliant la concentration au débit liquide. *Revue « Nature & Technologie » (NATEC), C- Sciences de l'Environnement*, *9*, 54–60.

Ghenim, A., Terfous, A., & Seddini, A. (2007). Study of suspended sediment load in semiarid Mediterranean regions: A case study from the watershed of wadi Sebdou (northwest Algeria). *Science et Changements Planétaires / Sécheresse*, *18*(1), 39–44. https://doi.org/10.1684/sec.2007.0067

Giménez, R., Casalí, J., Grande, I., Díez, J., Campo, M. A., Álvarez-Mozos, J., & Goñi, M. (2012). Factors controlling sediment export in a small agricultural watershed in Navarre (Spain). *Agricultural Water Management*, *110*, 1–8. https://doi.org/10.1016/j.agwat.2012.03.007

Giménez-Morera, A., Sinoga, J. D. R., & Cerdà, A. (2010). The impact of cotton geotextiles on soil and water losses from Mediterranean rainfed agricultural land. *Land Degradation & Development*, *21*(2), 210–217. https://doi.org/10.1002/ldr.971

Godsey, S. E., Kirchner, J. W., & Clow, D. W. (2009). Concentration-discharge relationships reflect chemostatic characteristics of US catchments. *Hydrological Processes*, *23*(13), 1844–1864. https://doi.org/10.1002/hyp.7315

Gomi, T., Sidle, R. C., Ueno, M., Miyata, S., & Kosugi, K. (2008). Characteristics of overland flow generation on steep forested hillslopes of central Japan. *Journal of Hydrology*, *361*(3–4), 275–290. https://doi.org/10.1016/j.jhydrol.2008.07.045

Gonzales-Inca, C., Valkama, P., Lill, J.-O., Slotte, J., Hietaharju, E., & Uusitalo, R. (2018). Spatial modeling of sediment transfer and identification of sediment sources during snowmelt in an agricultural watershed in boreal climate. *Science of The Total Environment*, *612*, 303–312. https://doi.org/10.1016/j.scitotenv.2017.08.142

Govers, G., & Poesen, J. (1988). Assessment of the interrill and rill contributions to total soil loss from an upland field plot. *Geomorphology*, *1*(4), 343–354. https://doi.org/10.1016/0169-555X(88)90006-2

Griffiths, L., Lengliné, O., Heap, M. J., Baud, P., & Schmittbuhl, J. (2018). Thermal Cracking in Westerly Granite Monitored Using Direct Wave Velocity, Coda Wave Interferometry, and Acoustic Emissions. *Journal of Geophysical Research: Solid Earth*, *123*(3), 2246–2261. https://doi.org/10.1002/2017JB015191

Guccione, M. J., Burford, M. F., & Kendall, J. D. (1999). Pemiscot Bayou, a Large Distributary of the Mississippi River and a Possible Failed Avulsion. In N. D. Smith & J. Rogers (Eds.), *Fluvial Sedimentology VI* (1st ed., pp. 211–220). Wiley. https://doi.org/10.1002/9781444304213.ch16

Guesri, M., Megnounif, A., & Ghenim, A. N. (2020). Rainfall erosivity and sediment yield in Northeast Algeria: K'sob watershed case study. *Arabian Journal of Geosciences*, *13*(7), 299. https://doi.org/10.1007/s12517-020-5276-1

Haddadchi, A., & Hicks, M. (2021). Interpreting event-based suspended sediment concentration and flow hysteresis patterns. *Journal of Soils and Sediments*, *21*(1), 592–612. https://doi.org/10.1007/s11368-020-02777-y

Hagerty, D. J. (1991). Piping/Sapping Erosion. I: Basic Considerations. *Journal of Hydraulic Engineering*, *117*(8), 991–1008. https://doi.org/10.1061/(ASCE)0733-9429(1991)117:8(991)

Haines, W. B. (1930). Studies in the physical properties of soil. V. The hysteresis effect in capillary properties, and the modes of moisture distribution associated therewith. *The*

Journal of Agricultural Science, *20*(1), 97–116. https://doi.org/10.1017/S002185960008864X

Hajigholizadeh, M., Melesse, A., & Fuentes, H. (2018). Erosion and Sediment Transport Modelling in Shallow Waters: A Review on Approaches, Models and Applications. *International Journal of Environmental Research and Public Health*, *15*(3), 518. https://doi.org/10.3390/ijerph15030518

Hamshaw, S. D., Dewoolkar, M. M., Schroth, A. W., Wemple, B. C., & Rizzo, D. M. (2018). A New Machine-Learning Approach for Classifying Hysteresis in Suspended-Sediment Discharge Relationships Using High-Frequency Monitoring Data. *Water Resources Research*, *54*(6), 4040–4058. https://doi.org/10.1029/2017WR022238

Harold L. Alling. (1950). Initial Shape and Roundness of Sedimentary Rock Mineral Particles of Sand Size. *SEPM Journal of Sedimentary Research*, *Vol. 20*. https://doi.org/10.1306/D42693CD-2B26-11D7-8648000102C1865D

Hartkamp, C. A., Arribas, J., & Tortosa, A. (1993). Grain size, composition, porosity and permeability contrasts within cross-bedded sandstones in Tertiary fluvial deposits, central Spain. *Sedimentology*, *40*(4), 787–799. https://doi.org/10.1111/j.1365-3091.1993.tb01360.x

Harvey, A. M. (2002). Effective timescales of coupling within fluvial systems. *Geomorphology*, *44*(3–4), 175–201. https://doi.org/10.1016/S0169-555X(01)00174-X

Hasiotis, T., Papatheodorou, G., Bouckovalas, G., Corbau, C., & Ferentinos, G. (2002). Earthquake-induced coastal sediment instabilities in the western Gulf of Corinth, Greece. *Marine Geology*, *186*(3–4), 319–335. https://doi.org/10.1016/S0025-3227(02)00240-2

Hatfield, R. G., & Maher, B. A. (2008). Suspended sediment characterization and tracing using a magnetic fingerprinting technique: Bassenthwaite Lake, Cumbria, UK. *The Holocene*, *18*(1), 105–115. https://doi.org/10.1177/0959683607085600

He, M., Zheng, H., Huang, X., Jia, J., & Li, L. (2013). Yangtze River sediments from source to sink traced with clay mineralogy. *Journal of Asian Earth Sciences*, *69*, 60–69. https://doi.org/10.1016/j.jseaes.2012.10.001

Heap, M. J., Baud, P., Meredith, P. G., Vinciguerra, S., & Reuschlé, T. (2014). The permeability and elastic moduli of tuff from Campi Flegrei, Italy: Implications for ground deformation modelling. *Solid Earth*, *5*(1), 25–44. https://doi.org/10.5194/se-5-25-2014

Heap, M. J., Lavallée, Y., Petrakova, L., Baud, P., Reuschlé, T., Varley, N. R., & Dingwell, D. B. (2014). Microstructural controls on the physical and mechanical properties of edifice-forming andesites at Volcán de Colima, Mexico. *Journal of Geophysical Research: Solid Earth*, *119*(4), 2925–2963. https://doi.org/10.1002/2013JB010521

Heap, M. J., Mollo, S., Vinciguerra, S., Lavallée, Y., Hess, K.-U., Dingwell, D. B., Baud, P., & Iezzi, G. (2013). Thermal weakening of the carbonate basement under Mt. Etna volcano (Italy): Implications for volcano instability. *Journal of Volcanology and Geothermal Research*, *250*, 42–60. https://doi.org/10.1016/j.jvolgeores.2012.10.004

Heidel, S. G. (1956). The progressive lag of sediment concentration with flood waves. *Transactions, American Geophysical Union*, *37*(1), 56. https://doi.org/10.1029/TR037i001p00056

Herman, E. K., Tancredi, J. H., Toran, L., & White, W. B. (2007). Mineralogy of suspended sediment in three karst springs. *Hydrogeology Journal*, *15*(2), 255–266. https://doi.org/10.1007/s10040-006-0108-2

Hewlett, J. D., & Hibbert, A. R. (1967). Factors affecting the response of small watersheds to precipitation in humid areas. *Forest Hydrology*, *1*, 275–290.

Hooke, J. M. (1986). The significance of mid-channel bars in an active meandering river. *Sedimentology*, *33*(6), 839–850. https://doi.org/10.1111/j.1365-3091.1986.tb00986.x

Horowitz, A. J. (2008). Determining annual suspended sediment and sediment-associated trace element and nutrient fluxes. *Science of The Total Environment*, *400*(1–3), 315–343. https://doi.org/10.1016/j.scitotenv.2008.04.022

Horowitz, A. J., & Elrick, K. A. (1987). The relation of stream sediment surface area, grain size and composition to trace element chemistry. *Applied Geochemistry*, *2*(4), 437–451. https://doi.org/10.1016/0883-2927(87)90027-8

Horton, R. E. (1933). The Rôle of infiltration in the hydrologic cycle. *Eos, Transactions American Geophysical Union*, *14*(1), 446–460. https://doi.org/10.1029/TR014i001p00446

Hosseinalizadeh, M., Kariminejad, N., Rahmati, O., Keesstra, S., Alinejad, M., & Mohammadian Behbahani, A. (2019). How can statistical and artificial intelligence approaches predict piping erosion susceptibility? *Science of The Total Environment*, *646*, 1554–1566. https://doi.org/10.1016/j.scitotenv.2018.07.396

Hounslow, M. W., & Morton, A. C. (2004). Evaluation of sediment provenance using magnetic mineral inclusions in clastic silicates: Comparison with heavy mineral analysis. *Sedimentary Geology*, *171*(1–4), 13–36. https://doi.org/10.1016/j.sedgeo.2004.05.008

Houston, J. (2006). Variability of precipitation in the Atacama Desert: Its causes and hydrological impact. *International Journal of Climatology*, *26*(15), 2181–2198. https://doi.org/10.1002/joc.1359

Huang, J., Ji, M., Xie, Y., Wang, S., He, Y., & Ran, J. (2016). Global semi-arid climate change over last 60 years. *Climate Dynamics*, *46*(3–4), 1131–1150. https://doi.org/10.1007/s00382-015-2636-8

Huang, J., Zhang, W., Zuo, J., Bi, J., Shi, J., Wang, X., Chang, Z., Huang, Z., Yang, S., Zhang, B., Wang, G., Feng, G., Yuan, J., Zhang, L., Zuo, H., Wang, S., Fu, C., & Jifan, C. (2008). An overview of the Semi-arid Climate and Environment Research Observatory over the Loess Plateau. *Advances in Atmospheric Sciences*, *25*(6), 906–921. https://doi.org/10.1007/s00376-008-0906-7

Hudson, P. F. (2003). Event sequence and sediment exhaustion in the lower Panuco Basin, Mexico. *CATENA*, *52*(1), 57–76. https://doi.org/10.1016/S0341-8162(02)00145-5

Hueso-González, P., Ruiz-Sinoga, J. D., Martínez-Murillo, J. F., & Lavee, H. (2015). Overland flow generation mechanisms affected by topsoil treatment: Application to soil conservation. *Geomorphology*, *228*, 796–804. https://doi.org/10.1016/j.geomorph.2014.10.033

Hughes, A. O., Olley, J. M., Croke, J. C., & McKergow, L. A. (2009). Sediment source changes over the last 250 years in a dry-tropical catchment, central Queensland, Australia. *Geomorphology*, *104*(3–4), 262–275. https://doi.org/10.1016/j.geomorph.2008.09.003

Hughes, A., Quinn, J., & McKergow, L. (2012). Land use influences on suspended sediment yields and event sediment dynamics within two headwater catchments, Waikato, New Zealand. *New Zealand Journal of Marine and Freshwater Research*, *46*(3), 315–333. https://doi.org/10.1080/00288330.2012.661745

Imeson, A. C., Verstraten, J. M., Van Mulligen, E. J., & Sevink, J. (1992). The effects of fire and water repellency on infiltration and runoff under Mediterranean type forest. *CATENA*, *19*(3–4), 345–361. https://doi.org/10.1016/0341-8162(92)90008-Y

Irvine, K. N., & Drake, J. J. (1987). PROCESS-ORIENTED ESTIMATION OF SUSPENDED SEDIMENT CONCENTRATION. *Journal of the American Water Resources Association*, *23*(6), 1017–1025. https://doi.org/10.1111/j.1752-1688.1987.tb00851.x

Iturrizaga, L. (2012). Hummocky debris landforms in the Chapursan Valley (Karakoram range, Pakistan): A glacio-geomorphological investigation. *Geomorphology*, *169–170*, 1–16. https://doi.org/10.1016/j.geomorph.2011.10.023

Jackson, G., & Sheldon, J. (1949). The Vegetation of Magnesian Limestone Cliffs at Markland Grips Near Sheffield. *The Journal of Ecology*, *37*(1), 38. https://doi.org/10.2307/2256729

Jacobson, P. J., Jacobson, K. M., Angermeier, P. L., & Cherry, D. S. (1999). Transport, Retention, and Ecological Significance of Woody Debris within a Large Ephemeral River. *Journal of the North American Benthological Society*, *18*(4), 429–444. https://doi.org/10.2307/1468376

Jain, S. (2014). Weathering and Mass Wasting. In S. Jain, *Fundamentals of Physical Geology* (pp. 129–163). Springer India. https://doi.org/10.1007/978-81-322-1539-4_7

James, S. C., Jones, C. A., Grace, M. D., & Roberts, J. D. (2010). Advances in sediment transport modelling. *Journal of Hydraulic Research*, *48*(6), 754–763. https://doi.org/10.1080/00221686.2010.515653

Jansson, M. B. (2002). Determining sediment source areas in a tropical river basin, Costa Rica. *CATENA*, *47*(1), 63–84. https://doi.org/10.1016/S0341-8162(01)00173-4

Jarsjö, J., Bayer-Raich, M., & Ptak, T. (2005). Monitoring groundwater contamination and delineating source zones at industrial sites: Uncertainty analyses using integral pumping tests. *Journal of Contaminant Hydrology*, *79*(3–4), 107–134. https://doi.org/10.1016/j.jconhyd.2005.05.011

Jeong, S. W., Locat, J., Leroueil, S., & Malet, J.-P. (2010). Rheological properties of fine-grained sediment: The roles of texture and mineralogy. *Canadian Geotechnical Journal*, *47*(10), 1085–1100. https://doi.org/10.1139/T10-012

Jones, J. A. A. (2004). Pipe and piping. In: Goudie, A.S. (Ed.). In *Encyclopedia of Geomorphology* (pp. 784–788). Routledge.

Julien, P. Y., & Moglen, G. E. (1990). Similarity and length scale for spatially varied overland flow. *Water Resources Research*, *26*(8), 1819–1832. https://doi.org/10.1029/WR026i008p01819

Jungers, M. C., Heimsath, A. M., Amundson, R., Balco, G., Shuster, D., & Chong, G. (2013). Active erosion–deposition cycles in the hyperarid Atacama Desert of Northern Chile. *Earth and Planetary Science Letters*, *371–372*, 125–133. https://doi.org/10.1016/j.epsl.2013.04.005

Kabir, S. M. I., & Ahmari, H. (2020a). Evaluating the effect of sediment color on water radiance and suspended sediment concentration using digital imagery. *Journal of Hydrology*, *589*, 125189. https://doi.org/10.1016/j.jhydrol.2020.125189

Kabir, S. Md. I., & Ahmari, H. (2020b). Sediment Color Effects on the Estimation of Suspended Sediment Concentration from Digital Imagery. *World Environmental and Water Resources Congress 2020*, 40–50. https://doi.org/10.1061/9780784482940.005

Kamann, P. J., Ritzi, R. W., Dominic, D. F., & Conrad, C. M. (2007). Porosity and Permeability in Sediment Mixtures. *Groundwater*, *45*(4), 429–438. https://doi.org/10.1111/j.1745-6584.2007.00313.x

Kassoul, M., Abdelgader, A., & Belorgey, M. (1997). Caractérisation de la sédimentation des barrages en Algérie. *Revue Des Sciences de l'eau/Journal of Water Science*, *10*(3), 339–358.

Kataoka, K. S., Matsumoto, T., Saito, T., Nagahashi, Y., & Iyobe, T. (2019). Suspended sediment transport diversity in river catchments following the 2014 phreatic eruption at Ontake Volcano, Japan. *Earth, Planets and Space*, *71*(1), 15. https://doi.org/10.1186/s40623-019-0994-x

Keesstra, S. D., Davis, J., Masselink, R. H., Casalí, J., Peeters, E. T. H. M., & Dijksma, R. (2019). Coupling hysteresis analysis with sediment and hydrological connectivity in three agricultural catchments in Navarre, Spain. *Journal of Soils and Sediments*, *19*(3), 1598–1612. https://doi.org/10.1007/s11368-018-02223-0

Keesstra, S., Nunes, J. P., Saco, P., Parsons, T., Poeppl, R., Masselink, R., & Cerdà, A. (2018). The way forward: Can connectivity be useful to design better measuring and modelling schemes for water and sediment dynamics? *Science of The Total Environment*, *644*, 1557–1572. https://doi.org/10.1016/j.scitotenv.2018.06.342

Kehew, A. E., Milewski, A., & Soliman, F. (2010). Reconstructing an extreme flood from boulder transport and rainfall–runoff modelling: Wadi Isla, South Sinai, Egypt. *Global and Planetary Change*, *70*(1–4), 64–75. https://doi.org/10.1016/j.gloplacha.2009.11.008

Keshavarz, M., Pellet, F. L., & Loret, B. (2010). Damage and Changes in Mechanical Properties of a Gabbro Thermally Loaded up to 1,000°C. *Pure and Applied Geophysics*, *167*(12), 1511–1523. https://doi.org/10.1007/s00024-010-0130-0

Khettab, O. E. F. (2022). Quantifying the in-channel contribution to suspended-sediment concentration, a concept for sediment yield apportionment using limited data. *River Research and Applications*, *38*(7), 1254–1265. https://doi.org/10.1002/rra.4012

Kieta, K. A., Owens, P. N., & Petticrew, E. L. (2023). Determination of sediment sources following a major wildfire and evaluation of the use of color properties and polycyclic aromatic hydrocarbons (PAHs) as tracers. *Journal of Soils and Sediments*, *23*(12), 4187–4207. https://doi.org/10.1007/s11368-023-03565-0

Kinnell, P. I. A. (1991). The Effect Of Flow Depth On Sediment Transport Induced By Raindrops Impacting Shallow Flows. *Transactions of the ASAE*, *34*(1), 161–0168. https://doi.org/10.13031/2013.31639

Kinnell, P. I. A. (1993). Sediment Concentrations Resulting from Flow Depth/Drop Size Interactions in Shallow Overland Flow. *Transactions of the ASAE*, *36*(4), 1099–1103. https://doi.org/10.13031/2013.28440

Kinnell, P. I. A. (2005). Raindrop-impact-induced erosion processes and prediction: A review. *Hydrological Processes*, *19*(14), 2815–2844. https://doi.org/10.1002/hyp.5788

Klein, M. (1984). Anti clockwise hysteresis in suspended sediment concentration during individual storms: Holbeck catchment; Yorkshire, England. *CATENA*, *11*(2–3), 251–257. https://doi.org/10.1016/0341-8162(84)90014-6

Kobayashi, D., Ishii, Y., & Kodama, Y. (1999). Stream temperature, specific conductance and runoff process in mountain watersheds. *Hydrological Processes*, *13*(6), 865–876. https://doi.org/10.1002/(SICI)1099-1085(19990430)13:6%253C865::AID-HYP761%253E3.0.CO;2-O

Kobayashi, M., & Shimizu, T. (2007). Soil water repellency in a Japanese cypress plantation restricts increases in soil water storage during rainfall events. *Hydrological Processes*, *21*(17), 2356–2364. https://doi.org/10.1002/hyp.6754

Koiter, A. J., Owens, P. N., Petticrew, E. L., & Lobb, D. A. (2013). The behavioural characteristics of sediment properties and their implications for sediment fingerprinting as an approach for identifying sediment sources in river basins. *Earth-Science Reviews*, *125*, 24–42. https://doi.org/10.1016/j.earscirev.2013.05.009

Koiter, A. J., Owens, P. N., Petticrew, E. L., & Lobb, D. A. (2015). The role of gravel channel beds on the particle size and organic matter selectivity of transported fine-grained sediment: Implications for sediment fingerprinting and biogeochemical flux research. *Journal of Soils and Sediments*, *15*(10), 2174–2188. https://doi.org/10.1007/s11368-015-1203-6

Koiter, A. J., Owens, P. N., Petticrew, E. L., & Lobb, D. A. (2018). Assessment of particle size and organic matter correction factors in sediment source fingerprinting investigations: An example of two contrasting watersheds in Canada. *Geoderma*, *325*, 195–207. https://doi.org/10.1016/j.geoderma.2018.02.044

Koken, M., & Constantinescu, G. (2008). An investigation of the flow and scour mechanisms around isolated spur dikes in a shallow open channel: 1. Conditions corresponding to the initiation of the erosion and deposition process. *Water Resources Research*, *44*(8), 2007WR006489. https://doi.org/10.1029/2007WR006489

Kramer, N., & Wohl, E. (2017). Rules of the road: A qualitative and quantitative synthesis of large wood transport through drainage networks. *Geomorphology*, *279*, 74–97. https://doi.org/10.1016/j.geomorph.2016.08.026

Krein, A., Petticrew, E., & Udelhoven, T. (2003). The use of fine sediment fractal dimensions and colour to determine sediment sources in a small watershed. *CATENA*, *53*(2), 165–179. https://doi.org/10.1016/S0341-8162(03)00021-3

Kuenen, Ph. H. (1956). Experimental Abrasion of Pebbles: 2. Rolling by Current. *The Journal of Geology*, *64*(4), 336–368. https://doi.org/10.1086/626370

Kumar, S. (2019). Geospatial Approach in Modeling Soil Erosion Processes in Predicting Soil Erosion and Nutrient Loss in Hilly and Mountainous Landscape. In R. R. Navalgund, A. S. Kumar, & S. Nandy (Eds.), *Remote Sensing of Northwest Himalayan Ecosystems* (pp. 355–380). Springer Singapore. https://doi.org/10.1007/978-981-13-2128-3_17

Lança, R., Fael, C., Maia, R., Pêgo, J. P., & Cardoso, A. H. (2013). Clear-Water Scour at Pile Groups. *Journal of Hydraulic Engineering*, *139*(10), 1089–1098. https://doi.org/10.1061/(ASCE)HY.1943-7900.0000770

Lanckriet, S., Asfaha, T., Frankl, A., Zenebe, A., & Nyssen, J. (2016). Sediment in Alluvial and Lacustrine Debris Fans as an Indicator for Land Degradation Around Lake Ashenge (Ethiopia). *Land Degradation & Development*, *27*(2), 258–269. https://doi.org/10.1002/ldr.2424

Langendoen, E. J. (2000). *Concepts: Conservational channel evolution and pollutant transport system*.

Langlois, J. L., Johnson, D. W., & Mehuys, G. R. (2005). Suspended sediment dynamics associated with snowmelt runoff in a small mountain stream of Lake Tahoe (Nevada). *Hydrological Processes*, *19*(18), 3569–3580. https://doi.org/10.1002/hyp.5844

Lavee, H., & Poesen, J. W. A. (1991). Overland flow generation and continuity on stone-covered soil surfaces. *Hydrological Processes*, *5*(4), 345–360. https://doi.org/10.1002/hyp.3360050403

Lawler, D. M., Petts, G. E., Foster, I. D. L., & Harper, S. (2006). Turbidity dynamics during spring storm events in an urban headwater river system: The Upper Tame, West Midlands,

UK. *Science of The Total Environment*, *360*(1–3), 109–126. https://doi.org/10.1016/j.scitotenv.2005.08.032

Le Bissonnais, Y. (1996). Aggregate stability and assessment of soil crustability and erodibility: I. Theory and methodology. *European Journal of Soil Science*, *47*(4), 425–437. https://doi.org/10.1111/j.1365-2389.1996.tb01843.x

Le Bouteiller, C., Naaim-Bouvet, F., Mathys, N., & Lavé, J. (2011). A new framework for modeling sediment fining during transport with fragmentation and abrasion. *Journal of Geophysical Research*, *116*(F3), F03002. https://doi.org/10.1029/2010JF001926

Lefrançois, J., Grimaldi, C., Gascuel-Odoux, C., & Gilliet, N. (2007). Suspended sediment and discharge relationships to identify bank degradation as a main sediment source on small agricultural catchments. *Hydrological Processes*, *21*(21), 2923–2933. https://doi.org/10.1002/hyp.6509

Lenzi, M. A. (2004). Displacement and transport of marked pebbles, cobbles and boulders during floods in a steep mountain stream. *Hydrological Processes*, *18*(10), 1899–1914. https://doi.org/10.1002/hyp.1456

Lenzi, M. A., & Marchi, L. (2000). Suspended sediment load during floods in a small stream of the Dolomites (northeastern Italy). *CATENA*, *39*(4), 267–282. https://doi.org/10.1016/S0341-8162(00)00079-5

Lepesqueur, J., Hostache, R., Martínez-Carreras, N., Montargès-Pelletier, E., & Hissler, C. (2019). Sediment transport modelling in riverine environments: On the importance of grain-size distribution, sediment density, and suspended sediment concentrations at the upstream boundary. *Hydrology and Earth System Sciences*, *23*(9), 3901–3915. https://doi.org/10.5194/hess-23-3901-2019

Li, G., Zheng, T., Fu, Y., Li, B., & Zhang, T. (2017). Soil detachment and transport under the combined action of rainfall and runoff energy on shallow overland flow. *Journal of Mountain Science*, *14*(7), 1373–1383. https://doi.org/10.1007/s11629-016-3938-y

Li, Q., Matthew Benson, W., Harlan, M., Robichaux, P., Sha, X., Xu, K., & Straub, K. M. (2017). Influence of Sediment Cohesion on Deltaic Morphodynamics and Stratigraphy Over Basin-Filling Time Scales. *Journal of Geophysical Research: Earth Surface*, *122*(10), 1808–1826. https://doi.org/10.1002/2017JF004216

Lin, W. (2002). Permanent strain of thermal expansion and thermally induced microcracking in Inada granite. *Journal of Geophysical Research: Solid Earth*, *107*(B10). https://doi.org/10.1029/2001JB000648

Little, D., & Field, J. (2003). The Rhyzosphere, Biology and the Regolith. *Advances in Regolith*. https://openresearch-repository.anu.edu.au/handle/1885/85461

Liu, J., Chen, M., Chen, Z., & Yan, W. (2010). Clay mineral distribution in surface sediments of the South China Sea and its significance for in sediment sources and transport. *Chinese Journal of Oceanology and Limnology*, *28*(2), 407–415. https://doi.org/10.1007/s00343-010-9057-7

Liu, J., Li, B., Tian, W., & Wu, X. (2018). Investigating and predicting permeability variation in thermally cracked dry rocks. *International Journal of Rock Mechanics and Mining Sciences*, *103*, 77–88. https://doi.org/10.1016/j.ijrmms.2018.01.023

Liu, J., Xian, B., Wang, J., Ji, Y., Lu, Z., & Liu, S. (2017). Sedimentary architecture of a sub-lacustrine debris fan: Eocene Dongying Depression, Bohai Bay Basin, east China. *Sedimentary Geology*, *362*, 66–82. https://doi.org/10.1016/j.sedgeo.2017.09.014

Liu, W., Birgand, F., Tian, S., & Chen, C. (2021). Event-scale hysteresis metrics to reveal processes and mechanisms controlling constituent export from watersheds: A review☆. *Water Research*, *200*, 117254. https://doi.org/10.1016/j.watres.2021.117254

Lizaga, I., Latorre, B., Gaspar, L., & Navas, A. (2022). Combined use of geochemistry and compound-specific stable isotopes for sediment fingerprinting and tracing. *Science of The Total Environment*, *832*, 154834. https://doi.org/10.1016/j.scitotenv.2022.154834

Lloyd, C. E. M., Freer, J. E., Johnes, P. J., & Collins, A. L. (2016a). Technical Note: Testing an improved index for analysing storm discharge–concentration hysteresis. *Hydrology and Earth System Sciences*, *20*(2), 625–632. https://doi.org/10.5194/hess-20-625-2016

Lloyd, C. E. M., Freer, J. E., Johnes, P. J., & Collins, A. L. (2016b). Using hysteresis analysis of high-resolution water quality monitoring data, including uncertainty, to infer controls on nutrient and sediment transfer in catchments. *Science of The Total Environment*, *543*, 388–404. https://doi.org/10.1016/j.scitotenv.2015.11.028

Lørup, J. K., & Styczen, M. (1990). Soil Erosion Modelling. In M. B. Abbott & J. C. Refsgaard (Eds.), *Distributed Hydrological Modelling* (Vol. 22, pp. 93–120). Springer Netherlands. https://doi.org/10.1007/978-94-009-0257-2_6

Lowe, A. T., & Eyring, L. (1975). Chemical hysteresis in phase transitions in the terbium oxide-oxygen system. *Journal of Solid State Chemistry*, *14*(4), 383–394. https://doi.org/10.1016/0022-4596(75)90060-2

Lu, J., Zheng, F., Li, G., Bian, F., & An, J. (2016). The effects of raindrop impact and runoff detachment on hillslope soil erosion and soil aggregate loss in the Mollisol region of Northeast China. *Soil and Tillage Research*, *161*, 79–85. https://doi.org/10.1016/j.still.2016.04.002

Lucas, D., Fankhauser, K., Maurer, H., McArdell, B., Grob, R., Herzog, R., Bleiker, E., & Springman, S. M. (2020). Slope Stability of a Scree Slope Based on Integrated Characterisation and Monitoring. *Water*, *12*(2), 447. https://doi.org/10.3390/w12020447

Lucas, D., Herzog, R., Iten, M., Buschor, H., Kieper, A., Askarinejad, A., & Springman, S. M. (2020). Modelling of landslides in a scree slope induced by groundwater and rainfall. *International Journal of Physical Modelling in Geotechnics*, *20*(4), 177–197. https://doi.org/10.1680/jphmg.18.00106

Ma, B., Yu, X., Ma, F., Li, Z., & Wu, F. (2014). Effects of Crop Canopies on Rain Splash Detachment. *PLoS ONE*, *9*(7), e99717. https://doi.org/10.1371/journal.pone.0099717

MacVicar, B. J., Piégay, H., Henderson, A., Comiti, F., Oberlin, C., & Pecorari, E. (2009). Quantifying the temporal dynamics of wood in large rivers: Field trials of wood surveying, dating, tracking, and monitoring techniques. *Earth Surface Processes and Landforms*, *34*(15), 2031–2046. https://doi.org/10.1002/esp.1888

Major, J. J. (2003). Post-Eruption Hydrology and Sediment Transport in Volcanic River Systems. *Water Resources IMPACT*, *5*(3), 10–15.

Malik, I., Pawlik, Ł., Ślęzak, A., & Wistuba, M. (2019). A study of the wood anatomy of Picea abies roots and their role in biomechanical weathering of rock cracks. *CATENA*, *173*, 264–275. https://doi.org/10.1016/j.catena.2018.10.018

Malmon, D. V., Reneau, S. L., Katzman, D., Lavine, A., & Lyman, J. (2007). Suspended sediment transport in an ephemeral stream following wildfire. *Journal of Geophysical Research: Earth Surface*, *112*(F2), 2005JF000459. https://doi.org/10.1029/2005JF000459

Malmström, M. E., Berglund, S., & Jarsjö, J. (2008). Combined effects of spatially variable flow and mineralogy on the attenuation of acid mine drainage in groundwater. *Applied Geochemistry*, *23*(6), 1419–1436. https://doi.org/10.1016/j.apgeochem.2007.12.029

Malutta, S., Kobiyama, M., Chaffe, P. L. B., & Bonumá, N. B. (2020). Hysteresis analysis to quantify and qualify the sediment dynamics: State of the art. *Water Science and Technology*, *81*(12), 2471–2487. https://doi.org/10.2166/wst.2020.279

Mao, L., Dell'Agnese, A., Huincache, C., Penna, D., Engel, M., Niedrist, G., & Comiti, F. (2014). Bedload hysteresis in a glacier-fed mountain river: BEDLOAD HYSTERESIS IN A GLACIER-FED MOUNTAIN RIVER. *Earth Surface Processes and Landforms*, *39*(7), 964–976. https://doi.org/10.1002/esp.3563

Maref, N., & Seddini, A. (2018). Modeling of flood generation in semi-arid catchment using a spatially distributed model: Case of study Wadi Mekerra catchment (Northwest Algeria). *Arabian Journal of Geosciences*, *11*(6), 116. https://doi.org/10.1007/s12517-018-3461-2

Marshall, D. H. (1933). Reducing Sediment Sampling Frequency at Streamflow Gaging Station Rio Grande at Otowi Bridge near San Ildefonso, New Mexico. *US Geological Survey Circular*, *953*, 4.

Martínez-Martínez, J., Benavente, D., Gomez-Heras, M., Marco-Castaño, L., & García-del-Cura, M. Á. (2013). Non-linear decay of building stones during freeze–thaw weathering processes. *Construction and Building Materials*, *38*, 443–454. https://doi.org/10.1016/j.conbuildmat.2012.07.059

Marttila, H., & Kløve, B. (2010). Dynamics of erosion and suspended sediment transport from drained peatland forestry. *Journal of Hydrology*, *388*(3–4), 414–425. https://doi.org/10.1016/j.jhydrol.2010.05.026

Marzen, M., Iserloh, T., Casper, M. C., & Ries, J. B. (2015). Quantification of particle detachment by rain splash and wind-driven rain splash. *CATENA*, *127*, 135–141. https://doi.org/10.1016/j.catena.2014.12.023

Masscheleyn, P. H., Delaune, R. D., & Patrick, W. H. (1991). Arsenic and Selenium Chemistry as Affected by Sediment Redox Potential and pH. *Journal of Environmental Quality*, *20*(3), 522–527. https://doi.org/10.2134/jeq1991.00472425002000030004x

Matgen, P., Fenicia, F., Heitz, S., Plaza, D., de Keyser, R., Pauwels, V. R. N., Wagner, W., & Savenije, H. (2012). Can ASCAT-derived soil wetness indices reduce predictive uncertainty in well-gauged areas? A comparison with in situ observed soil moisture in an assimilation application. *Advances in Water Resources*, *44*, 49–65. https://doi.org/10.1016/j.advwatres.2012.03.022

Matsuoka, N., & Murton, J. (2008). Frost weathering: Recent advances and future directions. *Permafrost and Periglacial Processes*, *19*(2), 195–210. https://doi.org/10.1002/ppp.620

Matsuoka, N., & Sakai, H. (1999). Rockfall activity from an alpine cliff during thawing periods. *Geomorphology*, *28*(3–4), 309–328. https://doi.org/10.1016/S0169-555X(98)00116-0

McBean, E. A., & Al-Nassri, S. (1988). Uncertainty in Suspended Sediment Transport Curves. *Journal of Hydraulic Engineering*, *114*(1), 63–74. https://doi.org/10.1061/(ASCE)0733-9429(1988)114:1(63)

McCave, I. N. (2008). Chapter 8 Size Sorting During Transport and Deposition of Fine Sediments. In *Developments in Sedimentology* (Vol. 60, pp. 121–142). Elsevier. https://doi.org/10.1016/S0070-4571(08)10008-5

McDiffett, W. F., Beidler, A. W., Dominick, T. F., & McCrea, K. D. (1989). Nutrient concentration-stream discharge relationships during storm events in a first-order stream. *Hydrobiologia*, *179*(2), 97–102. https://doi.org/10.1007/BF00007596

McDonald, D. M., & Lamoureux, S. F. (2009). Hydroclimatic and channel snowpack controls over suspended sediment and grain size transport in a High Arctic catchment. *Earth Surface Processes and Landforms*, *34*(3), 424–436. https://doi.org/10.1002/esp.1751

McGlynn, B. L., McDonnell, J. J., Seibert, J., & Kendall, C. (2004). Scale effects on headwater catchment runoff timing, flow sources, and groundwater-streamflow relations: SCALE EFFECTS ON CATCHMENT RUNOFF. *Water Resources Research*, *40*(7). https://doi.org/10.1029/2003WR002494

McGuire, K. J., & McDonnell, J. J. (2010). Hydrological connectivity of hillslopes and streams: Characteristic time scales and nonlinearities. *Water Resources Research*, *46*(10), 2010WR009341. https://doi.org/10.1029/2010WR009341

Meddi, M., & Ben Abbes, B. S. (2014). Analyse statistique et prévision des débits de crues dans le bassin versant de l'Oued Mekerra (Ouest de l'Algérie). *Revue Nature et Technologie*, *6*(1), 21–31.

Megnounif, A., & Ghenim, A. N. (2016). Rainfall irregularity and its impact on the sediment yield in Wadi Sebdou watershed, Algeria. *Arabian Journal of Geosciences*, *9*(4), 267. https://doi.org/10.1007/s12517-015-2280-y

Megnounif, A., & Ouillon, S. (2018). Empirical and analytical methods to characterize the efficiency of floods to move sediment in a small semi-arid basin. *Hydrology and Earth System Sciences*, *22*(12), 6335–6355. https://doi.org/10.5194/hess-22-6335-2018

Megnounif, A., Terfous, A., & Bouanani, A. (2005). Production et transport des matières solides en suspension dans le bassin versant de la Haute-Tafna (Nord-Ouest Algérien). *Revue Des Sciences de l'eau*, *16*(3), 369–380. https://doi.org/10.7202/705513ar

Megnounif, A., Terfous, A., Ghenaim, A., & Poulet, J.-B. (2007). Key processes influencing erosion and sediment transport in a semi-arid Mediterranean area: The Upper Tafna catchment, Algeria / *Processus clefs influençant l'érosion et le transport des sédiments dans une région semi-aride Méditerranéenne: le bassin versant de la Haute Tafna, Algérie*. *Hydrological Sciences Journal*, *52*(6), 1271–1284. https://doi.org/10.1623/hysj.52.6.1271

Megnounif, A., Terfous, A., & Ouillon, S. (2013). A graphical method to study suspended sediment dynamics during flood events in the Wadi Sebdou, NW Algeria (1973–2004). *Journal of Hydrology*, *497*, 24–36. https://doi.org/10.1016/j.jhydrol.2013.05.029

Melville, B. W. (1997). Pier and Abutment Scour: Integrated Approach. *Journal of Hydraulic Engineering*, *123*(2), 125–136. https://doi.org/10.1061/(ASCE)0733-9429(1997)123:2(125)

Mermut, A. R., Luk, S. H., Römkens, M. J. M., & Poesen, J. W. A. (1997). Soil loss by splash and wash during rainfall from two loess soils. *Geoderma*, *75*(3–4), 203–214. https://doi.org/10.1016/S0016-7061(96)00091-2

Meyer-Peter, E., & Müller, R. (1948). Formulas for Bed-Load transport. *IAHSR 2nd Meeting, Stockholm, Appendix 2*. https://repository.tudelft.nl/islandora/object/uuid%3A4fda9b61-be28-4703-ab06-43cdc2a21bd7

Milàn, J., & Bromley, R. G. (2007). The Impact of Sediment Consistency on Track and Undertrack Morphology: Experiments with Emu Tracks in Layered Cement. *Ichnos*, *15*(1), 19–27. https://doi.org/10.1080/10420940600864712

Misset, C., Recking, A., Legout, C., Poirel, A., Cazilhac, M., Esteves, M., & Bertrand, M. (2019). An attempt to link suspended load hysteresis patterns and sediment sources configuration in alpine catchments. *Journal of Hydrology*, *576*, 72–84. https://doi.org/10.1016/j.jhydrol.2019.06.039

Moog, D. B., & Whiting, P. J. (1998). Annual hysteresis in bed load rating curves. *Water Resources Research*, *34*(9), 2393–2399. https://doi.org/10.1029/98WR01658

Moore, D. (1966). Deltaic sedimentation. *Earth-Science Reviews*, *1*(2–3), 87–104. https://doi.org/10.1016/0012-8252(66)90001-8

Moss, A., & Green, P. (1983). Movement of solids in air and water by raindrop impact. Effects of drop-size and water-depth variations. *Soil Research*, *21*(3), 257. https://doi.org/10.1071/SR9830257

Mossa, J. (1996). Sediment dynamics in the lowermost Mississippi River. *Engineering Geology*, *45*(1–4), 457–479. https://doi.org/10.1016/S0013-7952(96)00026-9

Nadal-Romero, E., Regüés, D., & Latron, J. (2008). Relationships among rainfall, runoff, and suspended sediment in a small catchment with badlands. *CATENA*, *74*(2), 127–136. https://doi.org/10.1016/j.catena.2008.03.014

Nadal-Romero, E., Verachtert, E., Maes, R., & Poesen, J. (2011). Quantitative assessment of the piping erosion susceptibility of loess-derived soil horizons using the pinhole test. *Geomorphology*, *135*(1–2), 66–79. https://doi.org/10.1016/j.geomorph.2011.07.026

Nadir, M., & Boualem, R. (2016). Study of Beni Haroun dam pollution (Algeria). *Desalination and Water Treatment*, *57*(6), 2766–2774. https://doi.org/10.1080/19443994.2014.982192

Najafi, S., Dragovich, D., Heckmann, T., & Sadeghi, S. H. (2021). Sediment connectivity concepts and approaches. *CATENA*, *196*, 104880. https://doi.org/10.1016/j.catena.2020.104880

Nasseri, M. H. B., Schubnel, A., Benson, P. M., & Young, R. P. (2009). Common Evolution of Mechanical and Transport Properties in Thermally Cracked Westerly Granite at Elevated Hydrostatic Pressure. *Pure and Applied Geophysics*, *166*(5–7), 927–948. https://doi.org/10.1007/s00024-009-0485-2

Nasseri, M. H. B., Schubnel, A., & Young, R. P. (2007). Coupled evolutions of fracture toughness and elastic wave velocities at high crack density in thermally treated Westerly granite. *International Journal of Rock Mechanics and Mining Sciences*, *44*(4), 601–616. https://doi.org/10.1016/j.ijrmms.2006.09.008

Neal, C. W. M., & Anders, A. M. (2015). Suspended sediment supply dominated by bank erosion in a low-gradient agricultural watershed, Wildcat Slough, Fisher, Illinois, United States. *Journal of Soil and Water Conservation*, *70*(3), 145–155. https://doi.org/10.2489/jswc.70.3.145

Nearing, M. A. (2000). Evaluating soil erosion models using measured plot data: Accounting for variability in the data. *Earth Surface Processes and Landforms*, *25*(9), 1035–1043. https://doi.org/10.1002/1096-9837(200008)25:9%253C1035::AID-ESP121%253E3.0.CO;2-B

Nearing, M. A., Norton, L. D., Bulgakov, D. A., Larionov, G. A., West, L. T., & Dontsova, K. M. (1997). Hydraulics and erosion in eroding rills. *Water Resources Research*, *33*(4), 865–876. https://doi.org/10.1029/97WR00013

Nederbragt, A. J., Dunbar, R. B., Osborn, A. T., Palmer, A., Thurow, J. W., & Wagner, T. (2006). Sediment colour analysis from digital images and correlation with sediment composition.

Geological Society, London, Special Publications, *267*(1), 113–128. https://doi.org/10.1144/GSL.SP.2006.267.01.08

Nickling, W. G., & Neuman, C. M. (2009). Aeolian Sediment Transport. In A. J. Parsons & A. D. Abrahams (Eds.), *Geomorphology of Desert Environments* (pp. 517–555). Springer Netherlands. https://doi.org/10.1007/978-1-4020-5719-9_17

Nistor, C. J., & Church, M. (2005). Suspended sediment transport regime in a debris-flow gully on Vancouver Island, British Columbia. *Hydrological Processes*, *19*(4), 861–885. https://doi.org/10.1002/hyp.5549

Nolte, S., Koppenaal, E. C., Esselink, P., Dijkema, K. S., Schuerch, M., De Groot, A. V., Bakker, J. P., & Temmerman, S. (2013). Measuring sedimentation in tidal marshes: A review on methods and their applicability in biogeomorphological studies. *Journal of Coastal Conservation*, *17*(3), 301–325. https://doi.org/10.1007/s11852-013-0238-3

Nu-Fang, F., Zhi-Hua, S., Lu, L., & Cheng, J. (2011). Rainfall, runoff, and suspended sediment delivery relationships in a small agricultural watershed of the Three Gorges area, China. *Geomorphology*, *135*(1–2), 158–166. https://doi.org/10.1016/j.geomorph.2011.08.013

Nunes, J. P., Doerr, S. H., Sheridan, G., Neris, J., Santín, C., Emelko, M. B., Silins, U., Robichaud, P. R., Elliot, W. J., & Keizer, J. (2018). Assessing water contamination risk from vegetation fires: Challenges, opportunities and a framework for progress. *Hydrological Processes*, *32*(5), 687–694. https://doi.org/10.1002/hyp.11434

Nyssen, J., Pontzeele, J., & Billi, P. (2011). Effect of beaver dams on the hydrology of small mountain streams: Example from the Chevral in the Ourthe Orientale basin, Ardennes, Belgium. *Journal of Hydrology*, *402*(1–2), 92–102. https://doi.org/10.1016/j.jhydrol.2011.03.008

Ochiai, N., Iga, Y., Nohmi, M., & Ikohagi, T. (2013). Study of Quantitative Numerical Prediction of Cavitation Erosion in Cavitating Flow. *Journal of Fluids Engineering*, *135*(1), 011302. https://doi.org/10.1115/1.4023072

Oeurng, C., Sauvage, S., & Sánchez-Pérez, J. (2010). Dynamics of suspended sediment transport and yield in a large agricultural catchment, southwest France. *Earth Surface Processes and Landforms*, *35*(11), 1289–1301. https://doi.org/10.1002/esp.1971

Oguchi, C. T., & Yu, S. (2021). A review of theoretical salt weathering studies for stone heritage. *Progress in Earth and Planetary Science*, *8*(1), 32. https://doi.org/10.1186/s40645-021-00414-x

Oldfield, F., Rummery, T. A., Thompson, R., & Walling, D. E. (1979). Identification of suspended sediment sources by means of magnetic measurements: Some preliminary results. *Water Resources Research*, *15*(2), 211–218. https://doi.org/10.1029/WR015i002p00211

Olive, L. J., & Rieger, W. A. (1985). Variation in suspended sediment concentration during storms in five small catchments in southeast New South Wales. *Australian Geographical Studies*, *23*(1), 38–51. https://doi.org/10.1111/j.1467-8470.1985.tb00477.x

Oppel, H., & Mewes, B. (2020). On the Automation of Flood Event Separation From Continuous Time Series. *Frontiers in Water*, *2*, 18. https://doi.org/10.3389/frwa.2020.00018

Ostermann, M., Ivy-Ochs, S., Ruegenberg, F., & Vockenhuber, C. (2020). Characteristics and dating of the rock avalanche at Pragser Wildsee/Lago di Braies (Dolomites, Italy). *Alpine and Mediterranean Quaternary*, *33*(2), 183–189. https://doi.org/10.26382/AMQ.2020.07

Otmane, A., Baba-Hamed, K., Bouanani, A., & Safa, A. (2017). Prédétermination des valeurs de crues extrêmes et contribution de la plaine de Sidi Bel-Abbès dans le bilan hydrologique

du bassin versant de l'oued Mekerra. *Techniques Sciences Méthodes*, *7–8*, 27–48. https://doi.org/10.1051/tsm/201778027

Owens, P. N. (2008). Sediment behaviour, functions and management in river basins. In *Sustainable Management of Sediment Resources* (Vol. 4, pp. 1–29). Elsevier. https://doi.org/10.1016/S1872-1990(08)80003-7

Owens, P. N., Batalla, R. J., Collins, A. J., Gomez, B., Hicks, D. M., Horowitz, A. J., Kondolf, G. M., Marden, M., Page, M. J., Peacock, D. H., Petticrew, E. L., Salomons, W., & Trustrum, N. A. (2005). Fine-grained sediment in river systems: Environmental significance and management issues. *River Research and Applications*, *21*(7), 693–717. https://doi.org/10.1002/rra.878

Owens, P. N., Petticrew, E. L., & Van Der Perk, M. (2010). Sediment response to catchment disturbances. *Journal of Soils and Sediments*, *10*(4), 591–596. https://doi.org/10.1007/s11368-010-0235-1

Ozcan, O., Musaoglu, N., Seker, D. Z., & others. (2012). Environmental impact analysis of quarrying activities established on and near a river bed by using remotely sensed data. *Fresenius Environmental Bulletin*, *21*(11), 3147–3153.

Palmer, V. J. (1946). Retardance coefficients for low flow in channels lined with vegetation. *Eos, Transactions American Geophysical Union*, *27*(2), 187–197. https://doi.org/10.1029/TR027i002p00187

Parteli, E. J. R., Durán, O., Tsoar, H., Schwämmle, V., & Herrmann, H. J. (2009). Dune formation under bimodal winds. *Proceedings of the National Academy of Sciences*, *106*(52), 22085–22089. https://doi.org/10.1073/pnas.0808646106

Pawlik, Ł., Phillips, J. D., & Šamonil, P. (2016). Roots, rock, and regolith: Biomechanical and biochemical weathering by trees and its impact on hillslopes—A critical literature review. *Earth-Science Reviews*, *159*, 142–159. https://doi.org/10.1016/j.earscirev.2016.06.002

Peart, M., & Walling, D. (1982). Particle size characteristics of fluvial suspended sediment. *Recent Developments in the Explanation and Prediction of Erosion and Sediment Yield/Edited by DE Walling*.

Pedersen, H. S., & Hasholt, B. (1995). Influence of wind speed on rainsplash erosion. *CATENA*, *24*(1), 39–54. https://doi.org/10.1016/0341-8162(94)00024-9

Penck, A., & Brückner, E. (1909). *Die Alpen im Eiszeitalter*. Tauchnitz.

Phillips, J. D. (2003). Sources of nonlinearity and complexity in geomorphic systems. *Progress in Physical Geography: Earth and Environment*, *27*(1), 1–23. https://doi.org/10.1191/0309133303pp340ra

Phillips, J. D. (2009). Soils as extended composite phenotypes. *Geoderma*, *149*(1–2), 143–151. https://doi.org/10.1016/j.geoderma.2008.11.028

Phillips, J. D. (2016). Biogeomorphology and contingent ecosystem engineering in karst landscapes. *Progress in Physical Geography: Earth and Environment*, *40*(4), 503–526. https://doi.org/10.1177/0309133315624641

Piccolroaz, S., Calamita, E., Majone, B., Gallice, A., Siviglia, A., & Toffolon, M. (2016). Prediction of river water temperature: A comparison between a new family of hybrid models and statistical approaches: Prediction of River Water Temperature. *Hydrological Processes*, *30*(21), 3901–3917. https://doi.org/10.1002/hyp.10913

Pietroń, J., Jarsjö, J., Romanchenko, A. O., & Chalov, S. R. (2015). Model analyses of the contribution of in-channel processes to sediment concentration hysteresis loops. *Journal of Hydrology*, *527*, 576–589. https://doi.org/10.1016/j.jhydrol.2015.05.009

Pike, L., Gaskin, S., & Ashmore, P. (2018). Flume tests on fluvial erosion mechanisms in till-bed channels. *Earth Surface Processes and Landforms*, *43*(1), 259–270. https://doi.org/10.1002/esp.4240

Pitty, A. F. (2020). *Introduction to Geomorphology* (1st ed.). Routledge. https://doi.org/10.4324/9780429273131

Podmanicky, L., Balázs, K., Belényesi, M., Centeri, Cs., Kristóf, D., & Kohlheb, N. (2011). Modelling soil quality changes in Europe. An impact assessment of land use change on soil quality in Europe. *Ecological Indicators*, *11*(1), 4–15. https://doi.org/10.1016/j.ecolind.2009.08.002

Poeppl, R. E., Keesstra, S. D., & Hein, T. (2015). The geomorphic legacy of small dams—An Austrian study. *Anthropocene*, *10*, 43–55. https://doi.org/10.1016/j.ancene.2015.09.003

Poesen, J. (1989). Conditions for gully formation in the Belgian loam belt and some ways to control them. *Soil Erosion Protection Measures in Europe. Proc. EC Workshop. Freising, 1988*, 39–52.

Poggi-Varaldo, H. M., & Rinderknecht-Seijas, N. (2003). A Differential Availability Enhancement Factor for the Evaluation of Pollutant Availability in Soil Treatments. *Acta Biotechnologica*, *23*(23), 271–280. https://doi.org/10.1002/abio.200390034

Powell, D. M. (1998). Patterns and processes of sediment sorting in gravel-bed rivers. *Progress in Physical Geography: Earth and Environment*, *22*(1), 1–32. https://doi.org/10.1177/030913339802200101

Pradhan, S. P., & Siddique, T. (2019). Mass Wasting: An Overview. In S. P. Pradhan, V. Vishal, & T. N. Singh (Eds.), *Landslides: Theory, Practice and Modelling* (Vol. 50, pp. 3–20). Springer International Publishing. https://doi.org/10.1007/978-3-319-77377-3_1

Prathapar, S. A., & Bawain, A. A. (2014). Impact of sedimentation on groundwater recharge at Sahalanowt Dam, Salalah, Oman. *Water International*, *39*(3), 381–393. https://doi.org/10.1080/02508060.2014.895889

Prendergast, L. J., & Gavin, K. (2014). A review of bridge scour monitoring techniques. *Journal of Rock Mechanics and Geotechnical Engineering*, *6*(2), 138–149. https://doi.org/10.1016/j.jrmge.2014.01.007

Price, D. G. (1995). Weathering and weathering processes. *Quarterly Journal of Engineering Geology*, *28*(3), 243–252. https://doi.org/10.1144/GSL.QJEGH.1995.028.P3.03

Pringle, C. (2003). What is hydrologic connectivity and why is it ecologically important? *Hydrological Processes*, *17*(13), 2685–2689. https://doi.org/10.1002/hyp.5145

Prowse, C. W. (1984). Some Thoughts on Lag and Hysteresis. *Area*, *16*(1), 17–23. JSTOR.

Puech, C., & Chabi-Gonni, D. (1984). Méthode de calcul des débits de crus décennale. *CIEH, Ouagadougou*.

Pulley, S., & Collins, A. L. (2021). The potential for colour to provide a robust alternative to high-cost sediment source fingerprinting: Assessment using eight catchments in England. *Science of The Total Environment*, *792*, 148416. https://doi.org/10.1016/j.scitotenv.2021.148416

Pulley, S., Morten, C., Morgan, S., Cardenas, L. M., & Collins, A. L. (2022). Sediment detachment by raindrop impact on grassland and arable fields: An investigation of controls. *Journal of Soils and Sediments*, *22*(2), 692–703. https://doi.org/10.1007/s11368-021-03098-4

Pye, K. (1995). The nature, origin and accumulation of loess. *Quaternary Science Reviews*, *14*(7–8), 653–667. https://doi.org/10.1016/0277-3791(95)00047-X

Q., W., J., S., G., C., & L., X. (2002). Environmental effects induced by human activities in arid Shiyang River basin, Gansu province, northwest China. *Environmental Geology*, *43*(1–2), 219–227. https://doi.org/10.1007/s00254-002-0647-3

Quinton, J. N. (2004). Erosion and sediment transport. In *Environmental modelling: Finding simplicity in complexity*. John Wiley &, Sons, Ltd Chichester.

R. Chalov, S., Jarsjö, J., Kasimov, N. S., O. Romanchenko, A., Pietroń, J., Thorslund, J., & Promakhova, E. V. (2015). Spatio-temporal variation of sediment transport in the Selenga River Basin, Mongolia and Russia. *Environmental Earth Sciences*, *73*(2), 663–680. https://doi.org/10.1007/s12665-014-3106-z

Raigani, Z. M., Nosrati, K., & Collins, A. L. (2019). Fingerprinting sub-basin spatial sediment sources in a large Iranian catchment under dry-land cultivation and rangeland farming: Combining geochemical tracers and weathering indices. *Journal of Hydrology: Regional Studies*, *24*, 100613. https://doi.org/10.1016/j.ejrh.2019.100613

Ranalli, A. J. (2004). *A Summary of the Scientific Literature on the Effects of Fire on the Concentration of Nutrients in Surface Waters*. https://apps.dtic.mil/sti/citations/ADA439942

Rao, K. P. C., Steenhuis, T. S., Cogle, A. L., Srinivasan, S. T., Yule, D. F., & Smith, G. D. (1998). Rainfall infiltration and runoff from an Alfisol in semi-arid tropical India. I. No-till systems. *Soil and Tillage Research*, *48*(1–2), 51–59. https://doi.org/10.1016/S0167-1987(98)00124-X

Ravisangar, V., Dennett, K. E., Sturm, T. W., & Amirtharajah, A. (2001). Effect of Sediment pH on Resuspension of Kaolinite Sediments. *Journal of Environmental Engineering*, *127*(6), 531–538. https://doi.org/10.1061/(ASCE)0733-9372(2001)127:6(531)

Refsgaard, J. C., & Storm, B. (1990). Construction, Calibration And Validation of Hydrological Models. In M. B. Abbott & J. C. Refsgaard (Eds.), *Distributed Hydrological Modelling* (Vol. 22, pp. 41–54). Springer Netherlands. https://doi.org/10.1007/978-94-009-0257-2_3

Reneau, S. L., Katzman, D., Kuyumjian, G. A., Lavine, A., & Malmon, D. V. (2007). Sediment delivery after a wildfire. *Geology*, *35*(2), 151. https://doi.org/10.1130/G23288A.1

Reuschlé, T., Gbaguidi Haore, S., & Darot, M. (2003). Microstructural control on the elastic properties of thermally cracked granite. *Tectonophysics*, *370*(1–4), 95–104. https://doi.org/10.1016/S0040-1951(03)00179-3

Richards, L. A. (1931). CAPILLARY CONDUCTION OF LIQUIDS THROUGH POROUS MEDIUMS. *Physics*, *1*(5), 318–333. https://doi.org/10.1063/1.1745010

Richter, D., & Simmons, G. (1974). Thermal expansion behavior of igneous rocks. *International Journal of Rock Mechanics and Mining Sciences & Geomechanics Abstracts*, *11*(10), 403–411. https://doi.org/10.1016/0148-9062(74)91111-5

Riezebos, H. Th., & Epema, G. F. (1985). Drop shape and erosivity part II: Splash detachment, transport and erosivity indices. *Earth Surface Processes and Landforms*, *10*(1), 69–74. https://doi.org/10.1002/esp.3290100109

River, M., & Richardson, C. J. (2019). Suspended Sediment Mineralogy and the Nature of Suspended Sediment Particles in Stormflow of the Southern Piedmont of the USA. *Water Resources Research*, *55*(7), 5665–5678. https://doi.org/10.1029/2018WR024613

Rodríguez-Blanco, M. L., Soto-Varela, F., Taboada-Castro, M. M., & Taboada-Castro, M. T. (2018). Using hysteresis analysis to infer controls on sediment-associated and dissolved metals transport in a small humid temperate catchment. *Journal of Hydrology*, *565*, 49–60. https://doi.org/10.1016/j.jhydrol.2018.08.030

Rodríguez-Blanco, M. L., Taboada-Castro, M. M., & Taboada-Castro, M. T. (2010). Factors controlling hydro-sedimentary response during runoff events in a rural catchment in the humid Spanish zone. *CATENA*, *82*(3), 206–217. https://doi.org/10.1016/j.catena.2010.06.007

Rose, L. A., Karwan, D. L., & Godsey, S. E. (2018). Concentration-discharge relationships describe solute and sediment mobilization, reaction, and transport at event and longer timescales. *Hydrological Processes*, *32*(18), 2829–2844. https://doi.org/10.1002/hyp.13235

Rose, S. (2003). Comparative solute–discharge hysteresis analysis for an urbanized and a 'control basin' in the Georgia (USA) Piedmont. *Journal of Hydrology*, *284*(1–4), 45–56. https://doi.org/10.1016/j.jhydrol.2003.07.001

Rovira, A., & Batalla, R. J. (2006). Temporal distribution of suspended sediment transport in a Mediterranean basin: The Lower Tordera (NE SPAIN). *Geomorphology*, *79*(1–2), 58–71. https://doi.org/10.1016/j.geomorph.2005.09.016

Ruiz-Agudo, E., Putnis, C. V., Pel, L., & Rodriguez-Navarro, C. (2013). Template-Assisted Crystallization of Sulfates onto Calcite: Implications for the Prevention of Salt Damage. *Crystal Growth & Design*, *13*(1), 40–51. https://doi.org/10.1021/cg300744x

Rustomji, P. (2006). Analysis of gully dimensions and sediment texture from southeast Australia for catchment sediment budgeting. *CATENA*, *67*(2), 119–127. https://doi.org/10.1016/j.catena.2006.03.004

Sadeghi, S. H., & Singh, V. P. (2017). Dynamics of suspended sediment concentration, flow discharge and sediment particle size interdependency to identify sediment source. *Journal of Hydrology*, *554*, 100–110. https://doi.org/10.1016/j.jhydrol.2017.09.006

Salant, N. L., Hassan, M. A., & Alonso, C. V. (2008). Suspended sediment dynamics at high and low storm flows in two small watersheds. *Hydrological Processes*, *22*(11), 1573–1587. https://doi.org/10.1002/hyp.6743

Sánchez-Chardi, A., Ribeiro, C. A. O., & Nadal, J. (2009). Metals in liver and kidneys and the effects of chronic exposure to pyrite mine pollution in the shrew Crocidura russula inhabiting the protected wetland of Doñana. *Chemosphere*, *76*(3), 387–394. https://doi.org/10.1016/j.chemosphere.2009.03.036

Sanjuán, Y., Gómez-Villar, A., Nadal-Romero, E., Álvarez-Martínez, J., Arnáez, J., Serrano-Muela, M. P., Rubiales, J. M., González-Sampériz, P., & García-Ruiz, J. M. (2016). Linking Land Cover Changes in the Sub-Alpine and Montane Belts to Changes in a Torrential River. *Land Degradation & Development*, *27*(2), 179–189. https://doi.org/10.1002/ldr.2294

Sass, O., & Oberlechner, M. (2012). Is climate change causing increased rockfall frequency in Austria? *Natural Hazards and Earth System Sciences*, *12*(11), 3209–3216. https://doi.org/10.5194/nhess-12-3209-2012

Saukel, C., Stein, R., Vogt, C., & Shevchenko, V. P. (2010). Clay-mineral and grain-size distributions in surface sediments of the White Sea (Arctic Ocean): Indicators of sediment sources and transport processes. *Geo-Marine Letters*, *30*(6), 605–616. https://doi.org/10.1007/s00367-010-0210-2

Schaefli, B. (2016). Snow hydrology signatures for model identification within a limits-of-acceptability approach: Snow Hydrology Signatures. *Hydrological Processes*, *30*(22), 4019–4035. https://doi.org/10.1002/hyp.10972

Scheffers, A. M., May, S. M., & Kelletat, D. H. (2015a). Mass Movements: Landforms Shaped Under the Force of Gravity. In A. M. Scheffers, S. M. May, & D. H. Kelletat, *Landforms of the World with Google Earth* (pp. 163–182). Springer Netherlands. https://doi.org/10.1007/978-94-017-9713-9_8

Scheffers, A. M., May, S. M., & Kelletat, D. H. (2015b). Physical and Chemical Weathering. In A. M. Scheffers, S. M. May, & D. H. Kelletat, *Landforms of the World with Google Earth* (pp. 137–146). Springer Netherlands. https://doi.org/10.1007/978-94-017-9713-9_6

Scherer, G. W. (1999). Crystallization in pores. *Cement and Concrete Research*, *29*(8), 1347–1358. https://doi.org/10.1016/S0008-8846(99)00002-2

Scherer, G. W. (2004). Stress from crystallization of salt. *Cement and Concrete Research*, *34*(9), 1613–1624. https://doi.org/10.1016/j.cemconres.2003.12.034

Schilirò, L., Esposito, C., De Blasio, F. V., & Scarascia Mugnozza, G. (2019). Sediment texture in rock avalanche deposits: Insights from field and experimental observations. *Landslides*, *16*(9), 1629–1643. https://doi.org/10.1007/s10346-019-01210-x

Schleiss, A. J., Franca, M. J., Juez, C., & De Cesare, G. (2016). Reservoir sedimentation. *Journal of Hydraulic Research*, *54*(6), 595–614. https://doi.org/10.1080/00221686.2016.1225320

Seeger, M., Errea, M.-P., Beguería, S., Arnáez, J., Martí, C., & García-Ruiz, J. M. (2004). Catchment soil moisture and rainfall characteristics as determinant factors for discharge/suspended sediment hysteretic loops in a small headwater catchment in the Spanish pyrenees. *Journal of Hydrology*, *288*(3–4), 299–311. https://doi.org/10.1016/j.jhydrol.2003.10.012

Semenov, O. E. (2012). Dust Storms and Sandstorms and Aerosol Long-Distance Transport. In S.-W. Breckle, W. Wucherer, L. A. Dimeyeva, & N. P. Ogar (Eds.), *Aralkum—A Man-Made Desert* (Vol. 218, pp. 73–82). Springer Berlin Heidelberg. https://doi.org/10.1007/978-3-642-21117-1_5

Seng Low, H. (1989). Effect of Sediment Density on Bed-Load Transport. *Journal of Hydraulic Engineering*, *115*(1), 124–138. https://doi.org/10.1061/(ASCE)0733-9429(1989)115:1(124)

Sestini, G. (1989). Nile Delta: A review of depositional environments and geological history. *Geological Society, London, Special Publications*, *41*(1), 99–127. https://doi.org/10.1144/GSL.SP.1989.041.01.09

Shakesby, R., & Doerr, S. (2006). Wildfire as a hydrological and geomorphological agent. *Earth-Science Reviews*, *74*(3–4), 269–307. https://doi.org/10.1016/j.earscirev.2005.10.006

Sharif, Y. A., Elkholy, M., Hanif Chaudhry, M., & Imran, J. (2015). Experimental Study on the Piping Erosion Process in Earthen Embankments. *Journal of Hydraulic Engineering*, *141*(7), 04015012. https://doi.org/10.1061/(ASCE)HY.1943-7900.0001019

Sherriff, S. C., Rowan, J. S., Fenton, O., Jordan, P., Melland, A. R., Mellander, P.-E., & hUallacháin, D. Ó. (2016). Storm Event Suspended Sediment-Discharge Hysteresis and Controls in Agricultural Watersheds: Implications for Watershed Scale Sediment Management. *Environmental Science & Technology*, *50*(4), 1769–1778. https://doi.org/10.1021/acs.est.5b04573

Shields, A. (1936). Anwendung der Aehnlichkeitsmechanik und der Turbulenzforschung auf die Geschiebebewegung. *PhD Thesis Technical University Berlin*. https://repository.tudelft.nl/islandora/object/uuid%3A61a19716-a994-4942-9906-f680eb9952d6

Sivakumar, M. V. K. (2005). Impacts of Sand Storms/Dust Storms on Agriculture. In M. V. K. Sivakumar, R. P. Motha, & H. P. Das (Eds.), *Natural Disasters and Extreme Events in Agriculture* (pp. 159–177). Springer-Verlag. https://doi.org/10.1007/3-540-28307-2_10

Smith, C. E. (1998). Modeling high sinuosity meanders in a small flume. *Geomorphology*, *25*(1–2), 19–30. https://doi.org/10.1016/S0169-555X(98)00029-4

Smith, H. G., & Dragovich, D. (2009). Interpreting sediment delivery processes using suspended sediment-discharge hysteresis patterns from nested upland catchments, south-eastern Australia. *Hydrological Processes*, *23*(17), 2415–2426. https://doi.org/10.1002/hyp.7357

Soltani, A. A., Bermad, A., Boutaghane, H., Oukil, A., Abdalla, O., Hasbaia, M., Oulebsir, R., Zeroual, S., & Lefkir, A. (2020). An integrated approach for assessing surface water quality: Case of Beni Haroun dam (Northeast Algeria). *Environmental Monitoring and Assessment*, *192*(10), 630. https://doi.org/10.1007/s10661-020-08572-z

Spence, C. (2010). A Paradigm Shift in Hydrology: Storage Thresholds Across Scales Influence Catchment Runoff Generation: Paradigm shift in hydrology. *Geography Compass*, *4*(7), 819–833. https://doi.org/10.1111/j.1749-8198.2010.00341.x

Sreedhar, B. K., Albert, S. K., & Pandit, A. B. (2017). Cavitation damage: Theory and measurements – A review. *Wear*, *372–373*, 177–196. https://doi.org/10.1016/j.wear.2016.12.009

Staley, N. A., Wynn, T., Benham, B., Yagow, G., & Tech, V. (2006). Modeling channel erosion at the watershed scale: Model review and case study. *Center for TMDL and Watershed Studies, Biological Systems Engineering, Virginia Tech, Document*, *2006–0009*.

Steiger, J., Gurnell, A. M., & Petts, G. E. (2001). Sediment deposition along the channel margins of a reach of the middle River Severn, UK. *Regulated Rivers: Research & Management*, *17*(4–5), 443–460. https://doi.org/10.1002/rrr.644

Steiger, M. (2005a). Crystal growth in porous materials—I: The crystallization pressure of large crystals. *Journal of Crystal Growth*, *282*(3–4), 455–469. https://doi.org/10.1016/j.jcrysgro.2005.05.007

Steiger, M. (2005b). Crystal growth in porous materials—II: Influence of crystal size on the crystallization pressure. *Journal of Crystal Growth*, *282*(3–4), 470–481. https://doi.org/10.1016/j.jcrysgro.2005.05.008

Steiger, M., Charola, A. E., & Sterflinger, K. (2011). Weathering and Deterioration. In S. Siegesmund & R. Snethlage (Eds.), *Stone in Architecture* (pp. 227–316). Springer Berlin Heidelberg. https://doi.org/10.1007/978-3-642-14475-2_4

Stewart, C., Johnston, D. M., Leonard, G. S., Horwell, C. J., Thordarson, T., & Cronin, S. J. (2006). Contamination of water supplies by volcanic ashfall: A literature review and simple impact modelling. *Journal of Volcanology and Geothermal Research*, *158*(3–4), 296–306. https://doi.org/10.1016/j.jvolgeores.2006.07.002

Stewart, E. M., Ague, J. J., Ferry, J. M., Schiffries, C. M., Tao, R.-B., Isson, T. T., & Planavsky, N. J. (2019). Carbonation and decarbonation reactions: Implications for planetary habitability. *American Mineralogist*, *104*(10), 1369–1380. https://doi.org/10.2138/am-2019-6884

Stomph, T. J., De Ridder, N., Steenhuis, T. S., & Van De Giesen, N. C. (2002). Scale effects of Hortonian overland flow and rainfall-runoff dynamics: Laboratory validation of a process-based model. *Earth Surface Processes and Landforms*, *27*(8), 847–855. https://doi.org/10.1002/esp.356

Strohmeier, S., Knorr, K.-H., Reichert, M., Frei, S., Fleckenstein, J. H., Peiffer, S., & Matzner, E. (2013). Concentrations and fluxes of dissolved organic carbon in runoff from a forested catchment: Insights from high frequency measurements. *Biogeosciences*, *10*(2), 905–916. https://doi.org/10.5194/bg-10-905-2013

Strohmeier, S., Laaha, G., Holzmann, H., & Klik, A. (2016). Magnitude and Occurrence Probability of Soil Loss: A Risk Analytical Approach for the Plot Scale For Two Sites in Lower Austria. *Land Degradation & Development*, *27*(1), 43–51. https://doi.org/10.1002/ldr.2354

Stroosnijder, L. (2005). Measurement of erosion: Is it possible? *CATENA*, *64*(2–3), 162–173. https://doi.org/10.1016/j.catena.2005.08.004

Subehi, L., Fukushima, T., Onda, Y., Mizugaki, S., Gomi, T., Kosugi, K., Hiramatsu, S., Kitahara, H., Kuraji, K., & Terajima, T. (2010). Analysis of stream water temperature changes during rainfall events in forested watersheds. *Limnology*, *11*(2), 115–124. https://doi.org/10.1007/s10201-009-0296-2

Sun, J. (2002). Provenance of loess material and formation of loess deposits on the Chinese Loess Plateau. *Earth and Planetary Science Letters*, *203*(3–4), 845–859. https://doi.org/10.1016/S0012-821X(02)00921-4

Sun, J., Ge, X., Zhou, Y., Liu, D., Liu, J., Li, G., & Zheng, Y. (2023). Research on synergistic erosion by cavitation and sediment: A review. *Ultrasonics Sonochemistry*, *95*, 106399. https://doi.org/10.1016/j.ultsonch.2023.106399

Syvitski, J. P. M., Vörösmarty, C. J., Kettner, A. J., & Green, P. (2005). Impact of Humans on the Flux of Terrestrial Sediment to the Global Coastal Ocean. *Science*, *308*(5720), 376–380. https://doi.org/10.1126/science.1109454

Tananaev, N. I. (2015). Hysteresis effects of suspended sediment transport in relation to geomorphic conditions and dominant sediment sources in medium and large rivers of the Russian Arctic. *Hydrology Research*, *46*(2), 232–243. https://doi.org/10.2166/nh.2013.199

Tang, J.-W., Deng, J.-Y., You, X.-Y., & Wang, F. (2012). Forecast method for bank collapse in middle and lower Yangtze River(MLYZ). *Journal of Sichuan University: Engineering Science Edition*, *44*(1), 75–81.

Tansel, B., & Rafiuddin, S. (2016). Heavy metal content in relation to particle size and organic content of surficial sediments in Miami River and transport potential. *International Journal of Sediment Research*, *31*(4), 324–329. https://doi.org/10.1016/j.ijsrc.2016.05.004

Tao Shen, H., Shen, H., & Tsai, S.-M. (1990). Dynamic transport of river ice. *Journal of Hydraulic Research*, *28*(6), 659–671. https://doi.org/10.1080/00221689009499017

Thorley, R. M. S., Taylor, L. L., Banwart, S. A., Leake, J. R., & Beerling, D. J. (2015). The role of forest trees and their mycorrhizal fungi in carbonate rock weathering and its significance for global carbon cycling. *Plant, Cell & Environment*, *38*(9), 1947–1961. https://doi.org/10.1111/pce.12444

Thorslund, J., Jarsjö, J., Chalov, S. R., & Belozerova, E. V. (2012). Gold mining impact on riverine heavy metal transport in a sparsely monitored region: The upper Lake Baikal Basin case. *Journal of Environmental Monitoring*, *14*(10), 2780. https://doi.org/10.1039/c2em30643c

Tian, P., Zhai, J., Zhao, G., & Mu, X. (2016). Dynamics of Runoff and Suspended Sediment Transport in a Highly Erodible Catchment on the Chinese Loess Plateau. *Land Degradation & Development*, *27*(3), 839–850. https://doi.org/10.1002/ldr.2373

Tietjen, B., & Jeltsch, F. (2007). Semi-arid grazing systems and climate change: A survey of present modelling potential and future needs. *Journal of Applied Ecology*, *44*(2), 425–434. https://doi.org/10.1111/j.1365-2664.2007.01280.x

Torri, D., Sfalanga, M., & Del Sette, M. (1987). Splash detachment: Runoff depth and soil cohesion. *CATENA*, *14*(1–3), 149–155. https://doi.org/10.1016/S0341-8162(87)80013-9

Trimble, S. W. (1997). Contribution of Stream Channel Erosion to Sediment Yield from an Urbanizing Watershed. *Science*, *278*(5342), 1442–1444. https://doi.org/10.1126/science.278.5342.1442

Tsikouras, B., Pe-Piper, G., Piper, D. J. W., & Schaffer, M. (2011). Varietal heavy mineral analysis of sediment provenance, Lower Cretaceous Scotian Basin, eastern Canada. *Sedimentary Geology*, *237*(3–4), 150–165. https://doi.org/10.1016/j.sedgeo.2011.02.011

Tsoar, H. (2001). Types of Aeolian Sand Dunes and Their Formation. In N. J. Balmforth & A. Provenzale (Eds.), *Geomorphological Fluid Mechanics* (Vol. 582, pp. 403–429). Springer Berlin Heidelberg. https://doi.org/10.1007/3-540-45670-8_17

Turcotte, B., Morse, B., Bergeron, N. E., & Roy, A. G. (2011). Sediment transport in ice-affected rivers. *Journal of Hydrology*, *409*(1–2), 561–577. https://doi.org/10.1016/j.jhydrol.2011.08.009

Umbrell, E. R., Young, G. K., Stein, S. M., & Jones, J. S. (1998). Clear-Water Contraction Scour under Bridges in Pressure Flow. *Journal of Hydraulic Engineering*, *124*(2), 236–240. https://doi.org/10.1061/(ASCE)0733-9429(1998)124:2(236)

Upadhayay, H. R., Bodé, S., Griepentrog, M., Huygens, D., Bajracharya, R. M., Blake, W. H., Dercon, G., Mabit, L., Gibbs, M., Semmens, B. X., Stock, B. C., Cornelis, W., & Boeckx, P. (2017). Methodological perspectives on the application of compound-specific stable isotope fingerprinting for sediment source apportionment. *Journal of Soils and Sediments*, *17*(6), 1537–1553. https://doi.org/10.1007/s11368-017-1706-4

Urban, J. D., Tachovsky, J. A., Haws, L. C., Wikoff Staskal, D., & Harris, M. A. (2009). Assessment of human health risks posed by consumption of fish from the Lower Passaic River, New Jersey. *Science of The Total Environment*, *408*(2), 209–224. https://doi.org/10.1016/j.scitotenv.2009.03.004

U.S. Geological Survey. (2015). *National Field Manual for the Collection of Water-Quality Data. U.S. Geological Survey Techniques of Water-Resources Investigations, Book 9*. https://doi.org/10.3133/twri09

Vale, S. S., & Dymond, J. R. (2020). Interpreting nested storm event suspended sediment-discharge hysteresis relationships at large catchment scales. *Hydrological Processes*, *34*(2), 420–440. https://doi.org/10.1002/hyp.13595

Vale, S. S., Fuller, I. C., Procter, J. N., Basher, L. R., & Smith, I. E. (2016). Characterization and quantification of suspended sediment sources to the Manawatu River, New Zealand. *Science of The Total Environment*, *543*, 171–186. https://doi.org/10.1016/j.scitotenv.2015.11.003

Van Beek, R., Cammeraat, E., Andreu, V., Mickovski, S. B., & Dorren, L. (2008). Hillslope Processes: Mass Wasting, Slope Stability and Erosion. In J. E. Norris, A. Stokes, S. B. Mickovski, E. Cammeraat, R. Van Beek, B. C. Nicoll, & A. Achim (Eds.), *Slope Stability and Erosion Control: Ecotechnological Solutions* (pp. 17–64). Springer Netherlands. https://doi.org/10.1007/978-1-4020-6676-4_3

Van Dijk, A. I. J. M., Bruijnzeel, L. A., & Rosewell, C. J. (2002). Rainfall intensity–kinetic energy relationships: A critical literature appraisal. *Journal of Hydrology*, *261*(1–4), 1–23. https://doi.org/10.1016/S0022-1694(02)00020-3

Van Dijk, W. M., Van De Lageweg, W. I., & Kleinhans, M. G. (2013). Formation of a cohesive floodplain in a dynamic experimental meandering river. *Earth Surface Processes and Landforms*, *38*(13), 1550–1565. https://doi.org/10.1002/esp.3400

Vanmaercke, M., Zenebe, A., Poesen, J., Nyssen, J., Verstraeten, G., & Deckers, J. (2010). Sediment dynamics and the role of flash floods in sediment export from medium-sized catchments: A case study from the semi-arid tropical highlands in northern Ethiopia. *Journal of Soils and Sediments*, *10*(4), 611–627. https://doi.org/10.1007/s11368-010-0203-9

Vaughan, M. C. H., Bowden, W. B., Shanley, J. B., Vermilyea, A., Sleeper, R., Gold, A. J., Pradhanang, S. M., Inamdar, S. P., Levia, D. F., Andres, A. S., Birgand, F., & Schroth, A. W. (2017). High-frequency dissolved organic carbon and nitrate measurements reveal differences in storm hysteresis and loading in relation to land cover and seasonality. *Water Resources Research*, *53*(7), 5345–5363. https://doi.org/10.1002/2017WR020491

Veerasingam, S., Venkatachalapathy, R., & Ramkumar, T. (2014). Distribution of clay minerals in marine sediments off Chennai, Bay of Bengal, India: Indicators of sediment sources and transport processes. *International Journal of Sediment Research*, *29*(1), 11–23. https://doi.org/10.1016/S1001-6279(14)60018-4

Verachtert, E., Maetens, W., Van Den Eeckhaut, M., Poesen, J., & Deckers, J. (2011). Soil loss rates due to piping erosion. *Earth Surface Processes and Landforms*, *36*(13), 1715–1725. https://doi.org/10.1002/esp.2186

Vercruysse, K., Grabowski, R. C., & Rickson, R. J. (2017). Suspended sediment transport dynamics in rivers: Multi-scale drivers of temporal variation. *Earth-Science Reviews*, *166*, 38–52. https://doi.org/10.1016/j.earscirev.2016.12.016

Vörösmarty, C. J., McIntyre, P. B., Gessner, M. O., Dudgeon, D., Prusevich, A., Green, P., Glidden, S., Bunn, S. E., Sullivan, C. A., Liermann, C. R., & Davies, P. M. (2010). Global threats to human water security and river biodiversity. *Nature*, *467*(7315), 555–561. https://doi.org/10.1038/nature09440

Vörösmarty, C. J., Meybeck, M., Fekete, B., Sharma, K., Green, P., & Syvitski, J. P. M. (2003). Anthropogenic sediment retention: Major global impact from registered river impoundments. *Global and Planetary Change*, *39*(1–2), 169–190. https://doi.org/10.1016/S0921-8181(03)00023-7

Walling, D. E. (2013). The evolution of sediment source fingerprinting investigations in fluvial systems. *Journal of Soils and Sediments*, *13*(10), 1658–1675. https://doi.org/10.1007/s11368-013-0767-2

Walling, D. E., & Moorehead, P. W. (1989). The particle size characteristics of fluvial suspended sediment: An overview. In P. G. Sly & B. T. Hart (Eds.), *Sediment/Water Interactions* (pp. 125–149). Springer Netherlands. https://doi.org/10.1007/978-94-009-2376-8_12

Walling, D., & Webb, B. (1982). Sediment availability and the prediction of storm-period sediment yields. *IAHS-AISH Publication*, *137*.

Walling, D., Woodward, J., & Nicholas, A. (1993). A multi-parameter approach to fingerprinting suspended-sediment sources. *IAHS Publication*, *215*, 329–338.

Walsh, J. B. (1965). The effect of cracks in rocks on Poisson's ratio. *Journal of Geophysical Research*, *70*(20), 5249–5257. https://doi.org/10.1029/JZ070i020p05249

Wang, C., Yu, X., & Liang, F. (2017). A review of bridge scour: Mechanism, estimation, monitoring and countermeasures. *Natural Hazards*, *87*(3), 1881–1906. https://doi.org/10.1007/s11069-017-2842-2

Wang, J., Yu, B., Ni, S., Guo, Z., & Cai, C. (2020). Effects of sediment load on the abrasion of soil aggregate and hydraulic parameters in experimental overland flow. *Journal of Integrative Agriculture*, *19*(4), 1117–1126. https://doi.org/10.1016/S2095-3119(19)62719-X

Wang, J.-G., Li, Z., Cai, C., & Yang, W. (2012). Effects of transport distance and flow discharge of overland flow on destruction of Ultisol aggregates. *Particuology*, *10*(5), 607–613. https://doi.org/10.1016/j.partic.2011.06.013

Wang, J.-G., Li, Z.-X., Cai, C.-F., Yang, W., Ma, R.-M., & Zhang, G.-B. (2013). Effects of stability, transport distance and two hydraulic parameters on aggregate abrasion of Ultisols in overland flow. *Soil and Tillage Research*, *126*, 134–142. https://doi.org/10.1016/j.still.2012.09.005

Wang, J.-G., Yu, B., Yang, W., Cheng, J., Song, Y., & Cai, C. (2017). The abrasion of soil aggregate under different artificial rough beds in overland flow. *CATENA*, *155*, 183–190. https://doi.org/10.1016/j.catena.2017.03.016

Wang, L., Shao, M., Wang, Q., & Gale, W. J. (2006). Historical changes in the environment of the Chinese Loess Plateau. *Environmental Science & Policy*, *9*(7–8), 675–684. https://doi.org/10.1016/j.envsci.2006.08.003

Wang, S., Flanagan, D. C., & Engel, B. A. (2019). Estimating sediment transport capacity for overland flow. *Journal of Hydrology*, *578*, 123985. https://doi.org/10.1016/j.jhydrol.2019.123985

Wang, S., Pan, C., Xie, D., Xu, M., Yan, Y., & Li, X. (2022). Grain size characteristics of surface sediment and its response to the dynamic sedimentary environment in Qiantang Estuary, China. *International Journal of Sediment Research*, *37*(4), 457–468. https://doi.org/10.1016/j.ijsrc.2021.12.002

Wang, X., Schubnel, A., Fortin, J., Guéguen, Y., & Ge, H. (2013). Physical properties and brittle strength of thermally cracked granite under confinement. *Journal of Geophysical Research: Solid Earth*, *118*(12), 6099–6112. https://doi.org/10.1002/2013JB010340

Wang, Y., Kuang, S., & Su, J. (2016). Critical caving erosion width for cantilever failures of river bank. *International Journal of Sediment Research*, *31*(3), 220–225. https://doi.org/10.1016/j.ijsrc.2016.05.003

Wardrop, D. H., & Brooks, R. P. (1998). The Occurrence and Impact of Sedimentation in Central Pennsylvania Wetlands. *Environmental Monitoring and Assessment*, *51*(1/2), 119–130. https://doi.org/10.1023/A:1005958429834

Westbrook, C. J., Cooper, D. J., & Baker, B. W. (2006). Beaver dams and overbank floods influence groundwater–surface water interactions of a Rocky Mountain riparian area. *Water Resources Research*, *42*(6), 2005WR004560. https://doi.org/10.1029/2005WR004560

Whipple, K. X., Hancock, G. S., & Anderson, R. S. (2000). River incision into bedrock: Mechanics and relative efficacy of plucking, abrasion, and cavitation. *Geological Society of America Bulletin*, *112*(3), 490–503. https://doi.org/10.1130/0016-7606(2000)112%253C490:RIIBMA%253E2.0.CO;2

Wicks, E., Koch, E., O'Neil, J., & Elliston, K. (2009). Effects of sediment organic content and hydrodynamic conditions on the growth and distribution of Zostera marina. *Marine Ecology Progress Series*, *378*, 71–80. https://doi.org/10.3354/meps07885

Williams, G. P. (1989). Sediment concentration versus water discharge during single hydrologic events in rivers. *Journal of Hydrology*, *111*(1–4), 89–106. https://doi.org/10.1016/0022-1694(89)90254-0

Williams, M. R., Livingston, S. J., Penn, C. J., Smith, D. R., King, K. W., & Huang, C. (2018). Controls of event-based nutrient transport within nested headwater agricultural watersheds of the western Lake Erie basin. *Journal of Hydrology*, *559*, 749–761. https://doi.org/10.1016/j.jhydrol.2018.02.079

Wilson, C. G., Kuhnle, R. A., Bosch, D. D., Steiner, J. L., Starks, P. J., Tomer, M. D., & Wilson, G. V. (2008). Quantifying relative contributions from sediment sources in Conservation Effects Assessment Project watersheds. *Journal of Soil and Water Conservation*, *63*(6), 523–532. https://doi.org/10.2489/jswc.63.6.523

Wilson, E. M. (1990). *Engineering Hydrology*. Macmillan Education UK. https://doi.org/10.1007/978-1-349-20610-0

Wilson, G. (2011). Understanding soil-pipe flow and its role in ephemeral gully erosion. *Hydrological Processes*, *25*(15), 2354–2364. https://doi.org/10.1002/hyp.7998

Wolf, S., Stenger, D., Steudtner, F., Esser, V., Lehmkuhl, F., & Schüttrumpf, H. (2023). Modeling anthropogenic affected sediment transport in a mid-sized European river catchment–extension of the sediment rating curve equation. *Modeling Earth Systems and Environment*, *9*(4), 3815–3835. https://doi.org/10.1007/s40808-023-01703-8

Wong, F. L., Woodrow, D. L., & McGann, M. (2013). Heavy mineral analysis for assessing the provenance of sandy sediment in the San Francisco Bay Coastal System. *Marine Geology*, *345*, 170–180. https://doi.org/10.1016/j.margeo.2013.05.012

Wood, P. A. (1977). Controls of variation in suspended sediment concentration in the River Rother, West Sussex, England. *Sedimentology*, *24*(3), 437–445. https://doi.org/10.1111/j.1365-3091.1977.tb00131.x

Wu, S., Liu, Y., Bougoure, J. J., Southam, G., Chan, T.-S., Lu, Y.-R., Haw, S.-C., Nguyen, T. A. H., You, F., & Huang, L. (2019). Organic Matter Amendment and Plant Colonization Drive Mineral Weathering, Organic Carbon Sequestration, and Water-Stable Aggregation in Magnetite Fe Ore Tailings. *Environmental Science & Technology*, *53*(23), 13720–13731. https://doi.org/10.1021/acs.est.9b04526

Wu, W., & Wang, S. S. Y. (2006). Formulas for Sediment Porosity and Settling Velocity. *Journal of Hydraulic Engineering*, *132*(8), 858–862. https://doi.org/10.1061/(ASCE)0733-9429(2006)132:8(858)

Wymore, A. S., Leon, M. C., Shanley, J. B., & McDowell, W. H. (2019). Hysteretic Response of Solutes and Turbidity at the Event Scale Across Forested Tropical Montane Watersheds. *Frontiers in Earth Science*, *7*, 126. https://doi.org/10.3389/feart.2019.00126

Xu, L., Wang, Y., Zhao, W., & Jiang, E. (2018). Review on Riverbank Soil Collapse. *MATEC Web of Conferences*, *246*, 01021. https://doi.org/10.1051/matecconf/201824601021

Xue, S., Jian, H., Yang, F., Liu, Q., & Yao, Q. (2022). Impact of water-sediment regulation on the concentration and transport of dissolved heavy metals in the middle and lower reaches of the Yellow River. *Science of The Total Environment*, *806*, 150535. https://doi.org/10.1016/j.scitotenv.2021.150535

Xue, Y. (1996). The Impact of Desertification in the Mongolian and the Inner Mongolian Grassland on the Regional Climate. *Journal of Climate*, *9*(9), 2173–2189. https://doi.org/10.1175/1520-0442(1996)009%253C2173:TIODIT%253E2.0.CO;2

Yair, A., & Lavee, H. (1985). Runoff generation in arid and semi-arid zones. *Hydrological Forecasting, John Wiley and Sons, New York, New York 1985. p 183-220, 23 Fig, 3 Tab, 78 Ref.*

Yan, C., & Zheng, H. (2017). A coupled thermo-mechanical model based on the combined finite-discrete element method for simulating thermal cracking of rock. *International Journal of Rock Mechanics and Mining Sciences*, *91*, 170–178. https://doi.org/10.1016/j.ijrmms.2016.11.023

Yang, C.-C., & Lee, K. T. (2018). Analysis of flow-sediment rating curve hysteresis based on flow and sediment travel time estimations. *International Journal of Sediment Research*, *33*(2), 171–182. https://doi.org/10.1016/j.ijsrc.2017.10.003

Yaseen, Z. M., Al-Juboori, A. M., Beyaztas, U., Al-Ansari, N., Chau, K.-W., Qi, C., Ali, M., Salih, S. Q., & Shahid, S. (2020). Prediction of evaporation in arid and semi-arid regions: A comparative study using different machine learning models. *Engineering Applications of Computational Fluid Mechanics*, *14*(1), 70–89. https://doi.org/10.1080/19942060.2019.1680576

Yue, S., Ouarda, T. B. M. J., Bobée, B., Legendre, P., & Bruneau, P. (2002). Approach for Describing Statistical Properties of Flood Hydrograph. *Journal of Hydrologic Engineering*, *7*(2), 147–153. https://doi.org/10.1061/(ASCE)1084-0699(2002)7:2(147)

Yuill, B. T., & Gasparini, N. M. (2011). Hydrologic controls on wash load sediment concentrations within a low-ordered, ephemeral watershed. *Journal of Hydrology*, *410*(1–2), 73–83. https://doi.org/10.1016/j.jhydrol.2011.09.011

Yusof, N. S. M., Babgi, B., Alghamdi, Y., Aksu, M., Madhavan, J., & Ashokkumar, M. (2016). Physical and chemical effects of acoustic cavitation in selected ultrasonic cleaning applications. *Ultrasonics Sonochemistry*, *29*, 568–576. https://doi.org/10.1016/j.ultsonch.2015.06.013

Zhang, C., Wang, Z., Jiang, A., & Zhang, Y. (2023). Source apportionment of suspended sediment using grain-size end-member analysis. *Marine Environmental Research*, *187*, 105904. https://doi.org/10.1016/j.marenvres.2023.105904

Zhao, C., Gao, J., Huang, Y., Wang, G., & Zhang, M. (2016). Effects of Vegetation Stems on Hydraulics of Overland Flow Under Varying Water Discharges. *Land Degradation & Development*, *27*(3), 748–757. https://doi.org/10.1002/ldr.2423

Zhao, G., Mu, X., Wen, Z., Wang, F., & Gao, P. (2013). SOIL EROSION, CONSERVATION, AND ECO-ENVIRONMENT CHANGES IN THE LOESS PLATEAU OF CHINA. *Land Degradation & Development*, *24*(5), 499–510. https://doi.org/10.1002/ldr.2246

Zheng, F., & Huang, C. (2005). Gully Erosion. In *Encyclopedia of Soil Science—Two-Volume Set* (2nd ed.). CRC Press.

Zhou, A., Tang, H., & Wang, D. (2005). Phosphorus adsorption on natural sediments: Modeling and effects of pH and sediment composition. *Water Research*, *39*(7), 1245–1254. https://doi.org/10.1016/j.watres.2005.01.026

Ziegler, A. D., Benner, S. G., Tantasirin, C., Wood, S. H., Sutherland, R. A., Sidle, R. C., Jachowski, N., Nullet, M. A., Xi, L. X., Snidvongs, A., Giambelluca, T. W., & Fox, J. M. (2014). Turbidity-based sediment monitoring in northern Thailand: Hysteresis, variability,

and uncertainty. *Journal of Hydrology*, *519*, 2020–2039. https://doi.org/10.1016/j.jhydrol.2014.09.010

Ziegler, A. D., Giambelluca, T. W., Tran, L. T., Vana, T. T., Nullet, M. A., Fox, J., Vien, T. D., Pinthong, J., Maxwell, J. F., & Evett, S. (2004). Hydrological consequences of landscape fragmentation in mountainous northern Vietnam: Evidence of accelerated overland flow generation. *Journal of Hydrology*, *287*(1–4), 124–146. https://doi.org/10.1016/j.jhydrol.2003.09.027

Zuecco, G., Penna, D., Borga, M., & van Meerveld, H. J. (2016). A versatile index to characterize hysteresis between hydrological variables at the runoff event timescale: A Hysteresis Index for Variables at the Runoff Event Timescale. *Hydrological Processes*, *30*(9), 1449–1466. https://doi.org/10.1002/hyp.10681

Zwieniecki, M. A., & Newton, M. (1995). Roots growing in rock fissures: Their morphological adaptation. *Plant and Soil*, *172*(2), 181–187. https://doi.org/10.1007/BF00011320

Data Citation

[Computer software] Omar El Farouk Khettab. (2020, June 23). blinksum/AIO_C-Q_Hysteresis_Tool: All-in-one Hysteresis Analysis Tool (Version 1.0.2). Zenodo. http://doi.org/10.5281/zenodo.3905265

[dataset] United States Geological Survey (USGS), USGS Current Conditions for USGS 16200000 NF Kaukonahua Str abv RB, nr Wahiawa, Oahu, HI. Retrieved September 14, 2018, from https://waterdata.usgs.gov/hi/nwis/uv/?site_no=16200000

[dataset] United States Geological Survey (USGS), USGS Current Conditions for USGS 16210500 Kaukonahua Str at Waialua, Oahu, HI. Retrieved September 14, 2018, from https://waterdata.usgs.gov/hi/nwis/uv/?site_no=16210500

[dataset] United States Geological Survey (USGS), USGS Current Conditions for USGS 16226200 N. Halawa Str nr Honolulu, Oahu, HI. Retrieved September 14, 2018, from https://waterdata.usgs.gov/hi/nwis/uv/?site_no=16226200

[dataset] United States Geological Survey (USGS), USGS Current Conditions for USGS 16226400 N. Halawa Str nr Quar. Stn. at Halawa, Oahu, HI. Retrieved September 14, 2018, from https://waterdata.usgs.gov/hi/nwis/uv/?site_no=16226400

[dataset] United States Geological Survey (USGS), USGS Current Conditions for USGS 16238000 Makiki Stream at King St. bridge, Oahu, HI. Retrieved September 14, 2018, from https://waterdata.usgs.gov/hi/nwis/uv/?site_no=16238000

[dataset] United States Geological Survey (USGS), USGS Current Conditions for USGS 03353200 EAGLE CREEK AT ZIONSVILLE, IN. Retrieved November 22, 2018, from https://waterdata.usgs.gov/nwis/uv?site_no=03353200

[dataset] United States Geological Survey (USGS), USGS Current Conditions for USGS 07105800 FOUNTAIN CREEK AT SECURITY, CO., Retrieved June 2, 2018, from https://waterdata.usgs.gov/nwis/uv?site_no=07105800

[dataset] United States Geological Survey (USGS), USGS Current Conditions for USGS 07194880 Osage Creek near Cave Springs, AR., Retrieved November 22, 2018, from https://waterdata.usgs.gov/ar/nwis/uv?site_no=07194880

[dataset] United States Geological Survey (USGS), USGS Current Conditions for USGS 01649190 PAINT BRANCH NEAR COLLEGE PARK, MD. Retrieved February 22, 2022, from https://nrtwq.usgs.gov/explore/plot?site_no=01649190
[dataset] United States Geological Survey (USGS), USGS Current Conditions for USGS 07144100 Little Arkansas River near Sedgwick, KS. Retrieved February 22, 2022, from https://nrtwq.usgs.gov/explore/plot?site_no=07144100
[dataset] United States Geological Survey (USGS), USGS Current Conditions for USGS 01479820 Red Clay Creek near Kennett Square, PA. Retrieved November 9, 2021, from https://waterdata.usgs.gov/usa/nwis/uv?01479820
[dataset] United States Geological Survey (USGS), USGS Current Conditions for USGS 01480870 East Branch Brandywine Creek below Downingtown, PA. Retrieved November 9, 2021, from https://waterdata.usgs.gov/usa/nwis/uv?01480870
[dataset] United States Geological Survey (USGS), USGS Current Conditions for USGS 05516665 YELLOW RIVER NEAR OAK GROVE, IN. Retrieved February 22, 2022, from https://waterdata.usgs.gov/in/nwis/uv/?site_no=05516665
[dataset] United States Geological Survey (USGS), USGS Current Conditions for USGS 07263296 Maumelle River near Wye, AR. Retrieved November 9, 2021, from https://waterdata.usgs.gov/ar/nwis/uv?site_no=07263296
[dataset] United States Geological Survey (USGS), USGS Current Conditions for USGS 01473169 Valley Creek at PA Turnpike Br near Valley Forge., Retrieved August 22, 2020, https://waterdata.usgs.gov/pa/nwis/uv?site_no=01473169
[dataset] United States Geological Survey (USGS), USGS Current Conditions for USGS 0136219503 ESOPUS CREEK BELOW LOST CLOVE RD AT BIG INDIAN NY. Retrieved November 9, 2021, from https://waterdata.usgs.gov/ny/nwis/uv/?site_no=0136219503
[dataset] United States Geological Survey (USGS), USGS Current Conditions for USGS 01589025 PATAPSCO RIVER NEAR CATONSVILLE, MD. Retrieved February 11, 2022, from https://waterdata.usgs.gov/md/nwis/uv/?site_no=01589025
[dataset] United States Geological Survey (USGS), USGS Current Conditions for USGS 01673000 PAMUNKEY RIVER NEAR HANOVER, VA. Retrieved February 11, 2022, from https://waterdata.usgs.gov/usa/nwis/uv?01673000
[dataset] United States Geological Survey (USGS), USGS Current Conditions for USGS 02035000 JAMES RIVER AT CARTERSVILLE, VA. Retrieved February 11, 2022, from https://nwis.waterdata.usgs.gov/nwis/uv/?site_no=02035000
[dataset] United States Geological Survey (USGS), USGS Current Conditions for USGS 02203863 SHOAL CREEK AT COLUMBIA DRIVE NEAR ATLANTA, GA. Retrieved February 15, 2022, from https://nwis.waterdata.usgs.gov/nwis/uv/?site_no=02203863
[dataset] United States Geological Survey (USGS), USGS Current Conditions for USGS 07061270 East Fork Black River near Lesterville, MO. Retrieved February 15, 2022, from https://nwis.waterdata.usgs.gov/nwis/uv/?site_no=07061270
[dataset] United States Geological Survey (USGS), USGS Current Conditions for USGS 08181500 Medina Rv at San Antonio, TX. Retrieved February 16, 2022, from https://nwis.waterdata.usgs.gov/nwis/uv/?site_no=08181500